STUDIES OF SITE-SELECTIVE GLYCOSYLATION OF DIHYDROFOLATE REDUCTASE

BY

Lai-Hock, TEY

A THESIS SUBMITTED TO

THE UNIVERSITY OF CARDIFF

FOR THE DEGREE OF

Doctor of Philosophy

SCHOOL OF CHEMISTRY

THE UNIVERSITY OF CARDIFF

June 2008

ProQuest LLC
789 East Eisenhower Parkway
P.O. Box 1346
Ann Arbor, MI 48106-1346

Abstract

Glycosylation is important for many molecular processes, although how glycosylation contributes to glycoprotein structure and function is not entirely clear. Other than that, the study of many of these events is complicated by the fact that natural glycoproteins normally occur as mixtures of glycoforms, therefore the isolation or synthesis of homogenous glycoproteins is an important task. Previous studies on deglycosylated proteins have shown that glycosylation reduces their catalytic activity and increase thermal stability. Therefore, we hypothesize that similar effects may be observed in the naturally unglycosylated dihydrofolate reductase from *Escherichia coli* (EcDHFR).

Four different surface-exposed sites for the incorporation of a single cysteine residue were selected based on the protein crystal structure, which may or may not affect its dynamics. Homogeneous glycoproteins have been synthesized via chemoselective ligation of a glycosyl haloacetammide with the thiol of a cysteine, to produce site-selectively glycosylated forms of EcDHFR. Techniques such as mass spectrometry, circular dichroism (CD) spectroscopy, fluorescence spectroscopy, ultraviolet (UV) visible spectroscopy and stopped-flow spectrophotometry have been used to identify and study the physical properties of different glycoforms of DHFR.

Although there were some changes of the kinetic activity of the mutants of EcDHFR, the values were comparable to those of the wild-type protein. Interestingly, in four of the five cases studied, $EcDHFR_{DM}$ D87C, there was an increase in thermal stability upon site-selective glycosylation, The other mutants showed no effect. With the exception of the effect seen for the thermal stability of the D87C mutant, this is not in accordance with the original hypothesis. This suggest that the effect seen in the D87C

mutant may be due to specific interactions of the carbohydrate moiety at certain points on the protein. An increase in resistance to thermal denaturation observed for proteins in sugar solutions may therefore also be due to binding of the sugars to specific sites on the protein.

In conclusion, an effective method for the synthesis of homogeneous glycosylated and non-glycosylated proteins has been developed and applied to the site selective glycosylation of EcDHFR. The results also suggested that the kinetic properties of EcDHFR are not significantly affected by glycosylation. It may be the large effects in terms of protein stability which due to glycosylation only occur in naturally glycosylated proteins, and not in the naturally unglycosylated EcDHFR.

Acknowledgement

Initially, I would like to thank all the members of the Allemann group for their warm welcome and facilitating my integration in the group. I am grateful to my PhD supervisor, Prof. Rudolf K. Allemann, who has given me an opportunity to research under his supervision and for his support and commitment throughout my PhD. I am also grateful to members of the group for their kindness and aid, in particular Dr. Mahmoud Akhtar, Rhiannon Evans, and Dr. Joel Loveridge, for correcting and proof reading this work. Other than them, I am deeply grateful to Dr. David Miller and Dr. Richard Swanwick, who assisted me in my projects and thesis writing.

I am also grateful to many other people and friends who have assisted me in this project and my life in UK. Thank you for all your help and support.

Last and not least, I am deeply grateful to my parents who have sponsored me for my education in UK. Without their support, I could not have finished my education, thank you.

TABLE OF CONTENTS

3. Chapter 3: Wild-type (WT) and cysteine free (DM) EcDHFR

4. Chapter 4: Synthesis and Analysis of EcDHFR triple mutants

LIST OF FIGURES

1. Chapter 1: Introduction

2. Chapter 2: Materials and Methods

3. Chapter 3: Wild-type (WT) and cysteine free (DM) EcDHFR

4. Chapter 4: Synthesis and Analysis of EcDHFR triple mutants

5. Chapter 5: Synthesis and Purification of Glycosylated EcDHFR

6. Chapter 6: Studies of the effect of Glycosylation on EcDHFR

LIST OF TABLES

2. Chapter 2: Materials and Methods

3. Chapter 3: Wild-type (WT) and cysteine free (DM) EcDHFR

4. Chapter 4: Synthesis and Analysis of EcDHFR triple mutants

5. Chapter 5: Synthesis and Purification of Glycosylated EcDHFR

6. Chapter 6: Studies of the effect of Glycosylation on EcDHFR

LIST OF ABBREVIATIONS

A	Absorbance
ABD	Adenosine binding domain
$A_{H/D}$	Arrhenius preexponential factor for hydrogen/deuterium
APS	Ammonium persulphate
ATP	Adenosine triphosphate
BSA	Bovine serum albumin
CD	Circular dichroism
DEAE	Diethyl aminoethyl
DHFR	Dihydrofolate reductase
DM	free cysteine mutants or double mutant
DMSO	Dimethylsulfoxide
DNA	Deoxyribonucleic acid
dNTP	Deoxynucleotide triphosphate
dsDNA	Double stranded DNA
Dol-P_2	Dolichol diphosphate
DTT	Dithiothreitol
E_A	Activation energy
EcDHFR	*Escherichia coli* DHFR
EDTA	Sodium diaminoethanetetraacetate
FRET	Fluorescence resonance energy transfer
Gal	Galactose
GalNAc	N-acetylgalactosamine
Glc	Glucose
GlcNAc	N-acetylglucosamine
h	Planck constant = 6.626176×10^{-34} J s
$\hbar$	Plank constant divided by 2π
H_2F	7,8-dihydrofolate
H_4F	5,6,7,8-tetrahydrofolate
Ig	Immunoglobulins
IPTG	Isopropyl-thio-β-*D*-galactopyranoside

K_D	Dissociation constant
KIE	Kinetic isotope effect
$K_iH_jPO_4$	Potassium phosphate buffer
k_{obs}	Observed binding constant
k_{off}	Dissociation binding constant
k_{on}	Association binding constant
Lac	lactose
LB medium	Luria Bertani medium
LD	Loop domain
MALDI-TOF	Matrix Assisted Laser Desorption Time of Flight
MRE	Mean residue ellipticity
MTEN	Mes tris ethanolamine saline buffer
MTX	Methotrexate
M_w	Molecular weight
$NADP^+$	Nicotinamide adenine dinucleotide phosphate oxidised form
(4R)-NADPD	(4R)-[^{2}H]-NADPH
NADPH	Nicotinamide adenine dinucleotide phosphate reduced form
$Na_iH_jPO_4$	Sodium phosphate buffer
NMR	Nuclear magnetic resonance spectroscopy
OD	Optical density
pABG	p-aminobenzoylglutamate
PAGE	Polyacrylamide gel electrophoresis
PCR	Polymerase chain reaction
PEG	Polyethylene glycol
pfu	Plaque forming units
PMA	Pyrimethamine
R	Molar gas constant = 8.314472 m^2 kg s^{-2} K^{-1} mol^{-1} (J K^{-1})
RER	Rough endoplasmic reticulum
rpm	Revolutions per minute
rRNA	Ribosomal RNA
RT	Room temperature

SDM	Site-directed mutagenesis
SDS	Sodium dodecyl sulphate
ssDNA	Single stranded DNA
TAS	Tris acetate saline
TBS	Tris borate saline
TCEP	Tris(2-carboxyethyl)phosphine
TEMED	N,N,N',N'-tetramethylenediamine
T_M	Melting temperature
T_{max}	Maximum growth temperature
TmDHFR	*Thermotoga maritima* DHFR
TMP	Trimethoprim
tRNA	Transfer RNA
T_S	Maximum stability of the protein
TS	Transition state
TST	Transition state theory
UDP	Uridine diphosphate
V_{max}	Maximum rate
WT	Wild type
$\Delta G°$	Standard free energy
ΔZ	Error
ε	Extinction coefficient
λ	Reorganization energy
λ_B	DeBroglie wavelength
$\nu_{H/D}$	Vibration frequency for hydrogen/deuterium
σ	Standard deviation
σ_M	Standard error of the mean

All amino acids are expressed in either the international three-letter code or single-letter code. Their position in the polypeptidic sequence of the protein is denoted by the succeeding number, *e.g.* Gly121 or G121 indicates a glycine residue at position 121 in the amino acid sequence.

Chapter 1

Introduction

1.1 Preface

The study of glycobiology has been carried out for decades to study the biological functions of the carbohydrate moieties in term of stability, catalytic activity, regulation of intracellular traffic and localization of glycoproteins, modulation of enzymatic and hormone activity, modification of immunological properties, participation cell-cell interaction and many other effects. Although much was known about the structure and biosynthesis of oligosaccharides in glycoproteins, the central question of how glycosylation contributes to glycoprotein structure and function is not entirely clear. Other than that, the study of many of these events is being complicated by the fact that natural glycoproteins normally occur as mixtures of glycoforms, therefore the making of homogenous glycoproteins has been an important task for glycobiology. Many techniques from biological methodology to chemical synthesis have been introduced, however most of them have the disadvantages of reductions in site-selectivity and yields. However, such disadvantages have been overcome through a combination of the introduction of unique cysteine residues at required sites using a selective chemical derivatisation strategy. This methodology has been proven by the synthesis of homogeneous glycoforms of the human glycoprotein hormone, erythroprotein.

One example of a glycoprotein that has been extensively studied is the enzyme ribonucleases (RNase), which exists *in vivo* both in non-glycosylated and glycosylated forms, the two molecules being named as RNase A and B. The oligosaccharide moiety of RNase B shields a large section of the protein from interactions with other molecules. Thus, glycosylation contributes to the stability of RNase against proteases, but also decreases its activity because binding to the substrate (RNA) is hindered. Other than that,

the effect of decrease in thermal stability due to deglycosylation has been observed in yeast external invertase, bovine serum fetuin, and glycoamylase from *Aspergillus niger*.

These studies have shown that the carbohydrate moiety does have an effect on the thermal stability of the glycoproteins. However it is not known whether these effects can be observed in a naturally non-glycosylated protein? In this work, the effect of site-specific glycosylation on the structural conformation, thermal stability and kinetic activity of the naturally non-glycosylated enzyme, dihydrofolate reductase (DHFR), will be described.

1.2 The importance of glycoproteins

Until about 1960, carbohydrates were thought to be rather uninteresting compounds and they have been considered as a nuisance that complicated protein purification by the protein chemist. Research of the last 30 years or so, however, has demonstarated that most proteins are, in fact, glycoproteins. The term 'glycobiology', introduced in 1988, focused on the role of oligosaccharides in the context of the proteins to which they were attached. Almost all the secreted and membrane-associated proteins of eukaryotic cells are glycosylated and protein glycosylation is one of the most abundant forms of covalent protein and lipid modification in eukaryotic cells [1-3]. There are two main types of protein glycosylation: *N*-glycosylation (Asn-X-Ser (or Thr), where X≠Pro and possibly Asp), in which the oligosaccharide is attached to the NH_2 group of asparagine (Asn) side chains (Figure 1.1a), and *O*-glycosylation, in which the oligosaccharide is attached to the OH groups of serine (Ser) or threonine (Thr) side chain (Figure 1.1). Inspection of the protein databases suggests that as many as 70% of proteins

have potential *N*-glycosylation sites. Unfortunately, glycoproteins often refuse to crystallize and NMR techniques do not allow unambiguous determination of the complete conformation of the sugar part, due to the glycan heterogeneity and flexibility. Therefore, time-consuming complex simulation methods are often used to explore the conformational space of N-glycans [4, 5].

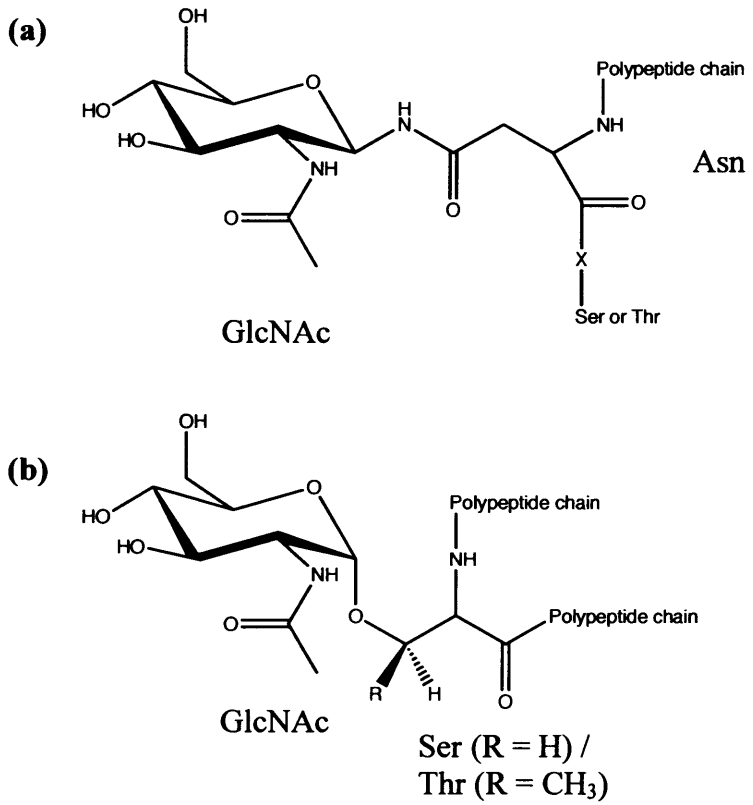

Figure 1.1: *Structures of oligosaccharide linkages. (a) N-linked glycosidic bond between GlcNAc and an Asn residue. (b) O-linked glycosidic bond between GlcNAc and Ser (Thr) residue.*

1.3 Synthesis of *O*-linked oligosaccharides

The synthesis of *O*-linked oligosaccharides occurs by the sequential addition of monosaccharide units to the newly synthesized protein as it passes through the Golgi complex. First, *N*-acetylgalactosamine (GalNAc) is transferred to the relevant Ser or Thr

residue of the protein by GalNAc transferase, an enzyme that uses uridine diphosphate-*N*-acetylgalactosamine (UDP-GalNAc) as the precursor (Figure 1.2). Other monosaccharides such as galactose (Gal), *N*-acetylglucosamine (GlcNAc), sialic acid, and fucose are then added using the corresponding sugar nucleotides as precursors. The exact type and number (up to about 10) of monosaccharides added depends on the protein substrate [6].

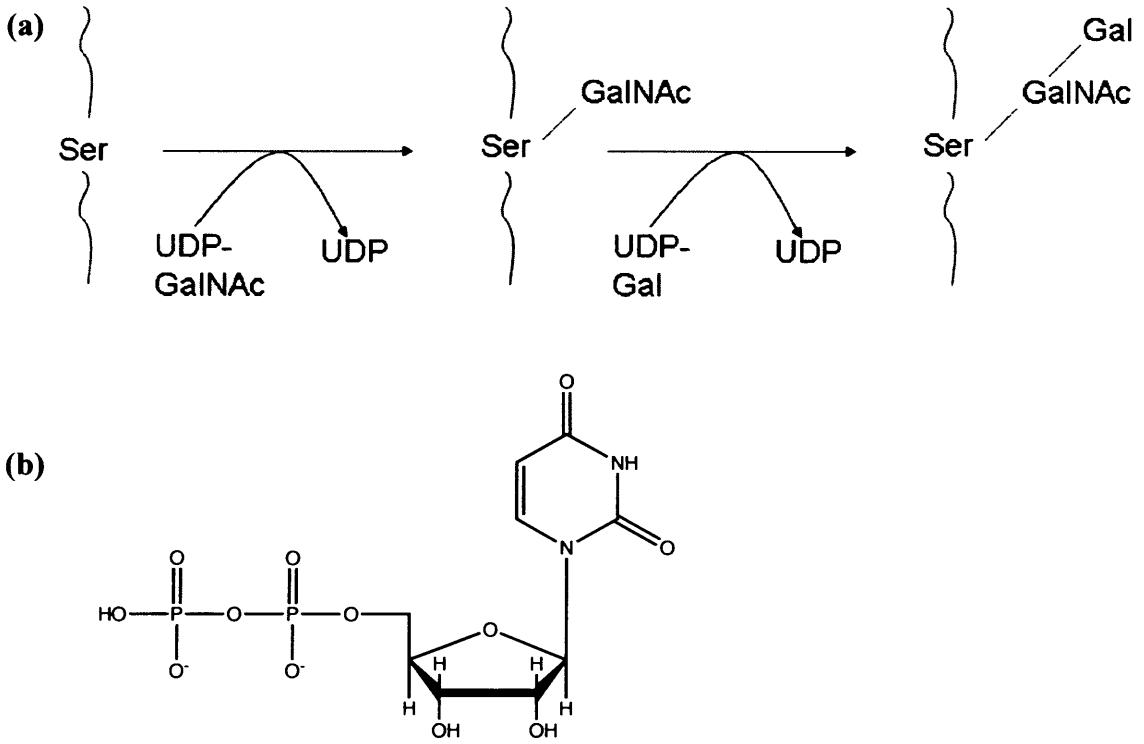

Figure 1.2: *(a) Synthesis of O-linked oligosaccharide. The example shown is an O-linked oligosaccharide in human immunoglobulin A (IgA). (b) The chemical structure of uridine diphosphate.*

1.4 Synthesis of *N*-linked oligosaccharides

The synthesis of *N*-linked oligosaccharides is much more complex than the *O*-linked oligosaccharides because they are not synthesized by adding monosaccharides directly to the protein but instead the oligosaccharide is made on a lipid carrier called

dolichol phosphate (Figure 1.3). Dolichol phosphate consists of 14-24 isoprene (C5) units (17-21 unis in animals and 14-24 units in fungi and plants) with a terminal phosphate group and it is anchored to the RER membrane. Involvement of lipid-linked oligosaccharides in N-linked glycoprotein synthesis was first demonstrated in 1972 by Armando Parodi and Luis Leloir, who showed that, when a lipid-linked oligosaccharide containing [^{14}C]glucose is incubated with rat liver microsomes (vesicular fragments of isolated ER), the radioactivity becomesw associated with protein. All *N*-linked oligosaccharides are based on a common pentasaccharide core structure consisting of three mannose (Man) residues and two *N*-acetylglucosamine (GlcNAc) residues (Figure 1.3).

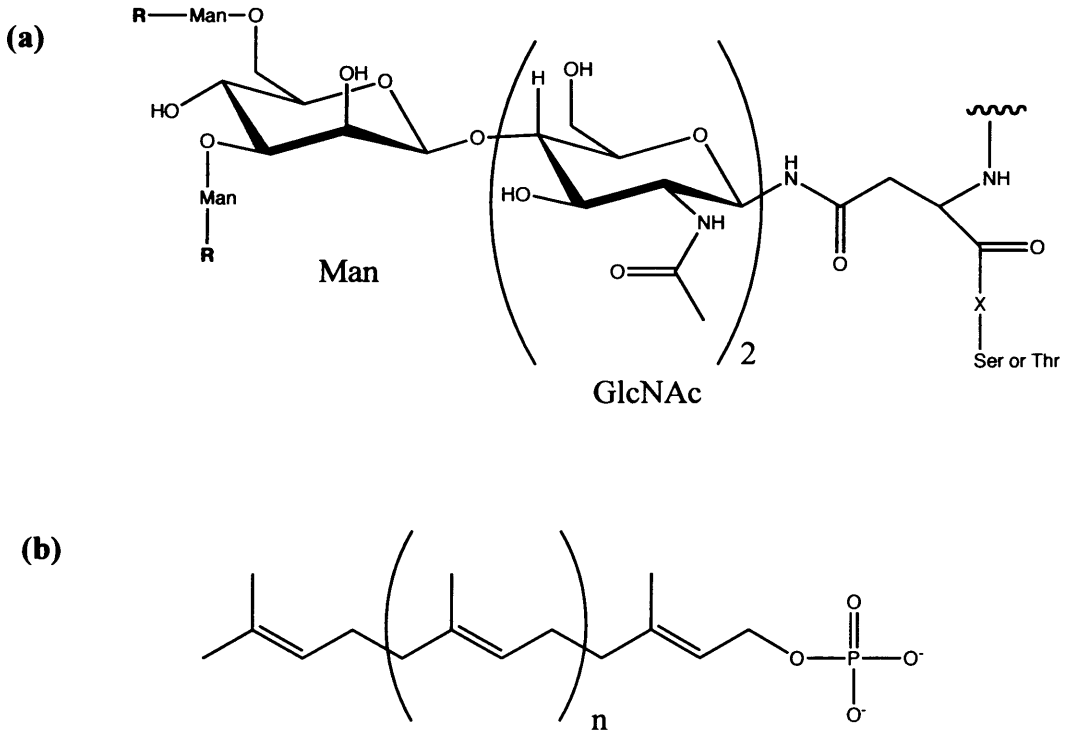

Figure 1.3: Figure (a) show the *structure of the common pentasaccharide core of N-linked oligosaccharides, and figure (b) show the structure of dolichol phosphate (n = 12-22 units).*

There are two different types of *N*-linked oligosaccharides; high mannose type oligosaccharides, where the R group in Figure 1.3 is consist of variable number of mannose residues, and complex type oligosaccharides, where the R group consists of a variety of other sugars such as GlcNAc, galactose, sialic acid and fucose.

Synthesis of the oligosaccharides is initiated by the dolichol phosphate (Dol-P) accepting monosaccharides from the cytosolic face of the RER membrane but when the $(Man)_5(GlcNAc)_2$-dolichol phosphate intermediate has formed, this will flip orientation to the luminal side of the RER membrane for accepting further monosaccharides (Figure 1.4). All of these subsequent transfers are from dolichol phosphate-linked monosaccharides that are made on the cytoplasmic side of the RER membrane then likewise flipped across to act as donors [7-10]. The final oligosaccharide, which is known as G-oligosaccharide [composed of $(Glc)_3(Man)_9(GlcNAc)_2$] is linked to the dolichol by a pyrophosphate bond. This provides the energy for transfering the oligosaccharides to the protein by a membrane-bound oligosaccharides transferase enzyme and which occurs in the RER (Figure 1.4). This reaction is also known as core glycosylation. Whilst the protein is still in the RER, the three glucose residues and a mannose residue will be removed. However, if the protein is unfolded or in a wrongly folded conformation, the glucose residues will be added back to the protein until a correctly folded form is achieved.

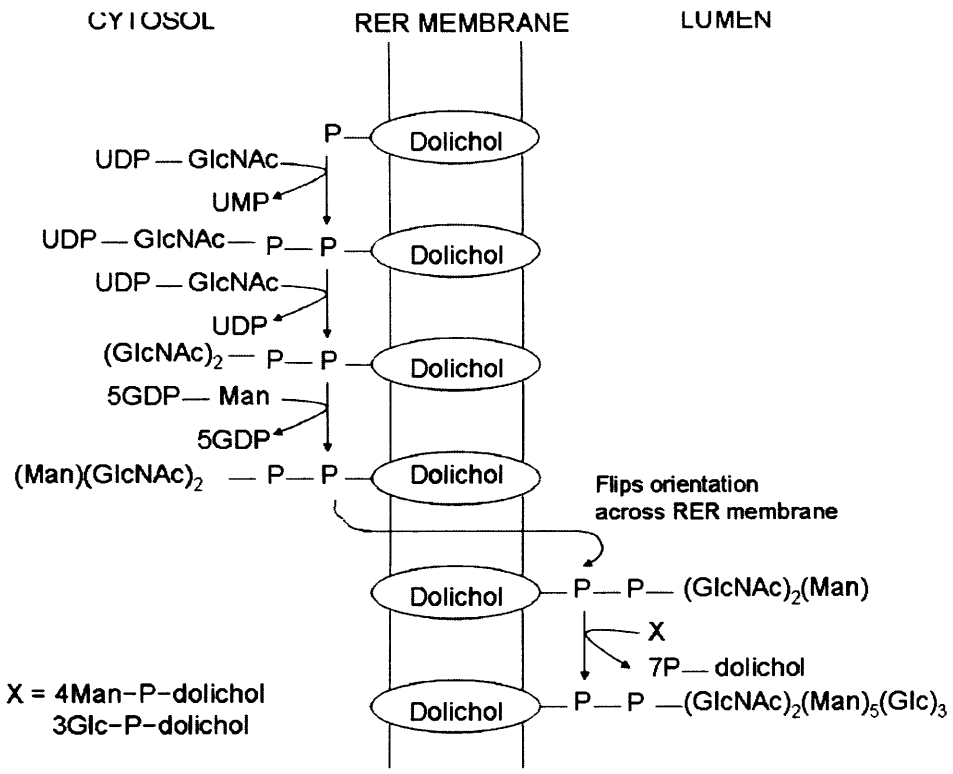

Figure 1.4: *Synthesis of N-linked oligosaccharides on a dolichol phosphate carrier in the RER membrane.*

Once the three glucose residues are finally removed, the protein may continue along the modification pathway transported to the Golgi complex *via* vesicles. As it moves through the Golgi complex, the 'trimming' or 'processing' of the oligosaccharide continues by removing another five mannose residues (Figure 1.5). Finally, mannose residues and other monosaccharides will be added to the oligosaccharides *via* a process known as terminal glycosylation to generate either the high mannose or complex type of oligosaccharides.

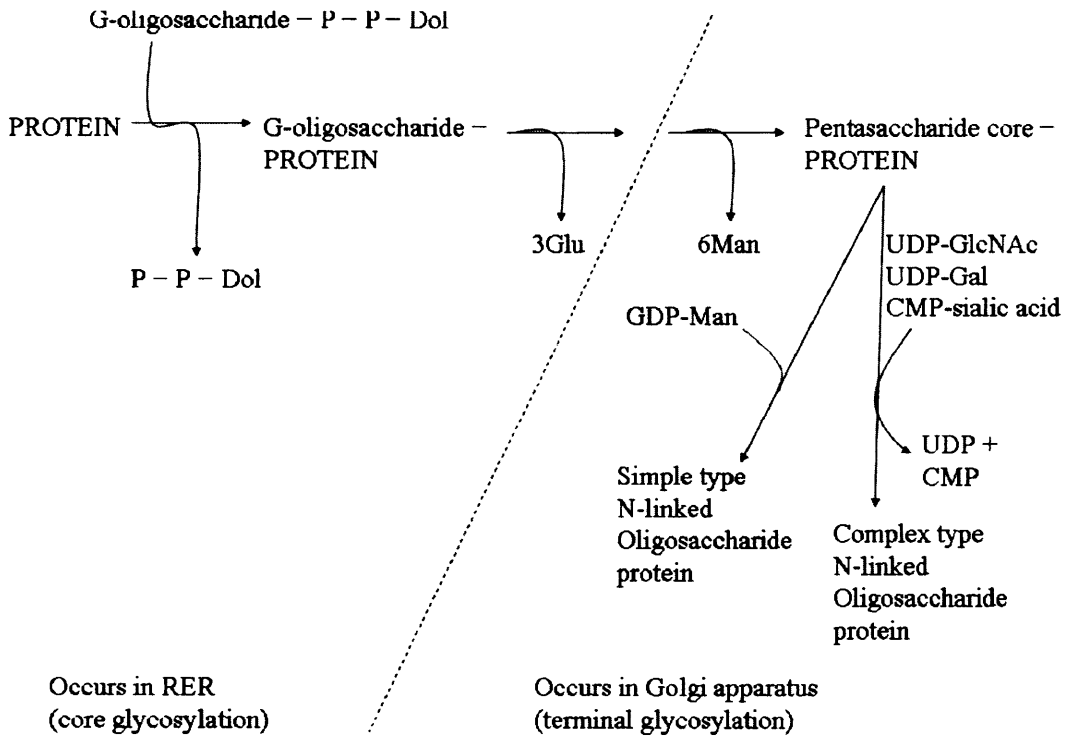

Figure 1.5: *Transfer of the oligosaccharides to the protein and further processing in the RER and Golgi.*

1.5 Importance and function of glycoproteins in eukaryotic cells

Glycoproteins have a wide range of important functions within eukaryotic cells. One type of glycoprotein found in the body is the mucins, which are secreted in the mucus of the respiratory and digestive tracts. The sugars attached to mucins give them considerable water-holding capacity and also make them resistant to proteolysis by digestive enzymes, which may be important in maintaining mucosal barriers.

Another important function of glycoproteins is immune cell recognition, especially in mammals [11]. Examples of glycoproteins in the immune system are the immunoglobulins (Ig) and the major histocompatibility complex (or MHC), which are

expressed on the surface of cells and interact with T-cells as part of the adaptive immune response.

Immunoglobulins (Ig) are large Y-shaped proteins used by the immune system to identify and neutralize foreign objects like bacteria and viruses. Each antibody recognizes a specific antigen unique to its target [12]. In binding their specific antigens, the antibodies can cause agglutination and precipitation of antibody-antigen products primed for phagocytosis by macrophages and other cells, block viral receptors, and stimulate other immune responses such as the complement pathway [13]. The complement pathway/system is a biochemical cascade of the immune system that helps clear pathogens from an organism, and promotes healing. It is derived from many small plasma proteins that work together to form the primary end result of cytolysis by disrupting the target cell's plasma membrane [12].

The major histocompatibility complex (MHC) is a large genomic region found in most vertebrates, especially in human. It is the most gene-dense region of the mammalian genome and plays an important role in the immune system, autoimmunity, and reproductive success. The MHC region encodes integral membrane proteins which are found on the surface of cells in all jawed vertebrates, and the function of these proteins are display the fragments of molecules from invading microbes or dysfunctional cells (*e.g.* tumor cells) to a particular type of white blood cell called a T cell that has the capacity to kill or co-ordinate the killing of the microbe, infected cell or malfunctioning cell.

Other examples of glycoproteins include components of the zona pellucida, which surrounds the oocyte, which is important for sperm-egg interaction, and structural glycoproteins, which occur in connective tissue. These help bind together the fibers, cells,

and ground substance of connective tissue. They may also help components of the tissue bind to inorganic substances, such as calcium in bone [14, 15].

Recent studies on the enzymes RNase, yeast external invertase, bovine serum fetuin, and glucoamylase have shown that glycosylation has a general stabilization effect on protein thermal stability and conformation [16]. The non-glycosylated protein and glycosylated protein, shows a difference in their thermal stability. Glycosylation appears to have an effect on stabilizing the protein. This similar phenomenon has also been observed in studies of the two heavily glycosylated β-1,3/1,4-glucanases by Olsen and co-workers [17]. They found that the glycosylated enzymes which were expressed in *Saccharomyces cerevisiae* were considerably more heat stable than their unglycosylated counterparts which are expressed in *E. coli*.

It is important to note that all the heavily glycosylated proteins, whether *N*-glycosylated or *O*-glycosylated or both, are thermally destabilized by removing their carbohydrate. If the results from the present study can be generalized, then we may expect that stabilization of protein conformation and thermal stability are common general properties conferred by the covalent attachment of carbohydrates to the polypeptide and are closely related to the extend of glycosylation.

However, due to the distinct differences in heat stability values were observed in those glycoproteins, these results do not explain the molecular basis by which carbohydrate affects the glycoprotein properties. One possible way for the attached carbohydrate moieties to stabilize the protein conformation is to form hydrogen bonds with the polypeptide. Studies of the crystal structure of glucose oxidase (GO) by Hecht and co-workers have shown that the *N*-linked mannose residues form strong hydrogen

bonds with the backbone nitrogen and the carbonyl oxygen of glutamic acid [18]. In addition, carbohydrate moieties may stabilize protein conformation simply by steric interactions of the carbohydrate with the adjacent peptide residues [19, 20].

Other example of glycoprotein that has been extensively studied is the mammalian ribonucleases (RNases) which has been regulate many important biological functions by catalyzing the degradation of single- and double-stranded ribonucleic acids (RNAs). Bovine pancreatic RNase is a mixture of unglycosylated RNase A (M_w = 13,682) and a collection of glycoforms (designated RNase B Man-5,-6,-7,-8 and -9) in which the oligomannose series, Man-5 to Man-9, is associated with the single N-glycosylation site at Asn34LeuSer. Various spectral properties (circular dichroism, optical rotatory disperson, and ultraviolet denaturation difference spectroscopy) of the glycosylated form, RNase B have been measured and were in good agreement with similar datas on the non-glycosylated form, RNase A. Other than that, the amino acid composition of RNase B is identical with that of RNase A and presumably the amino acid sequence of the two proteins is identical (ref). Previous studied of the 1D and 2D 1H NMR spectra of RNase A and the glycoforms of RNase B have showed no significant different too [21]. Previous studies by Dwek and co-workers have shown that the carbohydrate moieties that are attached on the protein were able to affect the enzymatic activity of the protein [19, 20]. The RNase A was more than three times as active as the glycosylated form, RNase B. The different size of the carbohydrate moiety attached to the protein may also affect the enzymatic activity.

In addition studies on the glucose oxidase (GO) in protein catalysis have shown that carbohydrate moieties have an effect on the kinetic properties of GO. GO catalyses

the oxidation of glucose to gluconolactone and the subsequent reduction of oxygen to hydrogen peroxide according to a ping-pong steady-state kinetic mechanism [22, 23]. Three glycoforms of GO, which vary in their degree of glycosylation have been characterized according to their molecular weight by Kohen and co-workers to investigate the kinetic properties of the enzyme, with the goal of determining the contribution of H-tunneling to the C-H bond cleavage step [22-24].

The properties of glucose and 2-deoxyglucose oxidation by GO have been investigated using both steady-state and pre-steady-state kinetic methods and have shown that 2-deoxyglucose is an ideal probe for their studies due to its sensitivity towards hydrogen transfer step [25, 26]. Focusing on 2-deoxyglucose to probe the chemical step, Kohen and co-workers measured the temperature dependence of competitive $H/^3H$ and $^2H/^3H$ kinetic isotope effects on the enthalpy of activation using [1-^{2}H]-2-deoxyglucose. Apparently, less glycosylation results in more tunneling and a lower enthalpy of activation. Interestingly, the crystal structure, kinetic analysis, and other studies suggest that the enzyme active site is not conformationally changed by the degree of glycosylation [18, 20, 27-31]

An alternative explanation for the effect of glycosylation on GO catalysis is through changes in protein dynamics. Recently, several works have reported that glycosylation can modify the dynamic stability and functional activity of an enzyme [20, 31]. In the latter studies, comparative X-ray crystallographic studies, circular dichroism (CD) and nuclear magnetic resonance (NMR) techniques, and NH-N^{2}H exchange data were used to demonstrate that the three-dimensional structure of RNase was unaffected by glycosylation whereas dynamic fluctuations were changed. In the studies of GO, the

enzyme activity was found to correlate with decreased glycosylation and protein rigidity which is due to the masses/sizes of the carbohydrate moieties attached on the surface of the protein. It was also shown that glycosylation had an effect on the isotopically sensitive hydrogen transfer step of the enzyme. This implied that protein dynamics may be involved in the transition state of the bond cleavage step.

In these experiments, two interesting questions arise: first, how glycosylation could modify protein dynamics; and second, how does such a change in protein dynamics affect tunneling in an enzymatic reaction?

A possible answer to the first question might lie in the relationship of surface changes to internal protein dynamics. Recent studies by Yedgar and co-workers provided direct evidence that viscosity decreases the specific volume and the adiabatic compressibility of the protein interior [32]. Based on the kinetics of tryptophan phosphorescence decay, Cioni and Strambini hypothesized that viscosity and hydrostatic pressure act similarly in decreasing internal free volume and increasing protein rigidity [33]. Studies by Rudd (1994) and Mer (1996) described a similar phenomenon where glycosylation decreased dynamic fluctuations throughout the molecule [20, 31]. It is possible that protein glycosylation leads to a change in solvation at the protein surface that resembles the effects of viscosity, and hydrostatic pressure.

As for the second question, many models connecting protein dynamics to its function have been described and reviewed [34-38]. Several investigators have simulated hydrogen transfer processes incorporating both protein dynamics and quantum-mechanical tunneling [39-42]. These models demonstrate that hydrogen tunneling in enzymatic systems may be mediated by thermal fluctuations, leading to a decrease in the

tunneling distance and disruption of the tunneling coherence with a concomitant localization of the particle to the product side. This process is also known as dissipative tunneling. From the studies of GO, there is evidence that the hydrogen transfer step in an enzyme-catalyzed reaction is modified by remote changes in glycosylation on the surface of the protein [24, 43].

As previously described, the native conformation of many proteins can be stabilized against thermal denaturation through glycosylation, however the mechanism of such stabilization is less clear [44-46]. The removal of carbohydrates from naturally glycosylated proteins through the use of glycosidases [47] or by mutagenesis of glycosylation sites [48, 49] can lead to decreased thermal stability of the protein. This is often accompanied by an increased tendency towards protein aggregation. Due to the heterogeneous nature of protein glycosylation both *in vivo* and *in vitro*, a comprehensive study if its effect on thermal stability has been elusive. However, studies of the stability of several unglycosylated proteins in the presence of high concentrations of saccharides such as glucose, sucrose, galactose and α,α-trehalose have led to the conclusion that these glycans stabilize the folded protein due to preferential binding of the native states [50-53]. Such observations suggest that glycosylation of natural proteins could establish a microenvironment that resembles that of unglycosylated proteins in solutions of high carbohydrate content.

Through these examples, we knew that at the cellular level, *N*- and *O*-glycans have been shown to contribute to a myriad of functions, including cell-adhesion events [54-57] during immune surveillance, inflammatory action, viral and bacterial infections [58]. There are other effects of glycosylation on protein such as participating in protein

folding [59], thermal stability [16], protection against proteolytic degradation [57, 60-63] and the protein catalytic activity [24, 43]. Glycoproteins usually exist as mixtures of various 'glycoforms' that differ in the structure of the oligosaccharides. In order to understand their function precisely, it is desired that glycoproteins are homogeneous and the oligosaccharide structure is well defined. Isolation of homogeneous glycoprotein is difficult; therefore various approaches to synthesise artificial glycoprotein have been developed [64]. These include modification of natural glycoproteins using glycosidases and/or glycosyltransferases [65], ligation of synthetic glycopeptides with expressed protein [66], and introducing synthetic sugar derivatives using a chemoselective ligation (*e.g.* coupling of a sugar bearing an haloacetamide group with a thiol of a free cysteine moiety) [67-71] (Scheme 1.1).

Recently, a full chemical synthesis of a large glycopeptide has been relatively successful [68, 72]. However the purity of the synthesized glycoproteins is paramount, and the yields of the product were low, and the synthesis was expensive. Therefore alternative methods are required to overcome these problems. The methodology of combination of the introduction of unique cysteine residues at required sites and a highly flexible but selective chemical derivatisation strategy allowed us to systematically study the effect of site-specific glycosylation on the thermal stability and catalytic activity of the naturally nonglycosylated enzyme, dihydrofolate reductase (DHFR).

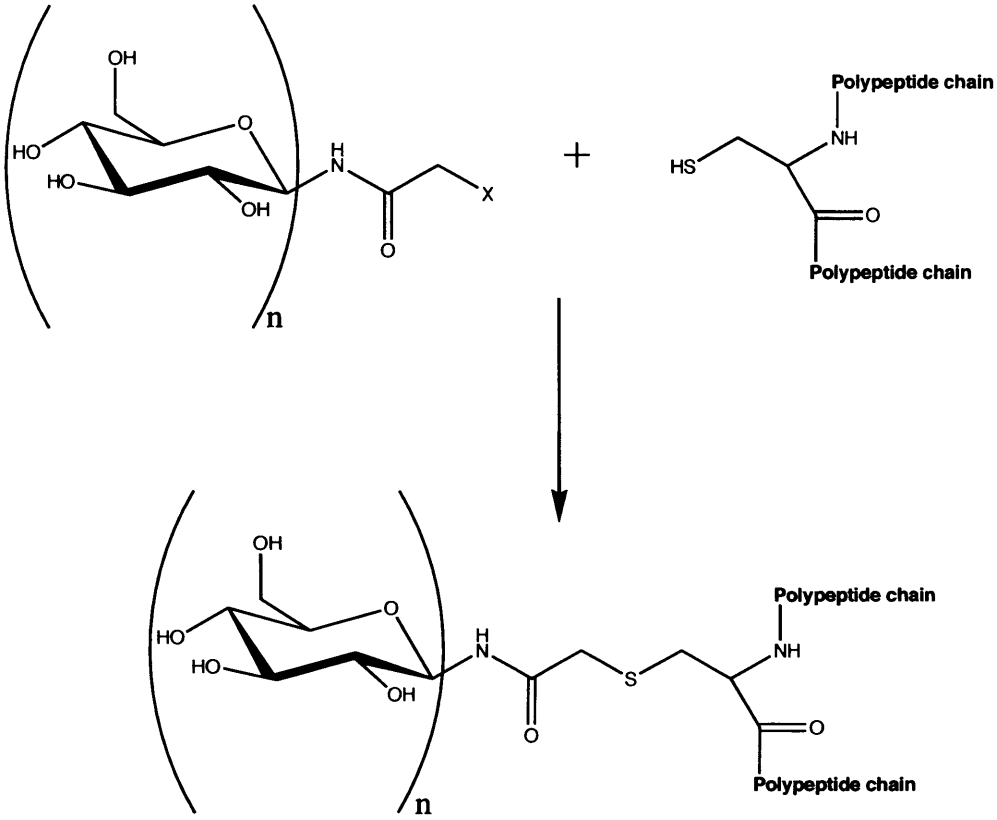

Scheme 1.1: *Chemoselective ligatiom of a glycosyl haloacetamide (X=Cl, Br, or I) with the thiol of a cysteine residue [67].*

1.6 Overview of dihydrofolate reductase (DHFR)

Dihydrofolate reductase (DHFR) is a ubiquitous enzyme which catalyses the reduction of 7,8-dihydrofolate (H_2F) to 5,6,7,8-tetrahydrofolate (H_4F) using nicotinamide adenine dinucleotide phosphate (NADPH) as a cofactor (Figure 1.6; also see Scheme 1.2). The reaction occurs by stereospecific hydride transfer of the pro-R hydrogen of NADPH to the C6 atom of the pterin ring with concurrent protonation of N5 of the substrate [73-75] (Figure 1.6). Both H_2F and H_4F are reduced derivatives of folate (folic acid). In many organisms, DHFR is also capable of catalyzing the reduction of folate to H_2F, although less efficiently [76]. H_2F is composed of a pterin ring linked *via* the 6-methyl group to a *para*-aminobenzoic acid moiety which is connected to one or several glutamate (Glu) residues through its α-amino group. The *para*-aminobenzoic *acid* and the glutamate

groups of the molecule are often referred to as the *para*-aminobenzoylglutamate (*p*ABG) portion (Scheme 1.2). DHFR plays a central role in maintenance of the intracellular pool of H_4F in prokaryotes and eukaryotes, which is essential for the biosynthesis of thymidylate, purines, several amino acids (*e.g.* serine), and hence for cell growth and proliferation [75, 77, 78].

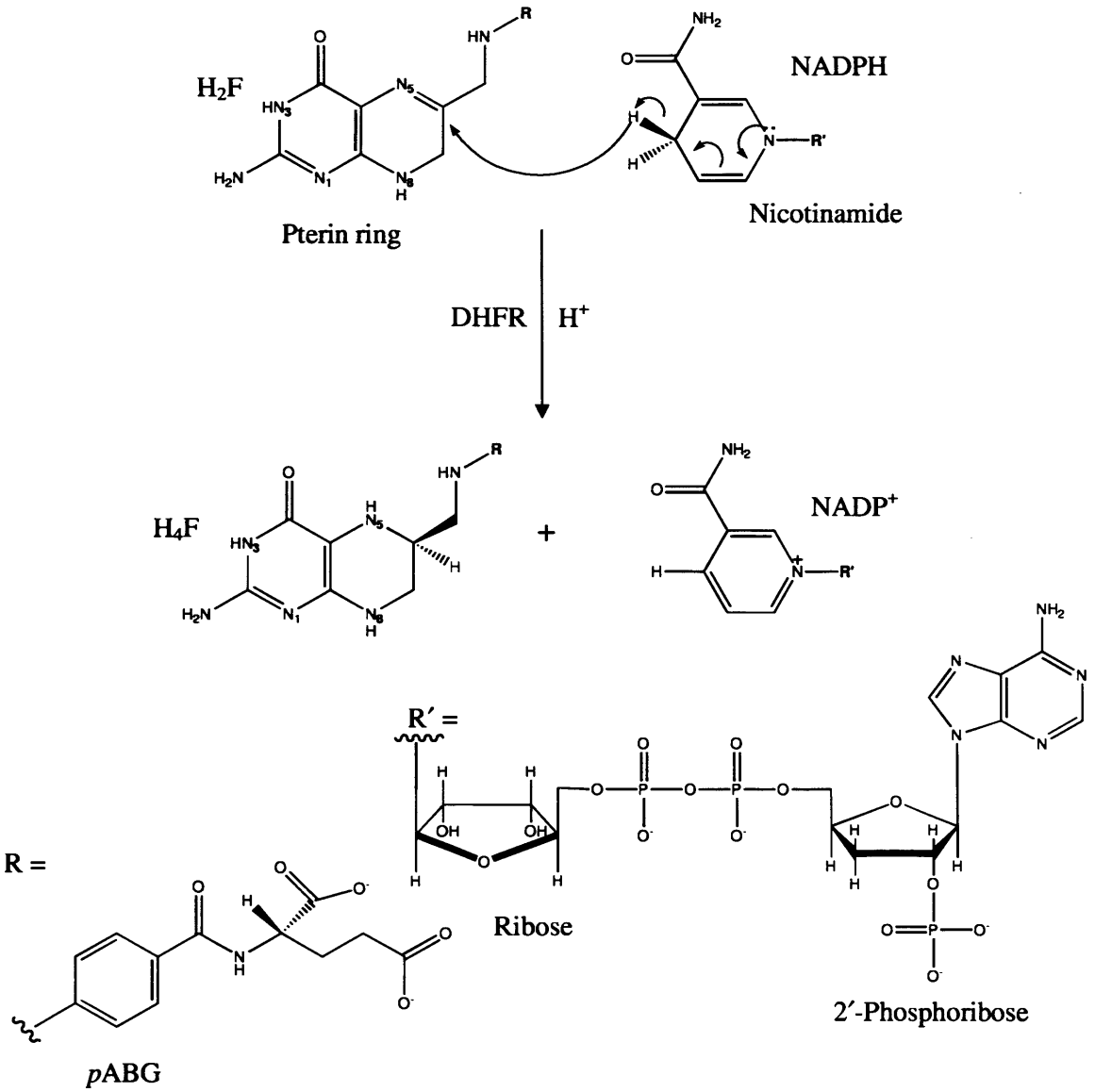

Scheme 1.2: *The reaction catalysed by DHFR and the structure of cofactor (NADPH) and substrate (H_2F).*

DHFR is the sole source of H_4F, and its low molecular weight (M_w ~18,000) coupled with a lack of disulfide bonds or metal ion requirements, makes it an ideal subject for kinetic measurements, X-ray crystallography, NMR spectroscopy, and site-directed mutagenesis studies [79-82]. DHFR is an important target for several anticancer and antibacterial drugs such as methotrexate (MTX), trimethoprim (TMP) and pyrimethamine (PMA), which act by inhibiting the enzyme in malignant cells (Figure 1.6). Trimethoprim, for example, binds to bacterial DHFRs 10^5 times tighter than it does to vertebrate DHFRs, [83] and the antimalarial agent pyrimethamine targets DHFR from *Plasmodium falciparum* [84]. The inhibition effects of MTX towards DHFR [79], have been demonstrated by Futterman [79, 85] and similar observation had been dicovered by Zakzewski and Nichol [79, 86]. After more than 40 years of studies, MTX remains one of the most potent chemotherapeutics in the treatment of leukaemia and lymphoma. DHFR is also the likely target in the treatment of rheumatoid arthritis by MTX.

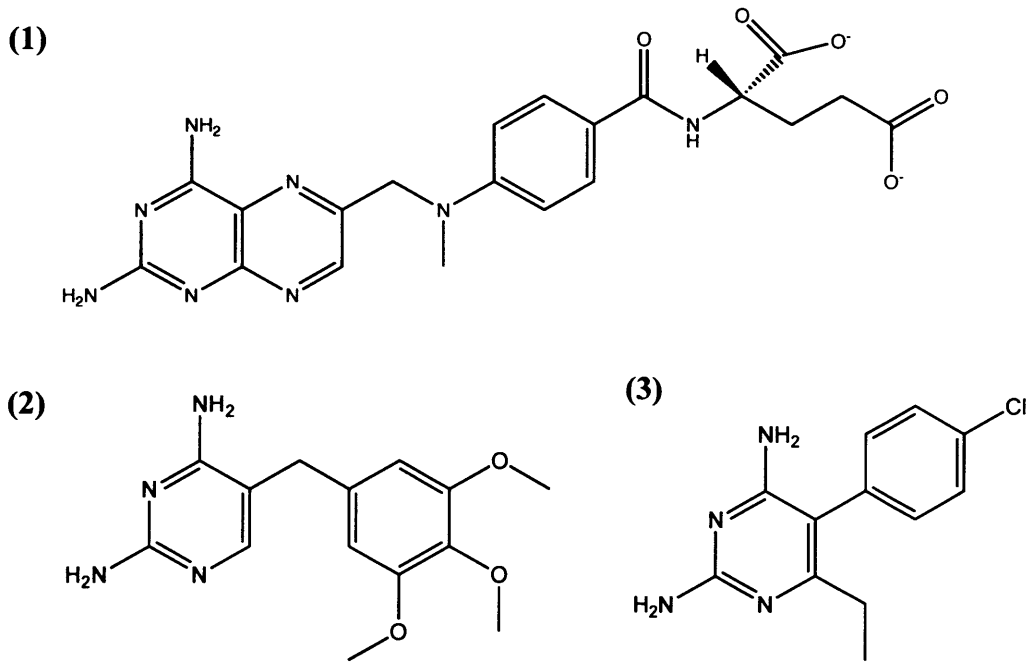

Figure 1.6: *Inhibitors of the reaction catalysed by DHFR. (1) is methotrexate (MTX), (2) is trimethoprim (TMP) and (3) is pyrimethamine (PMA).*

1.7 The importance of folic acid or folate

Folic acid or folate is a water-soluble B vitamin and occurs naturally in food and can also be taken as supplement. Folate gets its name from the Latin word *folium* meaning leaf, and it tends to be used as a general term referring to all forms of folate (*i.e.* H_2F, H_4F and their methylated forms). Leafy vegetables such as spinach, turnip greens, fortified cereal products, and certain other fruits and vegetables are discovered to be rich sources of folate.

A key observation by researcher Lucy Wills in 1931 led to the identification of folate as the nutrient needed to prevent anaemia during pregnancy. Dr. Wills demonstrated that anaemia could be reversed with brewer's yeast. Folate was identified as the corrective substance in brewer's yeast in the late 1930s and was extracted from spinach leaves in 1941. It was synthesized in 1964 by Yellapragada Subbarao.

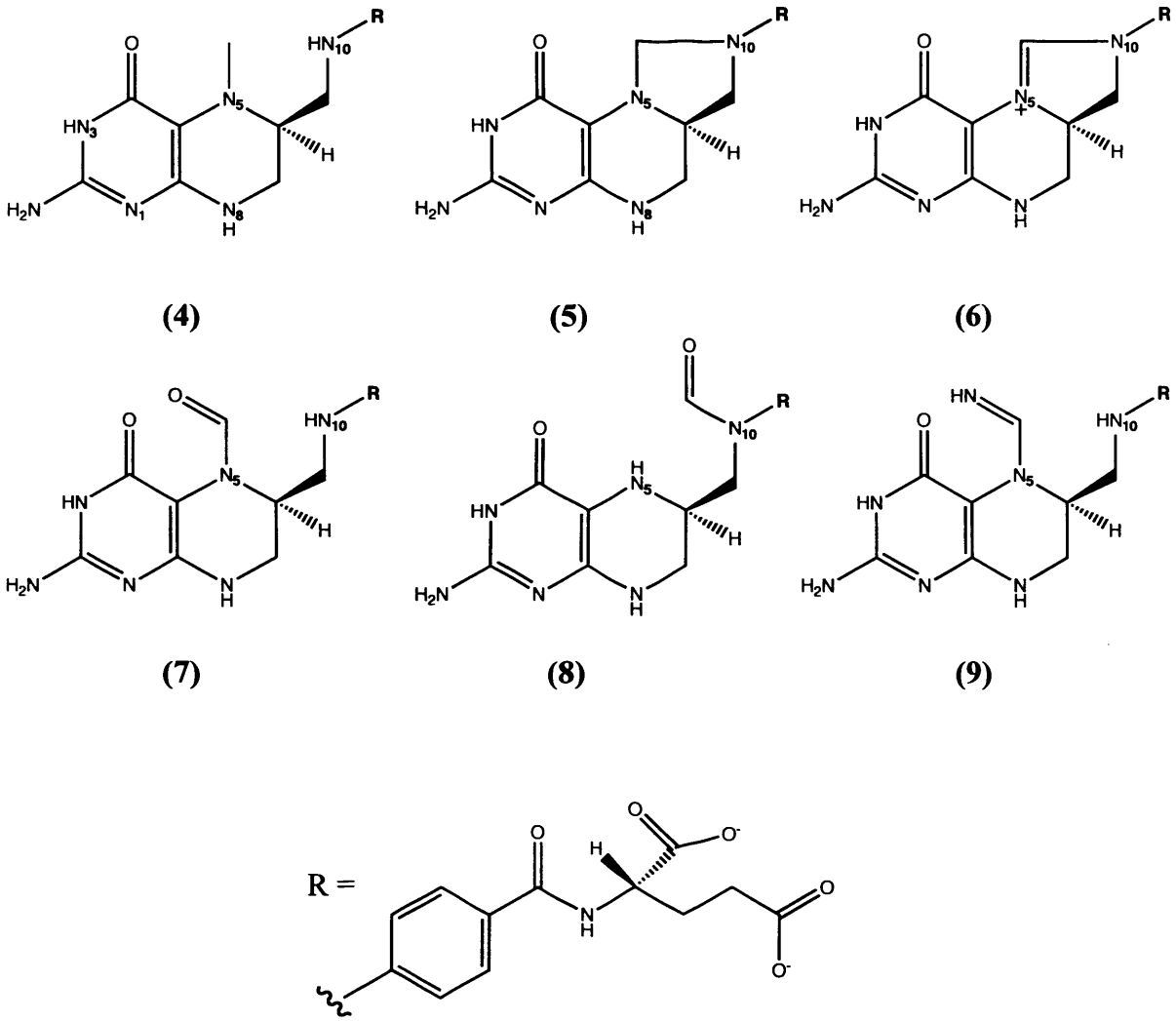

Figure 1.7: *Structures of one carbon unit carriers, derived from H_4F: N^5-methyl- H_4F (4), $N^{5,10}$-methylene- H_4F (5), $N^{5,10}$-methenyl- H_4F (6), N^5-formyl- H_4F (7), N^{10}-formyl- H_4F (8), and N^5-formimino- H_4F (9).*

Folate is necessary for the production and maintenance of new cells [87] especially during periods of rapid cell division and growth such as infancy and pregnancy. Folate is needed to replicate DNA, this is because H_4F, is a precursor of cofactors required for the production of purines, pyrimidines, and several amino acids [88].

H_4F is a carrier of one-carbon units, such as methyl ($-CH_3$), methylene ($-CH_2-$), methenyl (-CH=), formyl (-CHO) and formimino (-CH=NH) groups. These are carried by

H_4F bound to its N5 and N10 nitrogen atom (denoted as N^5 and N^{10}) (Figure 1.7). These folate derivatives are interconvertible and serve as substrates in a number of single-electron-transfer reactions. N^5-Methyl-tetrahydrofolate is known to be the source of the terminal methyl group of the amino acid methionine. $N^{5,10}$-Methylene-tetrahydrofolate is required by thymidylate synthase as a methyl group donor for the synthesis of dTMP (2'-deoxythymidine-5'-phosphate) from dUMP (2'-deoxyuridine-5'-phosphate) (Scheme 1.3) [88, 89].

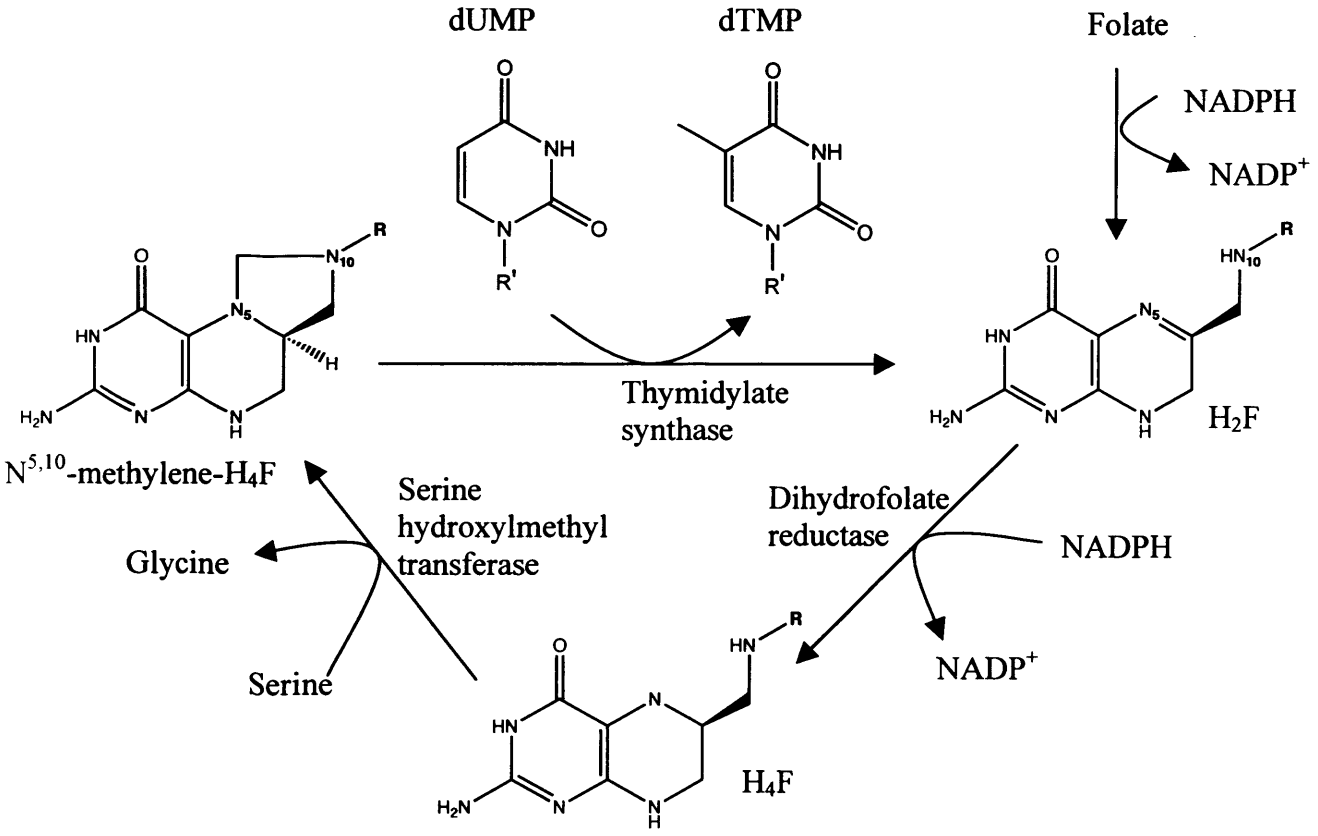

Scheme 1.3: *Schematic of the biosynthesis of dTMP from dUMP involving DHFR.*

1.8 Kinetic mechanism of DHFR

As a result of the biological and pharmacological importance of DHFR, this enzyme has been the subject of intensive kinetic and structural investigations for many years. For the past decades, several sources of DHFR have been investigated for the reaction mechanism. Most recent advances include the elucidation of a full kinetic pathway for DHFRs from *E. coli* (EcDHFR) [74], *Lactobacillus casei* (LcDHFR) [74], *Pneumocystis carinii [90]*, mouse [91] and human [92].

The complex catalytic cycle for EcDHFR has been reported by Benkovic and co-workers (Scheme 1.4) [74]. Under steady-state turnover conditions, with physiological concentrations of substrate and cofactor, the catalytic cycle is composed of five kinetically observable intermediates, dominated by a rapid hydride transfer from NADPH to H_2F and a slow release of the H_4F from the ternary product complex NADPH:DHFR:H_4F [74].

An important aspect for this cycle is that the chemical step of hydride transfer is not followed immediately by the release of the product. Following hydride transfer, the product (H_4F) is released only after the release of oxidised co-factor ($NADP^+$) and subsequent rebinding of NADPH into the active site. This step is also known as the rate-determining step (12.5 sec^{-1}). Thus, free enzyme will not be generated under physiological conditions, remaining primed for the next round of catalysis. The coordination of the ligand binding and release is maintained by a synergistic interaction between the substrate and co-factor binding site, in which the off-rates of oxidised cofactor ($NADP^+$) are elevated in the presence of bound product, and the off-rates of the product is elevated in the presence of reduced cofactor (NADPH). The chemical step is

associated with a pK_a of 6.5 and becomes the rate-determining step above pH 9 [93].

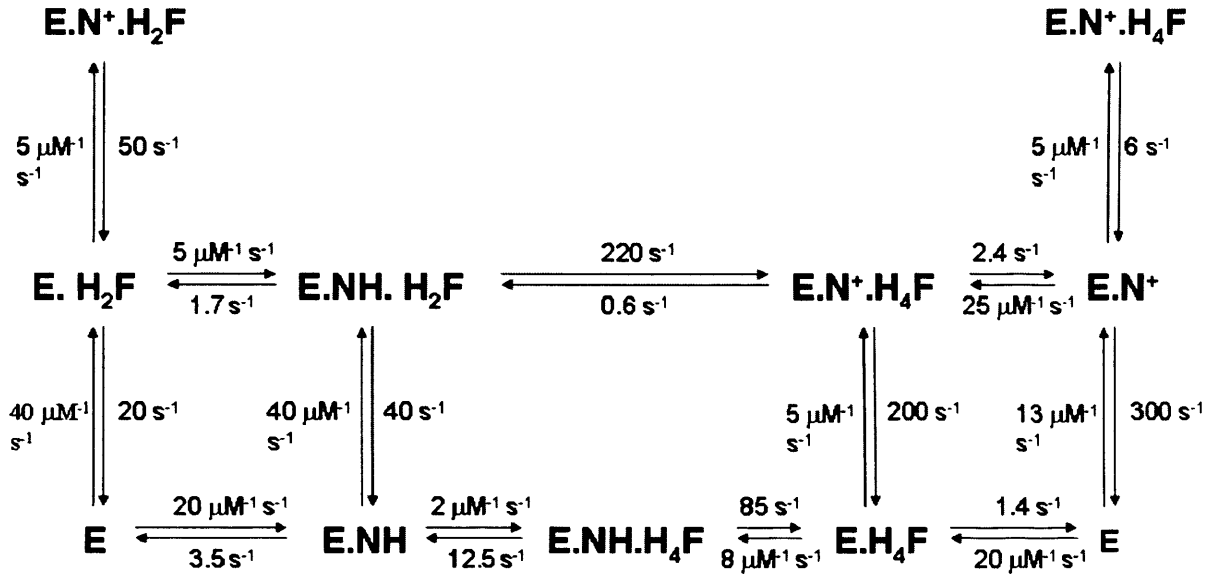

Scheme 1.4: *The catalytic cycle of EcDHFR. It shows the five primary imtermediates and the rate constant for DHFR catalysis pathway at pH 7 (2, 26). E = Enzyme, NH = NADPH, N^+ = $NADP^+$, H_2F = Dihydrofolate, and H_4F = Tetrahydrofolate.*

There are two different proposed mechanisms that explain the pH dependence of the hydride transfer reaction at the active site of EcDHFR. In both mechanisms the protonation of N5 atom of H_2F is very important for the rate of hydride transfer. In the first mechanism, Asp27 has been shown to play a major role as a proton acceptor. From the studied of crystallography [94], Raman spectroscopy [95] and computational analyses [96, 97] support a keto-enol tautomerization of the pterin substrate. The enol form is stabilized as a consequence of the expulsion of most of the water molecules on substrate binding leading to a significantly reduced dielectric environment and an increased pKa of N5 atom, thereby making its protonation feasible [93, 98]. An alternative mechanism suggests that the N5 atom is protonated directly by the solvent, recently receiving support from Molecular Dynamics (MD) calculations [99].

1.9 Structure of DHFR

The biological importance of DHFR in many biosynthetic pathways has prompted numerous structural studies. The first crystal structure of a DHFR enzyme was published 26 years ago from *E. coli* [100]. Since then, structural models based on X-ray crystallographic data have been constructed for the DHFR enzymes from *Lactobacillus casei* [100], chicken [101], human [102], mouse [103], *Pneumocystis carinii* [104] and *Leishmania maior [105].* However, the most extensive structural characterisation has been done on EcDHFR, including different substrate, inhibitor and cofactor complexes (for an extensive list of DHFR structures see [99] and references therein.

DHFRs are relatively small monomeric enzymes with molecular weights (M_w) normally ranging from 18,000 - 25,000. EcDHFR contains 159 amino acid residues and its molecular structure consists of a central eight-stranded beta-sheet (composed of β-strands A-H) and four flanking α-helices (designated as α_B, α_C, α_E, and α_F) (Figure 1.8) [106]. The active site cleft divides the protein into two structural domains: the adenosine binding domain (residues 38-88, ABD) and the major domain. The adenosine binding domain is the smaller of the two domains and provides the binding site for the adenosine moiety of the cofactor. The major domain is dominated by three loops [Met20 (residues 9-24), F-G (residues 116-132), and G-H (residues 142-150)] on the ligand binding face, surrounding the active site. These loops make up approximately 40–50% of the major domain, hence it is sometimes called the loop domain. Met20 and F-G loops are also referred as loop 1 and loop 2. X-ray crystal structures and NMR studies show that upon the binding of the enzyme to various ligands, Lys38 and Val88 perform a hinge-bending

motion, allowing the adenosine binding domain to move relative close to the major domain resulting in closure of the active site cleft [107].

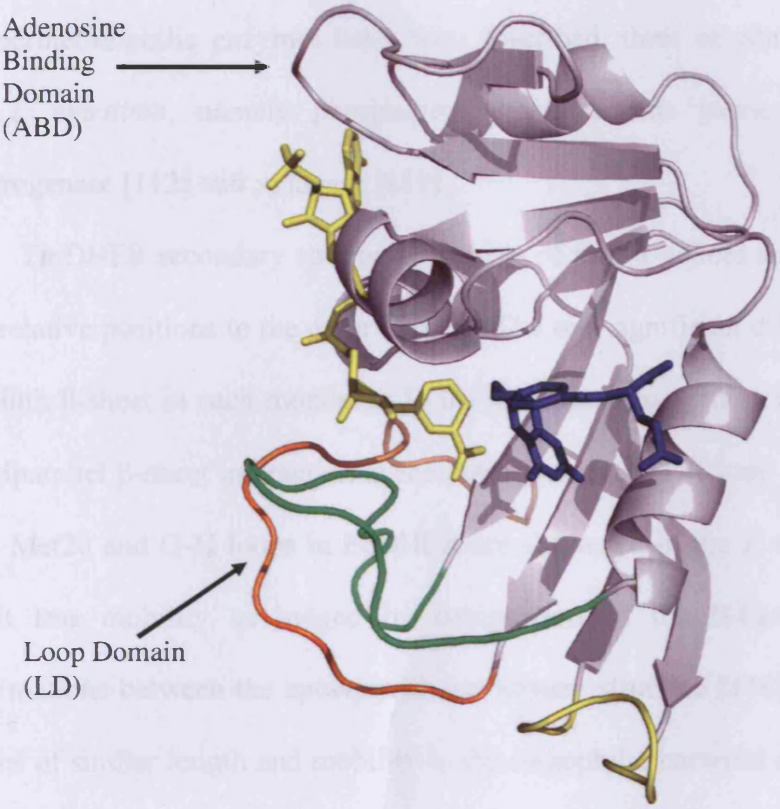

Figure 1.8: *Structural overview of EcDHFR. The major domain loops are indicated in green (Met20), orange (F-G), and yellow (G-H). The adenosine binding domain is red. Folate and NADP$^+$ are drawn in stick format and indicated in blue and yellow respectively in the ternary complex (1RA2). The structure is oriented so that the co-factor nicotinamide ring is in the plane of the paper [78, 108].*

Comparison of the various structures of DHFR from various species seems to adopt similar secondary and tertiary structural arrangements. The DHFR isolated from the hyperthermophilic bacterium *Thermotoga maritima* (TmDHFR) is the only hyperthermophilic DHFR isolated to date. Its X-ray crystal structure (Figure 1.9b) revealed similarity of the overall fold and tertiary structure with EcDHFR (Figure 1.9a).

TmDHFR has a size of approximate twice the size of the EcDHFR, because it is composed of two monomeric forms of EcDHFR. The dimeric form of TmDHFR most likely plays a central role in the thermostabilisation of the enzyme, as indicated by biophysical [109] and computational studies [110]. In the literature an increasing number of hyperthermophilic enzymes have been described, three of which have been isolated from *T. maritima*, namely phosphoribosyl anthranilate isomerase [111], glutamate dehydrogenase [112] and xylanase [113].

TmDHFR secondary structures consists of four α-helices and eight β-sheets in the same relative positions to the other DHFRs. The one significant difference is the addition of a ninth β-sheet in each monomer. In the dimer structure, these two extra strands form an antiparallel β-sheet interaction at the dimer interface. The loop regions corresponding to the Met20 and G-H loops in EcDHFR are shortened in the *T. maritima* structure and exhibit less mobility as judged by comparison of the B-factors of their relative conformations between the apoenzyme and ternary structure [110]. The CD loop region remains of similar length and mobility to the mesophilic bacterial enzymes, the F-G loop on the other hand is elongated in the *T. maritima* structure. However, the residues of the loop can be seen to be involved in the dimer interface and to be forming two inter-subunit salt bridges between lysine 129 from one subunit and two glutamate residues (136 and 138) from the other.

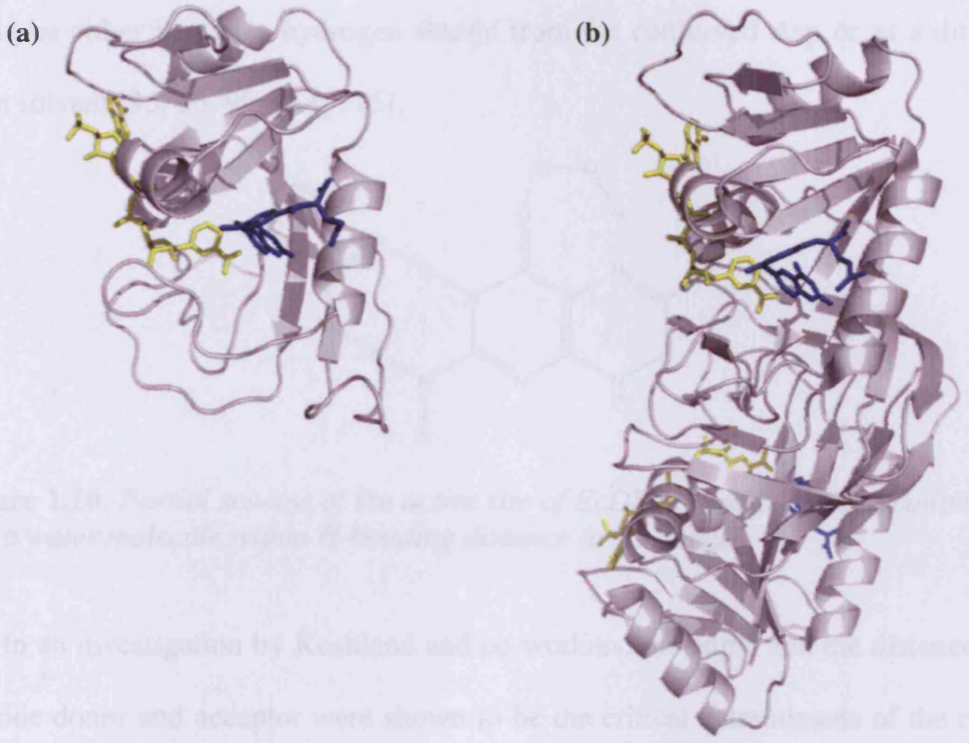

Figure 1.9: *Crystal structure of DHFR from E. coli (a) and T. maritima (b). MTX and $NADP^+$ are drawn in stick format and indicated in blue and yellow respectively in the ternary complex. The structure of EcDHFR and TmDHFR dimmer were taken from the PDB files 1RX3 and 1D1G, respectively [99, 110].*

1.10 The chemical step during the catalysis

As mention above, the DHFR-catalysed reduction of H_2F involves protonation of N5 of H_2F and hydride transfer from NADPH to C6 of H_2F. The source of the proton transferred to N5, by contrast to the source of the hydride, has been the major subject of debate. In EcDHFR, extensive crystallographic and nuclear magnetic resonance (NMR) studies of the apo-enzyme and various binary and ternary complexes have revealed the relative orientation of H_2F and NADPH in the active site. Through extensive investigation, the presence of the conserved ionisable amino acid residue Asp27 in the

active site and a water molecule within hydrogen bonding distance to N5 of H_2F are assumed to be mechanically important for the reaction (Figure 1.10) This water molecule could be either part of a hydrogen shuttle from the conserved Asp or as a direct donor from solvent [95, 96, 99, 114, 115].

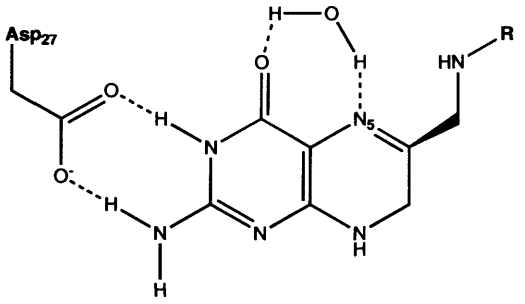

Figure 1.10: *Partial scheme of the active site of EcDHFR, indicate the location of Asp27 and a water molecule within H-bonding distance to N5 of H_2F.*

In an investigation by Koshland and co-workers, the angle and the distance between hydride donor and acceptor were shown to be the critical determinants of the rate of the hydride transfer [116]. From *ab initio* calculations the optimal C-C bond distance of the transferring and accepting carbons was determined to be 2.6 Å [117]. In the model of productive substrate binding [118] shown in Figure 1.12, Asp27 forms hydrogen bonds with Trp22, with Thr113, and with both the 2-amino and 3-amino groups of the pterin ring. Substitution of Asp27 with asparagine or serine generates a mutant form of EcDHFR that is 300 times slower and binds the substrate 20 times more weakly [93]. Thr113 hydrogen bonds indirectly to the pterin ring system through a fixed water molecule. Loss of the hydroxyl group, by substitution of Thr113 with valine, results in a 200 and 50 fold decrease in the affinity for H_2F and H_4F respectively [119]. The rate of the hydride transfer in the Thr113Val mutant enzyme decreases only six fold, which is consistent with the minor role for Thr113 in the proton transfer step.

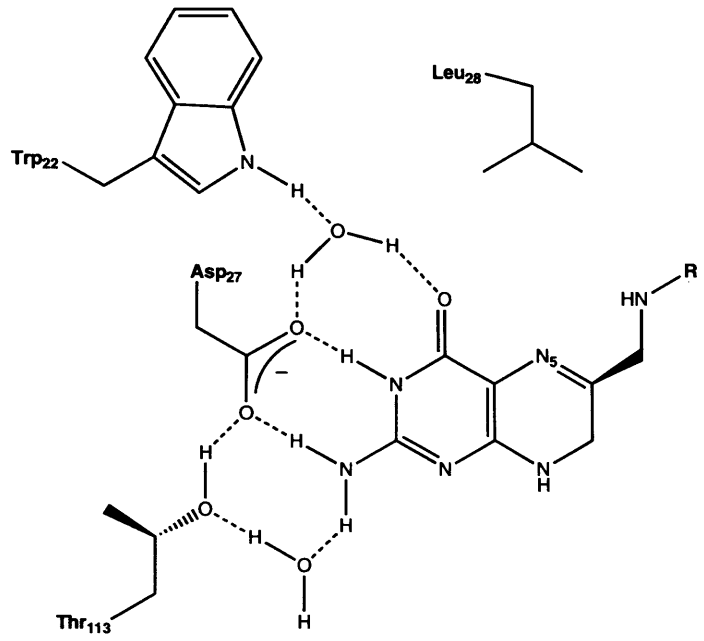

Figure 1.11: *The hydrogen bond network of the substrate in the active site, as derived from the crystal structure of the EcDHFR.NADP$^+$.H_2F ternary complex [118].*

Residue Trp22 coordinates the pterin ring system through hydrogen bonding with another fixed water molecule and it has been proposed that the hydrogen bonds formed by this residue are more important for binding substrate rather than for coordinating and orienting putative fixed water involved in the chemical step [120]. When Trp22 is substituted with phenylalanine, substrate affinity decreases six fold, but the hydride transfer rate decreases only three fold. The hydride transfer step for the EcDHFR catalysed reaction is *p*H dependent and the rate decreased with increasing *p*H showing an inversion point at *p*H 6.5. This apparent pK_a was attributed to Asp27 [121], since it is the only residue in the active site that seems to be able to protonate the substrate. Asp27 is more than 5 Å away from N5 of the pterin ring. The protonation of N5 was therefore proposed to occur by an indirect mechanism involving an adjacent water molecule, which

was stabilised in the active site by the enol tautomer of the substrate's pterin ring (Figure 1.11) [96].

The water molecule at the position site B (Figure 1.12) has only been observed in EcDHFR structures when the Met20 loop is in the open conformation, which is contrary to the proposal that such a water molecule may be involved in the reaction. An alternative mechanism has been suggested, in which protonation of the N5 atom of H_2F directly from solvent is responsible for the *p*H dependence [95]. This mechanism has received support from recent theoretical calculations by Brooks III and co-workers [115].

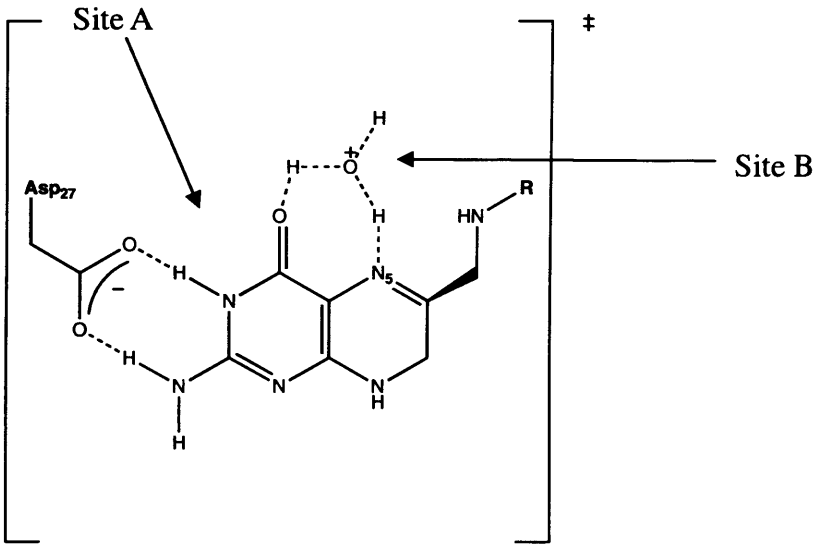

Figure 1.12: *The mechanism of the substrate protonation as proposed by Miller and Benkovic [98].*

1.11 Active site loop conformations

Within the active site, the substrate and cofactor bind in a hydrophobic cleft at the juncture of the two structural domains. In the ternary complex with $NADP^+$ and folate, the pterin ring (H_2F) and the nicotinamide ring (NADPH) bind in close proximity in the active site *via* van der Waals contact [118]. The Met20 loop lies directly over the active site protecting it from the solvent, and helps determine the active site's architecture. Part of the loop domains, which are the F-G and G-H loops, also play a stabilizing role of hydrogen bonding interactions with the Met20 loops.

Extensive X-ray studies of EcDHFR have provided evidence of how the enzyme changes its conformation to facilitate the reaction; it shows the Met20 loop appears in four characteristic conformations: occluded, closed, open, and disordered conformations (Figure 1.13) [108]. The occluded and closed conformations have also been observed in solution NMR experiments, and chemical shifts sensitive to the conformational change have been identified [115]. The open conformation has been observed only in certain crystal forms and seems to be stabilised by crystal lattice contacts [99, 115]. The Met20 loop is disordered in X-ray structures of the apo-enzyme and of the MTX complex. The electron density maps suggest that the disorder may result from the time-averaged fluctuations between the occluded and closed conformations [108].

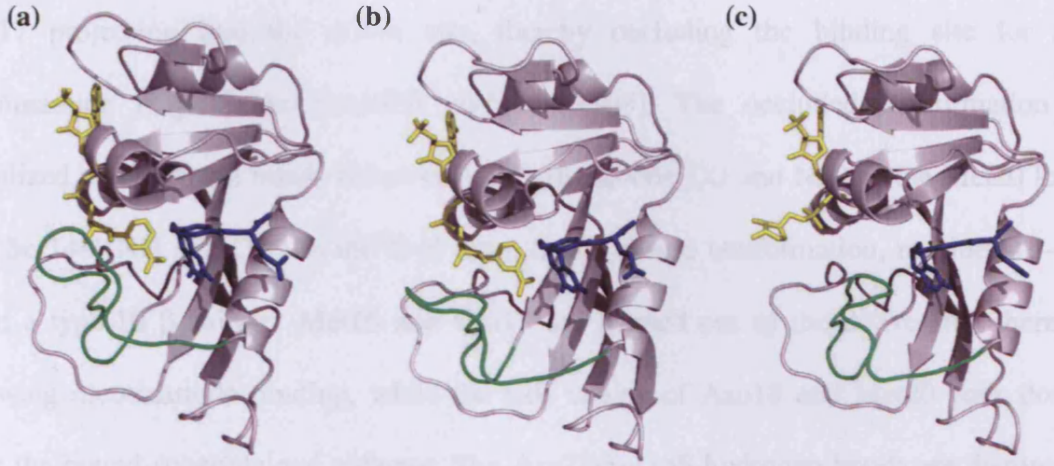

Figure 1.13: *X-ray structure of EcDHFR, showing the three conformations of the Met20 loop. The substrate and cofactor is showed in blue and yellow, respectively. The protein structure is showed in grey with the Met20 loop in green. The loop is closed over the active site in 1RX2 (a), open away in 1RA2 (b) and occluded into the nicotinamide binding site in 1RX6 [108].*

Changes in the conformation of the active site loops depend on the binding of ligands at the substrate and co-factor binding sites. If substrate is bound, the Met20 loop assumes the occluded loop conformation. Binding of the NADPH will lead to the formation of the closed conformation, in which the Met20 loop is closing the active site and protects it from solvent. Thus, loop movement is coordinated with the stages of the catalytic cycle. It is important to note that only the closed conformation allows positioning of the co-factor and substrate reactive centre in close proximity within the active site pocket, as observed, in the structures of the E:folate:$NADP^+$ and E:MTX:NADPH complexes, believed to be good models of the Michaelis complex and transition state, respectively [108].

The comparison between the occluded and closed conformations shows difference in structure in the central portion of the Met20 loop and in the pattern of hydrogen bonds

formed between the Met20 loop and the F-G and G-H loops (Figure 1.14). In the occluded state, the central region of the Met20 loop forms a 3_{10}-helix, with Met16 and Glu17 projecting into the active site, thereby occluding the binding site for the nicotinamide ring of the NADPH co-factor [108]. The occluded conformation is stabilized by hydrogen bonds between Asn23 (backbone CO and NH) in the Met20 loop and Ser148 (NH and Oγ) in the G-H loop. In the closed conformation, residues 16–19 form a type III'β-hairpin. Met16 and Glu17 are flipped out of the active site, thereby allowing nicotinamide binding, while the side chains of Asn18 and Met20 pack down over the bound substrate and cofactor. The Asn23/Ser148 hydrogen bonds are disrupted, and new hydrogen bonds are formed between the backbone NH and Oδ of Asp122 in the F-G loop and the backbone CO and NH of Gly15 and Glu17, respectively. The magnitude of the structural rearrangement is large; the hydrogen bond donors and acceptors in the closed complex are more than 9 Å (Asp122 to Gly15) and 11 Å (Asp122 to Glu17) apart in the occluded conformation [78]. A NMR study by Osborne and co-workers monitored the chemical shifts of the characteristic interactions between the Met20 loop and the ligands and concluded that the open conformation is in fact an intermediate between the closed and occluded forms of the Met20 loop. When the Met20 loop is in the open conformation, it extends away from the reactants, allowing the nicotinamide-ribose portion of NADPH and the pterin ring of H_2F in or out of the active site.

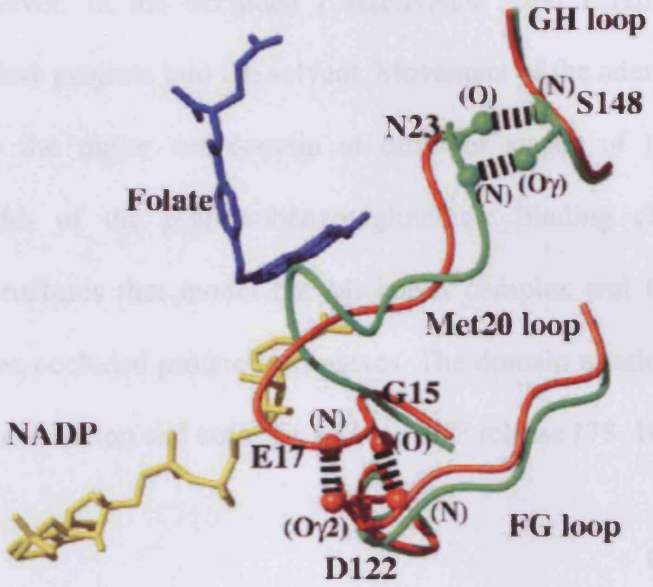

Figure 1.14: *Diagram of the Met20 loop and its integrations with the F-G loops in an overlay of the α-carbon traces for the closed (red) and occluded (green) conformations of EcDHFR. The positions of the folate and NADP$^+$ ligands in the ternary complex (1RX2) are shown in blue and yellow respectively [78].*

1.12 Loop and sub-domain movement during the catalytic cycle

A proposed detailed structural model for the conformational changes during the catalytic cycle was described by Sawaya & Kraut [99], based on the analysis of isomorphous crystal structures of *E. coli* DHFR complexes analogous to the five kinetic intermediates and to the transition state for hydride transfer, suggested that the Met20 loop is in the *closed conformation* in the holoenzyme, the Michaelis complex, and the transition state, but occludes the nicotinamide binding pocket in the three product complexes (Scheme 1.5).

In the Michaelis complex and transition state, the nicotinamide-ribose moiety occupies its binding pocket within the active site, in close proximity to the pterin ring of the substrate. However, in the occluded E:H_4F:$NADP^+$ and E:H_4F:NADPH product complexes, this moiety projects into the solvent. Movement of the adenosine binding sub-domain relative to the major sub-domain at different stages of the catalytic cycle modulates the width of the *p*-aminobenzoylglutamate binding cleft. This cleft is narrowest in the structures that model the Michaelis complex and transition state and becomes wider in the occluded product complexes. The domain rotations may play a role in transition state stabilization and cofactor-assisted H_4F release [78, 108].

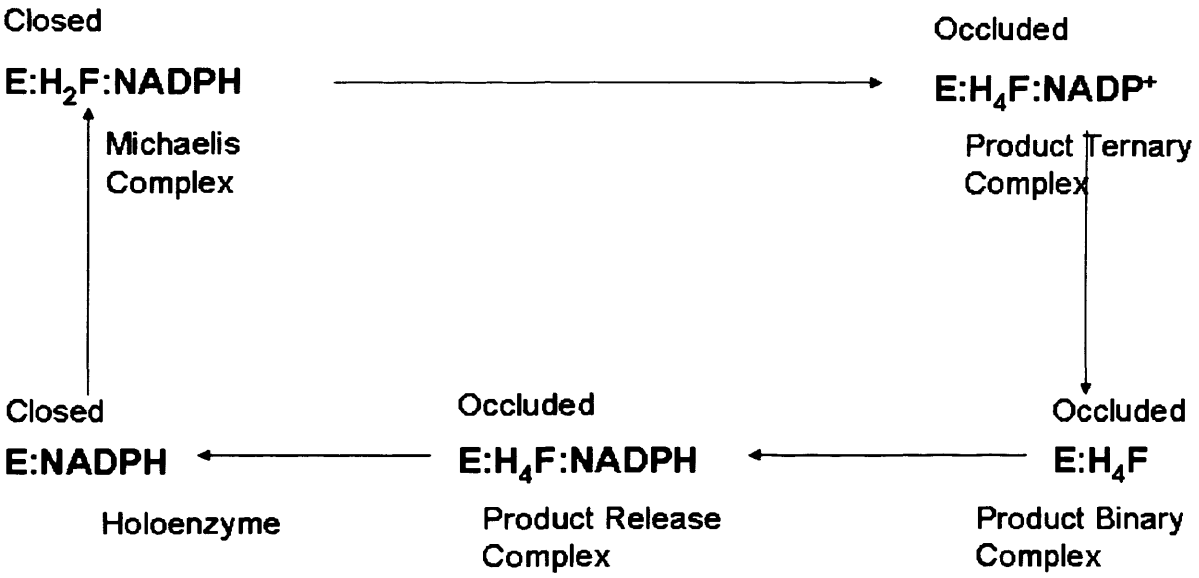

Scheme 1.5: *Schematic diagram indicating conformational changes in the active site loops through the catalytic cycle of DHFR.*

1.13 Loop dynamics

Given the important contacts made with substrate and cofactor and the compelling evidence for loop conformational changes during the catalytic cycle, much effort has been focused on the role of Met20 loop dynamics in ligand binding and catalysis. The existence of two isoforms of apo-EcDHFR (E1 and E2) was discovered by Dunn and King from their kinetic studies with trimethoprim (TMP) [122-124]. The second isomer was detected as a slow ligand-independent phase that followed an initial ligand-dependent burst phase in stopped-flow fluorescence kinetics. Interconversion between the isoforms occurs at a rate of 0.035 s^{-1} [125].

For the *E. coli* apo-enzyme, a second conformational equilibrium, faster than that between E1 and E2, is detectable by NMR spectroscopy within the Met20 loop. When magnetization transfer between the pair of resonances observed for the side chain imino proton of Trp22 was measured, the rate of fluctuations in the Met20 loop was estimated at ~35 s^{-1} [114]. This rate is comparable to the rate of product dissociation (12 s^{-1}) from the E:THF:NADPH ternary complex [74]. Conformational exchange on a similar timescale was also observed for the Met20 loop in the MTX [126] and folate [127] binary complexes.

The existence of slowly interconverting conformational states in DHFR from several sources has been demonstrated by NMR spectroscopy [127-129]{references within [78]}. Because the chemical shift is a highly sensitive probe of structure, a single spin giving rise to multiple peaks in an NMR spectrum is indicative of a conformational process that is slow on the NMR chemical shift timescale. Although a direct link is difficult to establish, the conformational exchange that gives rise to splitting of

resonances occurs on a slow timescale and is likely related to interconversion of the E1 and E2 isoforms that were identified from the biphasic substrate and cofactor binding kinetics. As in the case of the E1/E2 interconversion, binding of folate or NADPH to the apoenzyme appears to stabilize a single conformer, resulting in a single set of resonances in the NMR spectrum.

In a mutagenesis study, substitution of the central portion of the Met20 loop (residues 16–19) with a single glycine residue slows hydride transfer by more than 500-fold without significantly affecting the Michaelis constants (K_M) for substrate (H_2F) or cofactor (NADPH) [130]. Coincidentally, the mutation results in a single set of NMR peaks and disappearance of the slow ligand-independent phase observed in fluorescence quenching experiments. On the basis of these observations, Met20 loop movement may be a limiting factor in substrate turnover [114].

Recent studies by Benkovic and co-workers at the central portion of the Met20 loop for determine the relationship between the dynamic of the loop with the catalytic reaction of the DHFR by substituting with a single cysteine residue at the position 18 of the loop and the results showed not much affects in kinetic measurements. However when they acylated that site with a large hydrophobic fluorophore, ALEXA 488 there is a significant difference in kinetic activity and affinity for binding with NADPH (K_D) [126].

Although NMR experiments on the folate binary complex of *E. coli* DHFR failed to reveal any resonance splitting [131, 132], evidence for an equilibrium between two conformational substates has recently come from high-pressure $^{15}N/^{1}H$ 2D NMR studies in the pressure range between 30 and 2000 bar [127, 133, 134]. Upon increasing the pressure to 2000 bar, several resonances in the spectrum of the folate complex split or

broaden, revealing a second conformational state whose population is strongly temperature dependent. The second conformer appears to be more open and more hydrated than the first, and Akasaka and coworkers [127] proposed that it might represent an open conformation of the Met20 loop comparable to that observed in X-ray structures. The population of the secondary conformer is estimated to be 10% at 1 bar and 15 °C, and it lies about 5 kJ/mol in energy above the occluded ground state conformer. Its low, temperature-dependent population probably explains why it was not observed in NMR experiments at normal pressure.

Kraut and co-workers measured fluorescence decay for 13 EcDHFR mutants with slower rates of catalysis [135]. Excluding mutations at the critical Asp27, they found a striking correlation between dynamically quenched fluorescence and the rate of hydride transfer in the NADPH holoenzyme. From the loss of electron density in X-ray structures of the wild-type enzyme, they postulated that motions in the Met20 loop and the nicotinamide ring are primarily responsible for fluorescence quenching.

There has thus been a lot of evidence showing flexibility of the Met20 loop on a timescale (~2–40 s^{-1}) relevant to processes of substrate and cofactor binding and product release. This may also contribute to catalysis through active site compression and stabilisation of the transition state [96]. In the closed conformation inferred for the Michaelis complex and the transition state, the side chain of Met20 is directed towards the active site and packs against the nicotinamide and pterin rings by shielding the active site from solvent, generating a low dielectric and raising the *p*Ka of the putative proton-donating aspartate residue [96].

1.14 Changes in protein flexibility during the catalytic cycle

Variations in crystallographic temperature factors (B-factors) for EcDHFR suggested that the amplitude of motions varies along the polypeptide chain, as well as between different liganded complexes of the enzyme [99, 107, 118]. The variation between structures was largely in the Met20 and F-G loops, which exhibited low B-factors (suggesting little motion) in the closed complexes and higher B-factors (implying more motion) in the occluded complexes. In the extreme case, the Met20 loop in the apo-enzyme had no observable electron density (indicating that it is completely disordered). Thus, it was suggested that loop flexibility, as well as structure, depends on ligand binding and therefore varies during the catalytic cycle [99].

B-factors reflect only amplitudes of motion, not timescales, and cannot discriminate time-dependent motions from static disorder. A more detailed picture of protein dynamics at the level of individual residues is obtained using solution NMR spin-relaxation methods. Insights into molecular motions that occur on timescales faster than the overall tumbling of the macromolecule can be derived from the longitudinal (R_1) and transverse (R_2) nuclear spin-relaxation rates, and the [H]-^{15}N heteronuclear NOE. The relaxation data are commonly treated using the Lipari-Szabo model-free analysis [136, 137].

NMR studies provided a dynamic description of the structural elements of EcDHFR. The first comprehensive NMR study of dynamics in EcDHFR focused on the amide backbone and tryptophan side chain motions of the folate binary complex [131]. A full model-free analysis of the longitudinal (R_1) and transverse (R_2) nuclear spin-relaxation rates, and [H]-^{15}N heteronuclear NOE values gave a highly detailed view of

the magnitude and timescale of motions in DHFR [138]. The study identified several regions with below-average S_2 order parameters, indicative of large-amplitude motions on the picosecond-nanosecond timescale that are independent of the molecular tumbling. These included the hinge residues Lys38 and Val88, residues Gly67 and Asp69 in the adenosine binding loop, and several residues in the Met20 loop and the F-G loop. The decreased order parameters for residues in these regions are associated with internal correlation times on the order of 1–2 nanoseconds, significantly shorter than the overall rotational correlation time of the molecule, around 9 ns [138].

NMR measurements were extended to complexes that model intermediates in the catalytic cycle [138]. The ternary complex with folate and 5,6-dihydroNADPH (E:folate:DHNADPH) assumes an occluded loop conformation in which the adenosine ring of the cofactor is bound, but the nicotinamide ring is flipped out from the active site pocket into the solvent [108, 138]; this complex is a model for both the ternary product complex (E:H_4F:$NADP^+$) and the product release complex (E:H_4F:NADPH). In the ternary complex with folate and $NADP^+$ (E:folate: $NADP^+$), the Met20 loop is in the closed conformation and both the substrate pterin ring and the cofactor nicotinamide ring are inserted into the active site pocket; this complex is a model for the Michaelis complex formed during the catalytic cycle [99]. Finally, the folate binary complex was used as a model for the H_4F product binary complex [138]. A details of the studies has been reviewed in the paper published by Osborne MJ, Wright PE and co-workers [78].

1.15 Dynamics of protein

The rate enhancement exhibited by enzyme catalysed reactions is not fully understood. It is commonly accepted that the observed rate enhancement occurs mainly through transition state stabilisation. However, the contribution of protein dynamics has been shown to have a major role [78]. Numerous mutations have been introduced into EcDHFR to probe the role in catalysis of flexibility and conformational change in the Met20 and distal loops. The role of the hydrogen bonding networks formed between the Met20 and F-G loops and the Met20 and G-H loops in the closed and occluded conformers, respectively, has been investigated by Benkovic and co-workers [70, 75, 126].

As describe above, mutation of Gly121 to valine (G121V) results in a 40-fold decrease in NADPH binding affinity and a striking 200-fold decrease in the hydride transfer rate [75]. Furthermore, the G121V mutation introduces a new step into the catalytic cycle that reflects a slow (3.5 s^{-1}) conformational change prior to hydride transfer. This step has been interpreted as the exchange of the nicotinamide ring of the NADPH into the active site to form the reactive Michaelis complex. Deletion of Gly121 has shown similar effects on the kinetics [139]. This is rather surprising, since mutations far from the active site are expected to cause only slight alterations in the active site geometry by communicating structural changes through intervening residues. However, if protein fluctuations are involved in catalysis, mutations far from the active site could affect the catalytic rates by simply changing the global dynamic of the protein.

In order to support this theory, Rajagopalan *et al.* measured the rate for the forward and reverse hydride transfer step for the M42F, M42W, G121A, G121S and the four possible double mutant combinations [140]. They observed that while all the single mutations severely reduced the hydride transfer rate, the double mutation displayed non-additive effects (*i.e.*, the effect of double mutation is greater than the effect of the single mutation). This suggested a coupling of the F-G loop to distant regions of the enzyme. It is important, however to mention that recent experimental evidence seems to lead to different conclusions. Swanwick *et al.* used CD spectroscopy and stopped flow fluorescence refolding from the urea-denatured state to investigate the structure of the G121V mutant. In this study, G121V appears to be trapped in a highly fluorescent state; suggesting that the reduced catalytic activity of G121V is the consequence of non-local effects on the structure of the enzyme [77].

Earlier studies by Brooks and coworkers, using MD simulations, suggest that distant residues are coupled, exhibiting so called 'correlated motions' and these studies attempt to understand the effect of distal mutation on the chemical transformation step *via* thermodynamic factors [115]. It also showed that mutants can perturb the active site structurally, even if it is distant from the active site, thus rationalizing the observation by Benkovic and coworkers that distal mutation does affect the rate [75].

A portion of the network of coupled promoting motions in DHFR between Met20 loop and βF-βG loop is shown in Figure 1.15. When the H_2F substrate and NADPH co-factor are bound to the EcDHFR, the Met20 loop adopts the closed conformation, in which the Met20 loop is interacting strongly with NADPH. As mentioned above, the closed conformation is stabilized by H-bonding interactions with the βF-βG loop (residue

117-131). Specifically, the amide backbone of both Ile14 and Gly15 in the Met20 loop will form hydrogen bonds with Asp122 and Thr123in the βF-βG loop. These hydrogen bonds are not present in occluded and open conformation of the Met20 loop. Thus, a pre-organised structure that juxtaposes the substrate and coenzyme in an orientation conductive to reaction is been provided by the closed conformation [141].

Hybrid quantum/classical molecular dynamics (MD) simulations for the G121V mutant indicate that this is due to an increase in the free-energy barrier and suggest that the mutation may disrupt the network of coupled transition state promoting motions [142]. Therefore, we observe a dramatic decrease in the hydride transfer rate for the mutant EcDHFR [75]. This interpretation has however recently been questioned by two recent independent MD simulations for wild-type (WT) and mutant forms of EcDHFR [77, 143], suggesting that non-additivity in the kinetic effect of double mutants at these sites might have in origin on long range structural perturbation.

Previous studies on the Met20 loop by Benkovic and co-workers have shown that when a large hydrophobic compound (*i.e.* Alexa 488) was attached at position 18, there was an effect in the DHFR enzymatic reactivity [126]. However, the structure of the protein is similar to the wild-type protein. The attachment of the hydrophobic molecule seems have affected the dynamic of the protein, which led to the decrease of the enzymatic activity of the protein. A similar observation has been observed in the mammalian RNases and GO, where attachment of different carbohydrate moieties was able to affect their enzymatic activity but not their structures.

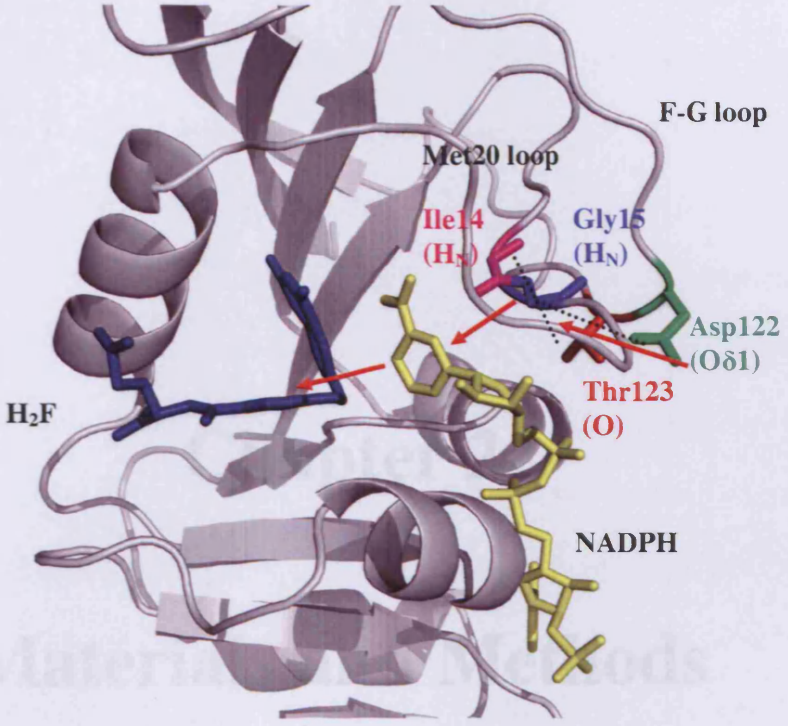

Figure 1.15: A *portion of the network of coupled promoting motions in DHFR, which proposed by Agrawal et al. [141]. The red arrows indicate the direction of promoting motion.*

Therefore, we have selected four different individual exposed sites for attachment of a carbohydrate moiety to study whether there is any effect on the protein stability and enzymatic reactivity. Four different types of carbohydrate moieties vary from monosaccharide to trisaccharides have been used in our experiments and the results of these studied will be discuss in following chapters.

Chapter 2

Materials and Methods

2.1 Materials

Oligonucleotide primers for site-directed mutagenesis were purchased from Alta Biosciences (University of Birmingham) and Operon Biotechnologies GmbH (Germany). *Pyrococcus furiosus* (*Pfu*) DNA Polymerase was purchased from Promega. DNA markers solution was from New England Biolabs (NEB). N,N'-methylene-bis-acrylamide and N,N,N',N'-tetramethylenediamide (TEMED), and AG® 501-X8 ion exchange resins were purchased from BIO-RAD. The DNA template of cysteine free EcDHFR (DM EcDHFR) DNA (C85A/C152S) was previously synthesized in our lab by Dr. Richard Swanwick and Dr. Masood Javeed The miniprep mutagenesis kit was obtained from Qiagen. *E. coli* BL21(DE3) cells were from Novagen. Micro size pore syringe filters were purchased from Millipore. Glycosyl iodoacetamides were contributed by Professor Sabine Flitsch (University of Manchester) and Dr. Nicola J. Davis. All other chemicals were purchased from Fluka, Sigma-Aldrich, Merck, Fisher or Melford, unless otherwise stated

.

2.2 Preparation of culture media

All media described in this chapter have been prepared according to Sanbrook *et al.* 1989 [144].

2.2.1 Luria Bertani (LB) medium

To prepare 1 litre (L) of media, the following were dissolved in 950 ml of deionised water;

10 g	Bacto-tryptone/peptone
10 g	NaCl
5 g	Yeast extract

The *p*H was adjusted to 7.5 with NaOH, the volume adjusted to 1 L, and sterilised in an autoclave at 121 °C, 15 lb.inch^{-2} for 20 minutes.

2.2.2 LB Ampicillin/Agar plates

For the preparation of agar plates 15 g of agar powder was added to 1 L of LB media prior to sterillisation. After cooling to ~55 °C, ampicillin was added to a concentration of 100 μg/ml *via* aseptic technique and the solution carefully mixed and poured into Petri dishes. After solidification, plates were stored inverted at 4 °C.

2.2.3 2xYT medium

To prepare 1 L of media, the following were dissolved in 950 ml of deionised water;

16 g	Bacto-tryptone
5 g	NaCl
10 g	Yeast extract

The *p*H was adjusted to 7.5 with NaOH, the volume adjusted to 1 L, and sterilised in an autoclaved at 121 °C, 15 lb.inch^{-2} for 20 minutes

2.3 The strains of *E. coli*

2.3.1 Expression strains

2.3.1.1 *E.coli* BL21(DE3)

The designation DE3 indicates that the strains contain the λDE3 lysogen that carries the gene for T7 RNA polymerase under control of the *lac*UV5 promoter. Isopropyl-β-D-thiogalactopyranoside (IPTG) is required to induce expression of T7 RNA polymerase.

2.3.1.2 *E. coli* BL21(DE3) pLysS

The pLysS plasmid produces T7 lysozyme, an inhibitor of T7 RNA polymerase which functions to lower the basal levels of recombinant protein which may be toxic to the cells or lower cell growth and viability prior to induction.

2.3.2 Cloning strains

The *E. coli* XL1-Blue strain was used for the preparation of high-quality plasmid DNA due to its ability to repair nicks in the transfected plasmid following site directed mutagenesis. These cells have high transformation efficiency and are supplied with the Quick-site directed mutagenesis kit.

2.4 Preparation of sterile solutions

2.4.1 Ampicillin solution (50 mg/ml)

Ampicillin sodium salt (100 mg) was dissolved in 2 ml sterile deionised water, filter sterilised using a 0.22 μm syringe filter, aliquoted and stored at -20 °C.

2.4.2 Chloramphenicol solution (34 mg/ml)

Chloramphenicol (34 mg) was dissolved in 1 ml ethanol (EtOH) and filter sterilised using a 0.22 μm syringe filter, aliquoted and stored at -20 °C.

2.4.3 Isopropyl-β-D-thiogalactopyranoside (IPTG) solution (0.2 g/ml)

IPTG (2 g) was dissolved in 10 ml sterile deionised water and filter sterilised using a 0.22 μm syringe filter, aliquoted and stored at -20 °C. IPTG working concentration for large scale expression was 0.12 mg/ml.

2.4.4 Competent Cell Buffer A

A 100 mM solution of calcium chloride ($CaCl_2$) was prepared in deionised water, sterilised in an autoclave at 121 °C, 15 $lb.inch^{-2}$ for 20 minutes and stored at 4 °C.

2.4.5 Competent Cell Buffer B

A solution of 100 mM $CaCl_2$/15 % glycerol was prepared in deionised water, sterilised in an autoclave at 121 °C, 15 $lb.inch^{-2}$ for 20 minutes and stored at 4 °C.

2.5 Preparation of non-sterile solutions

2.5.1 DNA Loading buffer (Agarose Gels)

The following reagents were added to 847.5 µl of deionised water;

2.5 µl	0.25% w/v Bromophenol blue
2.5 mg	Xylencyanol FF
150.0 µl	Glycerol

Solutes were fully dissolved and the solution, stored at room temperature (RT).

2.5.2 50x TAE electrophoresis buffer (Agarose Gels)

A solution of 50x TAE electrophoresis buffer was prepared as follows;

242.0 g	Tris Base
100.0 ml	EDTA (0.5 M, *p*H 8.0)
57.1 ml	Glacial acetic acid

Solutes were fully dissolved, the volume adjusted to 1 L with deionised water and stored at RT.

2.5.3 Ethidium Bromide solution (EtBr)

Ethidium bromide solution was prepared as follows. 10 mg of EtBr was dissolved in 1 ml of deionised water. Solutes were fully dissolved, the tube/sample wrapped with foil to prevent light exposure and stored at 4 °C.

2.5.4 MTEN buffer

The following solutes were dissolved in 150 ml deionised water to prepare the final concentration of each solute;

1.95 g	2-[N-morpholino]ethanesulfonic acid (MES) (50 mM)
0.66 g	Tris-base (25 mM)
0.30 ml	Diethanolamine (25 mM)
1.17 g	NaCl (100 mM)

The *p*H was adjusted to *p*H 7.0 with 1 M NaOH/HCl and the total volume taken to 200 ml with deionised water and stored at RT.

2.5.5 Phosphate buffer

Phosphate buffers at different *p*H values were prepared from 1 M stock solutions of potassium phosphate ($K_iH_iPO_4$, see table 2.1) and sodium phosphate ($Na_iH_iPO_4$, see table 2.2) buffers, and stored at RT. The total volume at the required *p*H was taken to 1 L with deionised water to prepare a working concentration of 100 mM phosphate buffer.

Table 2.1: *Proportions of K_2HPO_4 and KH_2PO_4 for the preparation of K_iPO_4 buffers at given pH.*

*p*H	Volume of 1 M K_2HPO_4 (ml)	Volume of 1 M KH_2PO_4 (ml)
6.0	13.2	86.8
6.4	27.8	72.2
6.8	49.7	50.3
7.0	61.5	38.5
7.2	71.7	28.3
7.4	80.2	19.8
7.6	86.6	13.4
7.8	90.8	9.2
8.0	94	6.0

Table 2.2: *Proportions of Na_2HPO_4 and NaH_2PO_4 for the preparation of buffers at given pH.*

*p*H	Volume of 1 M Na_2HPO_4 (ml)	Volume of 1 M NaH_2PO_4 (ml)
6.0	12.0	88.0
6.4	25.5	74.5
6.8	46.3	53.7
7.0	57.7	42.3
7.2	68.4	31.6
7.4	77.4	22.6
7.6	84.5	15.5
7.8	89.6	10.4
8.0	93.2	6.8

2.5.6 Tris buffer

To 950 ml of deionised water the following was added to prepare the final concentration of each solute;

6.06 g	Tris-base (50 mM)
1.80 g	EDTA (5mM)

Solutes were fully dissolved, the *p*H adjusted to 8.0 with 1 M NaOH/HCl and the volume was taken to 1 L with deionised water. For preparation of 0.15 M NaCl – Tris buffer (50 mM), 8.76 g of NaCl was added per 1 L buffer.

2.5.7 SDS-PAGE Solutions

2.5.7.1 Buffer 1 (1.5 M Tris-HCl, *p*H 8.8)

Tris-base (27.5g) was dissolved in 80.0 ml deionised water. The *p*H was adjusted to *p*H 8.8 with 5 M HCl, the total volume was taken to 150 ml with deionised water and stored at 4 °C.

2.5.7.2 Buffer 2 (0.5 M Tris-HCl, *p*H 6.8)

Tris-base (6.0 g) was dissolved in 60.0 ml deionised water. The *p*H was adjusted to *p*H 6.8 with 5 M HCl, the total volume was taken to 100 ml with deionised water and stored at 4 °C.

2.5.7.3 SDS solution 10 % (w/v)

Sodium dodecyl sulphate (SDS, 10.0 g) was dissolved in 100.0 ml deionised water. The solution was stored at RT.

2.5.7.4 Protein loading buffer

Protein loading buffer consisted of:

1.25 ml	Tris-HCl (0.5 M, *pH* 6.8)
2.50 ml	Glycerol
0.20 ml	10% (w/v) Bromophenol blue
2.00 ml	10% (w/v) SDS
3.55 ml	Deionised water

The solution was stored at RT. Immediately prior to use, β-Mercaptoethanol (β-ME) was added to a final concentration of 5 % (v/v). Protein samples were diluted 1:2 with the loading buffer and heated at 90 °C for 5 min.

2.5.7.5 10x Electrode (Running) buffer, *p*H 8.3

The following was dissolved in 950.0 ml deionised water;

30.3 g	Tris-base
144.0 g	Glycine
10.1 g	SDS

The *p*H was adjusted to 8.3, the total volume taken to 1 L and stored at RT. Immediately prior to running a gel, 10x electrode buffer was diluted to 1x buffer via addition of deionised water.

2.5.7.6 Staining solution

SDS-PAGE staining solution comprised;

0.25 ml	Coomassie Brilliant Blue (1.25 g/500 ml)
90.00 ml	Ethanol: deionised water (1:1. v/v)
10.00 ml	Glacial acetic acid

The solution was stored at RT. Staining solution was used to stain SDS-PAGE gel at RT for 20 minutes whilst stirring.

2.5.7.7 De-stain solution

SDS-PAGE de-stain solution comprised;

100 ml	Glacial acetic acid
120 ml	Isopropanol
800 ml	Deionised water

The solution was stored at RT. De-stain solution was used to destain Coomassie Brilliant Blue stained SDS-PAGE gels at RT whilst stirring.

2.5.8 Tannic Assay

It is an alternative method for determine protein concentration and this method was developed by Mejbaum-katzenellenbogen & Dobryszycka *et al.* 1959 [145]

2.5.8.1 Tannic reagent

The following reagents were added to 196 ml 1 M HCl and dissolved by heating to 80 °C;

4 ml	Phenol
20 g	Tannic acid

The solution was stored at RT.

2.5.8.2 Gum Arabic solution

0.4 g of gum arabic was added to 200 ml deionised water and dissolved by heating to 30 °C. The solution was stored at RT.

2.6 Site-directed mutagenesis

2.6.1 Primer design

Primers were designed as per manufacturer's instructions {QuickChange™ Site-Directed Mutagenesis Kit [146]}. Primers (forward and reverse) containing the desired mutation must anneal to the same sequence on complementary strands of the DNA, which should contain between 25 and 45 bases and the desired mutation should be positioned in the middle of the primer sequence. Guanine and cytosine bases should compromise at least 40% of the primer sequence, with the melting temperature (T_m) being at least 78 °C. The T_m for each primer was calculated using the following formula:

$$T_m = 81.5 + 0.41\ (\%GC) - 675/N - \%mismatch \qquad \textit{Equation 2.1}$$

(N is the length in bases and %GC and %mismatch are whole numbers)

Primers sequences used for the production of the desired mutants described within this work were as follows:

D87C Forward: 5' –CGCGGCGGCGGGT**TGC**GTACCAGAAATCATGG- 3'

D87C Reverse: 5' –CCATGATTTCTGGTAC**GCA**ACCCGCCGCCGCG- 3'

N18C Forward: 5' –CGCGTTATCGGCATGGAA**TGC**GCCATGCCGTGG- 3'

N18C Reverse: 5' –CCACGGCATGGC**GCA**TTCCATGCCGATAACGCG- 3'

R52C Forward: 5' –CTGGGAATCAATCGGT**TGC**CCGTTGCCAGGAC- 3'

R52C Reverse: 5' –GTCCTGGCAACGG**GCA**ACCGATTGATTCCCAG- 3'

D132C Forward: 5' –CCGGATTACGAGCCGGAT**TGC**TGGGAATCGG- 3'

D132C Reverse: 5' –CCGATTCCCA**GCA**ATCCGGCTCGTAATCCGG- 3'

(Text in **bold** indicates the position of the desired cysteine mutation)

2.6.2 dNTP mix

To prepare a stock solution of 2 mM dNTP mixture solution, 2 µl each of 20 mM of dATP, dGTP, dCTP, and dTTP were mixed. The total volume was taken to 20 µl with sterile deionised water, the solution was mixed thoroughly and stored at -20 °C.

2.6.3 Mutagenic polymerase chain reaction (PCR) protocol

The reactions were set up in 0.5 ml sterile Eppendorf tubes where the following was added;

1 µl	DNA template (5 – 50 ng)
4 µl	Forwards primer (125 ng)
4 µl	Reverse primer (125 ng)
1 µl	dNTP mix (2 mM)
5 µl	*Pfu* DNA polymerase buffer (0.5 U)
1 µl	*Pfu* DNA polymerase

The total volume was taken to 50 µl with sterile deionised water, the reaction mixture was covered with mineral oil and ready for Section 2.6.4.

2.6.4 Mutagenic PCR procedure

The polymerase chain reaction (PCR) was carried out according to the recommended thermal cycling conditions for *Pfu* DNA polymerase ["XL1-Blue competent cells", Instruction manual [146]], summarized in Table 2.3.

Table 2.3: *Recommended thermal cycling conditions for Pfu DNA polymerase-mediated PCR amplification.*

Step	Temperature (°C)	Time (sec)	Number of cycles
Initial Denaturation	95	30	1
Denaturation	95	30	
Annealing	55	60	16
Elongation	68	300	
Final Extension	68	60	1

2.6.5 Agarose gel electrophoresis

To prepare 1% agarose gel, 1.0 g of agarose powder was dissolved in 100 ml of 0.5x TAE buffer (dilute 1 ml 50x TAE buffer with 99 ml of deionised water) by heating in a microwave oven for 1 min. EtBr (0.2 mg/ml) was added and the mixture poured into a Mini Gel Kit Tray (CBS Scientific) to solidify. The gel was covered in 1x TAE buffer. DNA samples were prepared by mixing 5 µl PCR product with 1 µl of DNA loading buffer. The gel was run for 30 min at 8 volts/cm. EtBr fluorescence was visualised using an ultraviolet (UV) lamp at 245 nm [147].

2.6.6 Digestion with *Diplococcus pneumoniae* restriction endonuclease (*Dpn*I)

Restriction digestion with *Dpn*I was carried out immediately following site-directed mutagenesis in order to remove template DNA. Site directed mutagenesis products were incubated with *Dpn*I for 1 h at 37 °C as according to manufacturers' instructions. *Dpn*I recognizes and digests methylated sequences only (Figure 2.1). *Dpn*I functions by reading the methylation status of its recognition sequence, comparing the methylation status of the two adenines within the recognition sequence. If both adenines are unmethylated (a signal that the DNA is not host DNA) the enzymes avoids the restriction site. The enzyme acts as an endonuclease secondary to a maintenance methylase, thus template DNA gets digested and the newly synthesized (mutant) DNA is.untouched.

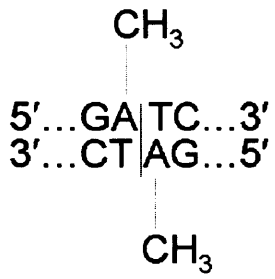

Figure 2.1: *Methylated sequence recognized by DpnI.*

2.7 Experimental protocols

2.7.1 Preparation and storage of DNA constructs

This section describes the procedures and materials required for the construction, manipulation, and storage of the DNA construct used during the course of this research. All DNA constructs including primers and plasmids were stored at –20 °C.

2.7.1.1 Purification of plasmid DNA

Plasmid DNA was purified according to manufacturers instructions from transformed *E. coli* strains (XL1-Blue) using a QIAGEN Miniprep Kit (QIAprep® Spin Miniprep Kit). A single colony was picked from a LB ampicillin agar plate and grown in 5 ml LB-ampicillin medium overnight (~10 h) at 37 °C, 160 *rpm*. The cells were harvested by centrifugation (3,430 g) and the manufacturer's protocol followed based on the Birnboim and Doly method [148]. Eluted DNA was stored at –20 °C.

2.7.1.2 Quantification of oligonucleotides and plasmid DNA

Quantification of all oligonucleotides and plasmid DNA was performed using a Shimadzu Biospec-mini spectrophotometer. Optical density (OD) measurements were taken at 260 nm and 280 nm. An OD_{260} value of 1.0 equates to 50 μg/ml of double stranded DNA (dsDNA), 30 μg/ml of oligonucleotide, or 40 μg/ml of single stranded DNA (ssDNA). The value derived from the ratio of OD_{260}/OD_{280} gave an indication of the purity of the DNA sample. An observed value between 1.8 and 2.0 indicates the DNA sample was pure and free from protein contamination.

2.7.1.3 Sequencing of plasmid DNA

DNA at a concentration between 200-500 ng/μl was added to 3.5 μl of 1 μM T7 primer. The total volume was brought to 10 μl with sterile deionised water. DNA sequencing was performed at the University of Birmingham Genomics Laboratory, Birmingham, UK. Alternatively 15 μl of 100 ng/μl DNA was sequenced by Lark Technologies, Essex, UK.

2.7.1.4 Cleavage of plasmid DNA using restriction enzymes

Plasmid DNA were restriction digested to check for the presence of a particular insert (without the need for sequencing) and allow the sub-cloning of inserts between various vectors. In all cases the manufacturer's procedures were followed; 0.3 μg of plasmid DNA (10 μl) was mixed with 1-5 U (~1 μl) of restriction enzyme, 10x buffer (~1 μl) and sterile deionised water. The reaction mixture was incubated at 37 °C for a defined period of time varying from an hour to overnight (o/n). In the case of double digests, where the plasmid DNA was simultaneously cut by two different restriction enzymes, a buffer

compatible with both enzymes was used as specified by the manufacturer.

2.7.1.5 DNA purification and visualisation

Double stranded DNA (dsDNA, >100 base pairs) was visualised by agarose gel electrophoresis (Section 2.6.5). DNA of different sizes run at different speeds through the agarose gel and separate according to their size and shape (*i.e.* supercoiled or linear). PCR products were compared directly to a DNA ladder (Bioline) to verify they were at the correct size.

2.7.1.6 DNA ethanol (EtOH) precipitates

Following sequencing of plasmid DNA, EtOH precipitates and glycerol stocks were made of all new constructs. Procedures described in this section were carried out at rt and cell solutions were centrifuged at 3,430 g in Eppendorf® 5415R centrifuge using aseptic technique. Once the standard plasmid DNA preparation was complete (Section 2.7.1.1), EtOH precipitates were prepared by eluting the bound DNA from the QIAprep column into 100 µl of sterile deionised water. 7.5 M ammonium acetate (50 µl) and 100% absolute EtOH (375 µl) were added to the DNA eluent and incubated for 10 minutes followed by centrifugation at 3,430 g, 15 minutes. The supernatant was carefully removed and the DNA pellet washed with 250 µl of 80% EtOH (v/v in deionised water) followed by centrifugation at 3,430 g, 10 minutes and stored at –80 °C.

2.7.1.7 Glycerol stocks

Glycerol stocks were prepared by incubating *E. coli* XL1-Blue competent cells containing the plasmid of interest at 37 °C, 180 rpm until an OD_{600} of ~0.6 was reached. A small volume of the culture (1 ml) was then aseptically mixed with 100 µl of 80% sterile glycerol (v/v deionised water), mixed and stored at –80 °C. Glycerol stocks could then be streaked on a pre-warmed agar plate containing the appropriate antibiotic and incubated o/n at 37 °C.

2.7.1.8 Preparation of competent cells

**E. coli* competent cells were streaked on a sterile LB agar plate and incubated at 37 °C o/n. A single colony was picked and grown o/n in 5 ml of LB medium at 37 °C, 180 rpm. The following day, the o/n culture was incubated in 50 ml 2x YT medium at 37 °C, 180 rpm until an OD_{600} of 0.5 was reached. The culture was then centrifuged for 10 min at 8,000 g, the supernatant discarded, and the pellet re-suspended in 20 ml of pre-chilled Competent Cell Buffer A (See Section 2.4.4) on ice for 20 min. The solution was centrifuged as before and the supernatant discarded. The pellet was re-suspended in 5-10 ml of Competent Cell Buffer B (See Section 2.4.5) and placed on ice for 1 h. The competent cells were aliquoted into 100 µl, fast-frozen in liquid nitrogen, and stored at –80 °C.

*XL1-Blue competent cells used to extract DNA and BL21(DE3) competent cells used to extract protein.

2.8 Protein purification and characterization

This section describes the procedures and materials required for the production, purification and analysis of EcDHFR wild-type (WT) and mutants. All enzymes were stored at 4 °C and assays at 20 °C unless otherwise stated.

2.8.1 Transformation of DNA constructs into competent cells

Plasmid DNA containing the required DNA construct was transformed into *E. coli* BL21(DE3) cells. 0.1 μg plasmid construct (1 μl) was added to 100 μl of cell suspension previously thawed on ice, and then incubated on ice for 30 minutes. The mixture was heat shocked via water bath at 42 °C for 30 sec. Preheated LB medium (1 ml) was added to the cell suspension and incubated at 37 °C, 180 rpm for 1 hour, followed by centrifugation (3,430 g) for 2 min. The pellet was re-suspended with 100 μl LB-medium and plated on a preheated sterile LB agar plate containing the appropriate antibiotic (See Ssection 2.2.2). Inverted plates were incubated o/n at 37 °C then stored at 4 °C.

2.8.2 Test induction

Test inductions were carried out to determine if the cells were producing the protein of interest. Two colonies were picked and grown o/n in two separate sterile tubes containing 5 ml LB medium and 10 μl 0.27 M ampicillin. From each tube, 100 μl was grown in 5 ml fresh LB medium containing 10 μl 0.27 M ampicillin and incubated at 37 °C, 180 rpm until an OD_{600} of 0.5 was reached; 1 ml of the solution was then removed for SDS-PAGE analysis. The remaining culture was then induced with 40 μl of 0.4 mM IPTG and

incubated for 3 h at 37 °C, 180 rpm. A sample (1 ml) of the incubated mixture was taken every hour for SDS-PAGE analysis, centrifuged (3,430 g) and the supernatant discarded. Protein loading buffer (100 µl) was added and heated to 90 °C for 5 min. SDS-PAGE analysis was performed to test for cellular expression of protein (Section 2.5.7). Protein identification will be discussed at Section 2.8.4.

2.8.3 Large scale expression

A sterile 100 ml flask containing 60 ml of LB medium, 180 µl of 0.27 mM ampicillin, was inoculated with a single cell colony and grown o/n at 37 °C, 180 rpm. The cell culture was divided equally into six flasks containing 500 ml of sterile LB medium, 1 ml of 0.27 mM ampicillin and incubated further until an OD_{600} of 0.5 was reached. A 1 ml sample was removed from each flask for SDS-PAGE analysis. Protein expression was induced with 1.0 ml (60 mg/ml) IPTG for 3 to 4 h at 37 °C, 180 rpm. The cells were harvested at 11,000 g, for 10 minutes in Sorvall® RC-5B centrifuge. The supernatant was discarded and the pellet stored at –20 °C.

2.8.4 Protein identification using SDS-PAGE

The Mini-PROTEAN^{TM} 3 cell (BioRad) was used to identify the protein of interest and to monitor its purification. The stacking gel was used to concentrate the samples and the resolving gel was used to separate the proteins by their molecular weight (M_w). The following solutions were prepared [Table 2.4] [149].

Table 2.4: *Solutions for SDS-PAGE.*

	dH_2O (ml)	30 % Acrylamide (ml)	*Buffer (ml)	10 % w/v SDS (ml)
Stacking (5 %)	5.7	1.7	2.5	0.1
Resolving (15 %)	2.4	5.0	2.5	0.1

***Resolving Gel buffer** – 1.5 M Tris-HCl (*p*H 8.8); **Stacking Gel buffer** – 0.5 M Tris-HCl (*p*H 6.8). See Section 2.5.6 for buffer preparation.

Immediately prior to pouring the gel, the following reagents were added;

Resolving Gel: 100 µl 10 % APS

10 µl TEMED

Stacking Gel: 50 µl 10 % APS

10 µl TEMED

Samples were mixed with protein loading buffer (1:2) and heated to 90 °C for 5 min. The samples were loaded into the gel wells and run for 50 min at 180 V in 1x running buffer (See Section 2.5.7.5). Gels were stained with staining solution followed by incubation with the de-stain solution to visualise protein bands (See Section 2.5.7), via UV light.

2.8.5 Purification of EcDHFR

As previously stated, BL21(DE3) *E. coli* cells were used for large scale expression of all proteins mutants. Frozen cells previously harvested during large scale expression were thawed on ice and re-suspended in 50 mM Tris buffer (*p*H 8.5, 15 ml). The suspension was sonicated for 5 min on ice and centrifuged at 27,000 g, 20 minutes in Sorvall® RC-5B. The filtered supernatant (0.22 μm filter, Millipore) was applied to a column contained immobilized methotrexate (MTX) resin (5 ml bed volume, Amersham Pharmacia Biotech AB), pre-equilibrated with lysate buffer (50 mM Tris buffer, *p*H 8.5) and washed (4x column volume) with the same buffer with 0.15 M NaCl. The column was extensively washed (20x column volume) with the same buffer. Bound protein was eluted with a buffer containing 50 mM Tris buffer (*p*H 8.5), 0.15 M NaCl, and 5 mM folic acid. The eluted protein was analysed by SDS-PAGE (Section 2.8.4). EcDHFR was dialysed o/n against 3 L of 5 mM phosphate buffer (*p*H 7.0) containing 5 mM EDTA with two changes of buffer. Dialysed protein was lyophilised to reduce the total volume of buffer. Two different methods have been used for further purification EcDHFR from folic acid (See Section 2.8.5.1 and Section 2.8.5.2).

2.8.5.1 DEAE anion exchange chromatography

A diethylaminoethyl (DEAE) sepharose column (15 ml bed volume, Amersham Pharmacia Biotech AB) was pre-equilibrated with lysate buffer. The column was extensively washed (10x column volume) with the same buffer. The lyophilised protein was dissolved in a small volume (~ 2 ml) of fresh dialysis buffer and applied to the DEAE-sepharose column. Bound protein was eluted with three column volumes of buffer

with a 0 to 1 M NaCl gradient in 50 mM of Tris buffer (*p*H 8.3) containing 5 mM EDTA. EcDHFR fractions were identified using SDS-PAGE and absorbance measured at 280 nm. Fractions containing EcDHFR were dialysed o/n against 3 L of dialysed buffer containing 5 mM EDTA with two changes of buffer. The flow rate was 2 ml/min.

2.8.5.2 SEPHADEX G-100 size exclusion chromatography

SEPHADEX G-100 contains beads for gel filtration prepared by cross-linking dextran with epichlorohydrin, and used to fractionate proteins from 4000 to 150,000 M_w. The lyophilised protein was dissolved in a small volume (~ 2 ml) of fresh dialysis buffer and applied to the SEPHADEX G-100 column (15 ml, Sigma-Aldrich) which has pre-equilibrated with lysate buffer. Bound protein was eluted with 50 ml 0.5 M NaCl in 50 mM of Tris buffer (*p*H 8.3) containing 5 mM EDTA. EcDHFR fractions were identified using SDS-PAGE and their absorbance measured at 280 nm. Fractions containing EcDHFR were dialysed o/n against 3 L of dialysed buffer containing 5 mM EDTA with two changes of buffer. The flow rate was 1.5 ml/min.

2.8.6 Protein identification using mass spectrometry

The mass of EcDHFR was determined by matrix assisted laser desorption ionization time-of flight mass spectrometry (MALDI-TOF) using a Bruker Biflex IV machine. The matrix used was *sinapic acid (10 mg/ml in 1:1, 1:2, 1:4 ratio dilution deionised water). Myoglobin (M_w~16,952) at a concentration of 10 pmol/μl was used to calibrate the machine.

*Alternative matrix such as α-cyano-4-hydroxy-cinnamic acid was used for analysis of peptides (M_w < 6,000).

2.8.7 Determine of protein concentration

Three alternative methods were used to determine the EcDHFR concentration. The accuracy of the protein concentration is very important prior for further analysis.

2.8.7.1 Absorbance measurement

The concentration of the WT EcDHFR enzyme was calculated using Shimadzu UV-2401PC, UV/Vis spectrophotometer using an extinction coefficient at 280 nm (ε_{280}) of 31,100 $cm^{-1}M^{-1}$ [74]. To determine presence of contaminating nucleic acids, if a ratio of the absorbance value at 280 nm compared to 260 nm < 1.6 (A_{280}/A_{260} <1.6) indicated a low level of contamination.

2.8.7.2 Micro-tannin Assay

The concentration of solutions of EcDHFR mutant proteins was determined using the micro-tannin assay calibrated against a standard concentration of bovine serum albumin (BSA) [150]. Optical density measurements were taken at 500 nm using a Shimadzu Bio-Spec-mini spectrophotometer. The accuracy for this assay was assumed to be between 10 and 80 μg of protein.

In a water bath, 1 ml of protein solution and the BSA solution was incubated for 5 min at 30 °C. Pre-warmed tannic reagent (1 ml) was added and the mixture incubated for a further 10 minutes. The solution was removed from the waterbath and 1 ml of gum arabic solution added and allowed to cool to RT (Section 2.5.8). An OD_{500} was taken to measure protein concentration.

2.8.7.3 Methotrexate (MTX) titration

The concentration of the EcDHFR mutant proteins was also calculated by observing the quench of the intrinsic tryptophan within the protein via MTX titration using a PerkinElmer LS 55 Luminescence spectrometer. The fluorescence emission spectrum of DHFR showed a maximum at 345 nm when excited at 290 nm. The total volume of MTX to quench the protein was used to determine the protein concentration;

$$M_1V_1 = M_2V_2 \qquad \textit{Equation 2.2}$$

Where M_1 is the initial concentration of sample, M_2 is the final concentration of sample, V_1 is the initial volume used, and V_2 is the final volume used.

2.8.8 Protein cleavage using trypsin digestion

EcDHFR was digested into polypeptides with the acetylated protease trypsin. EcDHFR protein (100 µl, 10 µM) in 100 mM ammonium hydrogen carbonate (*p*H 8 – 8.5) buffer was prepared. Trypsin (0.2 unit, 1 µl) was added to the protein sample, gentle mixed and incubated o/n at 37 °C. The protein sample was then lyophilized to remove the ammonium salt and stored at –20 °C. Prior to use, the protein was dissolved in 10 µl of deionised water or matrix for MALDI-TOF analysis (Section 2.8.6).

2.8.9 Protein storage

EcDHFR could be stored as a lyophilized product and its catalytic activity had no significant difference with protein solution, stored at –20 °C. EcDHFR could be stored at –20 °C for several months without any loss in activity.

2.9 Synthesis and purificatioin of glyco-EcDHFR

The methodology for derivatisation of the desired mutated glycosylated EcDHFR cysteine mutant (glycosyl haloacetamide) will be discussed in this section.

Protein sample (50 µl, 50 mM) was diluted with 150 µl of 50 mM phosphate buffer (*p*H 8.5), 1 mM TCEP, and incubated at 20 °C for 10 min. Glycosyl haloacetamide (5 mg) was dissolved in 100 µl of 50 mM phosphate buffer (*p*H 8.5) and mixed with the protein sample. The mixture was incubated in the dark at 4 °C for 36 h. The glycol-EcDHFR

protein was dialysed against 3 L of dialysis buffer containing 5 mM EDTA o/n and the protein sample was analysed using MALDI-TOF (Section 2.8.6) to determine any presence of free protein (unglycosylated protein) within the sample. For example, the unglycosylated DM-D87C EcDHFR with glucose-N-acetamide (GlcNAc) haloacetamide shows a molecular weight (M_w) at 17,989. Upon glycosylation, a peak indicating the M_w 18,237 is observed due to addition of one GlcNAc acetamide (M_w~248).

Purification of the glycol-EcDHFR was performed when at least 15 % of the protein sample contained sugar free proteins *via* MALDI-TOF analysis (Section 2.8.6). Mixtures of glycosylated and unglycosylated proteins were treated at *p*H 7.0 with 2-[(biotinoyl)-amino]-ethyl methanethiosulfonate (MTSEA) to produce mixtures of proteins that were either glycoslyated or biotinylated on the mutated Cys site. The sample mixture was incubated in 25 mM MES *p*H 7.5, 100 mM NaCl at 4 °C for 12 h. Reaction products were dialysed against dialysis buffer containing 5 mM EDTA o/n. The mixture was applied to avidin immobilized on agarose (~30 nmol avidin per ml of resin, Promega) and unbiotinylated proteins were eluted with 10 mM phosphate buffer (*p*H 7.5), 100 mM NaCl (Elution buffer). The overall yield varied from 25 – 65% [71].

2.10 Techniques for protein analysis

2.10.1 Circular dichroism (CD) spectroscopy and thermal denaturation

CD spectroscopy is a common technique used to characterise a protein's secondary structure and thermo-stability. In this work, CD spectroscopy was used to measure the melting temperature (thermo-stability) of EcDHFR and its glycosylated forms.

Experiments were performed using a Jasco 815 or Applied Photophysics Chirascan CD spectrometer. The resulting milli-degree values (θ) were converted to mean residue ellipticity (MRE or [Θ]) expressed as deg cm^2/dmol/residue. The value of the MRE was calculated using Equation 2.3;

$$[\Theta]\ MRE = [\theta] / (10 * m * c * l) \qquad \textit{Equation 2.3}$$

where [θ] is the measured ellipticity in mdeg, m is the number of residues, c is the concentration in M, and l is the path-length of the cuvette in cm.

EcDHFR (10 μM) in 5 mM phosphate buffer (*p*H 7.0) was placed in a stopped-lid quartz cuvette (10 mm path-length, Helman). Wavelengths were measured at every 1.0 nm ranging from 280.0 – 200.0 nm with a bandwidth of 1 mm, and a time per nm wavelength of 4 s used to obtain a far UV-CD spectrum of the enzyme.

In the temperature denaturation experiments, the temperature was increased at 0.4 °C/min. The temperature range used was from 20.0 – 80.0 °C. The unfolding of the protein was monitored at 222.0 nm and the melting temperature was taken as the midpoint of the observed transition. MRE_{222} was determined using Equation 2.3.

2.10.2 Kinetic assays

2.10.2.1 Preparation of substrates and co-factor

The preparation of 7,8-dihydrofolate (H_2F) was performed as previously described by Blakley (1984) [88]. Folic acid (38.2 mg) was dissolved in a freshly prepared, filtered solution of ascorbic acid (1.0 g/10 ml) and the *p*H was taken to 6.0 by drop wise addition of 1 M NaOH. The folate solution was reduced to tetrahydrofolate (H_4F) by addition of sodium dithionite (400 mg) at 4 °C. The formation of H_2F was achieved by slowly (1 ml/min) adding glacial acetic acid until the *p*H was 2.8. The solution was centrifuged at 27,000 g for 5 min at 4 °C. The white precipitate of H_2F was then re-suspended in 10 ml ascorbate solution (*p*H 6.0) and re-precipitated as described above. H_2F was re-suspended and washed with acetone and diethyl ether. All operations were performed anaerobically under nitrogen and all buffers were degassed before use. The presence of H_2F was confirmed by NMR and UV/Vis spectrophotometry by comparison with a known standard.

(4R)-[^{2}H]-NADPH (NADPD) was synthesised by reduction of $NADP^+$ (35 mg) using the $NADP^+$ dependent alcohol dehydrogenase from *Thermoanaerobium brokii* (3.8 units) and d_8 propan-2-ol (1.2 ml) [151]. The mixture was incubated in 25 mM ethanolamine (*p*H 7.8) at 42 °C. The reaction was completed in less than 1 h by monitored the absorbance reading at 340 nm. Purification of NADPD was achieved using anion exchange chromatography (Mono Q™ HR 5/5, Pharmacia) [152], using 25 mM ethanolamine (*p*H 7.8) as a calibrating buffer and eluting with a 75% gradient of NaCl over 10 min. Fractions that showed an absorbance ratio at 260 and 340 nm (A_{260}/A_{340}) of 2.4 or less

were collected, aliquoted and stored at –20 °C as lyophilized products.

NADPH and NADPD concentrations were determined by spectrophotometer using an ε_{340} of 6,220 $cm^{-1}M^{-1}$ [74]. Similarly the concentration of H_2F was determined using an ε_{282} of 28,000 $cm^{-1}M^{-1}$ at *p*H 7.4 [153].

2.10.2.2 Pre-steady state measurement of EcDHFR

Pre-steady state kinetic experiments were performed on an Applied Photophysics stopped-flow spectrophotometer using 2.5 ml syringes. Using the difference between the absorption and emission spectra of the co-factor in its reduced and oxidised forms, the loss of a hydride in NADPH was monitored during the reaction catalysed by DHFR. The nicotinamide ring of NADPH has a maximum fluorescence absorption at 340 nm and a maximum emission at 450 nm. However the oxidized form, $NADP^+$ has no adsorption or emission at these wavelengths. Therefore conversion of NADPH to $NADP^+$ resulted in a decrease in the relative fluorescence intensity at 450 nm upon excitation at 340 nm. A 450 nm cut off filter was used.

Pre-steady state kinetic measurements were monitored by measuring the fluorescence resonance energy transfer (FRET) between the protein and the reduced co-factor (NADPH). This technique relies on two important factors: 1) the overlap between the emission spectrum of tryptophan and the absorption spectrum of NADPH, and 2) the distance of the two chromophores (~10 to 100 Å). EcDHFR has a tryptophan residue in the active site, therefore exciting the reaction mixture at 292 nm results in the fluorescence resonance energy transfer (FRET) at 340 nm between the tryptophan and NADPH. This reaction can be followed by observing the decay of fluorescence of the reduced co-factor at 450 nm. EcDHFR (8 μM) solution was pre-incubated with NADPH

(4 μM) for at least 15 min at 20 °C to avoid hysteretic behavior [74]. As mentioned previously, a 450 nm cut off filter was used The reaction was initiated by rapidly mixing, at a controlled temperature, an equal volume of H_2F (100 μM) solution. The reaction buffer used was 100 mM MTEN (*p*H 7.0, Section 2.5.4). The reaction was monitored using a 400 nm cut-off filter. The dead time of the experiment was 2 msec. The observed kinetic traces were fitted to single or double exponential decay using the provided software (Applied PhotoPhysics)

2.10.2.3 Steady state measurement of EcDHFR

Turn-over rates were measured spectrophotmetrically following the decrease in absorbance at 340 nm during the reaction ($\varepsilon_{340,\ NADPH\ +THF}$ = 11,800 $M^{-1}cm^{-1}$ [74, 154]. The temperature was held constant at 20 °C and *p*H 7.0 for steady state measurement. The enzyme (10 μM) was pre-incubated with NADPH (20 μM) for 15 min at RT to avoid hysteretic behavior [74]. The enzyme-NADPH mixture solution (5 μl) was added to 950 μl of 100 mM MTEN (*p*H 7.0) buffer. NADPH/D (100 μM final concentration) was added to the solution and the reaction was started by adding 10 μl of H_2F (100 μM final concentration). The rates were calculated from the linear fittings of the initial velocities (from 10 – 40 sec). Each experiment was performed in triplicate and average values were used for calculations. Plotting a graph using the average activities against corresponding concentration of NADPH/D / H_2F, the Michaelis constant (K_M) and the rate constant (k_{cat}) were able to be determined. The cuvette used had a 10 mm path-length (Helman). Pre-warming the buffer and utilising a temperature controlled cuvette holder carefully controlled the temperature through the reaction.

2.10.3 Equilibrium dissociation constants

The equilibrium dissociation constants (K_D) between ligands (folate or NADPH) and EcDHFR and its derivatised glycoforms were measured by monitoring the quenching the intrinsic tryptophan fluorescence as a function of ligand concentration by PerkinElmer LS 55 Luminescence spectrometer at 25 °C [123]. The solvent conditions were 50 mM NaCl /50 mM phosphate buffer (*p*H 7.0) containing 0.1 mM EDTA and 0.1 mM DTT. The protein concentration was 0.05 to 0.5 μM.

The fraction of protein bound to the ligand was calculated by dividing the observed fluorescence intensity of the protein-ligand complex by the sum of the intensities of the protein-ligand complex and free protein from the ligand titrations (Equation 2.4). By plotting the fraction of bound protein against the concentration of unbound (free) ligand [L], the concentration where half of the protein binding sites are occupied $\{[L]_{1/2}\}$ can be calculated. The data were fit to the Langmuir isotherm (Equation 2.5).

$$\Phi = I_{LP} / (I_P + I_{LP}) \qquad \textit{Equation 2.4}$$

$$\Phi = 1 / (1 + K_D^n / [L]^n) \qquad \textit{Equation 2.5}$$

Where Φ is the fraction of protein bound, I is the intensity of the protein only (I_P) or of protein-ligand complex (I_{LP}); [L] is the concentration of free ligand that is not bound to the protein.

2.10.4 Equilibrium unfolding

Equilibrium unfolding of EcDHFRs and its derivatised glycoforms in the presence of urea were monitored by the intensity of fluorescence at 345 nm and 20 °C with a PerkinElmer LS 55 Luminescence spectrometer [155-157]. The solvent conditions were 10 mM K_iPO_4 (*p*H 7.0) containing 0.1 mM EDTA and 0.1 mM DTT. The protein concentration was maintained at about 2 μM and freshly prepared urea solution was pre-treated with AG® 501-X8 ion exchange resin (BIO-RAD) to remove the formation of cyanate and ammonium ions from decomposition of urea [158]. All samples were fully equilibrated at each denaturant concentration by incubated for o/n at RT before the fluorescence intensities were measured. A minimum of 10 to 15 data points were required to adequately define the denaturation curve.

2.11 Errors and their propagation

2.11.1 Standard errors of the mean

The errors in this work are expressed as standard error of the mean (σ_{SEM}) defined as the standard deviation (σ) of the observations divided by the square root of the sample size:

Standard deviation

$$\sigma = [\Sigma (X - M)^2 / (n - 1)^2]^{1/2}$$

Standard error of the mean (SEM)

$$\sigma_{SEM} = \sigma / n^{1/2}$$

Where X is the value of the population, M is the mean of the population, and n is the number of samples within the population. The accuracy of the SEM value was dependent on the sample size. With bigger sample sizes, the sample mean becomes a more accurate estimate of the parametric mean, so the standard error of the mean becomes smaller.

In this work, if not otherwise stated, the errors are given as two standard errors of the average mean, indicating an accuracy of 95%.

2.11.2 Propagation of errors

The propagation of the errors for all calculations were as follows,

	Function	Error (Δ)
Sum	$Z = X + Y$	$\Delta Z = (\Delta X^2 + \Delta Y^2)^{1/2}$
Subtraction	$Z = X - Y$	$\Delta Z = (\Delta X^2 + \Delta Y^2)^{1/2}$
Multiplication	$Z = X * Y$	$\Delta Z = Z[(\Delta X/X)^2 + (\Delta Y/Y)^2]^{1/2}$
Division	$Z = X / Y$	$\Delta Z = Z[(\Delta X/X)^2 - (\Delta Y/Y)^2]^{1/2}$
Logarithm	$Y = \ln X$	$\Delta Y = (\Delta X) / X$
Exponential	$Y = e^X$	$\Delta Y = \Delta X * e^X$

Where X and Y represent a variable and ΔX and ΔY represent their errors, respectively. The measurement X and Y must be independent from each other. The calculated value is Z and its error is ΔZ.

Chapter 3

Wild-type (WT) and cysteine free (DM) EcDHFR

3.1 Introduction

In order to understand the effect of site-specific glycosylation on the physical and chemical properties of the naturally nonglycosylated enzyme dihydrofolate reductase, a site-directed mutagenesis approach was followed. Stability and kinetic parameter studies of the glycosylated proteins and the site-specific cysteine mutant EcDHFR were used to identify the effects of the presence of sugars on the protein. However, the interpretation of those results required the determination of reference values obtained from the wild-type enzyme and the nonglycosylated site-specific cysteine mutant EcDHFR. Therefore wild-type and the site-specific cysteine mutant EcDHFR protein were expressed, and the protein purified to analyse their stability and kinetic parameters. The X-ray structure of EcDHFR reveals two cysteine residues located at position 85 and 152 [118]. In order to synthesise a desired site-selective homogeneous glycosylated EcDHFR, the two cysteine residues at position 85 and 152 were required to be replaced.

The cysteine free double mutant EcDHFR has been made and investigated by Iwakura and co-workers [159]. They successfully replaced the Cys85 and Cys152 with various amino acid residues. They showed that the Cys85Ala and Cys152Ser double mutant (DM) or also known as the free cysteine mutant of EcDHFR has catalytic activity (k_{cat} = 9.4 ± 0.4 s^{-1}) and thermal stability (T_M = 50.9 ± 0.9 °C) comparable to the wild-type enzyme. Therefore in our work, we selected the cysteine free double mutant C85A/C152S (DM)-EcDHFR as the base template for synthesizing single site-specific cysteine mutants of EcDHFR *via* site-directed mutagenesis techniques.

This chapter presents a detailed description of the entire study of wild-type (WT) and the cysteine free double mutant C85A/C152S (DM)-EcDHFR (Figure 3.1), which

was used as the DNA template for synthesizing site-specific cysteine mutants for obtaining results that were taken as reference values in the following chapters.

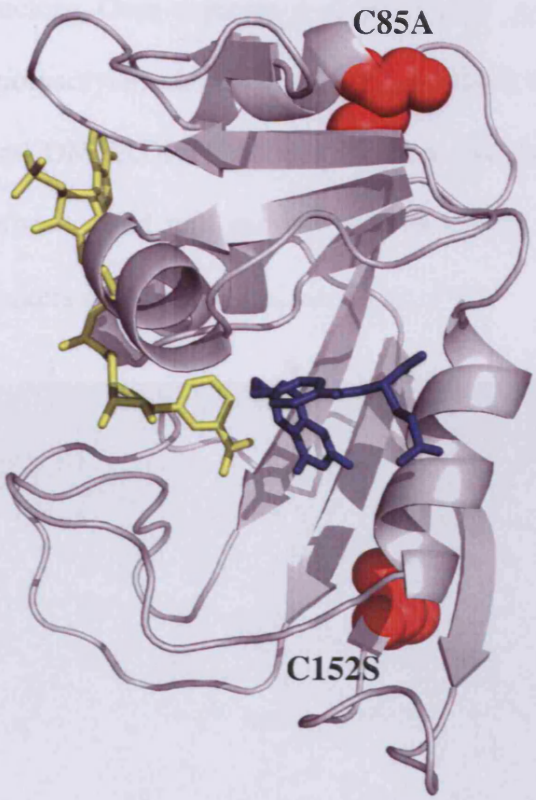

Figure 3.1: *Structural overview of EcDHFR. The two cysteine residues are labeled in red. Folate and NADP$^+$ are drawn in stick format and indicated in blue and yellow respectively in the ternary complex (1RA2). The structure is oriented so that the co-factor nicotinamide ring is in the plane of paper [78, 108].*

3.2 Expression of wild-type and cysteine free double mutant (DM) EcDHFR

A single *E. coli* BL21(DE3) colony containing WT or DM EcDHFR, was used to grow a culture to express the protein. These cells contain the λDE3 lysogen that carries the gene for T7 RNA polymerase under control of the *lac*UV5 promoter. Isopropyl-β-D-

thiogalactoside (IPTG), which binds to the *lac* repressor, can be used to induce production of the T7 RNA polymerase from the *lac*UV5 promoter. After induction with IPTG, T7 RNA polymerase transcribes the target gene carried in the plasmid. T7 RNA polymerase is promoter-specific, therefore it is commonly used to transcribe DNA which has been cloned into vectors. Over-expression of the DHFR protein was followed by sodium dodecyl sulfate polyacrylamide gel electrophoresis (SDS-PAGE) for visualization. The recombinant WT and DM EcDHFR proteins have a calculated mass about 18,000 molecular weight, therefore a band will showed at between the region of M_w ~20,000-14,000 by the protein markers at the SDS gel (See Figure 3.2).

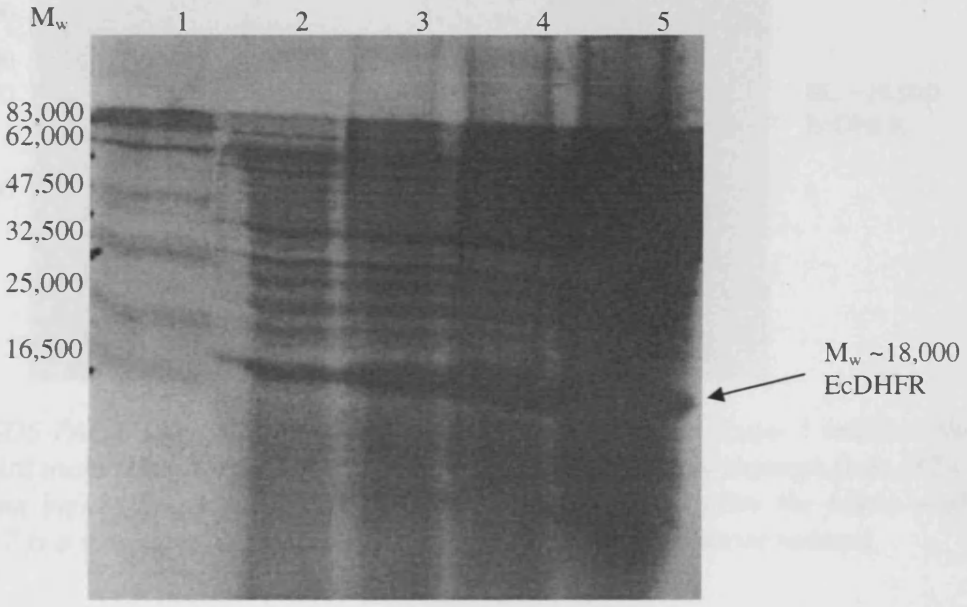

Figure 3.2: SDS-PAGE for l*arge-scale expression of EcDHFR. Lane 1 indicates the molecular weight marker; Lane 2 indicates the cells before induction with IPTG; and Lane 3-5 indicate the cells after induction with IPTG for 1, 3, and 4 h.*

3.3 Purification of EcDHFR

Initial purification of WT and DM EcDHFR was carried out using methotrexate (MTX) affinity chromatography. The column was pre-equilibrated using lysate buffer and the protein was eluted with lysate buffer containing 0.15 M NaCl and 5 mM folic acid. The eluted protein fraction from the MTX column was visualized by SDS-PAGE (Figure 3.3).

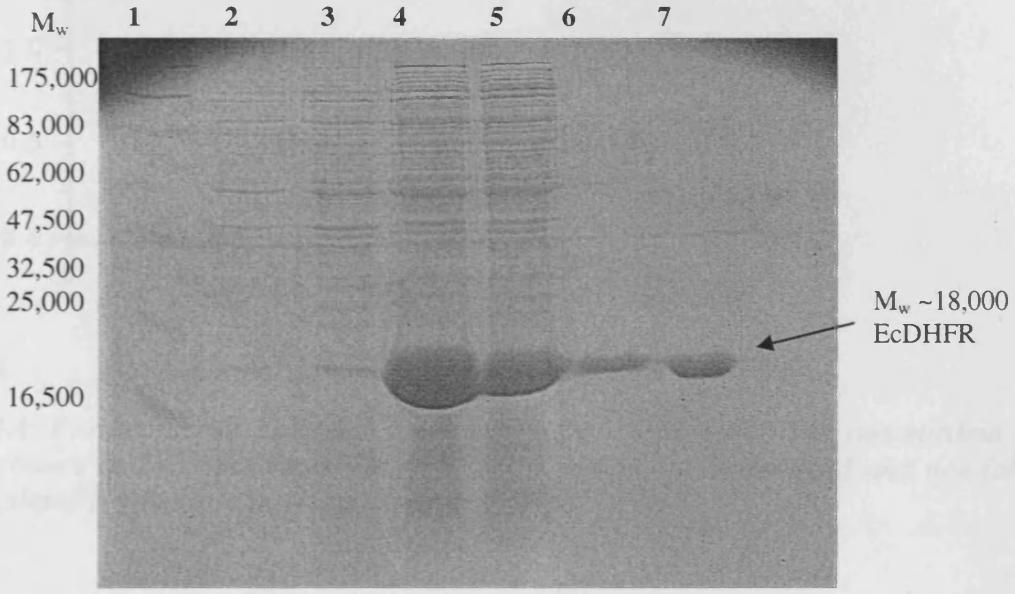

Figure 3.3*: SDS-PAGE purification of EcDHFR* via *MTX column. Lane 1 indicate the protein standard molecular weight, crude extract (lane 2 and 3), flow through from MTX-agarose column before folate wash (lane 4 and 5) and the eluent after the folate wash (lane 6) Lane 7 is a sample of WT EcDHFR after purify* via *MTX-agarose column.*

The eluted protein was dialyzed extensively with 5 mM of phosphate buffer (*p*H 7.0) to decrease the NaCl concentration and applied to a column contained diethylaminoethyl (DEAE) sepharose for further purification. The column was pre-equilibrated using column-lysate buffer (See Section 2.8.5.1) and the protein was eluted using a salt gradient (0 - 1.0 M NaCl) at a rate of 2 ml/min. Fractions were tested for protein by the absorbance at 280 nm. A typical elution profile of EcDHFR is shown

below in Figure 3.4. Two maxima in the absorbance were observed corresponding to a concentration of NaCl of 0.2 - 0.3 M and 0.4 – 0.5 M, respectively.

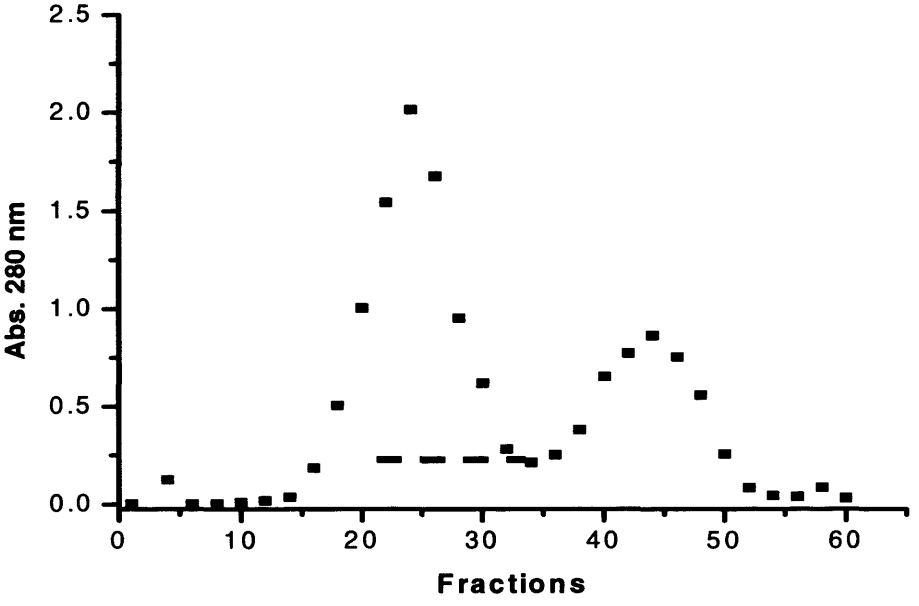

Figure 3.4: *Purification of EcDHFR* via *DEAE sepharose column. The two maxima in the absorbance at 280 nm denote the presence of DHFR with folic acid and non-folic acid complexes (--- denotes pooled fractions).*

As high absorbance at 280 nm can be produced by the presence of contaminating proteins and folate in addition to EcDHFR, several fractions corresponding to the two peaks of absorbance were analysed by SDS-PAGE (Figure 3.5). The aim of this experiment was to identify which protein fractions were least contaminated with folic acid. Other than that, through the observation of the color of the protein solution within the fractions, fractions between 20-30 contained least folic acid (colourless) and the fraction between 40 to 50 contain the most folic acid solution (yellow).

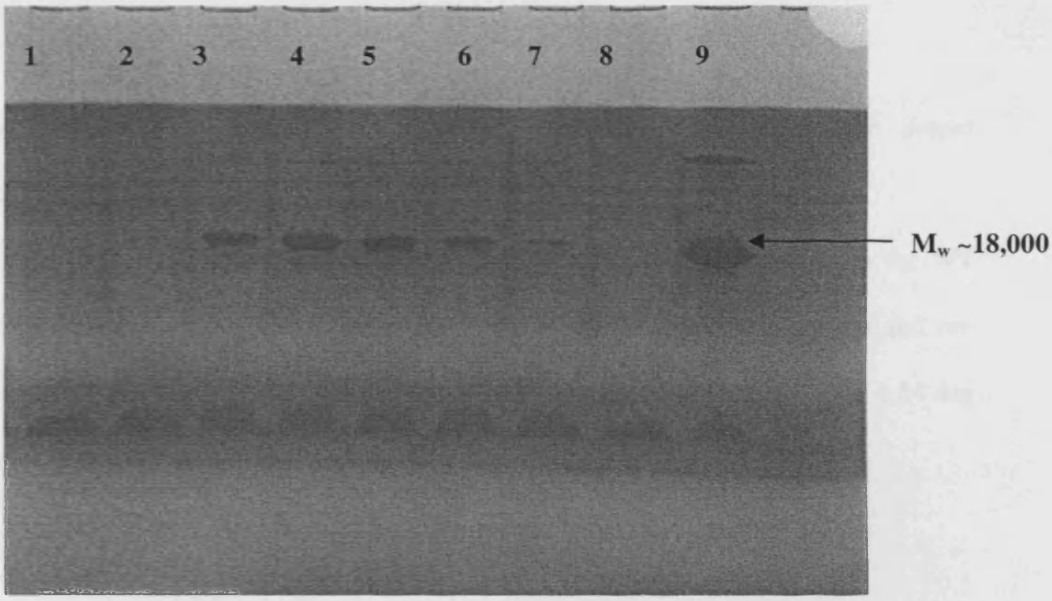

Figure 3.5: *Purification of EcDHFR by DEAE sepharose chromatography. Lane 9 is a sample of previously purified WT EcDHFR; Lane 1-8: fractions 8, 12, 16, 20, 25, 30, 35, and 40 respectively from the elution profile shown at Figure 3.4.*

Once the protein fractions that contained least contaminated with folic acid had been separated and identified the presence of protein within the solution by SDS-PAGE, further dialysis with 5 mM phosphate buffer (pH 7.0) was carried out. Dialyzed protein was lyophilized and stored at –20 °C. The concentration of EcDHFR protein solution was measured by the UV-absorbance measurement, tannin assay using BSA solutions as the standard curve, or MTX titration (Section 2.8.7).

3.4 Characterisation of EcDHFR

The far-UV CD spectrum of WT EcDHFR showed a minimum at 222 nm and a maximum at 195 nm at 25 °C (Figure 3.6). In good agreement with the values published previously [77, 160, 161], the mean residue ellipticities at 222 nm and 195 nm were –7,399 ± 182 deg cm^2 $dmol^{-1}$ and 9,856 ± 94 deg cm^2 $dmol^{-1}$ respectively. The far-UV

spectrum of EcDHFR indicated that the recombinant protein adopted the proper secondary structure.

The far-UV CD spectrum of DM EcDHFR which was very similar to the WT EcDHFR was also in good agreement with the values published by Iwakura and co-workers [159], the mean residue ellipticities at 222 nm and 195 nm were −7,689 ± 84 deg cm^2 $dmol^{-1}$ and 10,010 ± 60 deg cm^2 $dmol^{-1}$ respectively.(Figure 3.6).

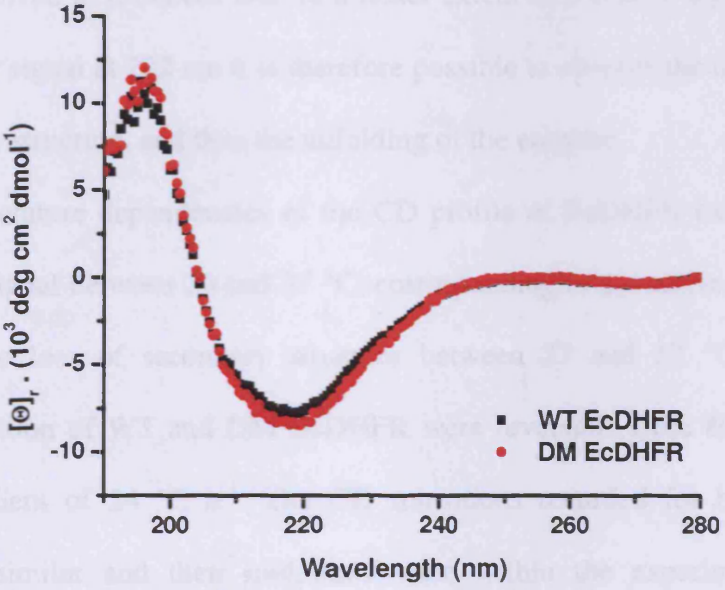

Figure 3.6: *Far-UV spectra of WT and DM EcDHFRs. All protein concentrations were 10 μM and the spectra were recorded by using a JASCO-815 spectrometer at 25 °C with a pathlength of 1 mm in 5 mM K_iPO_4 (pH 7.0).*

3.5 Thermal denaturation of EcDHFR

Thermal denaturation was used to measure the unfolding process of DHFR by a change in the CD signal at the wavelength of 222 nm as a function of temperature. This is also described as the melting temperature of a protein. The melting temperature (T_M) is where 50% of the population is unfolded (denatured) and the other half folded (native or non-denatured). The T_M of EcDHFR was measured at 222 nm (Figure 3.7). At this wavelength the CD spectra are dominated by the strong n-π^* transitions of the backbone amide bonds involved in α-helices and, to a lesser extent in β-sheets. By monitoring the change in the CD signal at 222 nm it is therefore possible to observe the disruption of the protein secondary structure, and thus the unfolding of the enzyme.

The temperature dependencies of the CD profile of EcDHFR exhibited a linear variation of the signal between 20 and 37 °C, corresponding to the native baseline, and a sharp cooperative loss of secondary structure between 37 and 57 °C (Figure 3.7). Thermal denaturation of WT and DM EcDHFR were reversible from 80 to 20 °C at a temperature gradient of 24 °C h^{-1}. The CD transitions recorded for both species of EcDHFR were similar and their midpoints were within the experimental error of measurements (50.7 ± 0.2 °C for WT and 50.9 ± 0.9 °C for DM EcDHFR). This shows that replacement of the two cysteine residues of EcDHFR caused no significance difference in thermal stability.

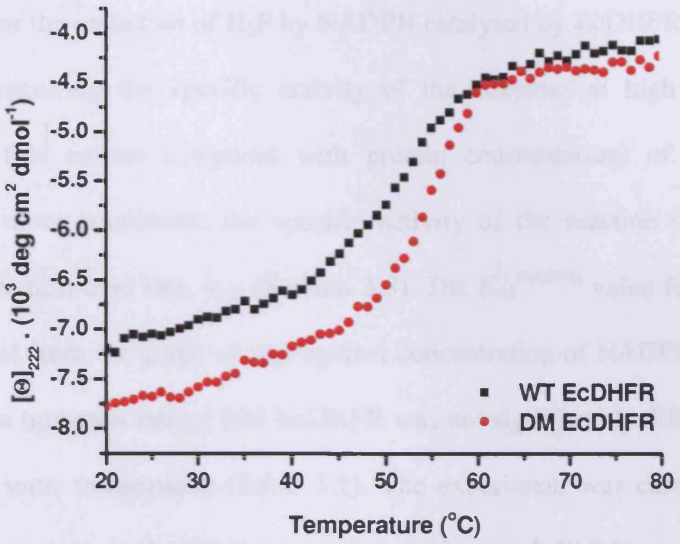

Figure 3.7: *Thermal denaturation of WT and DM EcDHFR. All protein concentrations were 10 μM and the spectra were recorded by using a JASCO-815 spectrometer from 20 to 80 °C with a pathlength of 1 mm in 5 mM K_iPO_4 (pH 7.0), and the scan rate was 24 °C h^{-1}.*

3.6 Steady state kinetics studies for EcDHFR

The velocity of the DHFR-catalysed turn-over rates of NADPH and H_2F were measured by UV spectroscopy. This relies on the difference of the absorbance maxima of the oxidised and reduced forms of the cofactor at 340 nm. At this wavelength NADPH showed a large peak while $NADP^+$ showed a very small peak. The steady state kinetics of the oxidation of NADPH to $NADP^+$ was therefore monitored by measuring the initial linear decrease of absorbance at 340 nm. The oxidation of the cofactor could be quantified by using the extinction coefficient for the reaction $\varepsilon_{340} = 11{,}800\ M^{-1}\ cm^{-1}$ [74, 154]. The specific activity, which is defined as the number of molecules of substrate(s) turned over by one molecule of enzyme per unit of time, was calculated per second. The

steady-state rate of the reduction of H_2F by NADPH catalysed by EcDHFR at *p*H 7.0 was calculated by measuring the specific activity of the enzymes at high concentration (usually 1000x fold excess compared with protein concentration) of substrate and cofactor. Under these conditions, the specific activity of the reaction is within good approximation the turn-over rate, k_{cat} (Section 3.8). The K_M^{NADPH} value for each protein can be determined from the graph of rate against concentration of NADPH used (Figure 3.8). At 25 °C the turn-over rate of DM EcDHFR was not significantly different than WT EcDHFR at the same temperature (Table 3.1). The experiment was carried out with a minimum of three repeats under the same conditions (Section 2.10.2.3).

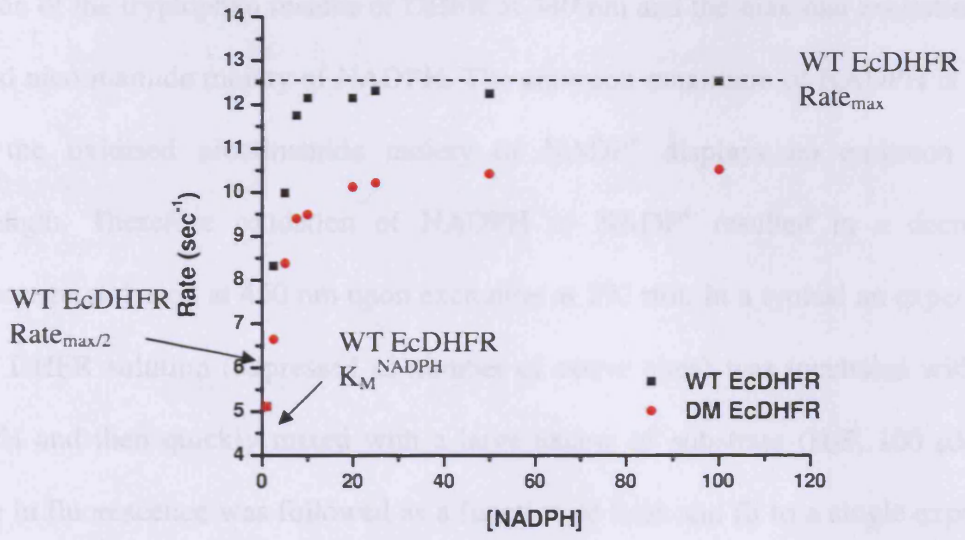

Figure 3.8: *A plot of rate of reaction of the WT and DM EcDHFRs against concentration of NADPH used. K_M^{NADPH} for each protein can be determined from the half of the maximal rate of reaction for each protein.*

Table 3.1: *Steady state kinetic parameters of WT and DM EcDHFRs. Kinetic measurements were carried out at 25 °C as previously described [162].*

EcDHFR	K_M^{NADPH} (μM)	k_{cat} (s^{-1})	k_{cat}/K_M^{NADPH} (s^{-1} μM^{-1})
WT	1.6 ± 0.1	12.2 ± 0.7	7.6
DM	2.1 ± 0.1	9.4 ± 0.4	4.5

3.7 Pre-steady state kinetics studies for EcDHFR

Stopped flow fluorescence can be used to measure the DHFR-catalysed hydride transfer. Similar to steady state kinetics, the ability of stopped flow to monitor the hydride transfer relies on the differences between the adsorption spectra of the reduced and oxidized cofactor. This technique relied additionally on the overlap of the maximal emission of the tryptophan residue of DHFR at 340 nm and the maximal excitation of the reduced nicotinamide moiety of NADPH. The emission maximum of NADPH is 450 nm while the oxidised nicotinamide moiety of $NADP^+$ displays no emission at this wavelength. Therefore oxidation of NADPH to $NADP^+$ resulted in a decrease of fluorescence emission at 450 nm upon excitation at 292 nm. In a typical an experiment 8 μM of DHFR solution (expressed as number of active sites) was incubated with 4 μM NADPH and then quickly mixed with a large excess of substrate (H_2F, 100 μM). The change in fluorescence was followed as a function of time and fit to a single exponential (Figure 3.9). Varying the concentration of NADPH (from 2 to 10 μM) did not affect the reaction rate [74]. The reaction catalysed by DM EcDHFR occurred at a rate of 191 ± 6 s^{-1} at *p*H 7.0 and 25 °C, similar to the hydride transfer rate for WT EcDHFR at the same temperature (Table 3.2). The experiment was carried out with a minimum of three repeats under the same conditions.

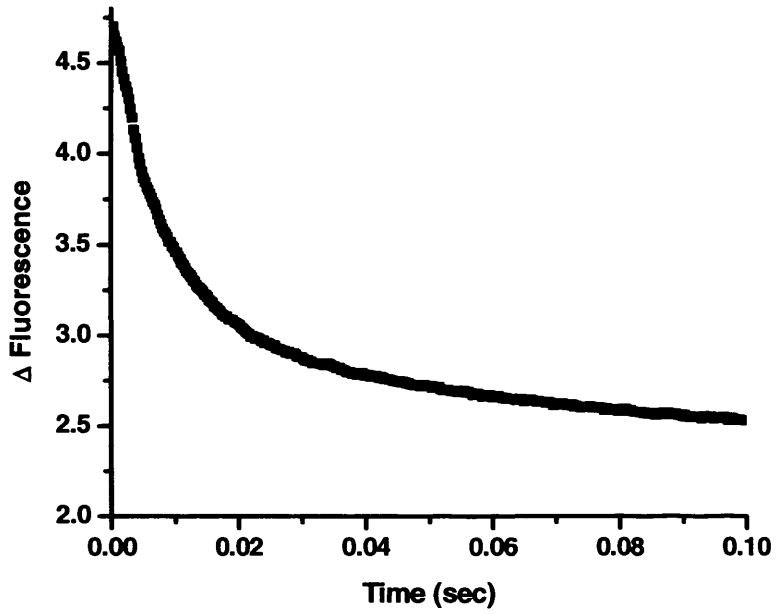

Figure 3.9: *Stopped flow fluorescence energy transfer experiment of EcDHFR with catalysed hydride transfer from NADPH to DHFR. The enzyme (8 μM) was preincubated NADPH (4 μM) in MTEN buffer (pH 7.0) and the reaction was initiated by the addition of an equal volume of* H_2F *(100 μM) at 25 °C (Section 2.10.2.2).*

Table 3.2: *Pre-steady state kinetic parameters of WT and DM EcDHFR. Kinetic measurements were carried out at 25 °C.*

EcDHFR	k_H (s^{-1})
WT	223 ± 5
DM	191 ± 6

3.8 Estimate for k_{cat}, K_M and catalytic efficiency for the EcDHFR catalysed reaction

The Michaelis-Menten model (Equation 3.1) is widely used to provide a phenomenological description of enzyme catalysis

$$E + S \underset{k_2}{\overset{k_1}{\rightleftharpoons}} ES \xrightarrow{k_{cat}} E + S \qquad \textit{Equation 3.1}$$

Where E represents the enzyme, S the substrate, ES the enzyme substrate complex and P is the reaction product. The rate constants k_1, k_2, and k_{cat} indicate the rate associated with each step of the catalytic process (note that k_{cat} is not hydride transfer, but it includes all the kinetic steps of the catalytic mechanism). The velocity of the reaction (V), expressed as rate of breakdown of the complex ES, can be expressed as a function of the reaction constants, the maximum velocity (V_{max}) and the concentration of the substrate ([S]) (Equation 3.2), where $k_{cat} = V_{max} / [E]_T$ and $K_M = (k_2 + k_{cat})/k_1$

$$V = (V_{max}.[S]) / (K_M + [S])$$

Equation 3.2

k_{cat} is the *turnover number* of the enzyme and represents the maximum number of substrate molecules converted to product per active site per unit of time, while K_M is defined as the concentration of the substrate at which the velocity of the reaction is half the maximum velocity and is generally a good indication of the affinity of the enzyme for the substrate. In these reactions, the Michaelis-Menten equation is used and the parameters k_{cat} and K_M indicate the speed of the reaction and the affinity for the enzyme to the substrate/cofactor, respectively. In the EcDHFR case, these catalytic parameters (k_{cat} and K_M) were calculated under pseudo first order conditions [74], by measuring the steady state reaction rate at saturating concentration of NADPH (or H_2F) and varying the concentration of the H_2F (or NADPH). From a previous study at *p*H 7.0 and 25 °C the values of K_M for H_2F and NADPH were 1.0 and 5.0 μM respectively, and the k_{cat} 10.1 and 12.2 s^{-1} respectively [74].

The calculated catalytic efficiency (k_{cat}/K_M) of DM EcDHFR for NADPH was slightly lower but not significantly different to that of WT EcDHFR at 25 °C (Table 3.1) and these results are comparable to those reported by Iwakura and co-workers [159].

3.9 Urea denaturation/equilibrium unfolding of EcDHFR

Previous studies showed that denaturing agents such as urea and guanidium hydrochloride (GdnHCl) exhibit favourable interactions with non-polar solutes and substituent groups, and polar groups of amides and peptides [155, 163]. Both polar and non-polar interactions provide the driving force for the denaturation of proteins by urea and related compounds. The nature of its interactions of denaturation with amine and peptide groups has been discussed elsewhere [164, 165].

A typical urea denaturation curve is shown in Figure 3.10a. When a protein unfolds by a two-state mechanism, the equilibrium constant, K, can be calculated from the experiment data by using:

$$K = [(y)_N - (y)] / [(y)-(y)_D] \qquad \textit{Equation 3.3}$$

Where (y) is the observed value of the parameter used to follow unfolding, and $(y)_N$ and $(y)_D$ are the values (y) would have for the native state and the denatured state under the same conditions where (y) was measured. In the original analyses of urea denaturation curves [166, 167], log K was found to vary linearly as a function of log [urea], and the slope of the plot was denoted by n, and the midpoint of the curve by $[urea]_{1/2}$ (where log K = 0). These parameters could than be used to calculate the dependence of the standard free energy of denaturation, $\Delta G°$ (= -RT ln K), on urea concentration with [156]:

$$d(\Delta G°)/d[urea] = RTn/[urea]_{1/2} \qquad \textit{Equation 3.4}$$

This equation was used by Alexander and Pace [166] to estimate the difference in stability among three genetic variants of a protein for the first time, and was the forerunner of the linear extrapolation method.

The linear extrapolation method (LEM) was first used to analyze urea and

GdnHCl denaturation curves by Greene and Pace [168]. When $\Delta G°$ is calculated as a function of urea concentration by using data such as those shown in Figure 3.10a, $\Delta G°$ is found to vary linearly with urea concentration as shown in Figure 3.10b. Based on results such as these for several proteins, this equation was proposed for analyzing the data:

$$\Delta G° = \Delta G°(H_2O) - m[\text{urea}]$$

Equation 3.5

where $\Delta G°(H_2O)$ is an estimate of the conformational stability of a protein that assumes that the linear dependence continues to 0 M denaturant (i.e. urea) and m is a measure of the dependence of ΔG on urea concentration, *i.e.*, the slope of the plot shown in Figure 3.10b. The same approach has been proposed for measuring the stability of RNA molecules [169].

The linear extrapolation method is now widely used for estimating the conformational stability of proteins and for measuring the difference in stability between proteins differing slightly in structure.

Equilibrium urea titrations were performed on EcDHFR and monitored by tryptophan fluorescence emission (Figure 3.9). This studied can be determined by titrating these EcDHFR with urea while monitoring the absorbance spectrum at 292 nm [160]. The observation of inflections in the fluorescence titration curves at ~2 M urea implies that DHFR undergoes a two-state unfolding transition. The difference in free energy, as determined by global fitting of the fluorescence data, between the native and denatured states of DM EcDHFR, 5.2 kcal mol^{-1} (Table 3.3), is similar to that for WT EcDHFR, 5.9 kcal mol^{-1} [159, 170]. This shows that the stability of the cysteine-free variant, DM EcDHFR, is similar to the WT protein, an observation previously reported by Iwakura and coworkers [159].

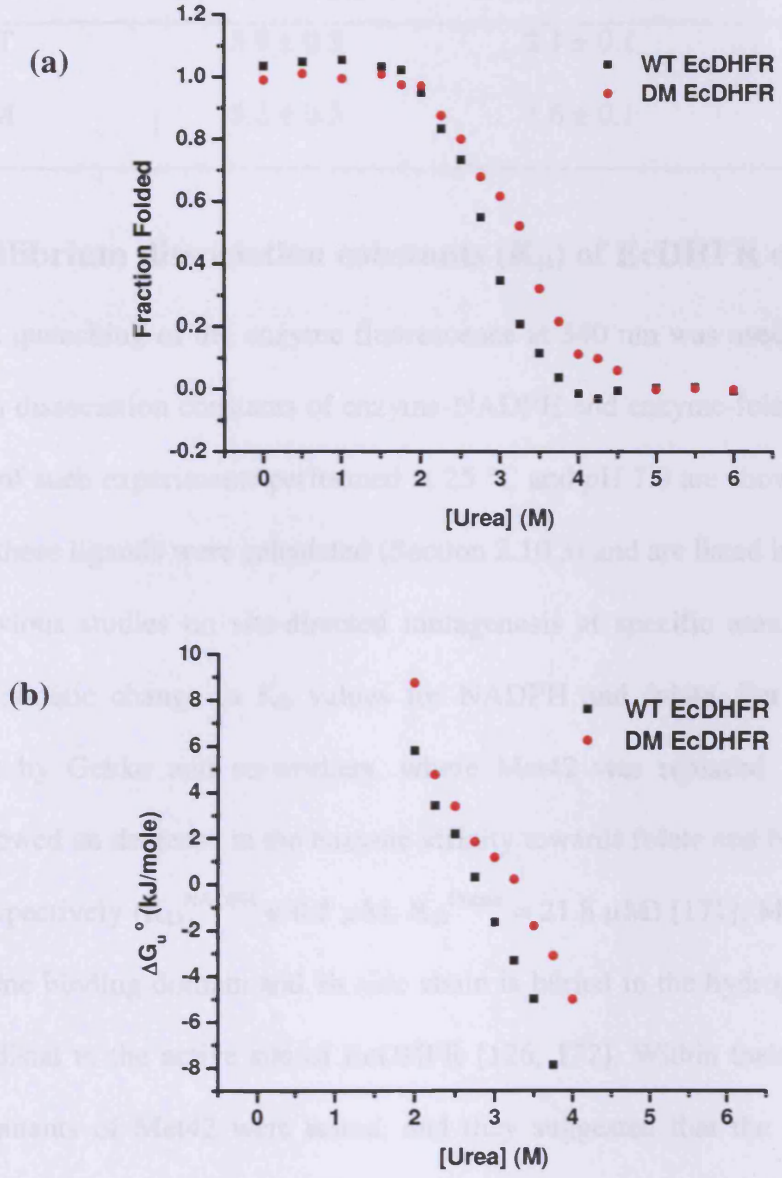

Figure 3.10: *Urea titration of WT and DM EcDHFR monitored by fluorescence. (a) Urea denaturation profile of the WT and DM EcDHFRs at 340 nm. All protein concentration were 2 μM and the spectra were recorded by using a PerkinElmer LS 55 Luminescence spectrometer at 20 °C in 5 mM K_iPO_4 (pH 7.0). (b) Plot of the free energy of unfolding in the presence of urea versus the urea concentration.*

Table 3.3: *Thermodynamic parameters obtained from equilibrium urea denaturation of EcDHFR*

EcDHFR	$\Delta G°$ (kcal mol^{-1})	m (kcal $mol^{-1}M^{-1}$)	C_m (M)
WT	5.9 ± 0.3	2.1 ± 0.1	2.8 ± 0.1
DM	5.2 ± 0.3	1.6 ± 0.1	3.1 ± 0.1

3.10 Equilibrium dissociation constants (K_D) of EcDHFR complexes

The quenching of the enzyme fluorescence at 340 nm was used to determine the equilibrium dissociation constants of enzyme-NADPH and enzyme-folate complexes and the results of such experiments performed at 25 °C and *p*H 7.0 are shown in Figure 3.11. The K_D of these ligands were calculated (Section 2.10.3) and are listed in Table 3.4.

Previous studies on site-directed mutagenesis at specific areas of DHFR have shown a dramatic change in K_D values for NADPH and folate. For example studies carried out by Gekko and co-workers, where Met42 was replaced with a trytophan residue, showed an decrease in the enzyme affinity towards folate and NADPH by 5- and 11- fold respectively (K_D^{NADPH} = 0.5 μM; K_D^{Folate} = 21.8 μM) [171]. Met42 is located in the adenosine binding domain and its side chain is buried in the hydrophobic core. This residue is distal to the active site of EcDHFR [126, 172]. Within their experiments, 14 different mutants of Met42 were tested, and they suggested that the introduction of a hydrophilic side chain at residue 42 disrupts the hydrophic interaction with the side chain of Ile50 (which comes directly into contact with the *p*-aminobenzoyl moiety of the substrate), consequently decreasing the affinity of the substrate. Thus the side-chain hydrophobicity at residue 42 would enhance the enzyme function mainly by decreasing the affinity of the substrate. These results showed that the affinities for coenzyme and

substrate may be influenced by the selected site of mutation.

From the results shown in Table 3.4, DM-EcDHFR has a similar K_D values for NADPH and folate to WT EcDHFR. These suggest that the affinities for coenzyme and substrate are not significantly changed in DM-EcDHFR.

The binding of the EcDHFR with its coenzyme and folate appears to be with a 1:1 stoichiometry, and this has been investigated by Dunn and coworkers [123]. Therefore we were able to use this technique to determine the equilibrium dissociation constants between the ligands and enzyme.

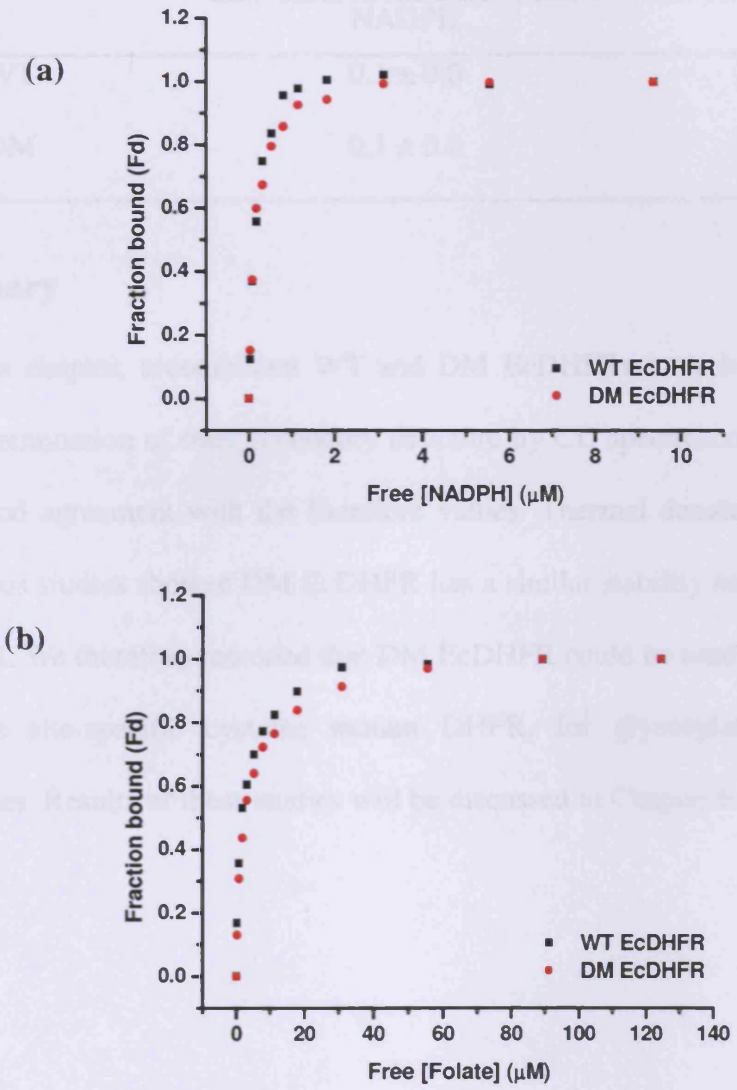

Figure 3.11: *NADPH (a) and folate (b) concentration dependence of the fluorescence intensity at 340 nm of WT and DM EcDHFRs. All protein concentrations were 0.05 μM (a) and 0.5 μM (b) and the spectra were recorded by using a PerkinElmer LS 55 Luminescence spectrometer at 25 °C in 50 mM K_iPO_4 (pH 7.0) containing 50 mM NaCl, 0.1 mM EDTA and 0.1 mM dithiothreitol (DTT). Curves are theoretical fits to Equation 2.5 (Section 2.10.3) with the parameter values listed in Table 3.4.*

Table 3.4: *Equilibrium dissociation constants of NADPH and folate parameter values of the WT and DM EcDHFRs at 25 °C and pH 7.0*

.

EcDHFR	K_D (μM)	K_D (μM)
	NADPH	Folate
WT	0.1 ± 0.0	2.1 ± 0.1
DM	0.1 ± 0.0	2.1 ± 0.2

3.11 Summary

In this chapter, recombinant WT and DM EcDHFRs have been expressed and purified. Determination of their secondary structure by CD spectroscopy showed similar results in good agreement with the literature values. Thermal denaturation studies and kinetic analysis studies showed DM EcDHFR has a similar stability and catalytic activity as WT DHFR. We therefore reasoned that DM EcDHFR could be used as a base template to synthesise site-specific cysteine mutant DHFR, for glycosylated with glycosyl haloacetamides. Results of these studies will be discussed in Chapter 6.

Chapter 4

Synthesis and Analysis of EcDHFR triple mutants

4.1 Introduction

Following the successful preparation of the DM EcDHFR and a comparison of its stability with the WT protein (see Chapter 3) the next aim was to synthesise different triple mutants of EcDHFR which would be able to undergo glycosylation (see Chapter 5). A single cysteine residue was introduced at specific sites of the DM EcDHFR *via* site-directed mutagenesis (see Section 2.6). Four different unique sites were selected. Positions 18 and 132 were located in the loop region, position 52 was located in the adenosine binding domain, and position 87 was located in the hinge region between the adenosine binding and loop domain of EcDHFR (Figure 4.1). These four exposed selected position was selected using the X-ray crystal structure of EcDHFR [107].

Loops are common secondary structural elements which are also defined by a contiguous segment of polypeptide. They lack regular dihedral angles and hydrogen bonding patterns and allow the protein backbone to reverse direction in three-dimensional space [173, 174]. They are variable in length and composition and are usually situated near the surface of proteins where they can play a role in ligand interaction and biological recognition. As has been pointed out by Leszczynski and co-workers, loops are excellent candidates for protein engineering studies [173].

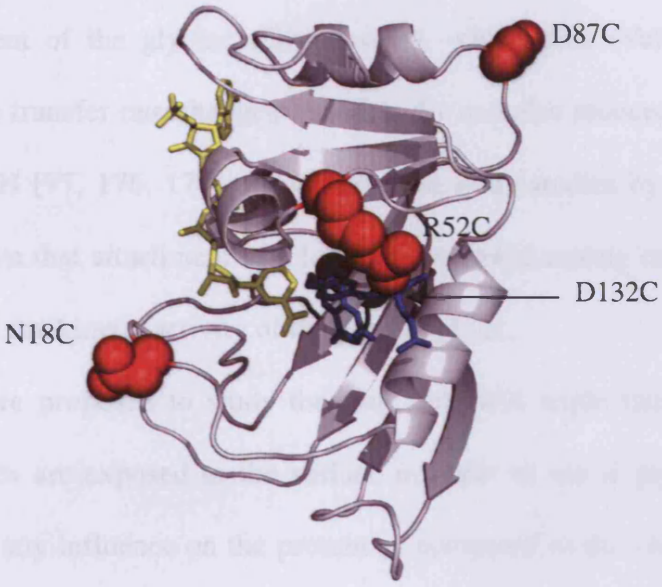

Figure 4.1: *Structural overview of EcDHFR. The four unique sites are labeled in red. Folate and NADP$^+$ are drawn in stick format and indicated in blue and yellow respectively in the ternary complex (1RA2). The structure is oriented so that the co-factor nicotinamide ring is in the plane of paper [78, 108].*

According to X-ray crystallographic studies, the Met20 loop is one of the most mobile structural element in the entire enzyme molecule. Three conformations of the protein have been observed during the protein catalysis [107]. The central section of Met20 loop, residues 16-20, is disordered in the apoenzyme and the NADP$^+$-holoenzyme crystal structures, generating an opening of the active-site cavity to solvent. The binding of ligands (*i.e.* folate, NADPH/NADP$^+$) causes the disordered segment of the loop to move as a result of stabilizing hydrogen bonds between residues in the Met20 and the F-G loops (See Section 1.7). The backbone nitrogen atoms of these loops displayed high dynamic mobility in NMR relaxation experiments, which has been interpreted to suggest a connection between the dynamic properties of these loops and the catalytic behaviour

of DHFR [138, 175].

Previous studies by site-directed mutagenesis at position 121, a highly mobile residue located in the middle of the F-G loop over 19 Å from the active site have shown that the replacement of the glycine (Gly) residue, with valine (Val) or leucine (Leu) slowed the hydride transfer rate changed dramatically and also reduced the affinity of the protein for NADPH [77, 176, 177]. In addition, previous studies by Benkovic and co-workers have shown that attachment of a large hydrophobic moiety on the surface of the Met20 loop altered the kinetic activity of the protein [126].

We therefore proposed to study the four EcDHFR triple mutants because their point mutation sites are exposed to the surface in order to see if glycosylation on this position will have any influence on the protein as compared to the observed results with DM and WT EcDHFR. This chapter presents a detailed description of the entire study of DM-N18C, DM-R52C, DM-D87C, and DM-D132C EcDHFR mutants for obtaining results that will be taken as reference values in the following chapters, where site-selective glycosylation is involved.

4.2 Expression and purification of the EcDHFR mutants

The four EcDHFR triple mutants (DM-N18C, DM-R52C, DM-D87C and DM-D132C) were constructed by oligonucleotide site-directed mutagenesis. To synthesize these proteins, a single *E. coli* BL21(DE3) colony containing DM-N18C, DM-R52C, DM-D87C or DM-D132C EcDHFR was expressed for protein. The expressed mutant enzymes were purified according to the protocol used for the wild-type protein (Sections 3.2 and 3.3). The recombinant EcDHFR triple mutants have calculated masses between

17,932 and 17,990, therefore within the SDS-PAGE analysis of the purified EcDHFR triple mutants showed a single band of similar mass to WT EcDHFR (see Figure 3.2). The concentration of the mutants was determined using the methotrexate (MTX) titration method (Section 2.8.7.3).

4.3 Characterisation and thermal denaturation of EcDHFR mutants

CD spectroscopy was used to investigate the structure of the four mutant enzymes by comparison with WT EcDHFR. The far-UV CD spectra of the mutants showed some differences. While the overall shape of the spectra were similar the molar ellipticity at 222 nm measured for the four mutants varied between -6,718 and -7,695 deg cm^2 $dmol^{-1}$ (Figure 4.2 and Table 4.1) From the observed values for each of the EcDHFR triple mutants at 222 nm, they are comparable to the WT EcDHFR. This suggests that while the secondary structure of the mutant may be similar to that of the wild-type protein, but the packing might be slightly different.

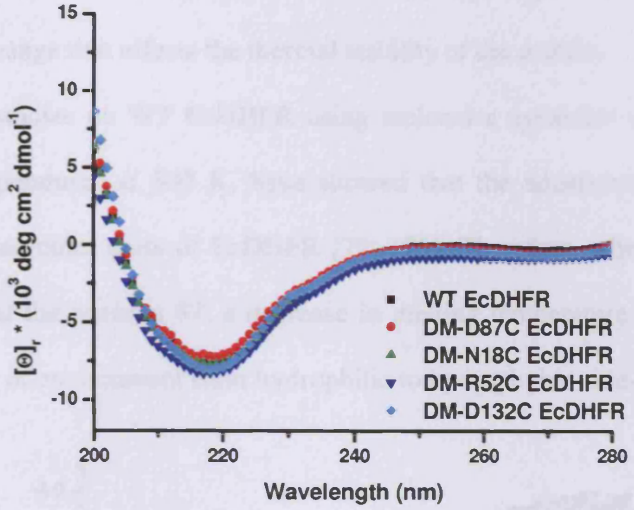

Figure 4.2: *Far-UV spectra of DM-N18C, DM-R52C, DM-D87C, DM-D132C and WT EcDHFRs. All protein concentration were 10 μM and the spectra were recorded using Applied Photophysics Chirascan CD spectrometer at 25 °C with a pathlength of 1 mm in 5 mM K_iPO_4 (pH 7.0).*

The thermal stability of the EcDHFR triple mutants was studied according to the protocol used for the WT and DM proteins. Thermal denaturation of the four triple mutant proteins was reversible from 20 to 80 °C at a temperature gradient of 24 °C h^{-1} (Figure 4.3). The CD transitions recorded for DM-N18C, DM-R52C, and DM-D132C EcDHFR were similar and their midpoints were within the experimental error of measurements (Table 4.1). Interestingly, DM-D87C has a lower thermal denaturation temperature by ~9 °C compared to WT EcDHFR, even though there is no highly significant difference in its secondary structure to the wild-type protein [159]. This suggested that replacement of cysteine residues of EcDHFR in a specific site may affects the protein thermal stability. Therefore, when position 87 is replaced with the hydrophobic side chain of a cysteine residue, the thermal stability of the protein is

reduced compared to the wild-type protein. This mutation might have generated a local conformational change that affects the thermal stability of the protein.

Previous studies on WT EcDHFR using molecular dynamics (MD) simulations against high temperatures at 500 K, have showed that the adenosine binding domain unfolds earlier than other parts of EcDHFR [77, 178]. Therefore, when we introduce a cysteine residue at the position 87, a decrease in melting temperature may be observed due to the change of environment from hydrophilic to hydrophobic side-chain residue.

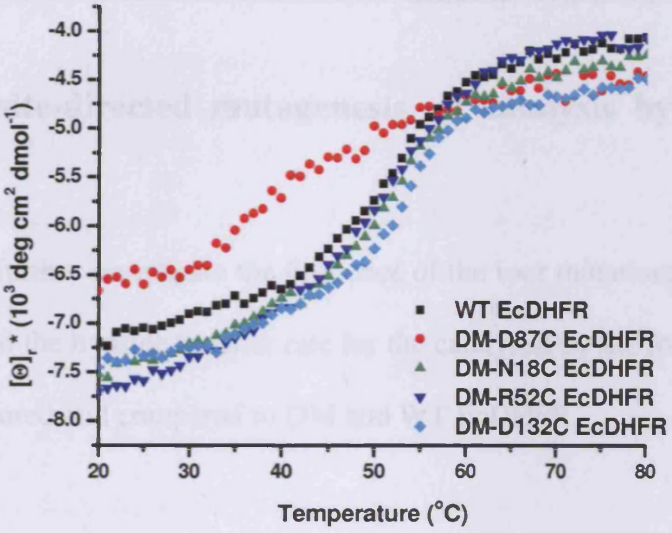

Figure 4.3: *Thermal denaturation of DM-N18C, DM-R52C, DM-D87C, DM-D132C and WT EcDHFRs. All protein concentrations were 10 μM and the spectra were recorded using a Applied Photophysics Chirascan CD spectrometer from 20 to 80 °C with a pathlength of 1 mm in 5 mM K_iPO_4 (pH 7.0), and the scan rate was 24 °C h^{-1}.*

Table 4.1: *Structural parameters for WT and DM EcDHFR, and the four triple mutants.*

EcDHFR	$[\Theta]_{222}$ deg cm^2 $dmol^{-1}$	T_M (°C)
WT	-7,399 ± 182	50.7 ± 0.2
DM	–7,689 ± 84	50.9 ± 0.9
DM-N18C	-7,398 ± 123	50.5 ± 0.4
DM-R52C	-7,695 ± 17	49.7 ± 0.5
DM-D87C	-6,718 ± 50	40.9 ± 0.3
DM-D132C	-7,417 ± 37	50.7 ± 0.3

4.4 Effects of site-directed mutagenesis on catalysis by the EcDHFR triple mutant

In order to further investigate the influence of the four mutations on EcDHFR, the steady-state rate and the hydride transfer rate for the catalysed by the four EcDHFR triple mutants were measured and compared to DM and WT EcDHFR.

4.4.1 Steady-state kinetic studies

The k_{cat} value of each mutant was measured by absorbance spectroscopy under conditions of excess substrate and cofactor (Section 3.6). K_M^{NADPH} was determined instead of K_M^{H2F}, because NADPH is more stable than H_2F, and the presence of impurities such as folate within the H_2F solution leads to inaccuracies in the determination of the H_2F concentration which is problematic when determining the K_M value.

From the observed results in Table 4.2, the mutant of DM-N18C has a similar k_{cat}/K_M^{NADPH} value to the DM and wild type protein. The DM-R52C, DM-D87C, and DM-D132C mutants have a lower k_{cat}/K_M^{NADPH} value than the DM and wild type protein. The difference catalytic efficiency values of each protein are due to the individual protein having a high K_M^{NADPH} value or low catalytic constant rate of reaction.

At 25 °C, the R52C mutant showed a ~2-fold decrease in the steady state rate; however there is not much difference in the K_M^{NADPH} value when compared with the wild-type protein (Table 4.2). Mutations at position 87 and 132 showed similar steady state rate as the wild type protein, however they had a lower catalytic efficiency because their K_M value is affected (Table 4.2). The mutants of DM-87C and DM-D132C showed two to three times lower affinity towards NADPH. It interesting to observe a lower catalytic efficiency for DM-D87C and DM-D132C, since these sites were located away from the catalytic centre and do not have any direct contact with the co-enzyme or substrates. Furthermore, no alteration of the protein secondary structure has been observed following the introduction of cysteine at these sites (Figure 4.2). The observed low values of k_{cat} or high values of K_M of these mutants may due to a change of local conformational by introduction of cysteine at the selected sites in the protein.

Table 4.2: *Steady state kinetic parameters for WT and DM EcDHFR, and the four triple mutants. Kinetic measurements were carried out at 25 °C*

EcDHFR	K_M^{NADPH} (μM)	k_{cat} (s^{-1})	k_{cat}/K_M^{NADPH} ($\mu M^{-1}s^{-1}$)
WT	1.6 ± 0.1	12.2 ± 0.7	7.6
DM	2.1 ± 0.1	9.4 ± 0.4	4.5
DM-N18C	1.5 ± 0.1	10.4 ± 1.5	6.9
DM-R52C	2.1 ± 0.1	4.9 ± 0.6	2.3
DM-D87C	4.9 ± 1.7	9.1 ± 0.1	1.9
DM-D132C	3.6 ± 0.1	12.6 ± 1.3	3.5

4.4.2. Pre-steady state kinetic studies

The hydride transfer reaction catalysed by DM-N18C, DM-R52C, DM-D87C, and DM-D132C were measured by stopped flow FRET at 25 °C under the conditions of excess H_2F (Section 3.6). This methodology is very sensitive, and allows observation not only of the reduction of NADPH to $NADP^+$, but also of conformational changes of the enzyme that will affects the distance between the two chromophores (the NADPH and the tryptophan). The resulting traces were fitted to a single exponential decay. The reaction catalyzed by the four triple mutants of EcDHFR showed very small changes in hydride transfer rate compared with the wild-type (Table 4.3). From the observation of the hydride transfer rate for the DM-R52C and DM-D132C (Table 4.2), when we introduced a hydrophobic residue such as the cysteine residue at that position, it has increased their single turn-over rates compared to DM and wild-type DHFR. The introduction of the cysteine residue on the loop seems have enhanced the hydride transfer rate of the triple mutants EcDHFR. Therefore we observed an increased of k_H rate from 223 to 309 s^{-1} for

the DM-R52C and DM-D132C EcDHFR. The experiment was carried out with a minimum of 3 repeats under the same conditions (Section 2.10.2.4).

Table 4.3: *Pre-steady state kinetic parameters for the DM-N18C, DM-R52C, DM-D87C, DM-D132C, DM and WT EcDHFR. Kinetic measurements were carried out at 25 °C.*

EcDHFR	k_H (s^{-1})
WT	223 ± 5
DM	191 ± 6
DM-N18C	174 ± 26
DM-R52C	305 ± 8
DM-D87C	162 ± 3
DM-D132C	309 ± 8

4.5 Urea denaturation/equilibrium unfolding of triple mutant EcDHFRs

The equilibrium urea titrations were performed on the EcDHFRs triple mutants and monitored by tryptophan fluorescence emission as previously described (Section 3.8). The difference in free energy, as determined by global fitting of the fluorescence urea titration data, between the native and denatured states of the DM-N18C, DM-R52C, and DM-D132C mutants showed similar difference in free energy (ΔG°)values to the wild-type protein (Table 4.4)

Interestingly, DM-D87C mutant showed the lowest ΔG° value, 2.7 kcal mol^{-1} (Table 4.3) compared to the other triple mutants and WT EcDHFR, and this value is about half that of the WT or DM EcDHFR [159]. This shows that the replacement of the cysteine residue at position 87 has an influence on the protein stability. Although we

observed no significant changes in the secondary structure for DM-D87C compared with the wild type protein *via* far-UV CD spectrum, the replacement of cysteine at 87 may have affected the protein's tertiary conformation. As mentioned earlier, position 87 is located at the hinge-bending region, and the replacement of a hydrophobic residue onto this site may have unfavorable effects on the two domains, which may lead to early protein degradation. Therefore a decrease in the thermal and chemical stability of DM-D87C EcDHFR has been observed.

Table 4.4: *Thermodynamic parameter values obtained from equilibrium urea denaturation for the DM-N18C, DM-R52C, DM-D87C, DM-D132C, DM and WT EcDHFR.*

EcDHFR	$\Delta G°$ (kcal mol^{-1})	M (kcal mol^{-1} M^{-1})	C_m (M)
WT	5.9 ± 0.3	2.1 ± 0.1	2.8 ± 0.1
DM	5.2 ± 0.3	1.6 ± 0.1	3.1 ± 0.1
DM-N18C	5.3 ± 0.3	2.3 ± 0.4	2.6 ± 0.1
DM-R52C	5.7 ± 0.2	2.1 ± 0.3	2.6 ± 0.1
DM-D87C	2.7 ± 0.2	1.4 ± 0.2	2.1 ± 0.1
DM-D132C	5.5 ± 0.3	2.6 ± 0.1	3.0 ± 0.1

4.6 Equilibrium dissociation constant (K_D) of EcDHFR triple mutants complexes

Measurement of the equilibrium dissociation constants for the complexes of NADPH/folate with the four triple mutants of EcDHFR was performed as described for the wild-type protein at 25 °C and *p*H 7.0 (Section 3.9). From the observed results (Table 4.5), all the EcDHFRs triple mutants have a similar K_D values for NADPH to WT EcDHFR. However there is a slight difference in K_D values for the protein:folate complexes. From Table 4.5, DM-R52C EcDHFR showed ~3 times higher values of K_D (folate) compared with the wild-type protein. By observing their single-turnover rate/hydride transfer rate (Tables 4.2 and 4.3), all these mutants showed comparable results to the wild-type enzyme, and this is in agreement with their K_D (NADPH) values. By comparing the steady state rates of these mutant proteins (Table 4.2), DM-R52C mutant showed a lower steady state rate than the wild type protein. It seems, when we substitute position 52 with a cysteine residue, it has an influence on the protein's affinity towards folate. Interestingly, no major conformational change had occured within the mutant protein, as noted from the far-UV CD spectrum. The binding affinity values between the NADPH and proteins are so low, that we are not able to conclude if there are any differences between the mutants of EcDHFRs. However, from the K_D binding between folate (homologous for H_2F/H_4F) and mutant proteins, we are able to observe that there is a correlation between the binding affinity with the steady state rate of reaction (Table 4.2). The mutant DM-R52C showed three times weaker binding to folate, compared with the DM and wild type protein, and also had the slowest turnover rate among the four triple mutant EcDHFRs (Tables 4.2 and 4.5).

Table 4.5: *Equilibrium dissociation constants of NADPH and folate parameter values of the DM-N18C, DM-R52C, DM-D87C, DM-D132C, DM and WT EcDHFRs at 25 °C and pH 7.0*

EcDHFR	K_D (μM)	
	NADPH	Folate
WT	0.10 ± 0.03	2.05 ± 0.05
DM	0.12 ± 0.02	2.11 ± 0.12
DM-N18C	0.22 ± 0.03	2.97 ± 0.25
DM-R52C	0.19 ± 0.05	6.32 ± 0.16
DM-D87C	0.13 ± 0.01	3.13 ± 0.21
DM-D132C	0.17 ± 0.08	2.11 ± 0.01

4.7 Conclusions

Recombinant DM-N18C, DM-R52C, DM-D87C, and DM-D132C EcDHFR mutants have been expressed and purified. CD spectra were comparable as the wild type protein showing that 2° structure of the protein was not affected. Thermal denaturation studies showed that the DM-N18C, DM-R52C, and DM-D132C EcDHFR mutants have similar stability to wild type protein, whereas the DM-D87C mutant does not. It has a lower thermal stability by 10 °C compared to the WT protein. In addition urea denaturation equilibrium unfolding studies showed that DM-D87C mutant has a lower ΔG° value compared to wild type protein. This result is in agreement with values obtained from thermal denaturation studies using CD spectroscopy. It seems that introduction of a hydrophobic residue into the highly exposed site 87 altered the protein stability. By comparing the amino acid sequence of DHFR between other species (*i.e. Moritella profunda*, *E. coli*, and *Enterobacter aerogenes*), the aspartic acid residue at

position 87, is a conserved residue. Therefore, we assume the introduction of a hydrophobic residue at position 87 might generate a local conformational change that affects the thermal stability of the protein. As the result lower thermal and chemical stability values are observed.

Kinetic studies of DM-N18C, DM-R52C, DM-D87C and DM-D132C EcDHFR mutants showed comparable results to wild type protein. Although there is a slight change in the values for some of the mutants compared with the wild type protein, these changes are not very large.

From the X-ray crystal structure of EcDHFR, R52 is located at the adenosine binding domain and situated near the glutamate moiety of the substrate (*i.e.* folate/H_2F). Although there was no direct evidence to show that there was an alteration of the bonding between R52C with the glutamate of the substrate. However, when we introduced the position 52 with cysteine residue, might generate a local conformational change that affects the postion 52 with the glutamate of the substrate. As the result, we observed a low binding affinity value between the DM-R52C with folate (Table 4.5). The weaker binding of this mutant towards folate, seems has affected the mutant catalytic rate.

This study shows that the introduction of a hydrophobic residue at a specific site can affect the stability and kinetic reactivity of the protein. These results will be used as a baseline for the investigation of whether glycosylation of those sites has any affect on the overall stability and kinetic reactivity of the protein.

Chapter 5

Synthesis and Purification of Glycosylated EcDHFR

5.1 Introduction

Glycosylation is important for many molecular processes such as molecular recognition, degradation and stability. Surface glycoproteins act as markers in the communication between cells during immune responses, inflammation and microbial virulence [179-181]. The correct glycosylation of proteins is important for their proper folding *in vivo* [182]. The presence of sugars on proteins has been shown to modulate their kinetic properties and stability [183].

However the scope of studies into specific *in vitro* glycosylation of proteins has until recently been limited and complicated by the fact that natural glycoproteins normally occur as mixtures of glycoforms that carry different sugars in different positions on the same protein backbone. The biological importance of glycoconjugates and their increasing importance as therapeutic agents make the synthesis of homogeneous glycoproteins an important task.

The different properties exhibited by each glycoforms within these microheterogeneous mixtures present cause regulatory difficulties [184] and problems in determining the exact function through structure-activity relationships. It has even been suggested that these naturally occurring mixture of glycoforms provide a spectrum of activities that can be biased in one direction or another as a means of fine-tuning [185]. Previous studies of single glycoforms by Dwek and co-workers [185] has been successful, however their methodology required abundant sources and extensive chromatography. There is therefore an urgent need for alternative sources of homogeneous glycoproteins.

The use of natural enzymes allows the site-selective introduction of sugars but is limited to natural glycans and by often relatively poor yields. Chemical glycosylation

reactions, however, which are more flexible with respect to the choice of glycan, suffer from limited site-selectivity. Despite significant advances in convergent synthesis using approaches such as native peptide ligation and ligation of a peptide with expressed protein fragments, the chemical synthesis of proteins is still a formidable task [186]. In addition, while methods for the synthesis of large structurally-defined oligosaccharides have recently been developed, oligosaccharide synthesis is still not routine [72].

Several methods have been described for the generation of neoglycoproteins (modified glycoprotein that resembles native glycoprotein) *via* site-selective glycosylation of proteins by chemical modification of biotechnologically produced proteins. Among the first approach was that of Flitsch and co-workers, who used the combination of the introduction of unique cysteine residues at the required sites, and a highly flexible but selective chemical derivatisation strategy (Scheme 5.1). The reaction of the free thiol group of a cysteine residue with a chemically-synthesized glycosyl iodoacetamide produces a stable linkage between the protein and the carbohydrate that resembles that found in the native glycosylation of asparagine residues [67, 70, 187]. Later this method was applied by Wong and co-workers to introduced chitotriose and a heptasaccharide stripped from the surface of horseradish peroxidase to bovine serum albumin (BSA) [69].

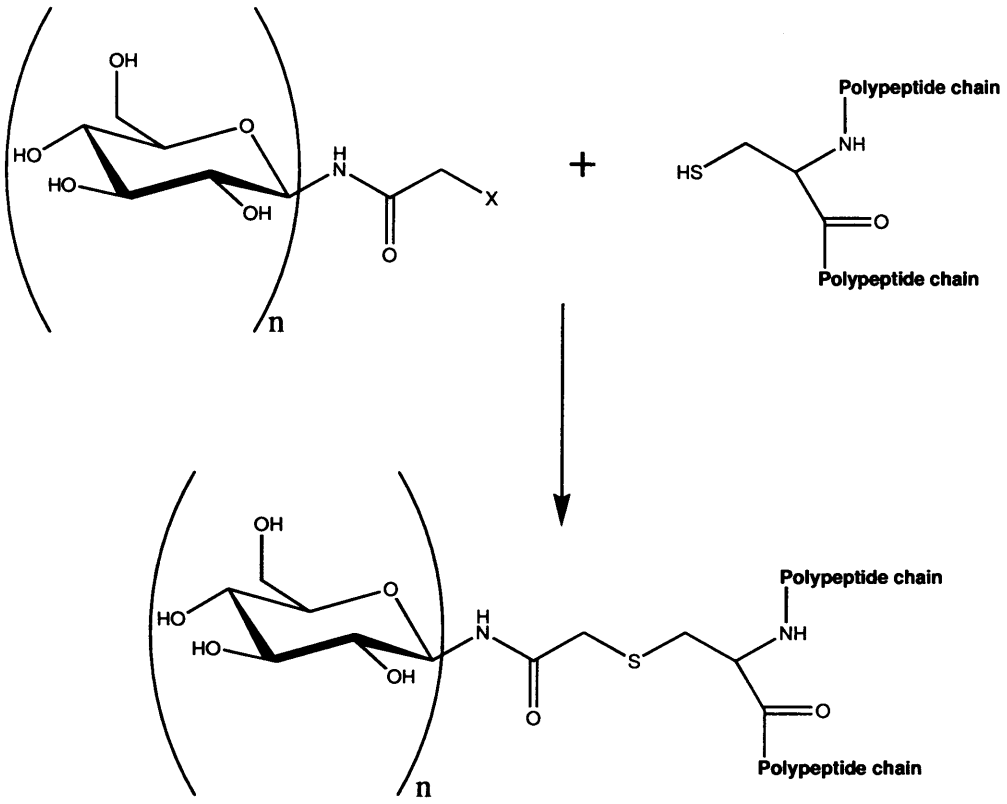

Scheme 5.1: *Generation of neoglycoproteins* via *alkylation of cysteine-containing proteins with glycosyl haloacetamides (X=Cl, Br, or I) [70]*

For full control of glycosylation both choices of site (site selectivity) and glycans are needed. A combined site-directed mutagenesis and chemical modification approach has solved this problem [188-191]. This approach provides a general method that allows both region- and glycan-specific glycosylation of proteins. The strategy involves the introduction of cysteine as a chemoselective tag at presented positions within a given protein and the reaction of its thiol group with glycomethanesulfonate (glycoMTS) reagents or glycosyl iodoacetamide (Scheme 5.2). Previous work by Davis and co-workers used glycoMTS reagents, which react specifically and quantitatively with thiols and allows the controlled formation of neutral disulfide linkage [191]. However this methodology does not produce high yields of homologous glycoproteins. A slight change

of the protein conformation would affect the glycosylation by producing lower yield of glycosylated proteins and this has been noted by Anderson and co-workers [192].

In an impressive, recent example of site-selective glycosylation through combined mutagenesis and modification, Flitsch and co-workers have used their iodoacetamide methodology (Scheme 5.1) to glycosylate three cysteine mutants of erythroprotein (EPO) (Scheme 5.2) [70]. The three natural asparagine (Asn) glycosylation sites (sites 24, 38 and 83) were mofified to cysteine residues for reaction with glycosyl iodoacetamide. Although the conversion rate from unglycosylated to glycosylated form is about 60% after 24 hours reaction time, it was possible to purify glycosylated EPO from unglycosylated EPO using a lectin-affinity column. This methodology is very simple and does not require any complex steps to synthesize and purify the end products.

Therefore it was decided to use this methodology to allow site-specific glycosylation of the naturally nonglycosylated enzyme, dihydrofolate reductase (DHFR). This chapter presents a detailed description of the glycosylation of EcDHFR.

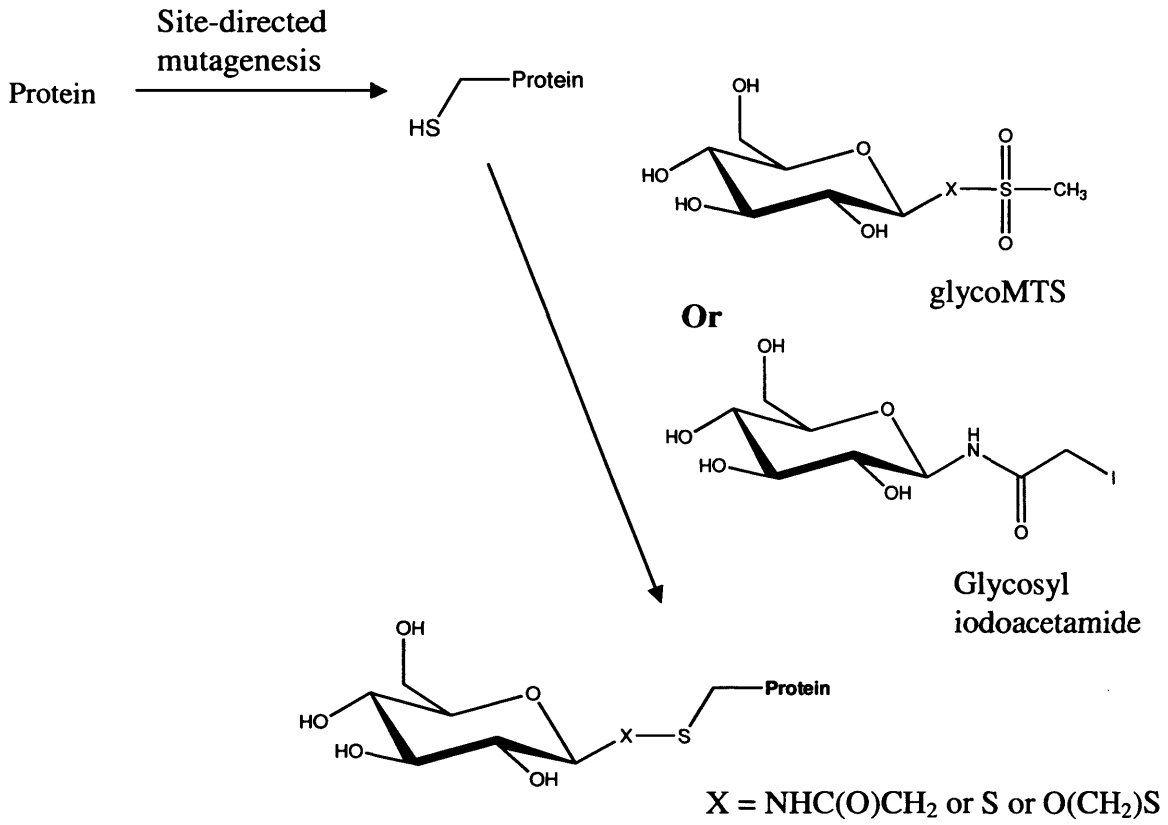

Scheme 5.2: *Site-selective glycoprotein synthesis through a combination of site-directed mutagenesis and chemical modification [70, 190, 191]*

5.2 Alkylation of EcDHFR triple mutants with glycosyl haloacetamides

This section describes the methodology for alkylation of the thiol group of a cysteine residue in EcDHFR triple mutants with glycosyl iodoacetamide. The reaction was first optimized with DM-D87C EcDHFR, using mass spectrometry to analyze the products. By comparing the molecular weight of the observed peaks in the mass spectrum with the non-glycosylated protein, it was possible to determine whether the protein was successfully glycosylated. Four different iodoacetamides were used; glucose, N-acetylglucosamine (GlcNAc), lactose, and maltosetriose iodoacetamide which range from monosaccharide to trisaccharide (Figure 5.1). These glycosyl iodoacetamides were synthesised and contributed by Flitsch and co-workers, and details of the synthetic work has been published [67].

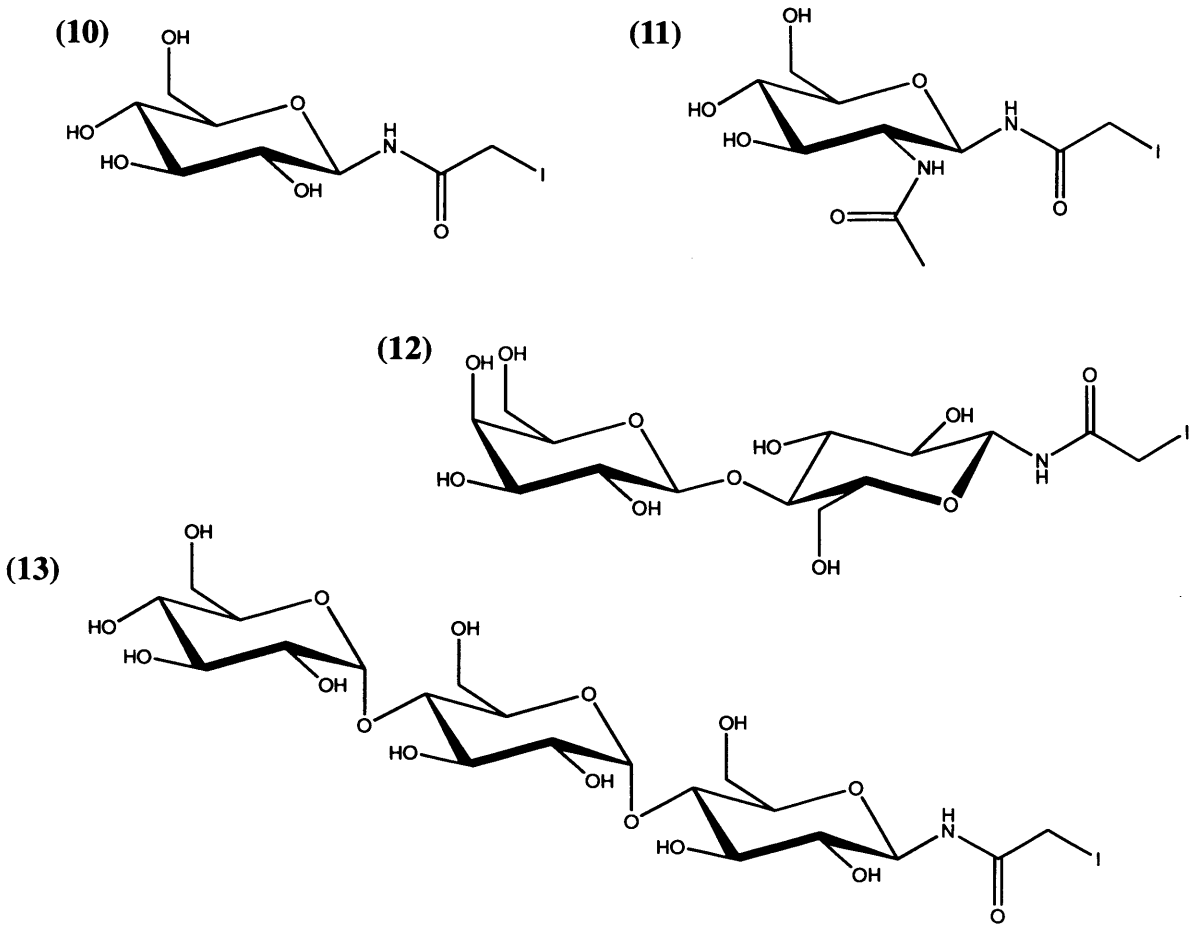

Figure 5.1: *The four different types of saccharides that were used: glucose (glc) iodoacetamide (10), GlcNAc iodoacetamide (11), lactose (lac) iodoacetamide (12), and maltotriose iodoacetamide (13)* [67].

At *p*H 8.5, 25 °C, the glycosyl iodoacetamide did not react efficiently with DM-D87C EcDHFR. Although the reaction was incubated for 24 hours t he percentage yields of the conversion from the non-glycosylated protein to glycosylated protein was about 30%. Further incubation of the mixtures for additional 24 hours increased the yield of glycosylated EcDHFR to 90%. However, two additional peaks were observed in the MALDI-TOF mass spectrum other than the mono-glycosylated EcDHFR. These peaks were observed at M_w ~18,472 and M_w ~18,743, which correspond to the attachment of an

additional one and two units of GlcNAc acetamide, respectively. Reducing the temperature to 4 °C prevented unwanted glycosylation, with the reaction stopping at the desired monoglycosylated product. The reaction was incubated for 48 hours the percentage yields of the conversion from the non-glycosylated protein to glycosylated protein was about 90%. At 37 °C, the intensity of the peak with molecular weight 18,743 became larger. From the observed results, the incubation mixture of temperatures greater than 4 °C and 48 hours, additional GlcNAc acetamides unit may react non-specifically on the DHFR protein (*i.e* lysine residue). The mass spectra of the alkylated DM-D87C EcDHFR with GlcNAc iodoacetamide at the three different temperatures are shown in Figure 5.2 and the observed molecular weight values were comparable to the calculated values for the glycosylated proteins. For example, non-glycosylated DM-D87C EcDHFR has a molecular weight (M_w) of 17,948 and after it is glycosylated with GlcNAc iodoacetamide at 4 °C, the molecular weight increases to 18,210.

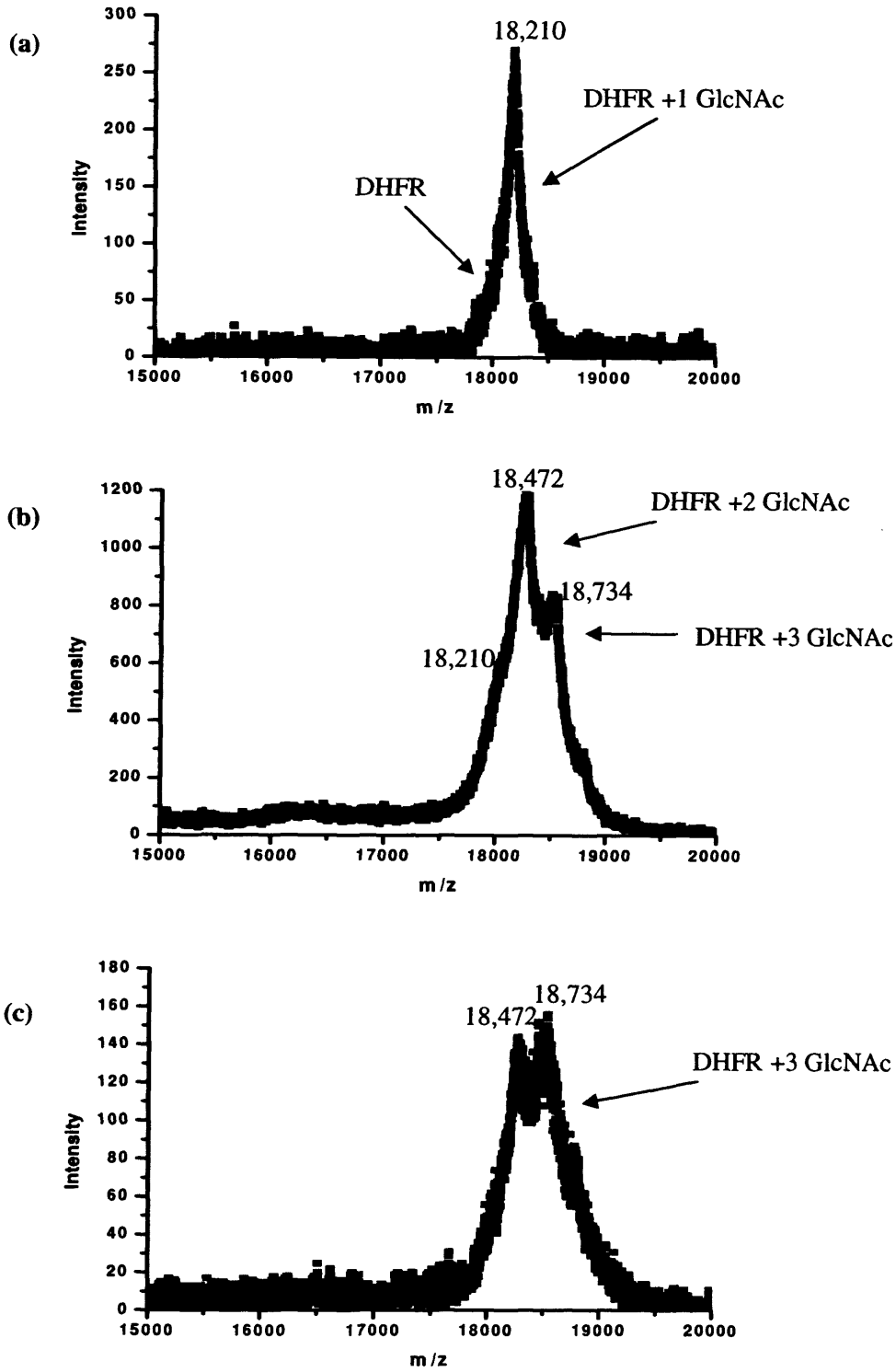

Figure 5.2: *MALDI-TOF mass spectra of DM-D87C EcDHFR alkylated with GlcNAc iodoacetamide at 4 °C (a), 25 °C (b), and 37 °C (c).*

The above experiments show temperature has an influence on the specificity of the alkylation reaction. Although, we have no solid evidence to show the correlation between the temperatures with the binding of glycosyl iodoacetamide, however from our experiments and observation, we conclude that the reaction between the glycosyl iodoacetamide with triple mutants EcDHFR is favored at 4 °C. Therefore only a single peak was observed in the MALDI-TOF mass spectra for the glycosylated EcDHFR (Figure 5.2a).

Figure 5.3 shows an example of the MALDI-TOF mass spectra for glycosylated DM-D87C EcDHFR with glucose, and lactose acetamide. The calculated mass for the glycosylated DM-D87C EcDHFR with glucose is ~18,170 and the glycosylated protein with lactose iodoacetamide is ~18,332. The observed molecular masses in Figure 5.3 were comparable to the calculated mass of the proteins. If the yield of the glycosylated protein was less than 90% compared with the non-glycosylated protein, then purification of the glycosylated protein was required. This was carried out by reacting with 2-[(biotinoyl)-amino]-ethyl methanesulfonate (MTSEA) and applying the solution to a column containing avidin resin, resulting in retention of biotinylated EcDHFR and elution of essentially pure mono-glycosylated proteins (Figure 5.2a) [71].

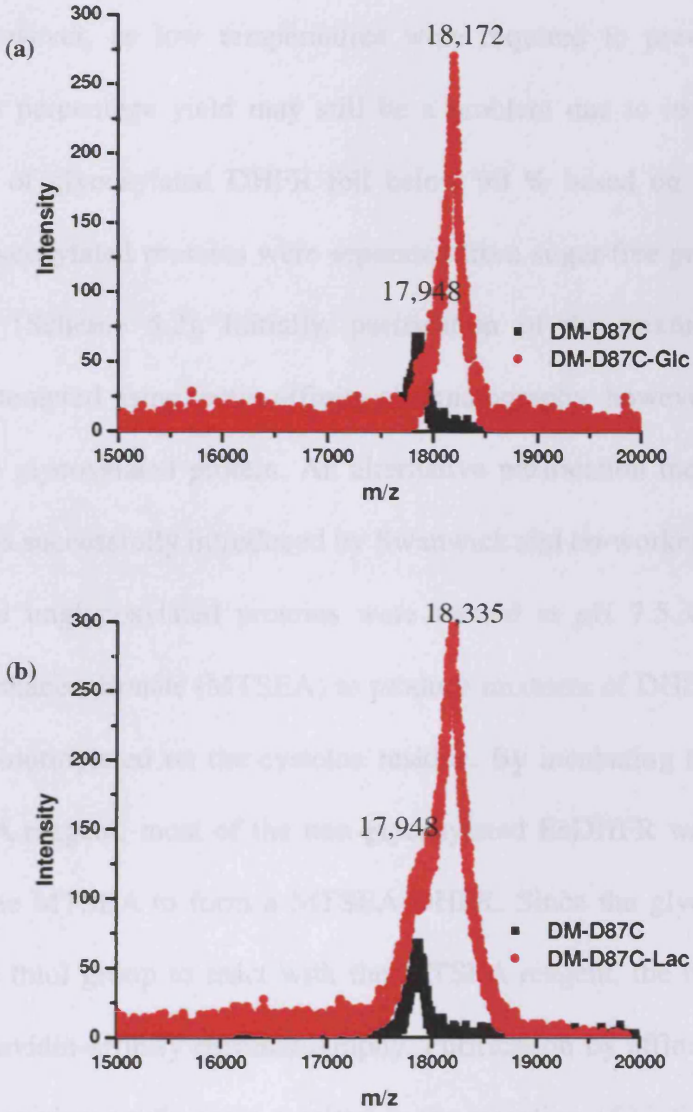

Figure 5.3: *MALDI-TOF mass spectra of DM-D87C EcDHFR glycosylated with glucose (a), and lactose acetamide (b). Within each spectrum, there is a mass spectrum of non glycosylated DM-D87C EcDHFR for comparison.*

5.3 Purification of glycosylated EcDHFR triple mutants

Production of high yields of the desired mono-glycosylated proteins was essential for analysis. However, as low temperatures were required to prevent bis-alkylation, obtaining a high percentage yield may still be a problem due to inefficient alkylation. When the yield of glycosylated DHFR fell below 90 % based on the observed mass spectrum, the glycosylated proteins were separated from sugar-free protein using affinity chromatography (Scheme 5.2). Initially, purification of the mixture of glycosylated EcDHFR was attempted using lectin-affinity chromatography, however no spectrum was observed for the glycosylated protein. An alternative purification method was therefore required, and was successfully introduced by Swanwick and co-workers [71]. Mixtures of glycosylated and unglycosylated proteins were treated at *p*H 7.5 with 2-[(biotinoyl)-amino]-ethyl methanesulfonate (MTSEA) to produce mixtures of DHFRs that were either glycosylated or biotinylated on the cysteine residue. By incubating the protein solution with the MTSEA reagent, most of the non-glycosylated EcDHFR was reacted with the thiol group of the MTSEA to form a MTSEA-DHFR. Since the glycosylated EcDHFR has no available thiol group to react with the MTSEA reagent, the two forms could be separated using avidin-affinity chromatography. Purification by affinity chromatography on a column containing avidin resin resulted in the retention of biotinylated protein and elution of essentially pure mono-glycosylated proteins (Scheme 5.2) [71].

conditions were used to glycosylate the remaining EcDHFR triple mutants. Therefore using this method, homogenous samples of EcDHFR carrying glucose (glc), GlcNAc, lactose (lac) and maltotriose on the cysteine residue of the EcDHFR triple mutants were successfully prepared in good overall yields (Scheme 5.2).

Table 5.1 shows the calculated molecular weight of the tryptic peptide for DM-D87C EcDHFR. These data were then compared to the observed peaks in the mass spectrum to demonstrate the presence of the carbohydrate moiety at the desired sites of the mutants.

Table 5.1: *Calculated molecular weights for the tryptic peptides of DM-D87C EcDHFR observed in the mass spectrum. The fragment containing the introduced cysteine residue is indicated in bold and underlined.*

Mass (M_w)	Position	Peptide Sequence
2460.3	13-33	VIGMENAMPWNLPADLAWFKR
2303.1	13-32	VIGMENAMPWNLPADLAWFK
2115.1	77-98	SVDEAIAAAG**C**VPEIMVIGGGR
2032.2	59-76	NIILSSQPGTDDRVTWVK
1635.8	45-58	HTWESIGRPLPGRK
1505.8	45-57	HTWESIGRPLPGR

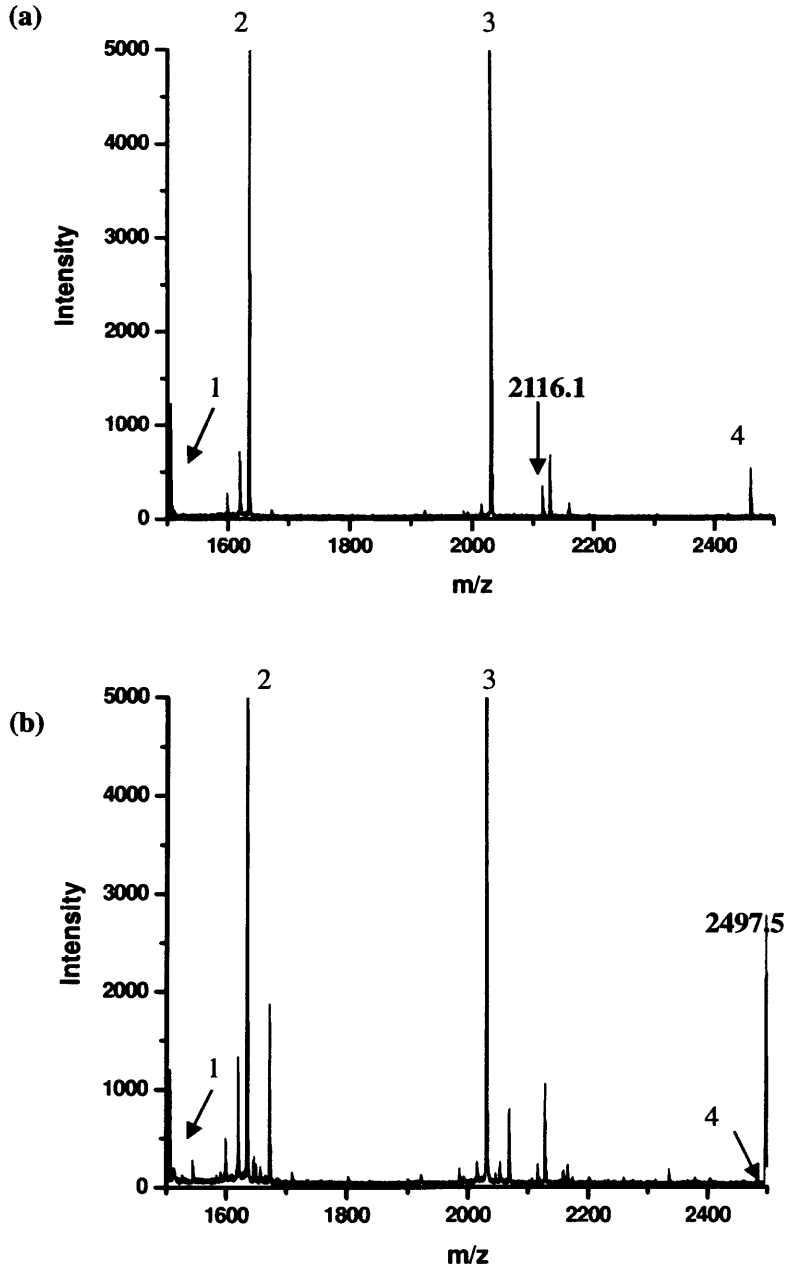

Figure 5.4: *Trypsin digests of DM-D87C EcDHFR (a) and DM-D87C EcDHFR carrying lactose on residue 87 (b). Mw ~ 2116.1 and 2497.5 are the singly charged ions for peptide contained SVDEAIAAAGCVPEIMVIGGGR, in its unglycosylated and lactose carrying forms, respectively. Peaks 1-4 correspond to the other tryptic peptides.*

5.4 Conclusions

A route for the purification to homogeneity of substantial quantities of neoglycoprotein has been described. Site-directed mutagenesis was used to introduce cysteine residues in specific positions of the target protein. The mutant proteins were derivatised with chemically synthesized glycosyl iodoacetamides and purified through scavenging of the unreacted sugar free proteins by biotin containing thiosulfonates followed by affinity chromatography to yield essentially pure glycosylated proteins.

This methodology does not require complex purification methods, therefore it is very easy to synthesis and purify a homogenous glycosylated proteins. This methodology was applied to the four different EcDHFRs triple mutants (*i.e.* DM-N18C, DM-R52C, DM-D87C and DM-D132C) to allow studies of the effect of the carbohydrate moieties on the physical, chemical and kinetic activity of the protein. In addition, it should be noted that the present methodology is very general and should be applicable to the derivitisation of cysteine sidechains with electrophilic thiol specific reagents other than glycosides, such as spectroscopic reporter groups, to produce homogeneously labelled material [193-195].

Chapter 6

Studies of the effect of Glycosylation on EcDHFR

6.1 Introduction

Chapters 4 and 5 describe the creation of four different triple mutants of EcDHFR, and an effective methodology of producing homogeneous glycoproteins. Here, the effect of the glycosylation on the triple mutants of EcDHFR, in terms of their structure, stability and kinetic reactivity of the protein, is described.

6.2 DM-N18C EcDHFR

Asn 18 is located in the Met20 loop, which is one of the most flexible structures in the entire protein (Figure 6.2) [107]. To synthesise this protein, a single *E. coli* BL21(DE3) colony containing DM-N18C EcDHFR was used in a large-scale preparation of the protein. Isopropyl-β-D-thiogalactoside (IPTG) was then added into the mixture for induction. Over expression of the DHFR protein was followed by sodium dodecyl sulfate polyacrylamide gel electrophoresis (SDS-PAGE) for visualization. The recombinant DM-N18C EcDHFR protein has a calculated mass about 17,947 molecular weight, therefore a band will be observe between the region of M_w ~20,000-14,000 which indicated by the protein markers at the SDS gel (Figure 6.1). The purification steps for the DHFR protein were then carried out using a column containing methotrexate (MTX) resin. After extensively dialysis the protein solution in 5 mM K_iPO_4 (*p*H 7.0) buffer to decreases the NaCl concentration and then applied to a column containing diethylaminoethyl (DEAE) resin for further purification.

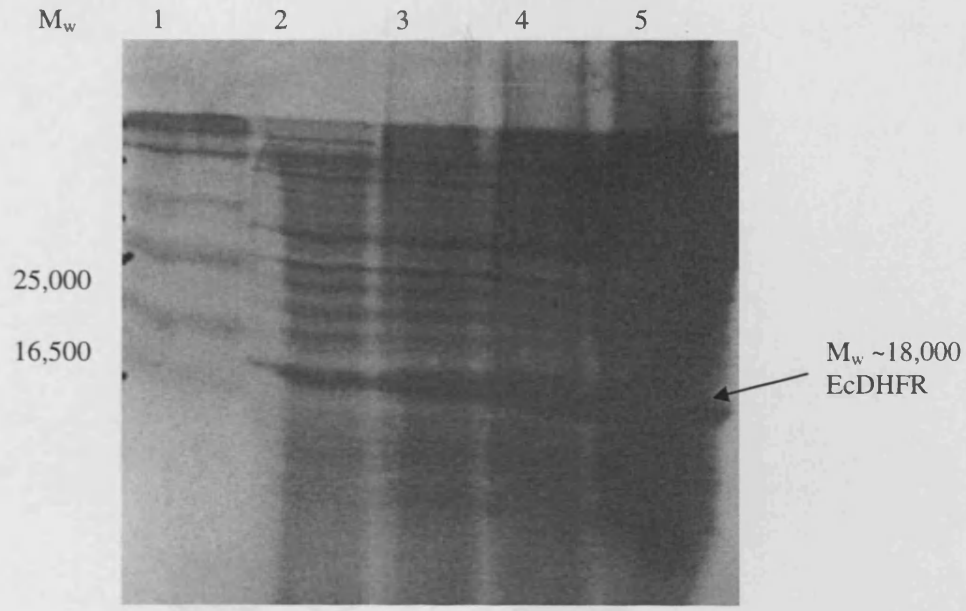

Figure 6.1: *SDS-PAGE for large-scale expression of EcDHFR. Lane 1 indicates the protein standard molecular weight; Lane 2 indicates the cells growth before induction with IPTG; and Lane 3-5 indicate the cells after induce with IPTG for duration 1, 3, and 4 h of incubation.*

Fragments of proteins solution contained the least folate was determined using UV-spectrophotometer at 280 nm. After that, we extensively washed the protein solution in 5 mM K_iPO_4 (*p*H 7.0) buffer to decreases the NaCl concentration. The DM-N18C EcDHFR protein was purified and its concentration was determined as the wild type EcDHFR (see Section 2.8.5-7 and Chapter 3).

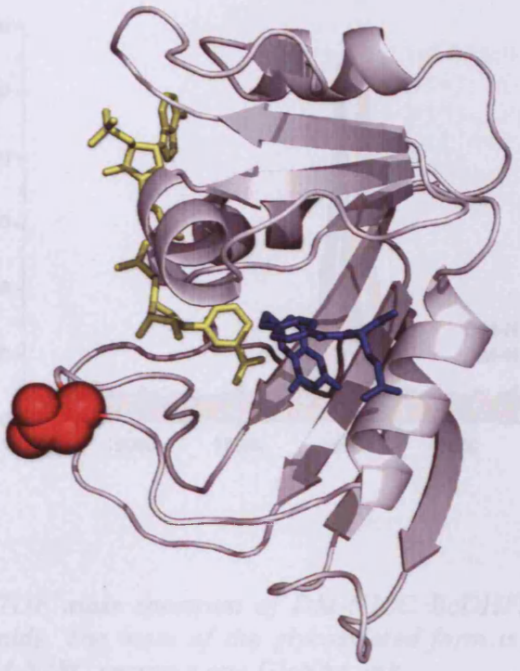

Figure 6.2: *Structural overview of EcDHFR. Position 18 is indicated in red. Folate and NADP+ are drawn in stick format and indicated in blue and yellow respectively in the ternary complex (1RA2). The structure is oriented so that the nicotinamide ring of the co-factor is in the plane of paper [78, 108].*

The purified protein was then alkylated with glycosyl haloacetamides and purified as described above (Sections 2.9 and 5.3). The concentration of the glycosylated protein was determined using the MTX titration method (Sectiom 2.8.7.3) and determined the presence of mono-glycosylated EcDHFR *via* MALDI-TOF spectroscopy (Figure 6.3).

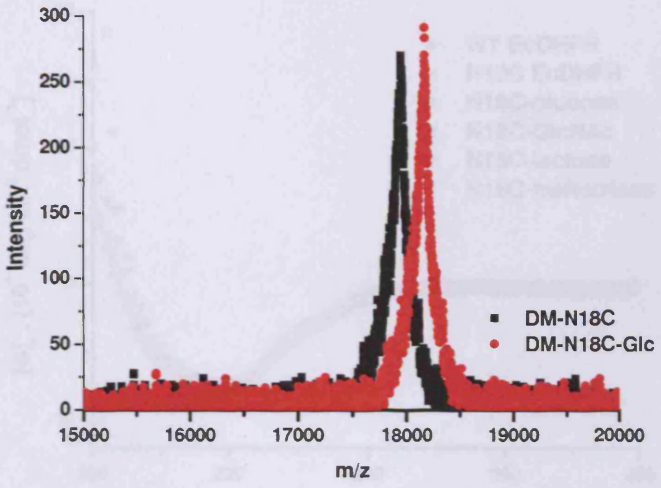

Figure 6.3: *MALDI-TOF mass spectrum of DM-N18C EcDHFR and its glycoyslated form with Glc acetamide. The mass of the glycosylated form is in agreement with the calculated mass of DM-N18C carrying one GlcNAc unit.*

6.2.1. Characterisation and thermal denaturation studies

CD spectroscopy was used to investigate the secondary structure of glycosylated DM-N18C EcDHFR. As DM EcDHFR, is comparable to WT EcDHFR in terms of structure, stability and kinetic reactivity (see Chapter 3), all the EcDHFR triple mutants and their glycosylated forms were compared directly to WT EcDHFR. Substrate and cofactor were not bound to any enzyme, therefore the spectra represented the enzymes in their native form (apoenzyme). The CD spectrum for the glycosylated forms of DM-N18C EcDHFR had a minimum at 222 nm and a maximum of 195 nm (Figure 6.4), which is similar to the unglycosylated DM-N18C and WT EcDHFR. No significant difference in the CD spectra were observed, showing that glycosylation at position 18 did not have a significant effect on the secondary structural elements of EcDHFR (Figure 6.4; Table 6.1).

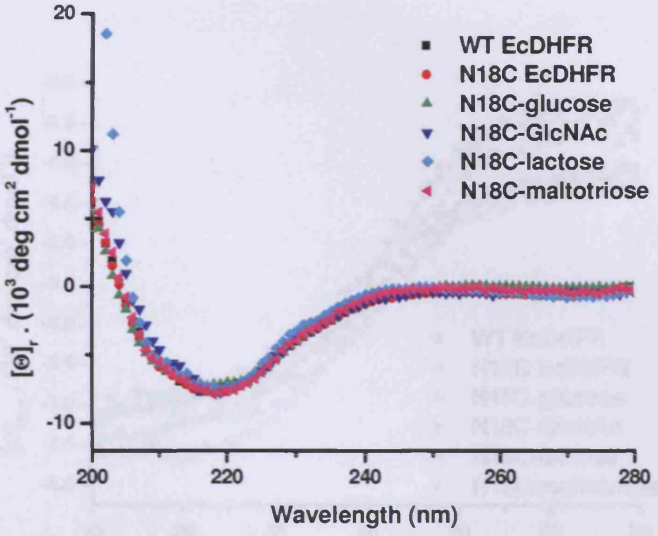

Figure 6.4: *Far-UV spectra of WT EcDHFRs, DM-N18C EcDHFR, and its glycoylated forms. All protein concentrations were 10 μM and the spectra were recorded by using a Applied Photophysics Chirascan CD spectrometer at 25 °C with a pathlength of 1 mm in 5 mM K_iPO_4 (pH 7.0).*

Thermal stability of the glycosylated forms of DM-N18C EcDHFR was determined by monitoring the change in the CD signal at 222 nm as a function of temperature. The temperature dependencies of the CD profile of glycosylated DM-N18C EcDHFR exhibited a small linear variation of the signal between 20 and 35 °C, corresponding to the native baselines, followed by a cooperative loss of secondary structure between 35 and 57 °C (Figure 6.5). Thermal denaturation of DM-N18C EcDHFR and its glycosylated forms were reversible from 20 to 80 °C at a temperature gradient of 24 °C h^{-1}. The CD transitions recorded for DM-N18C EcDHFR and its glycosylated forms were similar and their midpoints were within the experimental error of measurements (Table 6.1). The addition of glycans on the DM-N18C EcDHFR therefore caused no significant difference to the thermal stability.

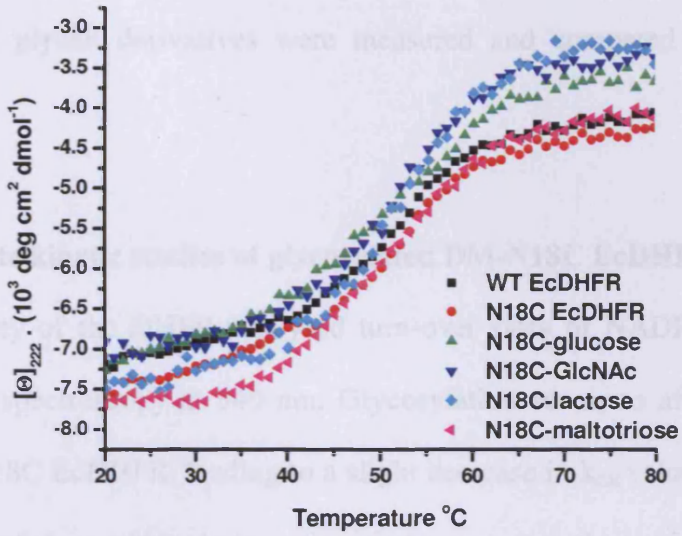

Figure 6.5: *Thermal denaturation of WT EcDHFR, DM-N18C EcDHFR, and its glycosylated forms. All protein concentrations were 10 μM and the spectra were recorded by using a Applied Photophysics Chirascan CD spectrometer at 25 °C with a pathlength of 1 mm in 5 mM K_iPO_4 (pH 7.0).*

Table 6.1: *Structural parameters for the WT, DM-N18C and its glycosylated forms of EcDHFR*

EcDHFR / Glycan	$[\Theta]_{222}$ (deg cm^2 dmol^{-1})	T_M (°C)
WT	-7,399 ± 182	50.7 ± 0.2
DM-N18C	-7,398 ± 123	50.5 ± 0.4
Glucose	-7,121 ± 149	50.5 ± 0.3
GlcNAc	-6,899 ± 23	51.0 ± 0.1
Lactose	-7,264 ± 230	50.6 ± 0.9
Maltotriose	-7,467 ± 221	51.0 ± 0.7

6.2.2. Effects of glycosylation on DM-N18C catalysis

In order to examine the effect of site-selective glycosylation on DM-N18C EcDHFR catalysis, the hydride transfer rate and the steady-state rate for the reaction for the four different glycan derivatives were measured and compared to the wild-type protein.

6.2.2.1 Steady state kinetic studies of glycosylated DM-N18C EcDHFR

The velocity of the DHFR-catalysed turn-over rates of NADPH and H_2F were measured by UV spectroscopy at 340 nm. Glycosylation seems to affect the turn-over rate of the DM-N18C EcDHFR, leading to a slight decrease in k_{cat} values at 25 °C (Table 6.2). As the size of the carbohydrate moiety is increased at the surface of DM-N18C EcDHFR, the k_{cat} value is lowered compared with WT EcDHFR. When a trisaccharide is attached to DM-N18C EcDHFR, the k_{cat} value is decreased about two fold compared with WT EcDHFR.

Interestingly, K_M^{NADPH} values were unaffected by glycosylation. It seems glycosylation on the position 18 of EcDHFR does not affect the Michaelis constant of the protein but it might affect the product release step. The attachment of a carbohydrate moiety on the Met20 loop may have affected the movement of the loop, therefore leading a decrease in k_{cat} value as the size of the carbohydrate moiety is increased. Due to the decrease of the k_{cat} value, the calculated catalytic efficiency (k_{cat}/K_M^{NADPH}) of the glycosylated DM-N18C EcDHFR also shows lower values compared to the DM-N18C and WT EcDHFR (Table 6.2). The experiment was carried out with a minimum of three repeats under the same conditions (Section 2.10.2.3).

Table 6.2: *Steady state kinetic parameters for WT EcDHFR, DM-N18C EcDHFR and its glycosylated forms. Kinetic measurements were carried out at 25 °C*

EcDHFR / Glycan	k_{cat} (s^{-1})	K_M^{NADPH} (μM)	k_{cat}/K_M^{NADPH} (s^{-1} μM)$^{-1}$)
WT	12.2 ± 0.7	1.6 ± 0.1	7.6
DM-N18C	10.4 ± 1.5	1.5 ± 0.1	6.9
Glucose	8.9 ± 0.4	1.4 ± 0.3	6.3
GlcNAc	7.6 ± 0.5	1.1 ± 0.1	6.9
Lactose	6.2 ± 0.7	1.4 ± 0.0	4.4
Maltotriose	4.8 ± 0.5	1.3 ± 0.6	3.7

6.2.2.2 Pre-steady state kinetic studies for glycosylated DM-N18C EcDHFR

The hydride transfer rate catalysed by DM-N18C EcDHFRs and its glycosylated forms were measured by stopped-flow FRET at 25 °C under the conditions of excess H_2F (Section 3.6). The resulting time course traces were fit to a single exponential decay and the rates are shown in Table 6.3. The reaction catalysed by the glycosylated DM-N18C showed a minor decrease in hydride transfer rate (Table 6.3). The addition of carbohydrate moiety on the Met20 loop may have disrupted the bonding between the Met20 loop and the backbone carbonyl oxygen of H45 in the helix. Therefore, the increased size of glycan on the Met20 loop may have delayed the complex formation. As the result, a lower value of single turn over rate for the protein compared with WT EcDHFR has been observed (Table 6.3). Interestingly, these values do not affected by the size of the carbohydrate moiety. The experiment was carried out with a minimum of 3 repeats under the same conditions (Section 2.10.2.4).

Table 6.3: *Pre-steady state kinetic parameters for the WT EcDHFR, DM-N18C EcDHFR and its glycosylated forms. Kinetic measurements were carried out at 25 °C*

EcDHFR / Glycan	k_H (s^{-1})
WT	223 ± 5
DM-N18C	174 ± 26
Glucose	179 ± 9
GlcNAc	160 ± 19
Lactose	132 ± 23
Maltotriose	156 ± 8

6.2.3 Urea denaturation/ equilibrium unfolding of DM-N18C EcDHFR and its glycosylated forms.

Equilibrium urea titrations were performed on the glycosylated DM-N18C EcDHFR and monitored by tryptophan fluorescence emission as previously described (Section 3.8). The difference in free energy, as determined by global fitting of fluorescence urea titration data, between the native and denatured states of the glycosylated DM-N18C EcDHFR is similar to that for WT EcDHFR (Table 6.4). Glycosylation at position 18 therefore seems to have no influence on the protein stability. This is comparable with the results from CD spectroscopy studies which showed no difference in secondary structure and thermal stability (Section 6.2.1).

Table 6.4: *Thermodynamic parameters obtained from equilibrium urea denaturation for WT EcDHFR, DM-N18C EcDHFR and its glycosylated forms.*

EcDHFR / Glycan	$\Delta G°$ (kcal mol^{-1})	m (kcal $mol^{-1}M^{-1}$)	C_m (M)
WT	5.9 ± 0.3	2.1 ± 0.1	2.8 ± 0.1
DM-N18C	5.3 ± 0.3	2.3 ± 0.4	2.6 ± 0.1
Glucose	5.7 ± 0.1	1.9 ± 0.1	2.7 + 0.2
GlcNAc	5.5 ± 0.2	1.8 ± 0.1	2.7+ 0.1
Lactose	5.6 ± 0.3	2.0 ± 0.1	2.5 + 0.2
Maltotriose	5.3 ± 0.3	2.1 ± 0.1	2.3 +0.1

6.2.4 Equilibrium dissociation constants (K_D) of glycosylated DM-N18C EcDHFR complexes.

Equilibrium dissociation constant studies for the complexes of NADPH and folate with the glycosylated DM-N18C EcDHFR were performed at 25 °C and *p*H 7.0 as described previously (Sections 3.9 and 4.6). The K_D^{NADPH} values for the glycosylated DM-N18C EcDHFRs (Table 6.5) are very small, therefore it is difficult to conclude that glycosylation has affected the protein affinity towards NADPH. Glycosylation on the Met20 loop therefore does not appear to show any influence on the K_D for NADPH binding with the protein. The K_D values with folate, on the other hand, increase slightly upon glycosylation (Table 6.5) and these values are significantly different to the WT and DM-N18C EcDHFRs. Glycosylation at position 18 of EcDHFR has showed an increased of about 1 μM for K_D^{Folate} value. However this effect does not correlate to the size of the carbohydrate moiety. On attachment of GlcNAc on the DM-N18C EcDHFR, its K_D^{Folate} value showed no significant difference to that of the protein glycosylated with lactose and maltotriose (Table 6.5). The relatively increased value of K_D^{Folate} of the glycosylated

protein may have direct affect on the k_{cat} and k_H of the protein. Therefore we were observed a minor changed of k_{cat} and k_H values of the protein along the increasing of the size of the glycan (Table 6.2 and Table 6.3).

Table 6.5: *Equilibrium dissociation constants of the complexes of NADPH and folate with WT EcDHFR, DM-N18C EcDHFR, and its glycosylated forms at 25 °C and* pH *7.0*

EcDHFR / Glycan	K_D (μM)	
	NADPH	Folate
WT	0.10 ± 0.03	2.05 ± 0.05
DM-N18C	0.22 ± 0.03	2.97 ± 0.25
Glucose	0.36 ± 0.01	3.30 ± 0.44
GlcNAc	0.34 ± 0.07	4.39 ± 0.19
Lactose	0.30 ± 0.06	4.2 ± 0.42
Maltotriose	0.36 ± 0.07	5.03 ± 1.35

6.3 DM-R52C EcDHFR

As mentioned previously, site 52 is located on the adenosine binding domain and is located near of the glutamate moiety of the folate/H_2F/H_4F (Figure 6.6). To synthesized this protein, a single *E. coli* BL21(DE3) colony containing DM-R52C EcDHFR was used to prepare a large-scale expression of the protein. Isopropyl-β-D-thiogalactoside (IPTG) was then added for induction. Over expression of the DHFR protein was followed by sodium dodecyl sulfate polyacrylamide gel electrophoresis (SDS-PAGE) for visualization. The recombinant DM-R52C EcDHFR protein has a calculated mass about 17,990 molecular weight, therefore a band will be observe between the region of M_w ~20,000-14,000 which indicated by the protein markers at the SDS gel. A similar observation for SDS gel as for previous triple mutants or WT EcDHFR will be observed (see Figure 6.1). The purification steps for the DHFR protein were then carried out using a column containing methotrexate (MTX) resin. After extensively dialysis the protein solution in 5 mM K_iPO_4 (*p*H 7.0) buffer to decreases the NaCl concentration and then applied to a column containing diethylaminoethyl (DEAE) resin for further purification.

The protein has purified and glycosylated as described previously (Sections 2.8.7.3, 2.9 and 4.2). The concentration of the glycosylated protein determined using the MTX titration method (Section 2.8.7.3) and determined the presence of mono-glycosylated EcDHFR using MALDI-TOF spectroscopy (Figure 6.7).

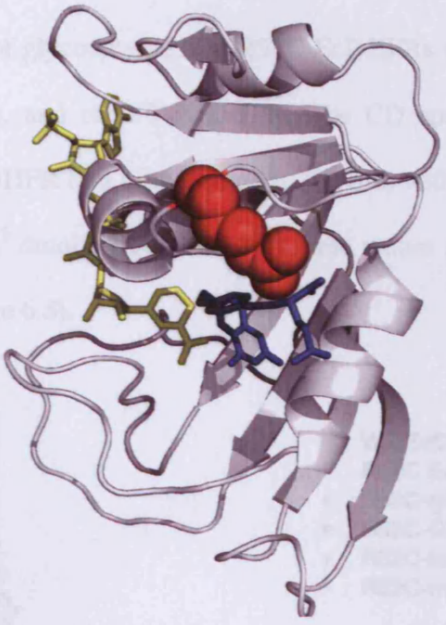

Figure 6.6: *Structural overview of EcDHFR. The position 52 is indicated in red. Folate and NADP$^+$ are drawn in stick format and indicated in blue and yellow respectively in the ternary complex (1RA2). The structure is oriented so that the co-factor nicotinamide ring is in the plane of paper [78, 108].*

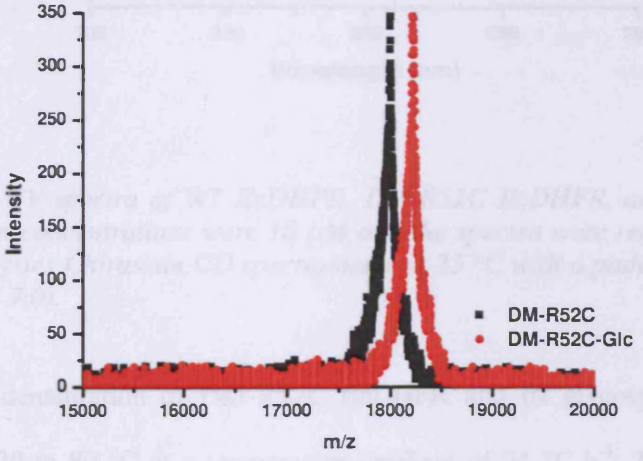

Figure 6.7: *MALDI-TOF mass spectra of DM-R52C EcDHFR and its glycoyslated form with Glc acetamide. The mass of the glycosylated form is in agreement with the calculated mass of DM-R52C carrying one Glc unit.*

6.3.1. Characterisation and thermal denaturation studies

The CD spectra of glycosylated DM-R52C EcDHFRs were compared to those of its un-glycosylated form, and of WT EcDHFR. The CD spectra for the glycosylated forms of DM-R52C EcDHFR had a minimum at 222 nm, with a MRE values between -6,967 and -7,695 deg cm^2 $dmol^{-1}$ (Table 6.6) and these values are comparable to those of the WT EcDHFRs (Figure 6.8).

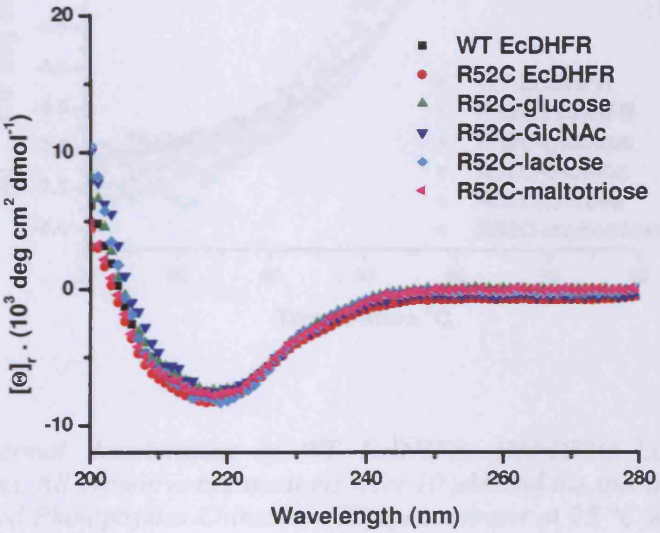

Figure 6.8: *Far-UV spectra of WT EcDHFR, DM-R52C EcDHFR, and its glycoylated forms. All protein concentrations were 10 μM and the spectra were recorded by using a Applied Photophysics Chirascan CD spectrometer at 25 °C with a pathlength of 1 mm in 5 mM K_iPO_4 (pH 7.0).*

Thermal denaturation of DM-R52C EcDHFR and its glycosylated forms was reversible from 20 to 80 °C at a temperature gradient of 24 °C h^{-1}. The CD transition recorded for DM-R52C EcDHFR and its glycosylated forms were similar and their midpoints were within the experimental error of measurements (Figure 6.9) Values for the

glycosylated forms were similar to those of the DM and WT EcDHFR. This shows that the addition of glycans to the DM-R52C EcDHFR caused no significant difference in thermal stability (Table 6.6).

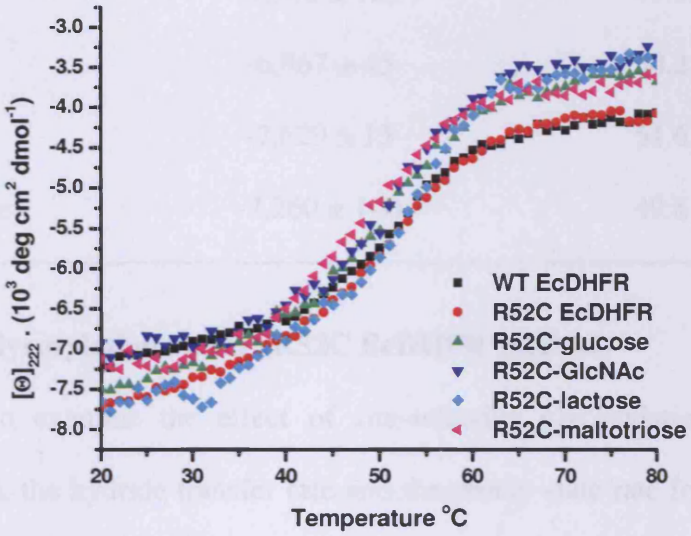

Figure 6.9: *Thermal denaturation of WT EcDHFR, DM-R52C EcDHFR and its glycosylated forms. All protein concentrations were 10 μM and the spectra were recorded by using a Applied Photophysics Chirascan CD spectrometer at 25 °C with a pathlength of 1 mm in 5 mM K_iPO_4 (pH 7.0).*

Table 6.6: *Structural parameters for WT EcDHFR, DM-R52C EcDHFR and its glycosylated forms.*

EcDHFR / Glycan	$[\Theta]_{222}$ (deg cm^2 $dmol^{-1}$)	T_M (°C)
WT	-7,399 ± 182	50.7 ± 0.2
DM-R52C	-7,695 ± 17	49.7 ± 0.5
Glucose	-7,366 ± 129	49.9 ± 0.2
GlcNAc	-6,967 ± 45	50.2 ± 0.9
Lactose	-7,629 ± 15	51.6 ± 0.1
Maltotriose	-7,260 ± 140	49.8 ± 1.0

6.3.2. Effects of glycosylation on DM-R52C EcDHFR catalysis

In order to examine the effect of site-selective glycosylation on DM-R52C EcDHFR catalysis, the hydride transfer rate and the steady-state rate for the reaction for the four different glycan derivatives were measured and compared to the wild-type protein.

6.3.2.1 Steady state kinetic studies for glycosylated DM-R52C EcDHFR

The DM-R52C EcDHFR showed an improvement in rate back towards that of the wild type protein with increasing glycan size, with an increased of k_{cat} values from 4.9 to 12.2 s^{-1} which was similar to that of the WT EcDHFR (Table 6.7). Interestingly, the K_M for NADPH for the glycosylated protein showed a comparable result to that of the WT ECDHFR. It seems that this is not significantly affected by site-selective protein glycosylation.

The catalytic efficiency (k_{cat}/K_M) of the glycosylated DM-R52C EcDHFR also

showed an improvement from 2.3 to 7.3 s^{-1} μM^{-1} and this value is similar as the WT EcDHFR (Table 6.7). Glycosylation on DM-R52C EcDHFR, appears to improve the catalytic efficiency of the protein and reformed the catalytic power of the DM-R52C EcDHFR similar to that of the wild type protein.

Table 6.7: *Steady state kinetic parameters for WT EcDHFR, DM-R52C EcDHFR and its glycosylated forms. Kinetic measurements were carried out at 25 °C*

EcDHFR / Glycan	k_{cat} (s^{-1})	K_M^{NADPH} (μM)	k_{cat}/K_M^{NADPH} (s^{-1} μM^{-1})
WT	12.2 ± 0.7	1.6 ± 0.1	7.6
DM-R52C	4.9 ± 0.6	2.1 ± 0.1	2.3
Glucose	7.1 ± 0.1	1.6 ± 0.5	4.4
GlcNAc	9.2 ± 0.2	1.3 ± 0.0	7.0
Lactose	12.2 ± 1.5	2.1 ± 0.4	5.8
Maltotriose	11.6 ± 0.3	1.6 ± 0.0	7.3

6.3.2.2 Pre-steady state kinetic studies for glycosylated DM-R52C EcDHFR

The hydride transfer rate catalysed by DM-R52C EcDHFR and its glycosylated forms were measured by stop flow FRET at 25 °C under the conditions of excess H_2F (Section 3.6). The resulting time course traces were fit to a single exponential decay and the rates are shown in Table 6.8. The reaction catalysed by the glycosylated DM-R52C showed a relatively small change in hydride transfer rate upon the increasing size of glycan, however these values are comparable with the wild type protein (Table 6.8). Although the non-glycosylated protein has a higher hydride transfer rate compared with the wild type protein, upon glycosylation the hydride transfer rate seems to shows similar

results to those of wild type protein. By introducing a hydrophilic compound (*i.e.* glycan moiety) at DM-R52C EcDHFR may have aided the protein in reaching a stable conformation with the glutamate moiety of the substrate.

Table 6.8: *Pre-steady state kinetic parameters for WT EcDHFR, DM-R52C EcDHFR and its glycosylated forms. Kinetic measurements were carried out at 25 °C*

EcDHFR / Glycan	k_H (s^{-1})
WT	223 ± 5
DM-R52C	305 ± 8
Glucose	235 ± 24
GlcNAc	266 ± 18
Lactose	175 ± 5
Maltotriose	169 ± 32

6.3.3 Urea denaturation/ equilibrium unfolding of DM-R52C EcDHFR and its glycosylated forms.

Equilibrium urea titrations were performed on the glycosylated DM-R52C EcDHFR and monitored by tryptophan fluorescence emission as previously described (Section 3.8). The difference in free energy, as determined by global fitting of fluorescence urea titration data, between the native and denatured states of the glycosylated DM-R52C EcDHFR is similar to that for WT EcDHFR with a value between 5.4 to 5.5 kcal mol^{-1} (Table 6.9). From the observed results, glycosylation at position 52 seems has no influence on the protein stability and it is comparable with the results from CD spectroscopy studies (Section 6.3.1).

Table 6.9: *Thermodynamic parameter values obtained from equilibrium urea denaturation for WT EcDHFRs, DM-R52C EcDHFR and its glycosylated forms*

EcDHFR / Glycan	$\Delta G°$ (kcal mol^{-1})	m (kcal $mol^{-1}M^{-1}$)	C_m (M)
WT	5.9 ± 0.3	2.1 ± 0.1	2.8 ± 0.1
DM-R52C	5.7 ± 0.2	2.1 ± 0.3	2.6 ± 0.1
Glucose	5.5 ± 0.2	1.9 ± 0.1	2.7 ± 0.1
GlcNAc	5.4 ± 0.2	1.6 ± 0.1	2.8 ± 0.1
Lactose	5.5 ± 0.2	1.6 ± 0.1	2.6 ± 0.1
Maltotriose	5.4 ± 0.1	1.9 ± 0.2	2.9 ± 0.1

6.3.4 Equilibrium dissociation constants (K_D) for glycosylated DM-R52C EcDHFR complexes.

Equilibrium dissociation constant studies for NADPH and folate with the glycosylated DM-R52C were performed at 25 °C and *p*H 7.0 as described for the WT and DM-R52C EcDHFRs (Section 3.9 and Section 4.6). The K_D values for NADPH with the glycosylated DM-R52C EcDHFRs are very small, therefore it is very difficult to conclude there is any significant difference among the proteins (Table 6.10). From the X-ray crystal structure, although position 52 is located on the adenosine binding domain, it does not make any direct contact with the NADPH structure. Therefore, we may not see any changes or influences on the K_D for NADPH binding. The K_D values for folate, on the other hand, decrease slightly with the size of the glycans (Table 6.10). However these changes are not significantly different to the unglycosylated DM-R52C EcDHFR. The relatively decreased value of the K_D for folate of the glycosylated protein may be due to formation of a stable conformation between the glutamate moiety of the folate and the

glycan moiety on the protein; therefore an improvement in the protein affinity towards folate, and the catalytic reactivity is observed (Table 6.6).

Table 6.10: *Equilibrium dissociation constants of NADPH and folate parameter values of WT EcDHFR, DM-R52C EcDHFR, and its glycosylated forms at 25 °C and pH 7.0*

EcDHFR / Glycan	K_D (μM)	
	NADPH	Folate
WT	0.10 ± 0.03	2.05 ± 0.05
DM-R52C	0.19 ± 0.05	6.32 ± 0.16
Glucose	0.24 ± 0.09	7.25 ± 0.46
GlcNAc	0.26 ± 0.03	6.59 ± 0.15
Lactose	0.33 ± 0.01	5.54 ± 0.16
Maltotriose	0.32 ± 0.05	2.67 ± 0.39

6.4 DM-D87C EcDHFR

As mention previously, site 87 is a solvent exposed residue within the hinge region that connects the adenosine binding and loop domains (Figure 6.10). To synthesis this protein, a single *E. coli* BL21(DE3) colony containing DM-D87C EcDHFR was used to prepare a large-scale expression of the protein. Isopropyl-β-D-thiogalactoside (IPTG) was then added for induction. Over expression of the DHFR protein was followed by sodium dodecyl sulfate polyacrylamide gel electrophoresis (SDS-PAGE) for visualization. The recombinant DM-D87C EcDHFR protein has a calculated mass about 17,948 molecular weight, therefore a band will be observe between the region of M_w ~20,000-14,000 which indicated by the protein markers at the SDS gel. A similar observation for

SDS gel as for previous triple mutants or WT EcDHFR would be observed (see Figure 6.1). The methodology for purifying this mutant was similar as for the other triple mutants and WT ECDHFR (see Section 2.8.7.3, 3.3, 6.2, and 6.3). The purified protein was then alkylated with glycosyl haloacetamides and purified as described above (Sections 2.9 and 5.3). The concentration of the glycosylated protein determined using the MTX titration method (Sectiom 2.8.7.3) and verified the production of mono-glycosylated protein using MALDI-TOF spectroscopy for determined the presence of carbohydrate moiety on the protein (Figure 6.11).

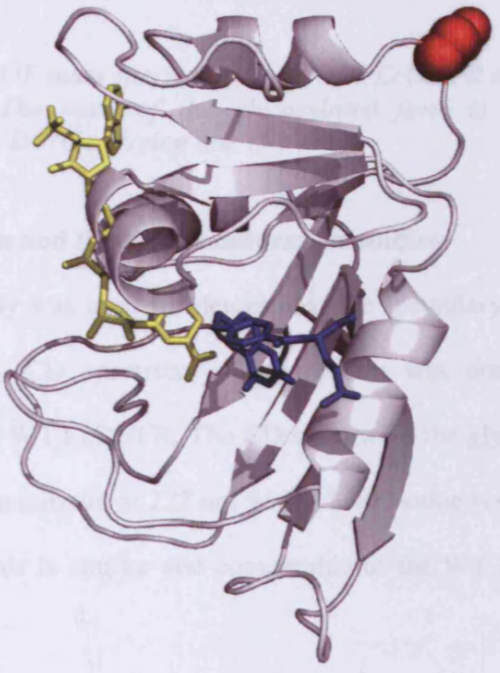

Figure 6.10: *Structural overview of EcDHFR. The position 87 is labelled in and indicated in red. Folate and NADP$^+$ are drawn in stick format and indicated in blue and yellow respectively in the ternary complex (1RA2). The structure is oriented so that the co-factor nicotinamide ring is in the plane of paper [78, 108].*

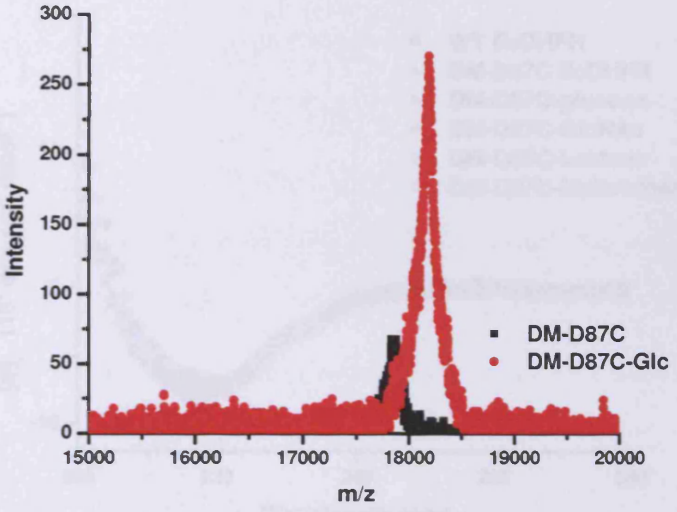

Figure 6.11: *MALDI-TOF mass spectra of DM-D87C EcDHFR and its glycoyslated form with Glc acetamide. The mass of the glycosylated form is in agreement with the calculated mass of DM-D87C carrying one Glc unit.*

6.4.1. Characterisation and thermal denaturation studies

CD spectroscopy was used for determined the secondary structure of DM-D87C EcDHFR. The far-UV CD spectrum of the protein was compared to those of its glycosylated forms and WT EcDHFR. The CD spectra for the glycosylated forms of DM-D87C EcDHFR had a minimum at 222 nm with a MRE value between -6,854 and -7,643 deg cm^2 $dmol^{-1}$, and this is similar and comparable to the WT EcDHFRs (Figure 6.12; Table 6.11).

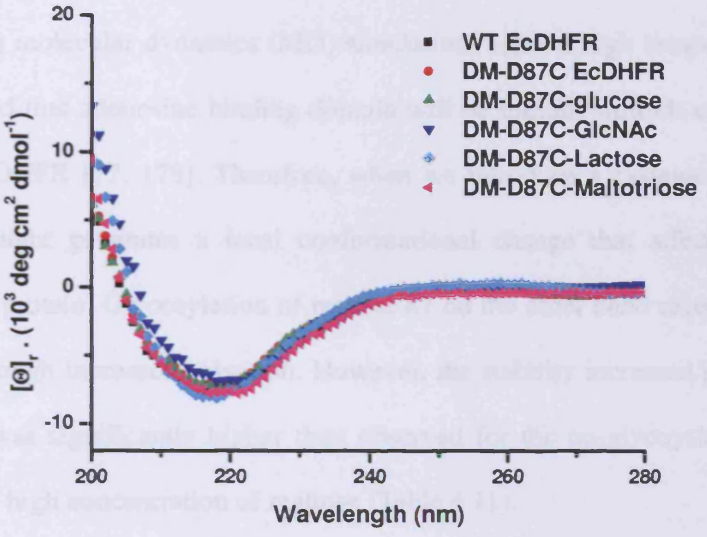

Figure 6.12: *Far-UV spectrum of WT EcDHFR, DM-D87C EcDHFR, and its glycoylated forms. All protein concentrations were 10 μM and the spectra were recorded by using a Applied Photophysics Chirascan CD spectrometer at 25 °C with a pathlength of 1 mm in 5 mM K_iPO_4 (pH 7.0).*

Thermal denaturation of DM-D87C EcDHFR and its glycosylated forms were reversible from 20 to 80 °C at a temperature gradient of 24 °C h^{-1}. Previous studies have shown the hinge region appears to lose its native structure relatively early in the temperature-induced unfolding process [77, 178]. Therefore, changes in T_M for the DM-D87C EcDHFR were observed when a hydrophobic residue was introduced at that site (Section 4.3, Table 6.11). The CD transitions showed an improvement in T_M for the glycosylated protein (Figure 6.13 and Table 6.11). Glycosylation at C87 has also increased the cooperativity of unfolding of the mutant protein. Although there is no significant difference in their secondary structure compared with the wild type protein, the addition of a glycan moiety at C87 has improved the protein thermal stability by

introducing a polar hydrophilic environment on that site. Previous studies on WT EcDHFR using molecular dynamics (MD) simulations against high temperatures at 500 K, have showed that adenosine binding domain will be initially unfolds compared other part of the EcDHFR [77, 178]. Therefore, when we introduce a cysteine residue at the position 87, might generates a local conformational change that affects the thermal stability of the protein. Glycosylation of residue 87 on the other hand reversed this effect most likely through increased solvation. However, the stability increased gained through glycosylation was significantly higher than observed for the un-glycoyslated protein in the presence of high concentration of maltose (Table 6.11).

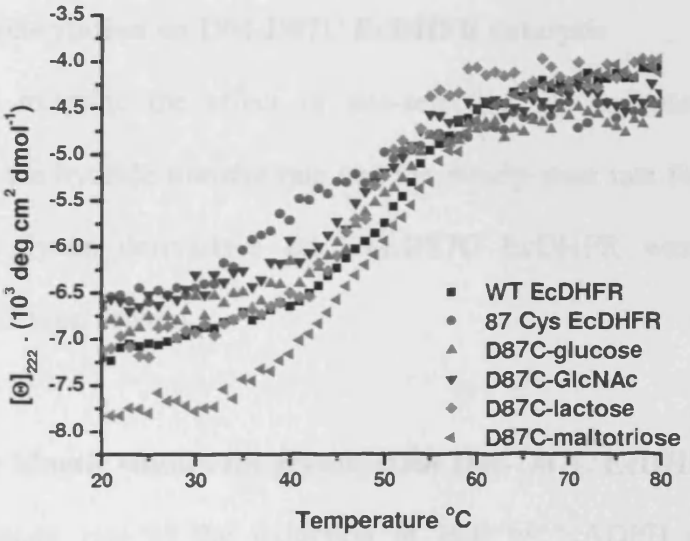

Figure 6.13: *Thermal denaturation of WT EcDHFR, DM-D87C EcDHFR and its glycosylated forms. All protein concentrations were 10 μM and the spectra were recorded by using a Applied Photophysics Chirascan CD spectrometer at 25 °C with a pathlength of 1 mm in 5 mM K_iPO_4 (pH 7.0).*

Table 6.11: *Structural parameters for WT EcDHFR, DM-D87C EcDHFR, and its glycosylated forms*

EcDHFR / Glycan	$[\Theta]_{222}$ (deg cm^2 $dmol^{-1}$)	T_M (°C)
WT	-7,399 ± 182	50.7 ± 0.2
DM-D87C	-6,718 ± 50	40.9 ± 0.3
Glucose	-6,869 ± 15	47.1 ± 0.3
GlcNAc	-6,661 ± 39	49.6 ± 1.1
Lactose	-7,171 ± 50	46.8 ± 2.1
Maltotriose	-7,660 ± 26	50.5 ± 0.3
+ 0.5 M Maltose	-7,029 ± 131	43.4 ± 0.4

6.4.2. Effects of glycosylation on DM-D87C EcDHFR catalysis

In order to examine the effect of site-selective glycosylation on DM-D87C EcDHFR catalysis, the hydride transfer rate and the steady-state rate for the reaction for the four different glycan derivatives on DM-D87C EcDHFR were measured and compared to the wild-type protein.

6.4.2.1 Steady state kinetic studies for glycosylated DM-D87C EcDHFR

The steady-state rate of the reduction of H_2F by NADPH catalysed by the glycosylated DM-D87C EcDHFRs at *p*H 7.0 was determined by measuring the specific activity of the enzymes at saturating condition for substrate and cofactor *via* UV spectroscopy at 340 nm. Upon glycosylation on DM-D87C EcDHFR, the k_{cat} values of the proteins were comparable to the WT EcDHFR. However the K_M^{NADPH} values for the proteins are higher than the wild type protein from 4.4 to 10.5 μM, leading to the lower

calculated catalytic efficiency (k_{cat}/K_M) values of the proteins (Table 6.12). A decreased catalytic efficiency (k_{cat}/K_M) values from 1.9 to 0.7 s^{-1} M^{-1}. Interestingly, glycosylation on the position C87 of the protein, which has no direct contact with NADPH according to the X-ray crystal structure (Figure 6.10), has an influence on the K_M for NADPH but no correlation with sugar size.

Table 6.12: *Steady state kinetic parameters for WT EcDHFR, DM-D87C EcDHFR, and its glycosylated forms. Kinetic measurements were carried out at 25 °C*

EcDHFR / Glycan	k_{cat} (s^{-1})	K_M^{NADPH} (μM)	k_{cat}/K_M^{NADPH} (s^{-1} μM^{-1})
WT	12.2 ± 0.7	1.6 ± 0.1	7.6
DM-D87C	9.1 ± 0.1	4.9 ± 1.7	1.9
glucose	7.3 ± 0.9	10.5 ± 1.5	0.7
GlcNAc	7.4 ± 0.1	6.3 ± 1.3	1.2
lactose	6.1 ± 2.4	7.0 ± 1.8	0.9
maltotriose	8.0 ± 0.5	4.4 ± 0.7	1.8

6.4.2.2 Pre-steady state kinetic studies for glycosylated DM-D87C EcDHFR

The hydride transfer rate catalysed by DM-D87C EcDHFR and its glycosylated forms were measured by stopped-flow FRET at 25 °C under the conditions of excess H_2F (Section 3.6). The resulting time course traces were fit to a single exponential decay and the rates are shown in Table 6.13. The reaction catalysed by the glycosylated DM-D87C protein showed a comparable hydride transfer rate upon glycosylation from 157 to 147 s^{-1} (Table 6.13). Interestingly, the position 87 is located in a solvent-exposed region and is away from the catalytic centre of the enzyme, yet has an effect on the protein catalytic

reactivity. On introduction of a cysteine residue at position 87, a decreased of the hydride transfer rate is observed. When we glycosylated this site, there is not much changes in the hydride transfer rate compared with the EcDHFR triple mutants. Glycosylation at position 87 seems have affected the catalytic reactivity of the DM-D87C EcDHFR, leading to lower catalytic efficiency values (Table 6.12) and hydride transfer rate compared with WT EcDHFR.

Table 6.13: Pre-steady state kinetic parameters for *WT EcDHFR, DM-D87C EcDHFR, and its glycosylated forms. Kinetic measurements were carried out at 25 °C*

EcDHFR / Glycan	k_H (s^{-1})
WT	223 ± 5
DM-D87C	162 ± 3
Glucose	157 ± 18
GlcNAc	149 ± 7
Lactose	147 ± 19
Maltotriose	154 ± 12

6.4.3 Urea denaturation/ equilibrium unfolding of DM-D87C EcDHFR and its glycosylated forms

Equilibrium urea titrations were performed on the glycosylated DM-D87C EcDHFR and monitored by tryptophan fluorescence emission as previously described (Section 3.8). The difference in free energy, as determined by global fitting of fluorescence urea titration data, between the native and denatured states of the glycosylated DM-D87C EcDHFR shows an improvement in the protein stability from 2.7 kcal mol^{-1} (DM-D87C) to 5.3 kcal mol^{-1} (DM-D87C-maltotriose) with increasing size of

the glycan moiety (Table 6.14). From the observed results, glycosylation at position 87 seems to have a positive influence on the protein stability. This is comparable with the results from the thermal denaturation studies which showed increased protein thermal stability upon glycosylation (Section 6.4.1).

Table 6.14: *Thermodynamic parameters obtained from equilibrium urea denaturation for WT EcDHFR, DM-D87C EcDHFR, and its glycosylated forms*

EcDHFR / Glycan	$\Delta G°$ (kcal mol^{-1})	M (kcal $mol^{-1}M^{-1}$)	C_m (M)
WT	5.9 ± 0.3	2.1 ± 0.1	2.8 ± 0.1
DM-D87C	2.7 ± 0.2	1.4 ± 0.2	2.1 ± 0.1
Glucose	4.2 ± 0.1	1.6 ± 0.1	2.0 ± 0.1
GlcNAc	4.3 ± 0.3	1.6 ± 0.1	2.0 ± 0.2
Lactose	5.1 ± 0.1	1.8 ± 0.1	2.1 ± 0.2
Maltotriose	5.3 ± 0.3	1.9 ± 0.1	2.2 ± 0.2

6.4.4 Equilibrium dissociation constants (K_D) of glycosylated DM-D87C EcDHFR complexes

Equilibrium dissociation constant studies between NADPH and folate with the glycosylated DM-D87C were performed at 25 °C and *p*H 7.0 as described for the WT and DM-D87C EcDHFRs (Section 3.9 and Section 4.6). The K_D values for the complexes of glycosylated DM-D87C EcDHFRs with NADPH (Table 5.15) are very similar to that of the wild type protein. Although the glycosylated DM-D87C protein has a relatively poor K_M for NADPH compared with WT EcDHFR, but it does not have any effect on the binding affinity between the protein and the NADPH. The K_D values for the complex of folate with the glycosylated proteins are also comparable to the wild type protein.

Interestingly, the K_D values for the complexes changes between the proteins and NADPH, does not match with the large values of K_M^{NADPH}. Glycosylation at position 87 has no effect on the protein affinity towards the NAPDH and folate.

Table 6.15: *Equilibrium dissociation constants of NADPH and folate parameters of WT EcDHFR, DM-D87CEcDHFR, and its glycosylated forms at 25 °C and* pH *7.0*

EcDHFR / Glycan	K_D (μM)	
	NADPH	Folate
WT	0.10 ± 0.03	2.05 ± 0.05
DM-D87C	0.13 ± 0.01	3.13 ± 0.21
Glucose	0.23 ± 0.11	2.56 ± 0.25
GlcNAc	0.26 ± 0.04	3.05 ± 0.06
Lactose	0.22 ± 0.02	2.92 ± 0.09
Maltotriose	0.33 ± 0.03	3.99 ± 0.89

6.5 DM-D132C EcDHFR

Position 132 is located in the end of the F-G loop of the protein (Figure 6.14). The mutant enzyme was produced in *E. coli* BL21(DE3) and purified according to the protocol used for WT EcDHFR (see Section 2.8.7.3 and 3.3). SDS-Page analysis of purified DM-D132C EcDHFR showed a single band of similar molecular weight to WT and the other EcDHFRs triple mutants (see Figure 6.1). The purified protein is then alkylated with glycosyl haloacetamides and purified as describe above (Sections 2.9 and 5.3). The concentration of the glycosylated protein is determined using the MTX titration method (Sectiom 2.8.7.3) and verified using MALDI-TOF spectroscopy (Figure 6.15).

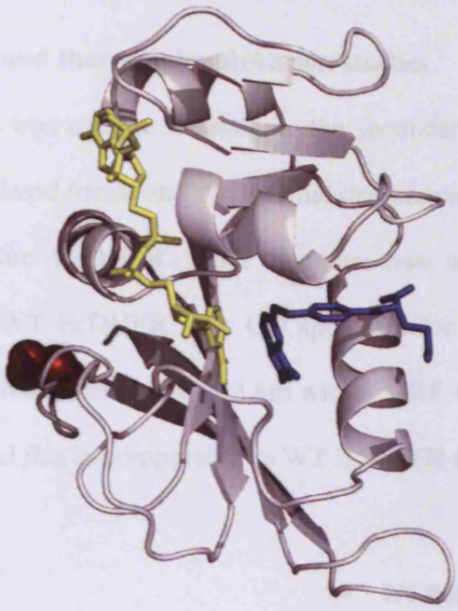

Figure 6.14: *Structural overview of EcDHFR. The position 132 is indicated in red. Folate and NADP$^+$ are drawn in stick format and indicated in blue and yellow respectively in the ternary complex (1RA2). The structure is oriented so that the co-factor nicotinamide ring is in the plane of paper [78, 108].*

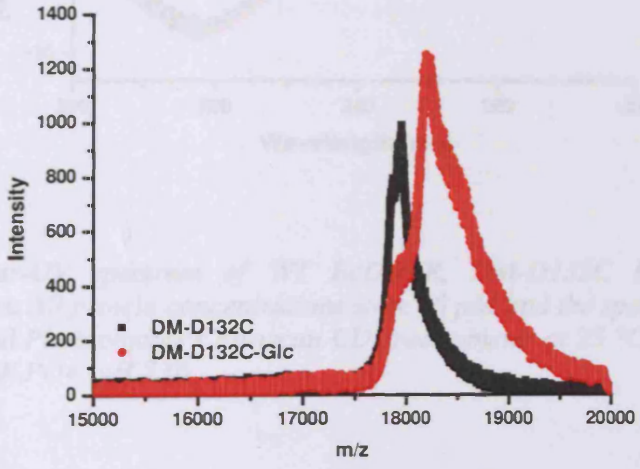

Figure 6.15: *MALDI-TOF mass spectra of DM-D132C EcDHFR and its glycoyslated form with Glc acetamide. The mass of the glycosylated form is in agreement with the calculated mass of DM-D132C carrying one Glc unit.*

6.4.1. Characterisation and thermal denaturation studies

CD spectroscopy was used to investigate the secondary structure of DM-D132C EcDHFR and its glycosylated forms and the thermal denaturation of the proteins. The far-UV CD spectrum of the EcDHFR triple mutants was compared to those of its glycosylated forms and WT EcDHFR. The CD spectrum for the glycosylated forms of DM-D132C EcDHFR had a minimum at 222 nm with a MRE value between -7,104 and -7,780 deg cm^2 $dmol^{-1}$, and this is comparable to WT EcDHFR (Figure 6.16; Table 6.16).

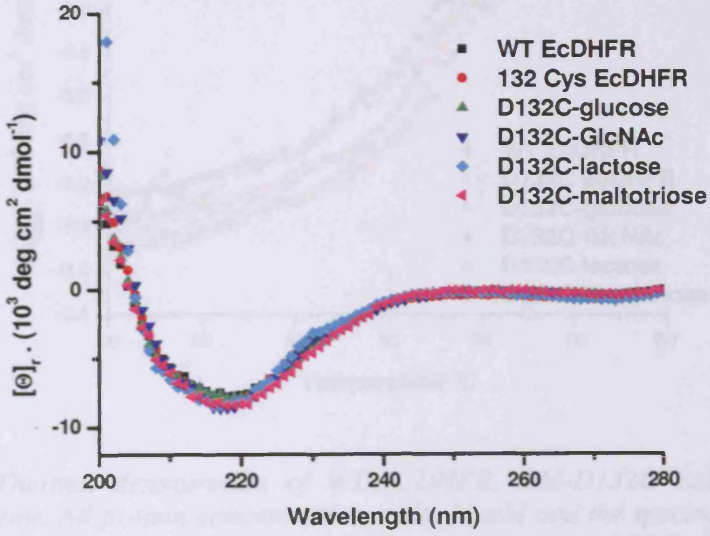

Figure 6.16: *Far-UV spectrum of WT EcDHFR, DM-D132C EcDHFR, and its glycosylated forms. All protein concentrations were 10 μM and the spectra were recorded by using a Applied Photophysics Chirascan CD spectrometer at 25 °C with a pathlength of 1 mm in 5 mM K_iPO4 (pH 7.0).*

Thermal denaturation of DM-D132C EcDHFR and its glycosylated forms was reversible from 20 to 80 °C at a temperature gradient of 24 °C h^{-1}. The CD transitions recorded for DM-D132C EcDHFR and its glycosylated forms were similar and their midpoints were within the experimental error of measurements (Figure 6.17 and Table 6.16). This shows that addition of glycans to the DM-R132C EcDHFR caused no significant difference in thermal stability.

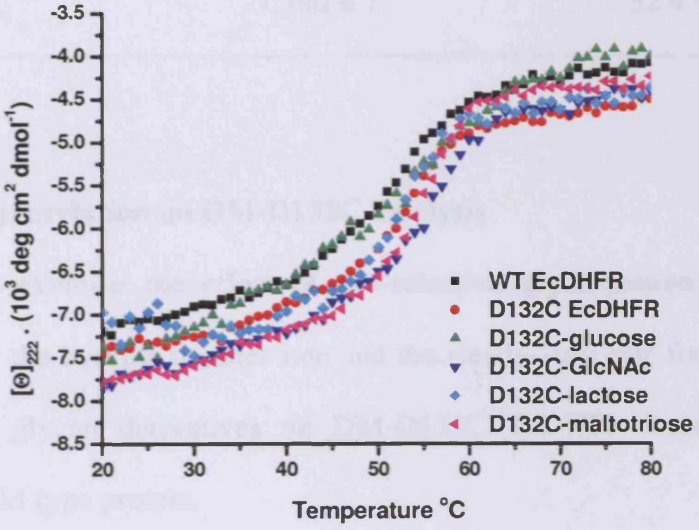

Figure 6.17: *Thermal denaturation of WT EcDHFR, DM-D132C EcDHFR, and its glycosylated forms. All protein concentrations were 10 μM and the spectra were recorded by using a Applied Photophysics Chirascan CD spectrometer at 25 °C with a pathlength of 1 mm in 5 mM K_iPO_4 (pH 7.0).*

Table 6.16: *Structural parameters for WT EcDHFR, DM-D132C EcDHFR, and its glycosylated forms.*

EcDHFR / Glycan	$[\Theta]_{222}$ (deg cm^2 $dmol^{-1}$)	T_M (°C)
WT	-7,399 ± 182	50.7 ± 0.2
DM-D132C	-7,417 ± 37	50.7 ± 0.3
Glucose	-7,424 ± 38	52.8 ± 0.9
GlcNAc	-7,766 ± 95	52.1 ± 1.6
Lactose	-7,104 ± 126	51.2 ± 0.7
Maltotriose	-7,780 ± 7	52.4 ± 0.6

6.5.2. Effects of glycosylation on DM-D132C catalysis

In order to examine the effect of site-selective glycosylation on DM-D132C EcDHFR catalysis, the hydride transfer rate and the steady-state rate for the reaction for the four different glycan derivatives on DM-D132C EcDHFR were measured and compared to the wild-type protein.

6.5.2.1 Steady state kinetic studies for glycosylated DM-D132C EcDHFR

Upon glycosylation of DM-D132C EcDHFR, the catalytic efficiency (k_{cat}/K_M) of the glycosylated DM-D132C EcDHFR improves compared with the non glycosylated DM-D132C EcDHFR from 3.5 to 7.5 s^{-1} μM^{-1} (Table 6.17). The k_{cat} values of the glycosylated proteins were not highly different to the WT EcDHFR, and the K_M^{NADPH} values for the glycosylated proteins (except D132C-glucose) were similar to the wild type protein, thereby increasing the catalytic efficiency of the protein and comparable to WT

EcDHFR. From the X-ray crystal structure, position 132 is located at the end of the F-G loop, with no direct contact with the ligands, however a change in the K_M values for NADPH is observed. Introduction of a hydrophobic residue into that region seems have disfavored the protein in catalytic reactivity which might due to local conformational change on the protein. However, when a carbohydrate moiety (hydrophilic compound) is introduce into that area, the K_M values for NADPH of the glycosylated protein is improved from 3.6 to 1.4 μM.

Table 6.17: *Steady state kinetic parameters for WT EcDHFR, DM-D132C EcDHFR, and its glycosylated forms. Kinetic measurements were carried out at 25 °C*

EcDHFR / Glycan	k_{cat} (s^{-1})	K_M^{NADPH} (μM)	k_{cat}/K_M^{NADPH} (s^{-1} μM^{-1})
WT	12.2 ± 0.7	1.6 ± 0.1	7.6
DM-D132C	12.6 ± 1.3	3.6 ± 0.1	3.5
Glucose	10.2 ± 0.8	2.7 ± 0.3	3.8
GlcNAc	9.7 ± 0.4	1.4 ± 0.0	6.9
Lactose	10.7 ± 0.4	1.6 ± 0.4	6.7
Maltotriose	11.3 ± 0.3	1.5 ± 0.2	7.5

6.5.2.2 Pre-steady state kinetic studies for glycosylated DM-D132C EcDHFR

The hydride transfer rate catalysed by DM-D132C EcDHFR and its glycosylated form were measured by stopped-flow FRET at 25 °C under the conditions of excess H_2F (Section 3.6). The resulting time course traces were fit to a single exponential decay and the rates are shown in Table 6.18. There is a slight decrease of hydride transfer rate for the glycoyslated proteins compared with the non-glycosylated DM-D132C EcDHFR

from 309 to 217 s^{-1}, which is comparable to that of the wild type protein (Table 6.18). Glycosylation at site 132 seems to have no large effects on the protein catalytic reactivity, therefore we did not observe a highly significant changes of the rates for the glycosylated proteins and WT EcDHFR.

Table 6.18: *Pre-steady state kinetic parameters for WT EcDHFR, DM-D132C EcDHFR, and its glycosylated forms. Kinetic measurements were carried out at 25 °C*

EcDHFR / Glycan	k_H (s^{-1})
WT	223 ± 5
DM-D132C	309 ± 8
Glucose	229 ± 7
GlcNAc	252 ± 22
Lactose	254 ± 15
Maltotriose	217 ± 18

6.5.3 Urea denaturation/ equilibrium unfolding of DM-D132C EcDHFR and its glycosylated forms

Equilibrium urea titrations were performed on the glycosylated DM-D132C EcDHFR and monitored by tryptophan fluorescence emission as previously described (Section 3.8). The difference in free energy, as determined by global fitting of fluorescence urea titration data, between the native and denatured states of the glycosylated DM-D132C EcDHFR, is similar to that for WT EcDHFR (Table 6.19). From the observed results, glycosylation at position 132 seems has no influence on the protein stability and it is comparable with the results from the thermal denaturation studies using CD spectroscopy (Section 6.5.1).

Table 6.19: *Thermodynamic parameters obtained from equilibrium urea denaturation for WT EcDHFR, DM-D132C EcDHFR, and its glycosylated forms*

EcDHFR / Glycan	$\Delta G°$ (kcal mol^{-1})	m (kcal $mol^{-1}M^{-1}$)	C_m (M)
WT	5.9 ± 0.3	2.1 ± 0.1	2.8 ± 0.1
DM-D132C	5.5 ± 0.3	2.6 ± 0.1	3.0 ± 0.1
Glucose	5.3 ± 0.2	2.2 ± 0.2	2.8 ± 0.1
GlcNAc	5.2 ± 0.3	1.8 ± 0.2	2.7 ± 0.2
Lactose	5.4 ± 0.3	1.7 ± 0.2	2.9 ± 0.1
Maltotriose	5.1 ± 0.2	1.7 ± 0.2	2.5 ± 0.1

6.5.4 Equilibrium dissociation constants (K_D) for glycosylated DM-D132C EcDHFR complexes.

Equilibrium dissociation constant studies between NADPH and folate with glycosylated DM-D132C were performed at 25 °C and *p*H 7.0 as described for the WT and DM-D132C EcDHFRs (Section 3.9 and Section 4.6). The K_D values for the glycosylated DM-D132C EcDHFRs with NADPH and folate were comparable to those of the wild type protein (Table 6.20). Although the observed K_D values for the protein glycosylated with lactose and maltotriose towards NADPH and folate were higher than the WT EcDHFR, these values were comparable to the WT EcDHFR. Position 132 is remote from the binding sites of both compounds. This would explain why glycosylation at 132 has no major influence on the K_D for either NADPH or folate.

Table 6.20: *Equilibrium dissociation constants of NADPH and folate parameters of WT EcDHFR, DM-D132C EcDHFR and its glycosylated forms at 25 °C and* pH *7.0*

EcDHFR / Glycan	K_D (μM)	
	NADPH	Folate
WT	0.10 ± 0.03	2.05 ± 0.05
DM-D132C	0.17 ± 0.08	2.11 ± 0.01
Glucose	0.32 ± 0.04	2.28 ± 0.08
GlcNAc	0.29 ± 0.04	2.23 ± 0.02
Lactose	0.37 ± 0.01	2.97 ± 0.16
Maltotriose	0.48 ± 0.13	2.80 ± 0.18

6.6 Conclusions

DM-N18C, DM-R52C, DM-D87C, and DM-D132C EcDHFR have been successfully glycosylated, and their secondary structures were analyzed by CD spectroscopy, showing similar results to the wild type protein. Thermal and urea denaturation studies showed that glycosylation does stabilized the protein. However these effects are dependent on the specific site of glycosylation. For example, the thermal stability of the DM-D87C EcDHFR is increased upon glycosylation. The stability gained through glycosylation was significantly higher than that observed for unglycosylated DM-D87C EcDHFR in the presence of high concentrations of maltose. The presence of 0.5 M maltose increased the melting temperature of all proteins examined by only approximately 3 °C. The increased stability frequently observed with naturally glycosylated proteins might therefore not simply be a nonspecific effect arising from changes in the solvation properties of the enzymes [53]. Site-specific effects can clearly

also contribute to the overall thermal stabilization of proteins, at least in the case of DHFR. All the results that observed for glycosylated DM-D87C EcDHFR have been published by our group [196].

At selected sites, the introduction of a carbohydrate moiety onto a protein has an effect on its catalytic reactivity. For example, the catalytic efficiency of the DM-R52C EcDHFR is increased upon glycosylation. However, glycosylation at position 18 does not increase the catalytic efficiency of the protein. Previous studies by Benkovic and co-workers on position 18 by attaching a large hydrophobic compound (*i.e.* Alexa 488) have showed similar results [126]. The increasing mass of the carbohydrate moiety attached at the central region of the Met20 loop has disrupted its flexibility in movement during complex formation within the protein. Therefore, glycosylation at the position 18 does have an effect of the protein dynamics. As a result, there is a decrease of its catalytic efficiency.

From our observed results, glycosylation seems to play an important role in protein stability and kinetics. However these effects were only observed at certain sites on EcDHFR.

Chapter 7

General Conclusions

Glycosylation is one of the major naturally occurring modifications of the covalent structure of proteins. Although much is known about the structure and biosynthesis of oligosaccharides in glycoproteins, the central question of how glycosylation contributes to the glycoprotein structure and function is not entirely clear. Studies on native glycosylated, carbohydrate-depleted, and recombinant non-glycosylated proteins have revealed such effects as stabilization of protein conformation, protection from proteolysis, protection from thermal denaturation, control of catalytic activity, and enhancement in nascent polypeptide solubility, but no effect was consistently observed for all glycoproteins. One method to study the effects of glycosylation systematically is the 'artificial' incorporation of glycans into proteins. The overall aim of this project was to use such an approach to determine the effect of site-specific glycosylation on the stability and kinetic reactivity of.DHFR, a naturally unglycosylated enzyme

The studies of glycosylated proteins required a substantial quantity of homologous glycoprotein, therefore an effective methodology was required. The method used combined site-directed mutagenesis to introduce cysteine residues in specific positions and subsequent derivatisation with chemically synthesized glycosyl haloacetamides (chloro or iodo). For purification, an innovative methodology was developed that uses scavenging of the unreacted sugar-free proteins by biotin-containing thiosulfonates followed by affinity chromatography yielding essentially pure glycosylated proteins. This is an efficient route for the synthesis of specifically glycosylated proteins to facilitate the study of the physical, chemical and biological effects of protein glycosylation.

The importance of site-specific glycosylation in stabilization of proteins against thermal denaturation was revealed clearly in our work. In the case of DM-D87C EcDHFR, site-selective glycosylation dramatically increased the resistance of the protein to thermal denaturation. The protein's melting temperature was increased significantly through the site-selective attachment of simple glycans by 6.0 to 9.0 °C. Glycosylation also stabilized DM-D87C EcDHFR against urea denaturation, increasing the free energy of unfolding value by 2.6 kcal mol^{-1}. However, this dramatic stabilization effect was not observed in the other three mutants of EcDHFR. The DM-N18C, DM-R52C, and DM-D132C mutants of EcDHFR showed little change in their observed thermal stability or resistance to urea denaturation upon glycosylation. This lack of effect on resistance to thermal denaturation has previously also been observed in DM-E120C [71]. Glu 120 is located on the water-exposed face of a surface loop next to Gly 121, which appears to be crucial for the activity of the enzyme. Thermal stability of DM-E120C EcDHFR was increased only slightly by the site-selective attachment of simple glycans. From these results, in general the changes of thermal stability of the proteins due to glycosylation is of the same order of magnitude as the decrease observed upon deglycosylation of naturally glycosylated proteins such as yeast external invertase, bovine serum fetuin and glucoamylase by 3.4, 4.0 and 1.9 °C, respectively [47]. Our data suggest that in certain circumstances significant increases in the thermal stability of proteins can be achieved even with the small carbohydrates used in the study, rather than with the often much larger oligosaccharides found in naturally glycosylated proteins. Resistance toward thermal denaturation due to glycosylation was only observable at specific sites on the protein.

The site-selectively glycosylated mutants of EcDHFRs showed similar kinetic activity (k_{cat}/K_M^{NADPH}) and hydride transfer rates to the wild-type protein. This suggests that the structures of the proteins were essentially unaltered. DM-R52C and DM-D132C EcDHFR showed slight improvement in their kinetic activity following site-selective glycosylation, while the kinetic activity of DM-N18C EcDHFR slightly decreased upon site-selective glycosylation and that of DM-D87C EcDHFR did not show any change. This is interesting because the mutation site at 87 is far from the active site (Asp 27) and hence has no direct contact with either the substrate or cofactor. The lack of effect on the kinetic activity values due to site-selective glycosylation has also been observed in the DM-E120C EcDHFR [71].

Although there were some improvements on kinetic activity values of the selected mutants of EcDHFR, the values were not significantly different to those of the wild-type protein. Interestingly, in four of the five cases studied, site-selective glycosylation does not show any large effects on the naturally nonglycosylated EcDHFR. There are several possible conclusions; the first is that the size of the carbohydrate moiety attached to the surface of the protein is too small for any large effects to be observed. Alternatively, the large effects shown by the carbohydrate moiety on glycoprotein in terms of stability and catalytic effects may only observe in natural glycoproteins. Finally, the increase in thermal stability upon site-selectively glycosylation on DM-D87C EcDHFR may be due to the specific interactions of the carbohydrate moiety at certain points on the protein. This final suggestion is supported by the fact that DM-D87C EcDHFR showed a large effect whereas the other four mutants did not. This suggests that the increase in resistance to thermal denaturation observed for proteins in sugar solutions is also due to binding of

the sugars to specific sites on the protein.

In conclusion, an effective method for the synthesis of homologous glycosylated and non-glycosylated proteins has been developed and applied to the site selective glycosylation of EcDHFR. While only minor effects on the kinetic properties of EcDHFR were observed, site-specific interactions between the proteins and the carbohydrate moieties led to significant effects on the stability of the protein.

References

1. Wormald, M.R., & Dwek, R. A., *Glycoproteins: glycan presentation and protein-fold stability [Minireview].* Structure, 1999. **7**: p. 155-160.

2. Rademacher, T.W., Parekh, R.B., & Dwek, R.A., *Glycobiology.* Annu. Rev. Biochem., 1988. **57**: p. 787-838.

3. Sharon, N., *Glycoproteins.* Trends Biochem. Sci., 1984. **9**: p. 198-202.

4. Bohne, A., Frank, M., Wetter, T., & Lieth, C-W. . *Glycosylation of Proteins: A Computer-Based Method for Rapid Exploration of Conformational Space of N-Glycans.* in *In Silico Biology.* 2001.

5. Hart, G.W., *Glycosylation.* Curr. Opin. Cell Biol., 1992. **4**: p. 1017-1023.

6. Jentoft, N., *Why are proteins O-glycosylated?* Trends Biochem. Sci., 1990. **15**: p. 291-294.

7. Abeijon, C., & Hirschberg, C.B., *Topography of glycosylation reactions in the endoplasmic reticulum.* Trends Biochem. Sci., 1992. **17**: p. 32-36.

8. Hirschberg, C.B., & Snider, M.D., *Topography of glycosylation in the rough endoplasmic reticulum and the Golgi apparatus.* Annu. Rev. Biochem., 1987. **56**: p. 63-87.

9. Schachter, H., *Enzymes associated with glycosylation.* Curr. Opin. Struct. Biol., 1991. **1**: p. 755-765.

10. Shaper, J.H., & Shaper, N.L., *Enzymes associated with glycosylation.* Curr. Opin. Struct. Biol., 1992. **2**: p. 701-709.

11. Sharon, N.L., & Lis, H., *Carbohydrates in cell recognition.* Sci. Am., 1993. **268**: p. 82-89.

12. Litman, G.W, Rast, .J., & Shamblott M.J., *Phylogenetic diversification of immunoglobulin genes and the antibody repertoire*, in *Mol. Biol. Evol.* 1993. p. 60-72.

13. Ravetch, J. & Bolland,.S., *IgG Fc receptors.* Annu Rev Immunol 2001. **19**: p. 275-290.

14. Parekh, R.B., *Effects of glycosylation on protein function.* Curr. Opin. Struct. Biol., 1991. **1**: p. 750-754.

15. Rasmussen, J.R., *Effect of glycosylation on protein function.* Curr. Opin. Struct. Biol., 1992. **2**: p. 682-686.

16. Wang, C.Q., Eufemi, M., Turano, C., & Giartosio, A., *Influence of the Carbohydrate Moiety on the Stability of Glycoproteins.* Biochemistry, 1996. **35**: p. 7299 - 7307.

17. Olsen, O., & Thomsen, K.K., J. Gen, Microbiology, 1991. **137**: p. 579-585.

18. Hecht, H.J., Kalisz, H.M., Hendle, J., Schmid, R.D., & Schomburg, D., *Crystal Structure of Glucose Oxidase from Aspergillus niger Refined at 2·3 Å Reslution.* J. Mol. Biol., 1993. **229**(1): p. 153-172.

19. Gerken, T.A., Butenhof, K.J., & Shogren, R., *Effects of glycosylation on the conformation and dynamics of O-linked glycoproteins: carbon-13 NMR studies of ovine submaxillary mucin.* Biochemistry, 1989. **28**: p. 5536-5543.

20. Rudd, P.M.,.Joao, H.C., Coghill, E., Fiten, P., Saunders, M.R., Opdenakker, G., & Dwek, R.A., *Glycoforms modify the dynamic stability and functional activity of an enzyme.* Biochemistry, 1994. **33**: p. 17-22.

21. Joao, H.C., Scragg, I.G., & Dwek, R.A., *Effects of glycosylation on protein conformation and amide proton exchange rates in RNase B.* FEBS Letters, 1992. **307**: p. 343-346.

22. Pazur, J.H., & Kleppe, K., *The Oxidation of Glucose and Related Compounds by Glucose Oxidase from Aspergillus niger.* Biochemistry, 1964. **3**: p. 578-583.

23. Crueger, A., & Crueger., W., *Microbial Enzymes and Biotechnology*, ed. W.M. Rogarty, & Kelly, C. T., Eds. 1990, London: Elsevier Applied Sciences.

24. Kohen, A., Jonsson, T., & Klinman, J.P., *Effects of Protein Glycosylation on Catalysis: Changes in Hydrogen Tunneling and Enthalpy of Activation in the Glucose Oxidase Reaction.* Biochemistry, 1997. **36**: p. 6854.

25. Bright, H.J., & Gibson, Q.H., *The Oxidation of 1-Deuterated Glucose by Glucose Oxidase* J. Biol. Chem., 1967. **242**: p. 994-1003.

26. Bright, H.J., & Appleby, M., *The pH Dependence of the Individual Steps in the Glucose Oxidase Reaction* J. Biol. Chem., 1969. **244**: p. 3625-3634.

27. Varghese, J.N., Epa, V.C., & Colman, P.M., *Three-dimensional structure of the complex of 4-guanidino-Neu5Ac2en and influenza virus neuraminidase* Protein Sciences, 1995. **4**: p. 1081-1087.

28. Shaw, A.L., Rothnagel, R., Chen, D., Ramig, R.F., Chiu, W., & Venkataram Prasad, B.V., *Three-dimensional visualization of the rotavirus hemagglutinin structure.* Cell, 1993. **74**: p. 693-701.

29. Puett, D., *Conformational Studies on a Glycosylated Bovine Pancreatic Ribonuclease* J. Biol. Chem., 1973. **248**: p. 3566-3572.

30. Williams, R.L., Greene, S.M., & McPherson, A., *The crystal structure of ribonuclease B at 2.5-A resolution* J. Biol. Chem., 1987. **262**: p. 16020-16031.

31. Mer, G., Hietter, H., & Lefevre J-F., *Stabilization of proteins by glycosylation examined by NMR analysis of a fucosylated proteinase inhibitor.* Nat. Struct. Biol., 1996. **3**(1): p. 45-53.

32. Priev, A., Almagor, A., Yedgar, S., & Gavish, B., *Glycerol Decreases the Volume and Compressibility of Protein Interior.* Biochemistry, 1996. **35**: p. 2061-2066.

33. Cioni, P., & Strambini, G.B., *Pressure Effects on Protein Flexibility Monomeric Proteins.* J. Mol. Biol., 1994. **242**: p. 291-301.

34. Welch, G.R., Samogyi, B., & Damjanovich, S., *The role of protein fluctuations in enzyme action: A review.* Prog. Biophys. Mol. Biol., 1983. **39**: p. 109-146.

35. Welch, G.R., *The Fluctuating Enzymes* ed. G.R. Welch, Ed. 1986, New York: J. Wiley and Sons.

36. Gregory, R.B., *Protein-Solvent Interactions*, ed. R.B. Gregory, Ed. 1995, New York: Marcel Dekker.

37. Williams, R.J.P., *Energised (entatic) States of Groups and of Secondary Structures in Proteins and Metalloproteins* Eur. J. Biochem., 1995. **234**(2): p. 363-381.

38. Mulholland, A.J., & Karplus, M., *Simulations of enzymic reactions.* Biochem. Soc. Trans., 1996. **24**: p. 247-254.

39. Sumi, H., & Ulstrup, J., *Dynamics of protein conformational fluctuation in enzyme catalysis with special attention to proton transfers in serine proteinases.* Biochim Biophys Acta, 1988. **955**: p. 26-42.

40. Borgis, D., & Hines, J. T., *The Enzyme Catalysis Process*, ed. A. Cooper, Houben, J., & Chien, L., Eds. 1989, New York: Plenum.

41. Bruno, W.J., & Bialek, W., *Vibrationally enhanced tunneling as a mechanism for enzymatic hydrogen transfer.* Biophys. J., 1992. **63**: p. 689-699.

42. Bala, P., Grochowski, P., Lesyng, B., & McCammon, J. A., *Quantum-Classical Molecular Dynamics Simulations of Proton Transfer Processes in Molecular Complexes and in Enzymes.* J. Phys. Chem, 1996. **100**: p. 2535-2545.

43. Seymour, S.L., & Klinman, J. P., *Comparison of Rates and Kinetic Isotope Effects Using PEG-Modified Variants and Glycoforms of Glucose Oxidase: The Relationship of Modification of the Protein Envelope to C-H Activation and Tunneling.* Biochemistry, 2002. **41**: p. 8747 - 8758.

44. Baek, W.O., & Vijayalakshmi, V. A., *Effect of chemical glycosylation histidines accessibility in immobilized metal ion affinity electrophoresis (IMAGE) system.* Biochim Biophys Acta, 1997. **1336**: p. 394-402.

45. Masárová, J., Misloviová, D., Gemeiner, P., & Michalková, E., *Stability enhancement of Escherichia coli penicillin G acylase by glycosylation with yeast mannan* Biotechnology and Applied Biochemistry, 2001. **34**: p. 127-133.

46. Broersen, K., Voragen, A. G. J., Hamer, R. J., & Harmen H. J. de Jongh, *Glycoforms of β-lactoglobulin with improved thermostability and preserved structural packing* Biotechnology and Bioengineering, 2004. **86**: p. 78-87.

47. Wang, C.Q., Eufemi, M., Turano, C., & Giartosio, A., *Influence of the Carbohydrate Moiety on the Stability of Glycoproteins.* Biochemistry, 1996. **35**: p. 7299 - 7307.

48. Kwon, K.-S., & Yu, M-H., *Effect of glycosylation on the stability of α1-antitrypsin toward urea denaturation and thermal deactivation.* Biochim Biophys Acta, 1997. **1335**: p. 265-272.

49. Gimenez-Roqueplo, A.-P., Célérier, J., Lucarelli, G., Corvol, P., & Jeunemaitre, X. , *Role of N-Glycosylation in Human Angiotensinogen* J. Biol. Chem., 1998. **273**: p. 21232-21238.

50. Crowe, J.H., Crowe, L. M., & Chapman, D., *Preservation of Membranes in Anhydrobiotic Organisms: The Role of Trehalose* Science, 1984. **223**: p. 701-703.

51. Carpenter, J.F., Crowe, L. M., & Crowe, J. H., *Stabilization of phosphofructokinase with sugars during freeze-drying: characterization of enhanced protection in the presence of divalent cations.* Biochim Biophys Acta, 1987. **923**: p. 109-115.

52. Xie, G., & Timasheff, S. N., *Mechanism of the stabilization of ribonuclease A by sorbitol: Preferential hydration is greater for the denatured than for the native protein.* Protein Sci., 1997. **6**: p. 211-221.

53. Xie, G., Timasheff, S. N., *The thermodynamic mechanism of protein stabilization by trehalose.* Biophys. Chem., 1997. **64**: p. 25-43.

54. Hynes, R.O., & Fox, C. F., *Tumor Cell Surfaces and Malignancy*, ed. A.R. Liss. 1980, New York.

55. Hynes, R.O., *Cell surface proteins and malignant transformation.* Biochimica et Biophysica Acta, 1976. **458**: p. 73-107.

56. Yamada, K.M., & Olden, K. , *Fibronectins-adhesive glycoproteins of cell surface and blood.* Nature, 1978. **275**: p. 179-184.

57. Olden, K., Hahn, E. L., & Yamada, K. M., *Cell Adhesion and Motility*, ed. A.S.G.P. Curtis, J. D., eds. 1980, Cambridge: Cambridge Univ. Press. 357-387.

58. Watt, G.M., & Boons, G-J., *A convergent strategy for the preparation of N-glycan core di-, tri-, and pentasaccharide thioaldoses for the site-specific glycosylation of peptides and proteins bearing free cysteines.* Carbohydrate Research, 2004. **339**(2): p. 181-193.

59. Parodi, A.J., *Protein Glucosylation and its role in protein folding.* Annual Review of Biochemistry, 2000. **69**: p. 31-67.

60. Schwarz, R.T., & Klenk, H-D. , *Inhibition of Glycosylation of the Influenza Virus Hemagglutinin* J. Virol., 1974. **14**: p. 1023-1034.

61. Schwarz, R.T., Rohrschneider, J. M., & Schmidt, M. F., *Suppression of glycoprotein formation of Semliki Forest, influenza, and avian sarcoma virus by tunicamycin.* J. Virol., 1976. **19**: p. 782-791.

62. Olden, K., Pratt, R. M., & Yamada, K. M., *Role of Carbohydrate in Biological Function of the Adhesive Glycoprotein Fibronectin.* PNAS, 1979. **76**: p. 3343-3347.

63. Prives, J.M., & Olden, K. , *Carbohydrate Requirement for Expression and Stability of Acetylcholine Receptor on the Surface of Embryonic Muscle Cells in Culture* PNAS, 1980. **77**: p. 5263-5267.

64. Kiichiro, T., Ichiro, M., & Yukishige, I., *Tight binding ligand approach to oligosaccharide-grafted protein.* Bioorganic & Medicinal Chemistry Letters 2004. **14**(9): p. 2285-2289.

65. Liu, H., Wang, L., Brock, A., Wong, C-H., & Schultz, P.G., *A Method for the Generation of Glycoprotein Mimetics.* J Am Chem Soc, 2003. **125**(7): p. 1702 - 1703.

66. Shin, Y., Winans, K. A., Backes, B.J., Kent, S. B. H., Ellman, J. A., & Bertozzi, C. R., *Fmoc-Based Synthesis of Peptide-αThioesters: Application to the Total Chemical Synthesis of a Glycoprotein by Native Chemical Ligation.* J Am Chem Soc, 1999. **121**(50): p. 11684-11689.

67. Davis, N.J., & Flitsch, S. L., *A novel method for the specific glycosylation of proteins.* Tetrahedron Lett, 1991. **32**(46): p. 6793-6796.

68. Davis, B.G., *Synthesis of Glycoproteins.* Chem. Rev., 2002. **102**: p. 579-601.

69. Wong, S.Y.C., Guile, G. R., Dwek, R. A., & Arsequell, G., *Synthetic glycosylation of proteins using N-(beta- saccharide) iodoacetamides: applications in site-specific glycosylation and solid-phase enzymic oligosaccharide synthesis. .* Biochem. J., 1994. **300**: p. 843-850.

70. Macmillan, D., Bill, R. M., Sage, K. A., Fern, D., & Flitsch, S. L., *Selective in vitro glycosylation of recombinant proteins: semi-synthesis of novel homogeneous glycoforms of human erythropoietin.* Chemistry & Biology, 2001. **8**: p. 133-145.

71. Swanwick, R.S., Daines, A. M., Flitsch, S. L., & Allemann, R. K., *Synthesis of homogenous site-selectively glycosylated proteins.* Org. Biomol. Chem, 2005. **3**: p. 572-574.

72. Plante, O.J., Palmacci, E. R., & Seeberger, P. H., *Automated Solid-Phase Synthesis of Oligosaccharides.* Science, 2001. **291**: p. 1523-1527.

73. Charlton, P.A., Young, D. W., Birdsall, B., Feeney, J., & Roberts, G. C. K., *Stereochemistry of reduction of folic acid using dihydrofolate reductase.* J. Chem. Soc., Chem. Commun, 1979(20): p. 922-924.

74. Fierke, C.A., Johnson, K. A., & Benkovic, S. J., *Construction and evaluation of the kinetic scheme associated with dihydrofolate reductase from Escherichia coli.* Biochemistry, 1987. **26**: p. 4085-4092.

75. Cameron, C.E., & Benkovic, S. J., *Evidence for a functional role of the dynamics of glycine-121 of Escherichia coli dihydrofolate reductase obtained from kinetic analysis of a site-directed mutant.* Biochemistry, 1997. **36**: p. 15792-15800.

76. Dann, J.G., Ostler, G., Bjur, R. A., King, R. W., Scudder, P., Turner, P. C., Roberts, G. C. K., & Burgen, A. S. V., *Large-scale purification and characterization of dihydrofolate reductase from a methotrexate-resistant strains of Lactobacillus casei.* Biochem. J., 1976. **157**: p. 559-571.

77. Swanwick, R.S., Shrimpton, P. J., & Allemann, R. K. , *Pivotal role of gly 121 in dihydrofolate reductase from Escherichia coli: the altered structure of a mutant enzyme may form the basis of its diminished catalytic performance.* Biochemistry, 2004. **43**: p. 4119-4127.

78. Schnell, J.R., Dyson, H. J., & Wright, P. E, *Structure, Dynamics, and Catalytic function of dihydrofolate reductase.* Annu. Rev. Biophys. Biomol. Struct, 2004. **33**: p. 119-140.

79. Huennekens, F.M., *In search of dihydrofolate reductase.* Protein Sciences, 1996. **5**(6): p. 1201-1208.

80. Gready, J.E., *Dihydrofolate reductase: Binding of substrates and inhibitors and catalytic mechanism.* Advan. Pharmacol. Chemother, 1980. **17**: p. 37-102.

81. Hitchings, G.H., *Selective inhibitors of dihydrofolate reductase.* In Vitro Cell Dev. Biol., 1989. **25**: p. 303-310.

82. Osborn, M.J., & Huennekens, F.M., *Enzymatic reduction of dihydrofolic acid.* J. Biol. Chem., 1958. **233**: p. 969-974.

83. Hitchings, G.H., & Burchall, J. J., *Inhibition of Folate Biosynthesis and Function as a Basis for Chemotherapy.* Advances in Enzymology Relative Areas Molecular Biology, 1965. **27**: p. 417-468.

84. Roth, C.C., *Recent Progress in the Medicinal Chemistry of 2,4-Diaminopyrimidines.* Progress in Medicinal Chemistry,, 1982. **19**: p. 269-331.

85. Futterman, S., *Enzymatic Reduction of folic acid and dihydrofolic acid to tetrahydrofolic acid.* J. Biol. Chem., 1957. **228**(2): p. 1031-1038.

86. Zakrzewski, S.F., *On the mechanism of chemical and enzymatic reduction of folate and dihydrofolate.* The Journal of Biological Chemistry, 1966. **341**(12): p. 2962-2967.

87. Kamen, B. *Folate and antifolate pharmacology.* in *Seminars in Oncology.* 1997.

88. Blakley, R.L., *Folates and Pterins.* 1984, New York: Wiley.

89. Stryer, L., *Biochemistry.* 5th ed. 1995, New York: W. H. Freeman Company.

90. Margosiak, S.A., Appleman, J. R., Santi, D. V., & Blakley, R. L., *Dihydrofolate Reductase from the Pathogenic Fungus Pneumocystis Carinii. Catalytic Properties and Interaction with Antifolates.* Archives of Biochemistry and Biophysics, 1993. **305**: p. 499-508.

91. Thillet, J., Adams, J. A., & Benkovic, S. J., *The Kinetic Mechanism of Wild-Type and Mutant Mouse Dihydrofolate Reductases.* Biochemistry, 1990. **29**: p. 5195-5202.

92. Appleman, J.R., Beard, W. A., Delcamp, T. J., Prendergast, N. J., Freisheim, J. H., & and R.L. Blakely, *Unusual Transient-State and Steady-State Kinetic Behaviour Is Predicted by the Kinetic Scheme Operational for Recombinant Human Dihydrofolate Reductase.* J. Biol. Chem., 1990. **265**: p. 2740-2748.

93. Howell, E.E., Villadranca, Jesus E., Wareen, Mark S., Oatley, Stuart J., and Kraut, Joseph., *Functional role of aspartic acid-27 in dihydrofolate reductase by mutagenesis.* Science, 1986. **231**: p. 1123-1129.

94. Lee, H., Reyes, V. M., & Kraut, J., *Crystal structures of Escherichia coli dihydrofolate reductase complexed with 5-formyltetrahydrofolate (folinic acid) in two space groups: Evidence of enolization of pteridine O4.* Biochemistry, 1996. **35**: p. 7012-7020.

95. Chen, Y.-Q., Kraut, J., Blakley, R. L., & Callender, R., *Determination by Raman spectroscopy of the pKa of N5 of dihydrofolate bound to dihydrofolate reductase: mechanistic implications.* Biochemistry, 1994. **33**(23): p. 7021-7026.

96. Cannon, W.R., Garrison, B. J., & Benkovic, S. J., *Electrostatic Characterization of Enzyme Complexes: Evaluation of the Mechanism of Catalysis of Dihydrofolate Reductase.* J Am Chem Soc, 1997. **119**(10): p. 2386-2395.

97. Cummins, P.L., & Gready, J. E., *Energetically most likely substrate and active-site protonation sites and pathways in the catalytic mechanism od dihydrofolate reductase* J Am Chem Soc, 2001. **123**: p. 3418-3428.

98. Miller, G.P., & Benkovic, S. J., *Stretching exercises - flexibility in dihhydrofolate reductase catalysis.* Chemistry and Biology, 1998. **5**(5): p. R105-R113.

99. Sawaya, M.R., & Kraut, J., *Loop and subdomain movements in the mechanism of Escherichia coli dihydrofolate reductase: crystallographic evidence.* Biochemistry, 1997. **36**: p. 586-603.

100. Matthews, D.A., Alden, R. A., Bolin, J. T., Freer, S. T., Hamlin, R., Xuong, N., Kraut, J., Poe, M., Williams, M., & Hoogsteen, K., *Dihydrofolate Reductase. X-Ray Structure of Binary Complex with Methotrexate.* Science, 1977. **197**(4302): p. 452-455.

101. Volz, K.W., D.A. Matthews, R.A. Alden, S.T. Freer, C. Hansch, B.T. Kaufman, & J. Kraut,, *Crystal Structure of Avian Dihydrofolate Reductase Containing Phenyltriazine and Nadph.* J. Biol. Chem., 1982. **257**(5): p. 2528-2536.

102. Oefner, C., A. Darcy, & F.K. Winkler, *Crystal Structure of Human Dihydrofolate Reductase Complexed with Folate.* Eur. J. Biochem., 1988. **174**: p. 377-385.

103. Stammers, D.K., J.N. Champness, C.R. Beddell, J.G. Dann, E. Eliopoulos, A.J. Geddes, D. Ogg, & A.C.T. North, *The Structure of Mouse L1210 Dihydrofolate Reductase Drug Complexes and the Construction of a Model of Human Enzyme.* FEBS Letters, 1987. **218**: p. 178-184.

104. Champness, J.N., A. Achari, S.P. Ballantine, P.K. Bryant, C.J. Delves, & D.K. Stammers, *Structure of Pneumocystis Carinii Dihydrofolate Reductase to 1.9 Angstrom Resolution.* Structure, 1994. **2**: p. 915-924.

105. Knighton, D.R., C.C. Kan, E. Howland, C.A. Janson, Z. Hostomska, K.M. Welsch, & D.A. Matthews,, *Structure of and Kinetic Channeling in Bifunctional Dihydrofolate Reductase-Thymidylate Synthase.* Nat. Struct. Biol., 1994. **1**: p. 186-194.

106. Bolin, J.T., Filman D. J., Matthews, D. A., Hamlin, R. C., & Kraut, J. , *Crystal structures of Escherichia coli and Lactobacillus casei dihydrofolate reductase refined at 1.7 A resolution. I. General features and binding of methotrexate.* J. Biol. Chem., 1982. **257**(22): p. 13673-13678.

107. Bystroff, C., & Kraut, J., *Crystal structure of unliganded Escherichia coli dihydrofolate reductase. Ligand induced conformational changes and cooperativity in binding.* Biochemistry, 1991. **30**: p. 2227-2239.

108. Osborne, M.J., Venkitakrishnan, R. P., Dyson, H. J., & Wright, P. E., *Diagnostic chemical shift markers for loop conformation and substrate and cofactor binding in dihydrofolate reductase complexes* Protein Sciences, 2003. **12**(10): p. 2230-2238.

109. Dams, T.J., R., *Stability and Folding of Dihydrofolate Reductase from the Hyperthermopohilic Bacterium Thermotoga Maritima.* Biochemistry, 1999. **38**: p. 9169-9178.

110. Dams, T., Auerbach, G., Bader, G., Ploom, T., Huber, R., Jaenicke, R. , *The crystal structure of dihydrofolate reductase from Thermotoga maritima: molecular features of thermostability.* J.Mol.Biol, 2000. **297**: p. 659-672.

111. Sterner, R., G.R. Kleemann, H. Szadkowski, A. Lustig, M. Hennig, & K. Kirschner,, *Phosphoribosyl Anthranilate Isomerase from Thermotoga Maritima Is an Extremely Stable and Active Homodimer.* Protein Sci., 1996. **5**(10): p. 2000-2008.

112. Knapp, S.V., W.M. de Vos, D. Rice, & R. Kladenstein,, *Crystal Structure of Glutamate Dehydrogenase from the Hyperthermophilic Eubacterium Thermotoga Maritima at 3.0 Å Resolution.* J. Mol. Biol., 1997. **267**: p. 916-932.

113. Winterhalter, C., P. Heinrich, A. Candussio, G. Wich, & Liebl.W, *Identification of a Novel Cellulose-Binding Domain within the Multidomain 120 Kda Xylanase Xyna of the Hyperthermophilic Bacterium Thermotoga Maritima.* Mol. Microbiol., 1995. **15**: p. 431-444.

114. Falzone, C.J., Wright, P. & Benkovic. S. J., *Dynamics of a flexible loop in dihhydrofolate reductase from Escherichia coli and its implecation for catalysis.* Biochemistry, 1994. **33**: p. 439-442.

115. Rod, T.H., & Brooks III, C. L., *How dihydrofolate reductase facilitates protonation of dihydrofolate.* J Am Chem Soc, 2003. **125**: p. 8718-8719.

116. Mesecar, A.D., B.L. Stoddard, & D.E. Koshland,, *Orbital Steering in the Catalytic Power of Enzymes: Small Structural Changes with Large Catalytic Consequences.* Science, 1997. **277**: p. 202-206.

117. Wu, Y.D.K.N.H., *Theoretical Transition Structures for Hydride Transfer to Methyleniminium Ion from Methylamine and Dihydropyridine - on the Nonlinearity of Hydride Transfers.* J Am Chem Soc, 1987. **109**: p. 2226-2227.

118. Bystroff, C., Oatley, S. J., & Kraut, J., *Crystal structures of Escherichia coli dihydrofolate reductase: the NADP+ holoenzyme and the folate-NADP+ ternary complex. Substrate binding and a model for the transition state.* Biochemistry, 1990. **29**: p. 3263-3277.

119. Fierke, C.A., & Benkovic, S. J., *Probing the functional role of thronine-113 of escherichia coli dihydrofolate reductase for its effect on turnover efficiency, catalysis and binding.* Biochemistry, 1989. **28**: p. 478-486.

120. Warren, M.S., Brown, K. A., Farnum, M. F., Howell, E. E., & Kraut, J., *Investigation of the functional role of tryptophan-22 in Escherichia coli dihydrofolate reductase by site-directed mutagenesis.* Biochemistry, 1991. **30**(46): p. 11092-11103.

121. Miller, G.P.S.J.B., *Strength of an Interloop Hydrogen Bond Determines the Kinetic Pathway in Catalysis by Escherichia Coli Dihydrofolate Reductase.* Biochemistry, 1998. **37**: p. 6336-6342.

122. Cayley, P.J., Dunn, S. M. J., & King, R. W., *Kinetics of substrate, coenzyme, and inhibitor binding to Escherichia coli dihydrofolate reductase.* Biochemistry, 1981. **20**: p. 874-879.

123. Dunn, S.M., Batchelor, J. G., & King, R. W., *Kinetics of ligand binding to dihydrofolate reductase: binary complex formation with NADPH and coenzyme analogues.* Biochemistry, 1978. **17**: p. 2356-2364.

124. Dunn, S.M., & King, R. W., *Kinetics of ternary complex formation between dihydrofolate reductase, coenzyme, and inhibitors.* Biochemistry, 1980. **19**: p. 766-773.

125. Chen, J.T., Taira, K., Tu, C. P., & Benkovic, S. J., *Probing the functional role of phenylalanine-31 of Escherichia coli dihydrofolate reductase by site-directed mutagenesis.* Biochemistry, 1987. **26**: p. 4093-4100.

126. Rajagopalan, P.T.R., Zhang, Z., McCourt, L., Dwyer, M., Benkovic, S. J., & Hammes, G. G., *Interaction of dihydrofolate reductase with methotrexate: ensemble and single-molecule kinetics.* Biochemistry, 2002. **99**: p. 13481-86.

127. Kitahara, R., Sareth, S., Yamada H, Ohmae, E., Gekko, K., & Akasaka, K., *High pressure NMR reveals active-site hinge motion of folate-bound Escherichia coli dihydrofolate reductase.* Biochemistry, 2000. **39**: p. 12789-12795.

128. Birdsall, B., Polshakov VI., & Feeney, J., *NMR studies of ligand carboxylate group interactions with arginine residues in complexes of Lactobacillus casei dihydrofolate reductase with substrates and substrate analogues.* Biochemistry, 2000. **39**: p. 9819-9825.

129. Zaborowski, E., Chung, J., Kroon, G.J.A., Dyson, H.J., & Wright, P.E., *Backbone HN, N, Cα, C' and Cβ assignments of the 19 kDa DHFR/NADPH complex at 9°C and pH 7.6.* J. Biomol. NMR, 2000. **16**: p. 349-350.

130. Li, L., Falzone, C. J., Wright, P. & Benkovic, S. J, *Functional role of mobile loop of Escherichia coli dihydrofolate reducatse in transition-state stabilization.* Biochemistry, 1992. **31**: p. 7826-7833.

131. Epstein, D.M.B., S. J. & Wright, P. E, *Dynamics of the dihhydrofolate reductase-folate complex: catalytic sites and regions known to undergo conformational change exhibit diverse dynamical features.* Biochemistry, 1995. **34**: p. 11037-11048.

132. Falzone, C.J., Benkovic, S. J., & Wright, P. E., *Partial 1H NMR assignments of the Escherichia coli dihydrofolate reductase complex with folate: evidence for a unique conformation of bound folate.* Biochemistry, 1990. **29**: p. 9667-9677.

133. Lassalle, M.W., Yamada, H., & Akasaka, K., *The Pressure-temperature Free Energy-landscape of Stapylococcal Nuclease Monitored by ^{1}H NMR* J. Mol. Biol., 2000. **298**: p. 293-302.

134. Akasaka, K., Tezuka, T., & Yamada, H., *Pressure-induced Changes in the Folded Structure of Lysozyme.* J. Mol. Biol., 1997. **271**: p. 671-678.

135. Farnum, M.F., Magde, D., Howell, E. E., Hirai, J. T., & Warren, M. S., *Analysis of hydride transfer and cofactor fluorescence decay in mutants of dihydrofolate reductase: possible evidence for participation of enzyme molecular motions in catalysis.* Biochemistry, 1991. **30**: p. 11567-11579.

136. Lipari, G., & Szabo, A., *Model-free approach to the interpretation of nuclear magnetic resonance relaxation in macromolecules. 1. Theory and range of validity.* J Am Chem Soc, 1982. **104**: p. 4546-4559.

137. Lipari, G., & Szabo, A., *Model-free approach to the interpretation of nuclear magnetic resonance relaxation in macromolecules. 2. Analysis of experimental results.* J Am Chem Soc, 1982. **104**: p. 4559-4570.

138. Osborne, M.J., Schnell, J., Benkovic, S. J., Dyson, H. J., & Wright, P. E., *Backbone Dynamics in Dihydrofolate Reductase Complexes: Role of Loop Flexibility in the Catalytic Mechanism.* Biochemistry, 2001. **40**(33): p. 9846-9859.

139. Miller, G.P., & Benkovic, S.J., *Deletion of a Highly Motional Residue Affects Formation of the Michaelis Complex for Escherichia Coli Dihydrofolate Reductase.* Biochemistry, 1998. **37**: p. 6327-6335.

140. Rajagopalan, P.T.R., Lutz, S., & Benkovic, S. J., *Coupling Interactions of Distal Residues Enhance Dihydrofolate Reductase Catalysis: Mutational Effects on Hydride Transfer Rates.* Biochemistry, 2002. **41**(42): p. 12618 - 12628.

141. Agarwal, P.K., Billeter, S. R., Rajagopalan, P. T. R., Benkovic, S. J., & Hammes-Schiffer, S., *Network of Coupled Promoting Motions in Enzyme Catalysis.* PNAS, 2002. **99**: p. 2794-2799.

142. Watney, J.B., Agarwal, P. K., & Hammes-Schiffer, S., *Effect of mutation on enzyme motion in dihydrofolate reducatase.* J Am Chem Soc, 2003. **125**: p. 3745-3750.

143. Rod, T.H., Radkiewicz, J. L., & Brooks III, C. L., *Correlated Motions and the Effect of Distal Mutation in Dihydrofolate Reductase Catalysis.* PNAS, 2003. **100**: p. 6980-6985.

144. Sanbrook, J., Fritsch, E.F., & Maniatis, T., *Molecular Cloning - A Laboratory Manual.* 2nd ed. 1984, NY: Cold Spring Harbor Laboratories.

145. Mejbaum-Katzenellenbogen, W., & Dobryszycka, W., *New method for quantitative determination of serum proteins separated by paper electrophoresis.* Clin. Chim. Acta, 1959. **4**: p. 515-522.

146. Kunkel, *QuickChange Site-Directed mutagenesis Kit.* 1985: Stratagene.

147. Vardevanyan, P.O., Antonyan, A. P., Parsadanyan, M. A., Davtyan, H. G., & Karapetyan, A. T., *The binding of ethidium bromide with DNA: interaction with single- and double-stranded structures.* Exp Mol Med, 2003. **35**(6): p. 527-533.

148. Birnboim, H.C., & Doly, J., *A rapid alkaline extraction for screening recombinant plasmid DNA.* Nuc. Acid Res, 1979. **7**: p. 1513-1523.

149. Laemmli, U.K., *Cleavage of Structural Proteins during the Assembly of the Head of Bacteriophage T4* Nature, 1970. **227**: p. 680-685.

150. Mejbaum-Katzenellenbogen, W., & Dobryszycka, W., *Immunochemical properties of the serum proteins after regeneration from the protein-tannin compounds.* Nature, 1962. **193**: p. 1288.

151. Jeong, S.-S., & Gready, J. E., *pH dependence of enzyme reaction rates and deuterium isotope effects on the reduction of a new mechanism-based substrate by dihydrofolate reductase (DHFR).* Biochemistry, 1995. **34**: p. 3734-3741.

152. Orr, G.A., & Blanchard, J. S., *High-Performance Ion-Exchange Separation of Oxidized and Reduced Nicotinamide Adenine Dinucleotides.* 1984. **142**(Analytical Biochemistry): p. 232-234.

153. Dawson, R.M.C., Elliott, D. C., Elliott, W. H., & Jones, K. M., *Data for Biochemical Research.* 1969, Oxford, U.K.: Oxford University Press.

154. Stone, S.R., & Morrison, J. F., *Kinetic mechanism of the reaction catalyzed by dihydrofolate reductase from Escherichia coli.* Biochemistry, 1982. **21**: p. 3757-3765.

155. Pace, C.N., *Determination and analysis of urea and guanidine hydrochloride denaturation curves.* Methods Enzymol., 1985. **131**: p. 267-280.

156. Tanford, C., *Isothermal unfolding of globular proteins in aqueous urea solutions.* J Am Chem Soc, 1964. **86**: p. 2050-2059.

157. Pace, C.N., Shirley, B. A., & Thomson, J. A., *Protein Structure: A Practical Approach*, ed. T.E. Creighton, ed. 1989, USA: Oxford University Press. 311-330.

158. Prakash, V., & Timasheff, S. N., *The calculation of partial specific volumes of proteins in 8 M urea solution.* Anal. Biochem, 1981. **117**: p. 330-335.

159. Iwakura, M., Jones, B. E., Luo, J, Matthews, C. R., *A Strategy for Testing the Suitability of Cysteine Replacements in Dihydrofolate Reductase from Escherichia coli.* J. Biochem, 1995. **117**: p. 480-488.

160. Touchette, N.A., Perry, K. P., & Matthews, C. R., *Folding of dihydrofolate reductase from Escherichia coli.* Biochemistry, 1986. **25**: p. 5445-5452.

161. Ohmae, E., Kurumiya, T., Makino, S., & Gekko, K. , *Acid and Thermal Unfolding of Eseherichia coli Dihydrofolate Reductase* J. Biochem, 1996. **120**: p. 946-953.

162. Maglia, G., & Allemann, R.K., *Hydride transfer during catalysis by dihydrofolate reductase from Thermotoga maritima.* Biochem. J. , 2003. **374**: p. 529-535.

163. Bolen, D.W., & Santoro, M. M., *Unfolding energy changes determined by the linear extrapolation method. 2. Incorporation of Delta Gn-u values in a thermodynamics cycle.* Biochemistry, 1988. **27**: p. 8069-8074.

164. Robinson, D.R., & Jencks, W. P., *The effects of the urea-guanidinium class on the activity coefficients of acetyltetraglycine ethyl ester and related compounds.* J Am Chem Soc, 1965. **97**: p. 2462-2470.

165. Roseman, M., & Jencks, W. P., *Interactions of urea and other polar compounds in water.* J Am Chem Soc, 1975. **97**(631-640).

166. Alexander, S.S., & Pace, C. N., *A comparison of the denaturation of bovine Beta-lactoglobulins A and B and goat-lactoglobulin.* Biochemistry, 1971. **10**: p. 2738-2743.

167. Pace, C.N., & Tanford, C., *Thermodynamics of the unfolding of beta-lactoglobulin A in aqueous urea solutions between 5 and 55 degrees.* Biochemistry, 1968. **7**: p. 198-208.

168. Greene, R.F.J., & Pace, C. N. , *Urea and guanidine hydrochloride denauration of ribonucleases, lysozyme, alpha-chymotrypsin, and beta-lactoglobulin.* J. Biol. Chem., 1974. **249**: p. 5388-5393.

169. Shelton, V.M., Sosnick, T. R., & Pan, T., *Applicability of urea in the thermodynamic analysis of secondary and tertiary RNA folding.* Biochemistry, 1999. **38**: p. 16831-16839.

170. Smith, V.F., & Matthews, R., *Testing the role of chain connectivitiy on the stability and structure of dihydrofolate reductase from E. coli: fragment complementation and circular permutation reveal stable, alternative folded forms.* Protein Sci., 2001. **10**: p. 116-128.

171. Ohmae, E., Fukumizu, Y., Iwakura, M., & Gekko, K., *Effects of Mutations at Methionine-42 of Escherichia coli Dihydrofolate Reductase on Stability and Function: Implication of Hydrophobic Interactions.* J. Biochem, 2005. **137**: p. 643-652.

172. Shaw, D., Odom, J. D., & Dunlap, R. B., *High expression and steady-state kinetic characterisation of methionine site-directed mutants of Escherichia coli menthionyl- and selenomethionyl-dihydrofolate reductase.* Biochim Biophys Acta, 1999. **1429**: p. 401-410.

173. Leszczynski, J.F., & Rose, G. D., *Loops in globular proteins: a novel category of secondary structure* Science, 1986. **234**: p. 859-855.

174. Richardson, J.S., *The Anatomy and Taxonomy of Protein Structure.* Adv. Protein Chem., 1981. **34**: p. 167-339.

175. Allemann, R.K., Evans, R.M., Tey, L-H., Maglia, G., Pang, J., Rodriguez, R., Shrimpton, P.J., & Swanwick, R.S., *Protein motions during catalysis by dihydrofolate reductases*, in *Phil. Trans. R. Soc. Lond. B.* 2006. p. 1317-1321.

176. Gekko, K., Yamagami, K., Kunori, Y., Ichihara, S., Kodama, M., & Iwakura, M., *Effects of point mutation in a flexible loop on the stability and enzymatic function of escherichia coli dihydrofolate reductase.* J. Biochem, 1993. **113**: p. 74-80.

177. Gekko, K., Kunori, Y., Takeuchi, H., Ichihara, S., & Kodama, M., *Point mutations at glycine-121 of Escherichia coli dihydrofolate reducatse: Important role of a flexible loop in the stability and function.* J. Biochem, 1994. **116**: p. 34-41.

178. Sham, Y.Y., Ma, B., Tsai, C.J., & Nussinov, R., *Molecular Dynamic simulation of E.coli dihydrofolate reductase and its protein fragments: relative stabilities in experiment and simulations.* Protein Sci., 2001. **10**: p. 135-148.

179. Lowe, J.B., *Glycosylation, Immunity, and Autoimmunity.* Cell, 2001. **104**: p. 809.

180. Lasky, L.A., *Selectin-Carbohydrate Interactions and the Initiation of the Inflammatory Response.* Annual Review of Biochemistry, 1995. **64**: p. 113-140

181. Sharon, N., & Lis, H., *Lectins-Proteins with a sweet tooth: Functions in cell recognition.* Essays in Biochemistry, 1995. **30**: p. 59.

182. Helenius, A., & Aebi, M., *Intracellular Functions of N-Linked Glycans* in *Science.* 2001. p. 2364-2369.

183. Vijayalekshmi, S., George, S. K., Andersson, L. K., Kihlberg, J., & Baltzer, L., *A surface exposed O-linked galactose residue destabilises the structure of a folded helix-loop-helix dimer.* Org. Biomol. Chem, 2003. **1**: p. 2455.

184. Bill, R.M., & Flitsch, S. L., *Chemical and biological approaches to glycoprotein synthesis.* Chem. Biol., 1996. **3**: p. 145.

185. Rudd, P.M., Joao, H. C., Coghill, E., Fiten, P., Saunders, M. R., Opdenakker, G., & Dwek, R. A., *Glycoforms modify the dynamic stability and functional activity of an enzyme.* Biochemistry, 1994. **33**: p. 17-22.

186. Muir, T.W., *Semisythesis of proteins by expressed protein ligation.* Annual Review of Biochemistry, 2003. **72**: p. 249-289

187. Bill, R.M., P.C. Winter, C.M. McHale, V.M. Hodges, G.E. Elder, J. Caley, S.L. Flitsch, R. Bicknell, & T.R. Lappin, *Expression and mutagenesis of recombinant human and murine erythropoietins in Escherichia coli.*, in *Biochim Biophys Acta.* 1995. p. 35-43.

188. Davis, B.G., & Jones, J. B., *Glycoprotein Synthesis: From Glycobiological Tools to Tailor-made Catalysts* Synlett, 1999: p. 1495.

189. Lloyd, R.C., Davis, B. G., & Jones, J. B., *Site-selective glycosylation of subtilisin Bacillus lentus causes dramatic increases in esterase activity.* Bioorg. Med. Chem, 2000. **8**: p. 1537.

190. Davis, B.G., Lloyd, R. C., & Jones, J. B., *Controlled Site-Selective Glycosylation of Proteins by a Combined Site-Directed Mutagenesis and Chemical Modification Approach.* J. Org. Chem, 1998. **63**: p. 9614.

191. Davis, B.G., Maughan, M.A.T., Green, M.P., & Ullman, A., *Glycomethanethiosulfonates: powerful reagents for protein glycosylation.* Tetrahedron: Asymmetry, 2000. **11**: p. 245-262.

192. Andersson, L., Stenhagen, G., & Baltzer, L., *The Site-Selective Glycosylation of a Designed Helix-Loop-Helix Polypeptide Motif.* J. Org. Chem, 1998. **63**: p. 1366-1367.

193. Altenbach, C., Flitsch, S. L., Khorana, H. G., & Hubbell, W. L., *Structural studies on transmembrane proteins. 2. Spin labeling of bacteriorhodopsin mutants at unique cysteines.* Biochemistry, 1989. **28**: p. 7806 - 7812.

194. Flitsch, S.L., & Khorana, H. G., *Structural studies on transmembrane proteins. 1. Model study using bacteriorhodopsin mutants containing single cysteine residues.* Biochemistry, 1989. **28**: p. 7800 - 7805.

195. Hubbell, W.L., Cafiso, D. S., & Altenbach, C., *Identifying conformational changes with site-directed spin labeling* Nat. Struct. Biol., 2000. **7**: p. 735-739.

196. Swanwick, R.S., Daines, A. M., Tey, L-H., Flitsch, S. L., & Allemann, R. K., *Increased Thermal Stability of Site-Selectively Glycosylated Dihydrofolate Reductase.* ChemBioChem, 2005. **6**: p. 1338-1340.

Publications

Increased Thermal Stability of Site-Selectively Glycosylated Dihydrofolate Reductase

Richard S. Swanwick,[a, b] Alison M. Daines,[c] Lai-Hock Tey,[a] Sabine L. Flitsch,[c] and Rudolf K. Allemann*[a, b]

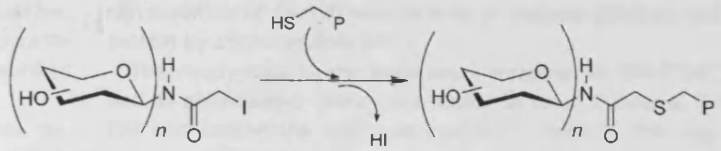

Scheme 1. Alkylation of site-selectively introduced cysteine mutants of DHFR;[12,16] $n = 0$–3.

Glycosylation is important for many molecular processes such as molecular recognition, degradation and stability. While it has long been established that the native conformation of many proteins can be stabilised against thermal denaturation through glycosylation,[1–3] the mechanism of such stabilisation is less clear. The removal of carbohydrates from naturally glycosylated proteins through the use of glycosidases[4] or by mutagenesis of glycosylation sites[5,6] can lead to decreased thermal stability of the protein. This is often accompanied by an increased tendency towards protein aggregation. Due to the heterogeneous nature of protein glycosylation both in vivo and in vitro, a comprehensive study of its effect on thermal stability has been elusive. However, studies of the stability of several unglycosylated proteins in the presence of high concentrations of saccharides such as glycerol, glucose, sucrose, galactose and α,α-trehalose have led to the conclusion that these glycans stabilise the folded protein due to preferential binding of the native state.[7–10] Such observations suggest that glycosylation of natural proteins could establish a microenvironment that resembles that of unglycosylated proteins in solutions of high carbohydrate content.

The scope of studies into specific in vitro glycosylation of proteins has until recently been limited. The use of natural enzymes allows the site-selective introduction of sugars but is limited to natural glycans and by often relatively poor yields. Chemical glycosylation reactions, however, which are more flexible with respect to the choice of glycan, suffer from limited site-selectivity. Such shortcomings have been overcome through a combination of the introduction of unique cysteine residues at required sites and a highly flexible but selective chemical derivatisation strategy (Scheme 1).[11–16] This methodology allowed us to study the effect of site-specific glycosylation on the thermal stability of the naturally nonglycosylated enzyme, dihydrofolate reductase (DHFR), systematically.

DHFR is a major target for antibacterial and anticancer drugs and has long served as a paradigm for the study of enzyme kinetics, protein dynamics and stability. DHFR has a compact folded form (Figure 1), which is comprised of two domains, the adenosine binding and loop domains. These domains are connected by a short polypeptide stretch centred around amino acid residues 86 and 87, known as the hinge region. Large-scale movements of external loops control access of the cofactor to the active site and propagation through the catalytic cycle.[17–19] Here we report dramatic increases in the thermal stability of *E. coli* DHFR as a result of site-selective glycosylation of individual surface residues.

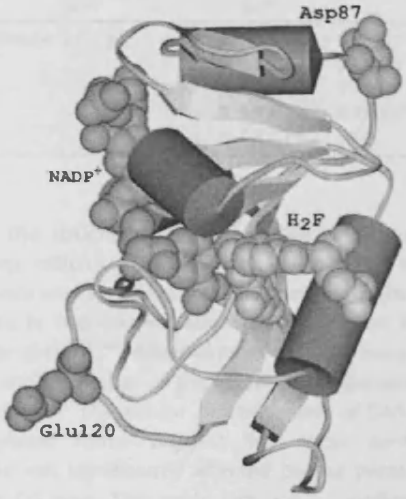

Figure 1. Diagram of the structure of *E. coli* DHFR indicating the positions of the two loop residues Asp87 and Glu120. The positions of dihydrofolate (H_2F) and cofactor ($NADP^+$) are shown in the space-filling models.[17]

Loop residues 87 and 120, located on opposite sides of the protein (Figure 1), were chosen for selective glycosylation. Glu120 is positioned on the water-exposed face of a surface loop next to Gly121, which appears to be crucial for the activity of the enzyme. Mutation of residue 121 significantly reduces the catalytic performance of DHFR through local conformational changes that affect the properties of the enzyme globally.[20–26] Asp87 is a solvent exposed residue within the hinge region that connects the adenosine binding and loop domains. The hinge region appears to lose its native structure relatively early in the temperature-induced unfolding process.[20,27] Site-selective glycosylation of positions 120 and 87 of DHFR was achieved through the replacement of Glu120 and Asp87 with cysteine by site-directed mutagenesis of the cysteine free double mutant DHFR-C85A/C152S (DM), which has folding, stability and kinetic properties very similar to those of the wild-type protein.[28] DM-E120C and DM-D87C were derivatised by

[a] *Dr. R. S. Swanwick, L.-H. Tey, Prof. R. K. Allemann*
School of Chemistry, Cardiff University
Park Place, Cardiff CF10 3AT (UK)
Fax: (+44)-2920-879014
E-mail: allemannrk@cardiff.ac.uk

[b] *Dr. R. S. Swanwick, Prof. R. K. Allemann*
School of Chemistry, University of Birmingham
Edgbaston, Birmingham, B15 2TT (UK)

[c] *Dr. A. M. Daines, Prof. S. L. Flitsch*
School of Chemistry, University of Edinburgh
King's Buildings, West Mains Road, Edinburgh, EH9 3JJ (UK)

  DOI: 10.1002/cbic.200500103

treatment with the iodoacetamides of *N*-acetyl glucosamine, glucose, maltose, lactose and maltotriose (*O*-α-D-glucopyranosyl-(1→4)-*O*-α-D-glucopyranosyl-(1→4)-D-glucose) and purified as described previously.[16]

CD-spectroscopy indicated no significant differences between the structures of wild-type DHFR, DM-E120C and DM-D87C and their glycosylated forms (Figure 2). However, when

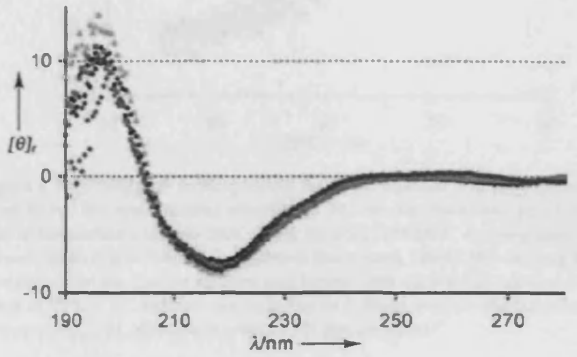

Figure 2. Representative CD-spectra for DHFR, DHFR mutants and their glycosylated forms. CD-spectra of DHFR (brown dots), DM (black dots), DM-D87C (red squares), DM-E120C (blue squares) and DM-D87C-lactose-acetamide (green triangles). All other glycan-carrying proteins described in the text exhibited CD-spectra that were essentially identical to the ones shown here. All protein concentrations were 10 μM and the spectra were recorded by using a JASCO-810 spectrometer at 25 °C with a path length of 1 mm in 10 mM KP_i pH 7.0. Mean residue ellipticities [Θ], are reported in units of 10^3 deg cm^2 dmol^{-1}.

the thermal stabilities of the proteins were investigated by measuring their CD-spectra as a function of temperature, the presence of the glycans led to significant stabilisation of the protein folds (Table 1). Glycosylation of Cys120 led to a small but significant increase in the melting temperature of the protein. Interestingly, the extent of stabilisation observed for disaccharides was about twice that seen for monosaccharides.

Table 1. Melting temperatures [°C] of DM, DM-E120C and DM-D87C and their glycosylated forms. The thermal stabilities of nonglycosylated DM and DM-D87C in the presence of 0.5 M maltose are also indicated. The melting temperatures were determined from the denaturation curves obtained from the dependence of the mean residue ellipticity at 222 nm $[\Theta]_{r,222}$ on temperature. All protein concentrations were 10 μM and the spectra were recorded on a JASCO-810 spectrometer with a path length of 1 mm in 10 mM KP_i pH 7.0.[20] The melting temperature for wild-type DHFR is 50.7 ± 0.2 °C.

Glycan	DM	DM-E120C	DM-D87C
none	50.8 ± 0.3	50.8 ± 0.4	40.9 ± 0.3
glucose		51.8 ± 0.2	47.1 ± 0.3
GlcNAc		52.5 ± 0.1	49.6 ± 1.1
lactose		54.1 ± 0.1	46.8 ± 2.1
maltose		54.2 ± 0.3	n.d.
maltotriose		n.d.	47.5[a]
acetamide		51.3[a]	39.6 ± 1.2
+0.5 M maltose	52.9 ± 0.4	n.d.	43.4 ± 0.4

[a] Single measurement.

Glycosylation of Cys120 with lactose or maltose stabilised the protein by approximately 3 °C.

The steady-state kinetic parameters measured for DM-E120C and its glycosylated forms were similar to those measured for DM and indeed the wild-type enzyme[29] (Table 2). This suggests that the structures were essentially unaltered. The surface FG loop, which contains Glu120, is connected through hydrogen bonds and van der Waals interactions to the M20 loop, which exists in two conformations depending on the state of the catalytic cycle.[17,30] Movements of the M20 loop, which display rates similar to that of the steady-state turnover, regulate ligand binding.[23] The similar reaction rates of DM-E120C and its glycosylated forms suggest that these conformational changes are not significantly affected by the presence of glycans in the FG loop. This could indicate a coordinated movement of the FG and M20 loops and is in agreement with results obtained by molecular mechanics simulations.[23,24,31]

Table 2. Steady state kinetic parameters of DHFR mutants and their glycosylated forms. Kinetic measurements were carried out at 25 °C as previously described.[29] The kinetic parameters for DHFR are $K_M^{NADPH} = 2.8 \pm 0.3$ μM and $k_{cat} = 8.8 \pm 0.2$ s^{-1}.

Glycan	DM		DM-E120C		DM-D87C	
	k_{cat} [s^{-1}]	K_M^{NADPH} [μM]	k_{cat} [s^{-1}]	K_M^{NADPH} [μM]	k_{cat} [s^{-1}]	K_M^{NADPH} [μM]
None	7.0 ± 0.4	2.7 ± 0.5	6.4 ± 1.4	2.3 ± 1.0	9.1 ± 0.1	4.9 ± 1.7
Glucose			7.8 ± 1.1	3.7 ± 1.4	7.3 ± 0.9	10.5 ± 1.5
GlcNAc			5.3 ± 1.7	3.9 ± 2.1	7.4 ± 0.1	6.3 ± 1.3
Lactose			7.1 ± 2.0	1.9 ± 1.7	6.1 ± 2.4	7.0 ± 1.8
Maltose			7.7 ± 1.9	6.8 ± 1.6	n.d.	n.d.

While replacing Glu120 with Cys had no effect on the stability of the protein, DM-D87C displayed significantly reduced stability compared to DM (Table 1). The melting temperature of DM-D87C was lowered by almost 10 °C and the thermally induced unfolding reaction displayed somewhat reduced cooperativity (Figure 3). However, the CD-spectrum of DM-D87C at 25 °C was comparable to that of DM (Figure 2); this suggests that no major conformational changes had occurred as a consequence of the amino acid change. Derivatisation of DM-D87C with glycosyl iodoacetamides dramatically increased the stability of the protein. Alkylation with *N*-acetyl glucosamine completely reversed the destabilising effect of Cys87, and the glycosylated protein displayed thermal stability that was identical to that of the parent protein (Table 1). The shape of the melting curve observed for glycosylated forms of DM-D87C was comparable to that of DM (Figure 3). As had been observed for glycosylated DM-E120C, the steady-state kinetic properties of the DM-D87C and its glycosylated forms at 25 °C, were similar to those observed for DM (Table 2). Together with the unaltered CD-spectra of the glycosylated proteins, the results suggested that the altered thermal stabilities of the proteins were not a consequence of global conformational changes, but due to the site-specific presence of glycans. Alkylation of DM-E120C and DM-D87C with nonglycosylated iodoacetamide alone did not lead to a significant increase of the

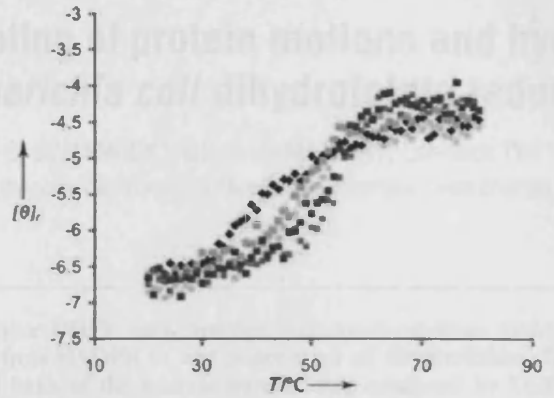

Figure 3. Representative melting curves for DHFR mutants and their glycosylated forms. The mean residue ellipticity at 222 nm was measured as a function of temperature for DM-D87C (black squares), DM-D87C carrying glucose (green squares) and *N*-acetylglucosamine (blue dots), DM-E120C carrying *N*-acetylglucosamine (purple squares) and lactose (red squares) by using a gradient of 20 °C h^{-1}. Conditions are as in Figure 2. Mean residue ellipticities at 222 nm $[\Theta]_{222}$ are reported in units of 10^3 deg cm^2 dmol^{-1}.

proteins' melting temperatures (Table 1). This indicated that the glycans were responsible for the increased stability of the glycoproteins. The unnatural linkage between the proteins and the glycans was clearly not the cause of their enhanced stability.

Asp87, which is located in the hinge region between the adenosine binding and loop domain of DHFR, contains one of the most solvent exposed side chains of the protein. Replacement of the polar carboxylate group of Asp87 with the hydrophobic side chain of cysteine might generate a local conformational change that affects the thermal stability of the protein. Glycosylation of residue 87 on the other hand reversed this effect most likely through increased solvation. However, the stability increase gained through glycosylation was significantly higher than that observed for the unglycosylated protein in the presence of high concentrations of maltose. The presence of 0.5 M maltose increased the melting temperature of all proteins examined by only approximately 3 °C (Table 1). The increased stability frequently observed with naturally glycosylated proteins, might therefore not simply be a nonspecific effect arising from changes in the solvation properties of the enzymes.[10] Site-specific effects can clearly also contribute to the overall thermal stabilisation of proteins, at least in the case of DHFR.

Our results show that site-selective glycosylation of DHFR can dramatically increase the resistance of the protein against thermal denaturation. The protein's melting temperature could be increased significantly through the site-selective attachment of simple glycans. It should be noted that the increase in thermal stability observed in our studies is of the same order of magnitude as the decreases observed upon deglycosylation of naturally glycosylated proteins, which were 3.4, 4.0 and 1.9 °C for yeast external invertase, bovin serum fetuin and glucoamylase, respectively.[4] Our data suggest that significant increases in the thermal stability of proteins can be achieved even with the small carbohydrates used in this study, rather than with the often much larger oligosaccharides found in naturally glycosylated proteins.

Acknowledgements

This work was financially supported by the BBSRC, the EPSRC and the Wellcome Trust.

Keywords: glycosylation · mutagenesis · oligosaccharides · selectivity · thermal stability

[1] W. O. Baek, M. A. Vijayalakshmi, *Biochim. Biophys. Acta* **1997**, *1336*, 394.
[2] J. Masarova, D. Mislovicova, P. Gemeiner, E. Michalkova, *Biotechnol. Appl. Biochem.* **2001**, *34*, 127.
[3] K. Broersen, A. G. J. Voragen, R. J. Hamer, H. H. J. de Jongh, *Biotechnol. Bioeng.* **2004**, *86*, 78.
[4] C. Q. Wang, M. Eufemi, C. Turano, A. Giartosio, *Biochemistry* **1996**, *35*, 7299.
[5] K. S. Kwon, M. H. Yu, *Biochim. Biophys. Acta* **1997**, *1335*, 265.
[6] A. P. Gimenez-Roqueplo, J. Célérier, G. Lucarelli, P. Corvol, X. Jeunemaitre, *J. Biol. Chem.* **1998**, *273*, 21 232.
[7] J. H. Crowe, L. M. Crowe, D. Chapman, *Science* **1984**, *223*, 701.
[8] J. F. Carpenter, L. M. Crowe, J. H. Crowe, *Biochim. Biophys. Acta* **1987**, *923*, 109.
[9] G. F. Xie, S. N. Timasheff, *Protein Sci.* **1997**, *6*, 211.
[10] G. F. Xie, S. N. Timasheff, *Biophys. Chem.* **1997**, *64*, 25.
[11] D. Macmillan, R. M. Bill, K. A. Sage, D. Fern, S. L. Flitsch, *Chem. Biol.* **2001**, *8*, 133.
[12] N. J. Davis, S. L. Flitsch, *Tetrahedron Lett.* **1991**, *32*, 6793.
[13] R. M. Bill, P. C. Winter, C. M. McHale, V. M. Hodges, G. E. Elder, J. Caley, S. L. Flitsch, R. Bicknell, T. R. J. Lappin, *Biochim. Biophys. Acta* **1995**, *1261*, 35.
[14] B. G. Davis, *Chem. Rev.* **2002**, *102*, 579.
[15] D. P. Gamblin, P. Garnier, S. van Kasteren, N. J. Oldham, A. J. Fairbanks, B. G. Davis, *Angew. Chem.* **2004**, *116*, 845; *Angew. Chem. Int. Ed.* **2004**, *43*, 827.
[16] R. S. Swanwick, A. M. Daines, S. L. Flitsch, R. K. Allemann, *Org. Biomol. Chem.* **2005**, *3*, 572.
[17] M. R. Sawaya, J. Kraut, *Biochemistry* **1997**, *36*, 586.
[18] M. J. Osborne, J. Schnell, S. J. Benkovic, H. J. Dyson, P. E. Wright, *Biochemistry* **2001**, *40*, 9846.
[19] M. J. Osborne, R. P. Venkitakrishnan, H. J. Dyson, P. E. Wright, *Protein Sci.* **2003**, *12*, 2230.
[20] R. S. Swanwick, P. J. Shrimpton, R. K. Allemann, *Biochemistry* **2004**, *43*, 4119.
[21] C. E. Cameron, S. J. Benkovic, *Biochemistry* **1997**, *36*, 15 792.
[22] G. P. Miller, S. J. Benkovic, *Chem. Biol.* **1998**, *5*, R105.
[23] P. K. Agarwal, S. R. Billeter, P. T. R. Rajagopalan, S. J. Benkovic, S. Hammes-Schiffer, *Proc. Natl. Acad. Sci. USA* **2002**, *99*, 2794.
[24] S. J. Benkovic, S. Hammes-Schiffer, *Science* **2003**, *301*, 1196.
[25] T. H. Rod, J. L. Radkiewicz, C. L. Brooks, *Proc. Natl. Acad. Sci. USA* **2003**, *100*, 6980.
[26] I. F. Thorpe, C. L. Brooks, *Proteins Struct. Funct. Bioinf.* **2004**, *57*, 444.
[27] Y. Y. Sham, B. Y. Ma, C. J. Tsai, R. Nussinov, *Proteins* **2002**, *46*, 308.
[28] M. Iwakura, B. E. Jones, J. B. Luo, C. R. Matthews, *J. Biochem.* **1995**, *117*, 480.
[29] G. Maglia, M. H. Javed, R. K. Allemann, *Biochem. J.* **2003**, *374*, 529.
[30] R. P. Venkitakrishnan, E. Zaborowski, D. McElheny, S. J. Benkovic, H. J. Dyson, P. E. Wright, *Biochemistry* **2004**, *43*, 16 046.
[31] J. L. Radkiewicz, C. L. Brooks, *J. Am. Chem. Soc.* **2000**, *122*, 225.

Received: March 15, 2005
Published online on July 8, 2005

Biochem. J. (2006) 394, 259–265 (Printed in Great Britain) doi:10.1042/BJ20051464

Coupling of protein motions and hydrogen transfer during catalysis by *Escherichia coli* dihydrofolate reductase

Richard S. SWANWICK*, Giovanni MAGLIA†, Lai-hock TEY* and Rudolf K. ALLEMANN*[1]

*School of Chemistry, Cardiff University, Main Building, Park Place, Cardiff CF10 3AT, U.K., and †School of Chemistry, University of Birmingham, Edgbaston, Birmingham B15 2TT, U.K.

The enzyme DHFR (dihydrofolate reductase) catalyses hydride transfer from NADPH to, and protonation of, dihydrofolate. The physical basis of the hydride transfer step catalysed by DHFR from *Escherichia coli* has been studied through the measurement of the temperature dependence of the reaction rates and the kinetic isotope effects. Single turnover experiments at pH 7.0 revealed a strong dependence of the reaction rates on temperature. The observed relatively large difference in the activation energies for hydrogen and deuterium transfer led to a temperature dependence of the primary kinetic isotope effects from 3.0 ± 0.2 at 5 °C to 2.2 ± 0.2 at 40 °C and an inverse ratio of the pre-exponential factors of 0.108 ± 0.04. These results are consistent with theoretical models for hydrogen transfer that include contributions from quantum mechanical tunnelling coupled with protein motions that actively modulate the tunnelling distance. Previous work had suggested a coupling of a remote residue, Gly^{121}, with the kinetic events at the active site. However, pre-steady-state experiments at pH 7.0 with the mutant G121V-DHFR, in which Gly^{121} was replaced with valine, revealed that the chemical mechanism of DHFR catalysis was robust to this replacement. The reduced catalytic efficiency of G121V-DHFR was mainly a consequence of the significantly reduced pre-exponential factors, indicating the requirement for significant molecular reorganization during G121V-DHFR catalysis. In contrast, steady-state measurements at pH 9.5, where hydride transfer is rate limiting, revealed temperature-independent kinetic isotope effects between 15 and 35 °C and a ratio of the pre-exponential factors above the semi-classical limit, suggesting a rigid active site configuration from which hydrogen tunnelling occurs. The mechanism by which hydrogen tunnelling in DHFR is coupled with the environment appears therefore to be sensitive to pH.

Key words: dihydrofolate reductase, dynamics, hydrogen transfer, kinetics, protein motions, tunnelling.

INTRODUCTION

It has long been accepted that electrons can be transferred in chemical reactions by quantum mechanical tunnelling with energies of activation deriving from heavy-atom motions [1]. However, only recently have several cases of hydrogen tunnelling been described where the probability of tunnelling was modulated by environmental dynamics and protein motions [2–15]. Several theoretical models that incorporate environmental motions have been developed to describe hydrogen transfer reactions [5,16–19]. The model proposed by Kuznetsov and Ulstrup [19] and developed further by Knapp and Klinman [5,13] for enzymatic transformations, which separates the faster e^- and H co-ordinates from the environmental co-ordinate, distinguishes between passive motions that influence the probability of the formation of an active site configuration conducive to hydride transfer, and active protein motions that modulate the tunnelling distance and hence the reaction rate.

DHFR (dihydrofolate reductase) has long served as a paradigm for the study of issues relating to enzyme structure, dynamics and catalysis. DHFR catalyses the reduction of H_2F (7,8-dihydrofolate) to H_4F (5,6,7,8-tetrahydrofolate) with the concurrent oxidation of NADPH. DHFR is essential for maintaining intracellular levels of H_4F, a cofactor involved in the biosynthesis of several amino acids, purines and thymidylate. DHFR from *Escherichia coli* is a monomeric enzyme comprising an eight-stranded β-sheet and four α-helices connected by flexible loop regions (Figure 1). The M20, βF-βG and βG-βH loops have been implicated in catalysis [20]. In the reactive ternary complex, when both H_2F and NADPH are bound, the M20 loop adopts the closed conformation, which is stabilized through hydrogen bonds between residues in the M20 and the βF-βG loops [21]. The backbone atoms of the βF-βG loop display high dynamic mobility in NMR relaxation experiments, which has been interpreted to suggest a connection between the dynamic properties and the catalytic behaviour of DHFR [22–25].

The complete kinetic scheme for DHFR from *E. coli* has been determined [26,27]. The reaction rate is strongly dependent on the pH of the solution. The chemical step, in which the *pro-R* hydrogen is transferred from C-4 of NADPH to C-6 of H_2F and N-5 of the substrate is protonated, is characterized by a single pK_a of approx. 6.5 with a rate variation of almost two orders of magnitude. This pK_a can most likely be attributed to protonation of the substrate in the ternary enzyme complex [28]. At physiological pH, the overall rate of the conversion of H_2F into H_4F is limited by product release, while the chemical step is fast and essentially irreversible [26]. However, at pH values of 9.5 and above, hydrogen transfer is much slower and fully rate-determining.

Several computational studies using combined QM/MM (quantum mechanical and molecular mechanical) and free-energy perturbation approaches have shed some light on the mechanism of the hydride transfer step in DHFR catalysis [28–35]. QM/MM simulations and genomic sequence analysis identified a network of hydrogen bonds and van der Waals interactions in DHFR from *E. coli* between the surface βF-βG loop and the active site that may influence protein dynamics and promote catalysis [18,36]. Replacement of Gly^{121}, a highly mobile residue located in the middle of the βF-βG loop over 19 Å (1 Å = 0.1 nm) from

Abbreviations used: DHFR, dihydrofolate reductase; DTT, dithiothreitol; H_2F, 7,8-dihydrofolate; H_4F, 5,6,7,8-tetrahydrofolate; KIE, kinetic isotope effect; NADPD, (4*R*)-[^{2}H]NADPH; QM/MM, quantum mechanical and molecular mechanical.

[1] To whom correspondence should be addressed (email allemannrk@cardiff.ac.uk).

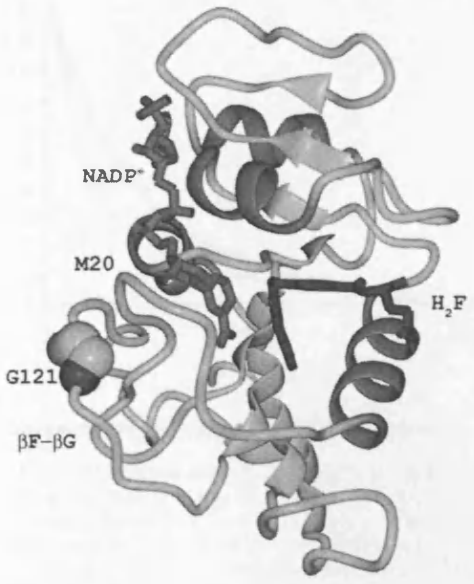

Figure 1 Structure of DHFR from *E. coli* bound to $NADP^+$ and H_2F

The PDB file 1RA2 [21] was used to generate the diagram. The βF-βG and the M20 loops as well as the position of the catalytically important loop residue Gly^{121} are indicated.

the active site (Figure 1), with valine or leucine slowed the hydride transfer rate dramatically and weakened binding of NADPH [37]. Experimental and theoretical results suggested that this reduction in the rate of hydride transfer was due to significant differences in the stability of the tertiary structural elements surrounding the site of the mutation [22,33,38].

Two previous experimental studies suggested a coupling between protein dynamics and DHFR catalysis. Pre-steady-state measurements with DHFR from *Thermotoga maritima* indicated that protein fluctuations were coupled with hydride transfer which at low temperature displayed a significant contribution from tunnelling [8]. Steady-state experiments at the non-physiological pH value of 9, where hydride transfer is largely rate-determining for the *E. coli* enzyme, suggested a relatively rigid active site geometry and hydride transfer by extensive tunnelling, modulated by passive dynamics [2].

Here, we report measurements of the hydride transfer catalysed by DHFR from *E. coli* and the G121V-DHFR mutant, in which valine replaced the loop residue Gly^{121}. While hydride transfer was slowed by almost two orders of magnitude in the mutant at physiological pH, hydrogen transfer was actively coupled with the environment for both proteins. The mechanism by which hydrogen transfer coupled with the environment was dependent on pH.

MATERIALS AND METHODS

Substrates and cofactors

H_2F was prepared by dithionite reduction of folate (Sigma) as described previously [39]. NADPH was purchased from Sigma. NADPD ((4*R*)-[^{2}H]NADPH) was prepared by reduction of $NADP^+$ (Sigma) using the $NADP^+$-dependent alcohol dehydrogenase from *Thermoanaerobium brokii* (Sigma) and purified by anion-exchange chromatography on Mono Q™ HR 5/5 (Amersham Biosciences). NADPH and NADPD concentrations were determined spectrophotometrically using a molar absorption coefficient (ε) at 339 nm of 6200 $M^{-1} \cdot cm^{-1}$. Similarly, the concentration of H_2F was measured assuming an ε of 28 000 $M^{-1} \cdot cm^{-1}$ at 282 nm for pH 7.4.

Protein purification

BL21(DE3) Star (Stratagene) cells were used for the production of DHFR from *E. coli* and its G121V mutant from a pET11c derived plasmid (Novagen) containing the respective coding regions essentially as described in [38]. Cells were grown in LB (Luria–Bertani) medium containing 0.27 mM ampicillin at 37 °C to an optical density at 600 nm of 0.6. Expression was induced by the addition of isopropyl β-thiogalactoside to a final concentration of 0.4 mM. Cells were harvested by centrifugation and resuspended in lysis buffer [25 mM potassium phosphate, pH 7.0, 0.5 M NaCl, 1 mM EDTA, 10 %, v/v, glycerol and 1 mM DTT (dithiothreitol)]. The suspension was sonicated for 5 min on ice and centrifuged at 50 000 ***g*** for 45 min. The supernatant was applied to a methotrexate column (10 ml; Sigma) pre-equilibrated with lysis buffer. The resin was extensively washed (~300 ml) with the same buffer and elution of bound protein was achieved with 100 mM sodium borate (pH 8.3), 0.5 M NaCl, 10 % glycerol and 3 mM folic acid. The eluted protein was dialysed extensively against 10 mM potassium phosphate (pH 7.0) containing 1 mM DTT. The dialysate was applied to a DEAE-Sepharose column (20 ml; GE Healthcare) previously equilibrated with 10 mM potassium phosphate (pH 7.0) containing 1 mM DTT and 5 mM EDTA. The bound protein was eluted with a gradient from 0 to 1 M NaCl in potassium phosphate (pH 7.0), 5 mM EDTA and 1 mM DTT and dialysed to remove salt. The protein concentrations were measured spectrophotometrically assuming an ε of 31 100 $M^{-1} \cdot cm^{-1}$ at 280 nm and by titration with methotrexate.

Pre-steady-state kinetic measurements

Pre-steady-state kinetic experiments were performed on an Applied Photophysics stopped-flow spectrophotometer essentially as described before [8]. Hydride transfer rates were measured following the fluorescence resonance energy transfer from the protein to reduced NADPH in potassium phosphate for optimal pH stability over the temperature range. The sample was excited at 292 nm and the emission was measured using an output filter with a cut-off at 400 nm. In a typical experiment for DHFR, the enzyme (40 μM, final concentrations) was preincubated with NADPH or NADPD (20 μM) in 100 mM potassium phosphate (pH 7.0) and 100 mM NaCl for at least 15 min to avoid hysteresis. The reaction was started by rapidly mixing with H_2F (200 μM) in the same buffer. For G121V-DHFR, the enzyme (20 μM) was preincubated with NADPH or NADPD (10 μM) and the experiments were run as above. The hydride transfer rates did not change when the concentration of NADPH was reduced to 5 μM or doubled to 20 μM.

Steady-state kinetic measurements

All steady-state kinetic experiments were performed in MTEN buffer (50 mM MES buffer, 25 mM Tris, 25 mM ethanolamine and 100 mM NaCl) at pH 9.5. The pH was carefully adjusted at the experimental temperature with the relevant calibration buffers [borate (pH 10; Fisher Chemicals) and phosphate (pH 7; Fisher Chemicals)] at that temperature. DHFR (50 nM) was preincubated with NADPH/NADPD (50 μM) for 10 min at the experimental temperature prior to the addition of excess H_2F (100 μM) to initiate the reaction. The steady-state rate was determined from the linear decrease in the absorbance of the reduced cofactor at 340 nm with time using a molar absorbance change for the DHFR

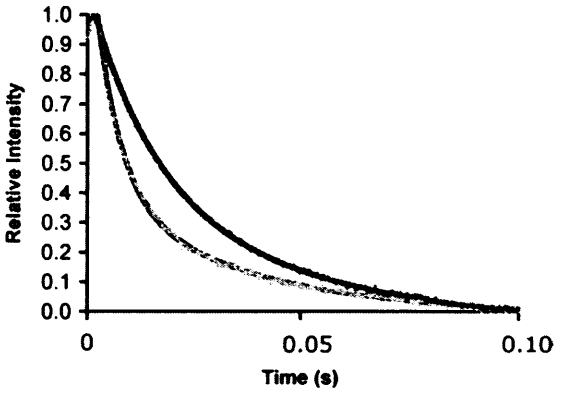

Figure 2 Fluorescence energy transfer during DHFR catalysis

Measurement of the rate of H- (light grey dots) and D- (dark grey) transfer catalysed by DHFR in a single turnover experiment measured by stopped-flow fluorescence resonance energy transfer from DHFR to the reduced cofactor at 25 °C. The relative intensity of fluorescence above 400 nm was measured after excitation at 292 nm. The fits to a double-exponential model for decreasing fluorescence intensity are also indicated. DHFR was preincubated with NADPH or NADPD and the reaction started through the addition of H_2F. Final concentrations were: DHFR, 40 μM; reduced cofactor, 20 μM and H_2F, 200 μM. The dead time of the experiments was approx. 0.002 s.

reaction of 11 800 $M^{-1} \cdot cm^{-1}$ [40]. Each data point was measured at least six times.

RESULTS AND DISCUSSION

Temperature dependence of hydride transfer and KIEs (kinetic isotope effects) for DHFR catalysis

The rate of hydride transfer (k_H) from NADPH to H_2F was measured at pH 7 and 25 °C in single-turnover experiments by monitoring fluorescence resonance energy transfer from DHFR to the reduced cofactor in the presence of excess enzyme [26,37]. The decrease of the fluorescence intensity was best described by a double exponential (Figure 2). The rate constant of the slow step (~6.5 s^{-1}) was independent of the concentration of NADPH and did not depend on whether NADPH or NADPD was used as the cofactor. It most likely represented the slow release of cofactor and/or product. At 25 °C, the rapid decrease in fluorescence intensity preceding this slow step occurred with a first-order rate constant of 203.7 ± 7.4 s^{-1} (see Supplementary Table 1 at http://www.BiochemJ.org/bj/394/bj3940259add.htm) in good agreement with previously published values of 220 s^{-1} [26,37] and 222.8 ± 1.3 s^{-1} [8]. The slight variation is most likely a consequence of the different buffers used in these experiments. In the experiments reported here potassium phosphate was used because of its good pH stability over wide ranges of temperature. When NADPD was used as the cofactor, the rate constant was reduced to 75.1 ± 5.4 s^{-1}, resulting in a KIE of 2.7 ± 0.2. This value was identical with the value of 2.8 that has been predicted computationally [31] and the published experimental value of 2.9 ± 0.2 at ambient temperature [41].

To evaluate whether hydride transfer during catalysis by DHFR was coupled to protein motions, the rate of the chemical step was measured at pH 7.0 as a function of the temperature between 5 and 40 °C for both ^1H (H)- and ^2H (D)-transfer. The temperature dependence of the rates was fitted to the empirical Arrhenius equation ($\ln k = \ln A - E_A/RT$, where k is a first-order rate constant, A is the pre-exponential factor and E_A is the experimental activation energy) to obtain the activation energy and the pre-exponential factor (Figure 3). The reaction rates showed a relatively strong dependence on the temperature, resulting in

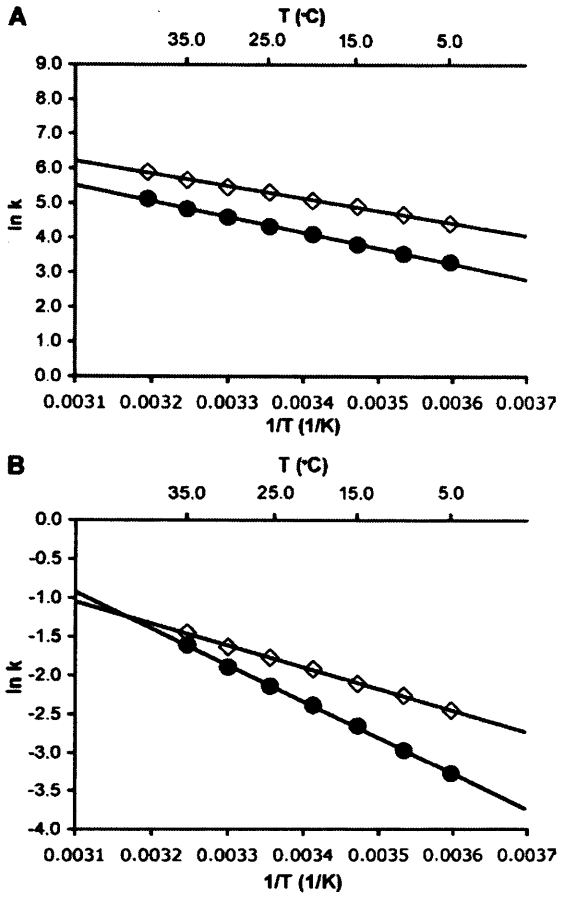

Figure 3 Arrhenius plots for H- and D-transfer during DHFR and G121V-DHFR catalysis at pH 7.0

Temperature dependence of the H- (◇) and D-transfer (●) rate constants for the reactions catalysed by DHFR (**A**) and G121V-DHFR (**B**) is shown. Each data point is the average of at least six measurements; the error bars are obscured by the symbols. Fitting the average rate value for every temperature to the Arrhenius equation yields the following parameters: DHFR, $E_A^H = 29.9 \pm 0.6$ kJ · mol^{-1}, $A_H = 3.3 \pm 0.8 \times 10^7$ s^{-1} and $E_A^D = 37.7 \pm 0.6$ kJ · mol^{-1}, $A_D = 3.07 \pm 0.80 \times 10^8$ s^{-1}; G121V-DHFR, $E_A^H = 23.3 \pm 0.3$ kJ · mol^{-1}, $A_H = 2.2 \pm 0.2 \times 10^3$ s^{-1} and $E_A^D = 39.0 \pm 0.6$ kJ · mol^{-1}, $A_D = 8.1 \pm 2.0 \times 10^5$ s^{-1}.

activation energies of E_A^H of 29.9 ± 0.6 kJ · mol^{-1} and E_A^D of 37.7 ± 0.7 kJ · mol^{-1}, leading to an inverse pre-exponential factor A_H/A_D of 0.108 ± 0.04 ($A_H = 3.3 \pm 0.8 \times 10^7$ s^{-1}; $A_D = 3.07 \pm 0.81 \times 10^8$ s^{-1}). The activation energy for H-transfer reported here was very similar to that measured previously in a different buffer but under identical conditions otherwise (28.2 ± 0.9 kJ · mol^{-1}) [8]. The relatively large difference in the activation energies for H- and D-transfer led to a temperature dependence of the primary KIEs (Figure 4). The KIE varied from 3.0 ± 0.2 at 5 °C to 2.2 ± 0.2 at 40 °C. The inverse ratio of the pre-exponential factors, which was well below the lower limit for the semi-classically calculated value of 0.71 [2,42], suggested a contribution from quantum mechanical tunnelling. Within a model of tunnelling through a rigid barrier, the temperature-dependent KIEs together with the observed values for A_H/A_D and $E_A^{H/D}$ suggest a moderate amount of tunnelling [43]. Two recent computational studies of hydrogen transfer during catalysis by DHFR from *E. coli* suggested that the barrier for hydrogen transfer was significantly lowered through the inclusion of quantum mechanical effects [31,36]. Garcia-Viloca et al. [31] obtained an overall quantum mechanical correction of 13.4 kJ · mol^{-1} to the classical activation energy for hydrogen transfer. Most of this

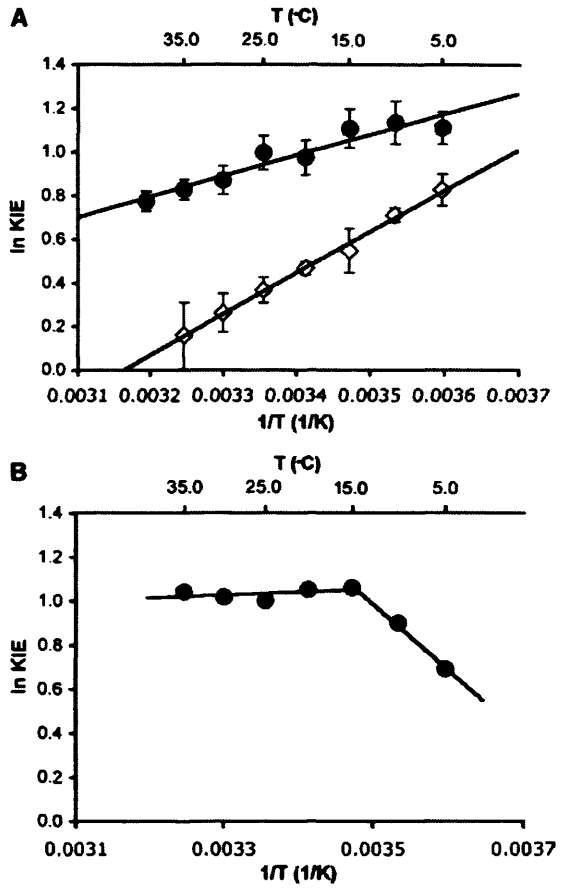

Figure 4 Temperature dependence of the KIEs for H- and D-transfer from NADPH/NADPD to H_2F

(**A**) Results from pre-steady-state measurements at pH 7.0 for catalysis by DHFR (●) and G121V-DHFR (◇). The best fit through the data yielded $\Delta E_A^{H/D}$ of 7.83 ± 0.98 kJ · mol^{-1} and A_H/A_D of 0.109 ± 0.043 for DHFR and $\Delta E_A^{H/D}$ of 15.83 ± 0.44 kJ · mol^{-1} and A_H/A_D of 0.0024 ± 0.0004 for G121V-DHFR. (**B**) Steady-state measurements for DHFR catalysis at pH 9.0 and 5.0. The best fit through the data between 15 and 35 °C is indicated and yields $\Delta E_A^{H/D}$ of 1.11 ± 0.79 kJ · mol^{-1} and A_H/A_D of 1.81 ± 0.19.

correction was attributed to quantization of nuclear vibrations, while only 2.9 kJ · mol^{-1} derived from hydrogen tunnelling. From the inverse ratio of the pre-exponential factors measured here, a previously proposed static model would predict moderate hydrogen tunnelling [43,44]. However, within the formalism of this model, elevated KIEs would be predicted in contrast with the rather small values measured here. The hydride transfer reaction catalysed by DHFR can therefore only be described adequately if protein motions coupled with hydrogen transfer are taken into account. Several theoretical approaches to hydrogen transfer models have been proposed that treat the hydrogen coordinates as fully quantum mechanical and incorporate various degrees of heavy atom motions to modulate the tunnelling barrier [16,17,45–47]. In one such model, a distinction was made between motions that actively modulate the tunnelling barrier and passive motions that merely help bring the substrates into reactive configurations (reviewed in [5,13]). This model predicts that when active dynamic motions are dominant and generate a temperature-dependent tunnelling distance, the KIEs become so temperature-dependent that the ratio of the pre-exponential factors is inverse. The experimentally observed inverse A_H/A_D and the temperature dependence of the KIEs suggest that at pH 7.0, DHFR actively modulates the tunnelling distance and hence the reaction rates [48]. Such active motions result in temperature-dependent KIEs and an inverse ratio of the pre-exponential factors, because the ideal tunnelling distance is different for the two isotopes. Such actively promoted tunnelling has been called rate-promoting vibrations [14,49,50], environmentally coupled tunnelling [13,43], and vibrationally enhanced ground state tunnelling [51]. The results reported here may also support the recent proposal of a correlation of changes in structural characteristics within DHFR from *E. coli* along the reaction pathway of hydrogen transfer through a network of hydrogen bonds and van der Waals interactions spanning the entire enzyme [18].

Steady-state kinetics of DHFR at pH 9.5

In a previous study, the temperature dependence of the deuterium and tritium isotope effects at pH 9.0, which was measured under steady-state conditions, also revealed environmentally coupled hydrogen transfer [2]. However, in contrast with the results presented here, for H-transfer at pH 7.0, the KIEs were independent of temperature. The rates for hydride transfer in DHFR catalysis have been shown to decrease steeply with increasing pH [26]. However, the rate of product release, which is rate-determining at physiological pH, is pH-independent; hence hydride transfer becomes rate limiting at elevated pH and, at pH 9.5 and above, the steady-state rate reflects the rate of the chemical step only [2,26]. Since at pH 9.0 the chemical step is not fully rate-determining, hydride transfer rates were measured under steady-state conditions at pH 9.5 to exclude kinetic complexity at pH 9.0 as a basis for the observed difference in the temperature dependence of transfer at elevated and physiological pH. We have therefore determined the temperature dependence of the steady-state turnover rates for the reduction of H_2F with NADPH and NADPD during DHFR catalysis at pH 9.5 [26] from the decrease in the absorbance at 340 nm due to the oxidation of the cofactor. At 25 °C, the rates for H- and D-transfer were 0.927 ± 0.012 and 0.341 ± 0.008 s^{-1}, resulting in a KIE of 2.72 ± 0.1 (see Supplementary Table 2 at http://www.BiochemJ.org/bj/394/bj3940259addd.htm). The KIE measured here was essentially identical to that calculated in a previous study [KIE (H/D) = 2.92 ± 0.076] from the measured H/T and D/T KIEs at pH 9.0 [2].

Within the temperature range of 15 and 35 °C the KIEs remained constant within the error of the experiment (Figure 4), while below 15 °C the KIEs decreased sharply. Fitting the KIEs between 15 and 35 °C to the Arrhenius equation resulted in a very small difference in the activation energy for H- and D-transfer ($\Delta E_A^{H/D} = 1.11 \pm 0.79$ kJ · mol^{-1}) and an isotope effect for the pre-exponential factor A_H/A_D of 1.81 ± 0.19, larger than the upper semi-classical limit of 1.41 [42]. A similar temperature dependence and enhanced KIE for the pre-exponential factors had been observed previously for the H/T and D/T KIEs at pH 9.0 [2]. A larger value for A_H/A_D of 4.0 ± 1.5 has been reported previously in steady-state experiments at pH 9.0 [2]. While an A_H/A_D ratio outside the semi-classical range has widely been accepted as an indication for quantum mechanical tunnelling, a recent computational study resulted in a ratio of pre-exponential factors of 1.9 [52], identical within error with the results reported here. Interestingly, a larger value was obtained when the tunnelling contributions were omitted.

The temperature-independent KIEs at elevated pH were in sharp contrast with the strong temperature dependence of the KIEs at pH 7 and suggested a relatively rigid active site configuration from which hydrogen transfer occurs with a contribution from environmentally coupled hydrogen tunnelling. Within the model linking catalysis and dynamics proposed by Klinman and coworkers [43], the elevated value for A_H/A_D together with the temperature-independent KIEs suggested contributions from passive

dynamics that do not actively modulate the tunnelling distance. This is in sharp contrast with the behaviour of DHFR at physiological pH, where hydrogen transfer is facilitated by active modulation of the tunnelling barrier. It is interesting to point out in this context that a recent computational study of DHFR catalysis revealed a small but significant temperature variation of the KIEs as a consequence of two competing temperature effects [53]. It is perhaps not surprising that in such a system the temperature dependence varies with reaction conditions.

DHFR has evolved an active site structure that is organized to support hydrogen tunnelling and to use active dynamics to promote hydrogen transfer at physiological pH. Relatively small increases in the pH of the solution, however, lead to a stiffening of the active site that no longer allows DHFR to actively promote hydrogen transfer, resulting in a reduction of the reaction rate by more than one order of magnitude. Interestingly, at pH 9.5, DHFR displays a temperature dependence of the reaction rates similar to that of the structurally more rigid DHFR from the thermophilic bacterium *T. maritima* [8]. Both enzymes appear to rely on passive motions only to generate active site configurations conducive to hydrogen transfer. In addition, the hydride transfer rates for the thermophilic DHFR at pH 7 and for the mesophilc DHFR at pH 9.5 were similar in the experimentally accessible temperature range [8,39]. These observations may suggest an evolutionary pattern in which catalysis progressed from a relatively rigid active site structure of DHFR from the ancient thermophile *T. maritima* to a more flexible and kinetically more efficient structure in *E. coli* that actively promotes hydrogen transfer at physiological pH.

Temperature dependence of hydride transfer and KIEs for catalysis by G121V-DHFR

Although residue 121 in the βF-βG loop of DHFR is on the exterior of the protein and approx. 19 Å from the centre of the enzyme, experimental studies have shown that mutations of Gly^{121} can reduce the rate of hydride transfer by up to 163-fold [20,37]. Together with NMR and computational studies, these results have been interpreted as evidence for the existence of a network of coupled dynamic motions that include residues in exterior loops of DHFR and promote hydride transfer [18]. It has been postulated that mutation of Gly^{121} disrupts this network of coupled motions leading to the observed reduction in the reaction rate and altered dynamic properties of the enzyme [52]. The rate of the hydride transfer from NADPH to H_2F catalysed by G121V-DHFR was measured at pH 7.0 in pre-steady-state experiments. The decrease in the fluorescence intensity was best described by a double exponential. A first event was observed that occurred with a rate constant of approx. 3.5 s^{-1} at 25 °C and did not show a KIE when NADPD replaced NADPH. This process had previously been interpreted as a conformational change associated with a rearrangement of the reduced nicotinamide ring into the enzyme's active site [20]. Surprisingly, this fast isotopically insensitive step had not been observed under similar conditions in a previous study of G121V-DHFR catalysis, perhaps due to the different buffers used in the two studies [37]. This initial step was followed by a slow decrease in the fluorescence intensity, the rate of which did not change when the concentration of NADPH was varied. The slow step was therefore most likely due to the oxidation of the cofactor that occurred with a first-order rate constant of 0.171 ± 0.004 s^{-1} at 25 °C (see Supplementary Table 3 at http://www.BiochemJ.org/bj/394/bj3940259add.htm). This rate constant is somewhat lower than that published previously [37], most likely as a consequence of the different reaction conditions. In the present study, potassium phosphate, which shows little variation of pH with changing temperature, was used rather than the amine-based MTEN buffer. At 25 °C, a KIE of 1.450 ± 0.042 was measured when NADPD was used instead of NADPH.

Similar to the wild-type enzyme, a relatively strong temperature dependence of the hydride transfer rates and the KIEs was observed between 5 and 35 °C (Figures 3 and 4). The rates increased almost 3-fold in the temperature range leading to activation energies of E_A^H of 23.3 ± 0.3 and E_A^D of 39.0 ± 0.6 kJ · mol^{-1} for H- and D-transfer respectively. The activation energy for H-transfer catalysed by G121V-DHFR was smaller than that measured for the wild-type, indicating that the reduced catalytic efficiency of the mutant was a consequence of a smaller pre-exponential factor ($A_H = 2.2 \pm 0.2 \times 10^3$ s^{-1}; $A_D = 8.1 \pm 2.0 \times 10^5$ s^{-1}). The difference in activation energies ($\Delta E_A = E_A^H - E_A^D$) of -15.7 kJ · mol^{-1} was twice that observed for wild-type DHFR, leading to more strongly inverse pre-exponential factors A_H/A_D of 0.0025 ± 0.0007. These data are consistent with a model in which the reaction occurred with a significant contribution from quantum mechanical tunnelling coupled with active dynamic motions.

The results presented here indicate that, while replacing residue 121 in DHFR with valine leads to a significant reduction in the rate of hydrogen transfer, the general mechanism by which the reaction is coupled with the environment is unaltered, at least in a qualitative sense. Molecular dynamics, CD and fluorescence experiments had suggested that the reduced catalytic efficiency of the mutant may arise from structural effects on the overall fold of the protein [38]. NMR experiments indicated that in G121V-DHFR the closed conformation, in which hydrogen transfer occurs in the wild-type, was destabilized [22]. Geometric constraints imposed by the bulky isopropyl group in G121V-DHFR may be transmitted to the active site to produce a lower number of active site configurations favourable for hydride transfer. In agreement with this explanation, a computational study by Thorpe and Brooks [33] suggested that H_2F and NADPH populate preferentially a region of configuration space of DHFR that is conducive to the reaction, while substrate and cofactor become trapped in unproductive configurations in G121V-DHFR. The results presented here indicate, however, that once NADPH and H_2F are bound in the reactive configuration, both mutant and wild-type actively promote hydride transfer.

The reduced catalytic efficiency of G121V-DHFR was mainly a consequence of the significantly reduced pre-exponential factors. The Eyring interpretation of the temperature dependence of the reaction rates relates activation energy and pre-exponential factor to activation enthalpy and entropy, $\Delta\eta^\ddagger$ and $\Delta S^\ddagger$. The activation enthalpies and entropies for hydride transfer by DHFR and G121V-DHFR were obtained by fitting the temperature dependence of the reaction rates to the Eyring equation [$k/T = k_B/h \exp(\Delta S^\ddagger/R) \exp(-\Delta H^\ddagger/RT)$, where k is a first-order constant, k_B the Boltzmann constant and h the Planck constant; R is the universal gas constant]. While the activation enthalpy favoured hydride transfer by G121V-DHFR by 6.3 ± 0.2 kJ · mol^{-1}, the activation entropy strongly favoured the reaction catalysed by the wild-type enzyme. An increase in the activation entropy ($-T\Delta S^\ddagger$) for the mutant indicated that a significantly higher molecular reorganization was required to reach the transition state in G121V-DHFR ($T\Delta S^\ddagger_{G121V} = -56.4 \pm 0.8$ kJ · mol^{-1}) than in the wild type enzyme ($T\Delta S^\ddagger_{WT} = -32.9 \pm 0.8$ kJ · mol^{-1}).

In summary, our results suggest that the mechanism by which hydrogen transfer in DHFR is coupled with protein fluctuations, depends on the pH of the environment. Under physiological conditions, DHFR increases the reaction rate through optimization of the coupling of environmental dynamics with quantum mechanical tunnelling. Only relatively small changes in pH lead to a stiffening of the active site and a loss of active promotion of

hydrogen transfer. On the other hand, the mechanism is relatively robust towards mutation of residue 121, the identity of which is known to be critical for efficient hydride transfer. Like in the wild-type enzyme, the tunnelling distance is modulated by active dynamics in the kinetically compromised mutant G121V-DHFR. The reduced hydride transfer rates of this mutant are therefore not the consequence of altered dynamics, but most likely of geometric constraints [33,38] that lead to a higher entropic cost for the formation of active site conformations conducive to the reaction.

This work was supported by the BBSRC (Biotechnology and Biological Sciences Research Council) and Cardiff University.

REFERENCES

1 Marcus, R. A. and Sutin, N. (1985) Electron transfers in chemistry and biology. Biochim. Biophys. Acta **811**, 265–322
2 Sikorski, R. S., Wang, L., Markham, K. A., Rajagopalan, P. T. R., Benkovic, S. J. and Kohen, A. (2004) Tunneling and coupled motion in the *Escherichia coli* dihydrofolate reductase catalysis. J. Am. Chem. Soc. **126**, 4778–4779
3 Basran, J., Patel, S., Sutcliffe, M. J. and Scrutton, N. S. (2001) Importance of barrier shape in enzyme-catalyzed reactions: vibrationally assisted hydrogen tunneling in tryptophan tryptophylquinone-dependent amine dehydrogenases. J. Biol. Chem. **276**, 6234-6242
4 Francisco, W. A., Knapp, M. J., Blackburn, N. J. and Klinman, J. P. (2002) Hydrogen tunneling in peptidylglycine α-hydroxylating monooxygenase. J. Am. Chem. Soc. **124**, 8194–8195
5 Knapp, M. J. and Klinman, J. P. (2002) Environmentally coupled hydrogen tunneling: linking catalysis to dynamics. Eur. J. Biochem. **269**, 3113–3121
6 Kohen, A. and Klinman, J. P. (1999) Hydrogen tunneling in biology. Chem. Biol. **6**, R191–R198
7 Kohen, A. and Klinman, J. P. (2000) Protein flexibility correlates with degree of hydrogen tunneling in thermophilic and mesophilic alcohol dehydrogenases. J. Am. Chem. Soc. **122**, 10738–10739
8 Maglia, G. and Allemann, R. K. (2003) Evidence for environmentally coupled hydrogen tunneling during dihydrofolate reductase catalysis. J. Am. Chem. Soc. **125**, 13372–13373
9 Rickert, K. W. and Klinman, J. P. (1999) Nature of hydrogen transfer in soybean lipoxygenase 1: separation of primary and secondary isotope effects. Biochemistry **38**, 12218–12228
10 Agrawal, N., Hong, B. Y., Mihai, C. and Kohen, A. (2004) Vibrationally enhanced hydrogen tunneling in the *Escherichia coli* thymidylate synthase catalyzed reaction. Biochemistry **43**, 1998–2006
11 Masgrau, L., Basran, J., Hothi, P., Sutcliffe, M. J. and Scrutton, N. S. (2004) Hydrogen tunneling in quinoproteins. Arch. Biochem. Biophys. **428**, 41–51
12 Doll, K. M., Bender, B. R. and Finke, R. G. (2003) The first experimental test of the hypothesis that enzymes have evolved to enhance hydrogen tunneling. J. Am. Chem. Soc. **125**, 10877–10884
13 Klinman, J. P. (2003) Dynamic barriers and tunneling. New views of hydrogen transfer in enzyme reactions. Pure Appl. Chem. **75**, 601–608
14 Antoniou, D., Caratzoulas, S., Kalyanaraman, C., Mincer, J. S. and Schwartz, S. D. (2002) Barrier passage and protein dynamics in enzymatically catalyzed reactions. Eur. J. Biochem. **269**, 3103–3112
15 Garcia-Viloca, M., Gao, J., Karplus, M. and Truhlar, D. G. (2004) How enzymes work: analysis by modern rate theory and computer simulations. Science **303**, 186–195
16 Borgis, D. and Hynes, J. T. (1996) Curve crossing formulation for proton transfer reactions in solution. J. Phys. Chem. **100**, 1118–1128
17 Bruno, W. J. and Bialek, W. (1992) Vibrationally enhanced tunneling as a mechanism for enzymatic hydrogen transfer. Biophys. J. **63**, 689–699
18 Agarwal, P. K., Billeter, S. R., Rajagopalan, P. T. R., Benkovic, S. J. and Hammes-Schiffer, S. (2002) Network of coupled promoting motions in enzyme catalysis. Proc. Natl. Acad. Sci. U.S.A. **99**, 2794–2799
19 Kuznetsov, A. M. and Ulstrup, J. (1999) Proton and hydrogen atom tunnelling in hydrolytic and redox enzyme catalysis. Can. J. Chem. **77**, 1085–1096
20 Rajagopalan, P. T. R., Lutz, S. and Benkovic, S. J. (2002) Coupling interactions of distal residues enhance dihydrofolate reductase catalysis: mutational effects on hydride transfer rates. Biochemistry **41**, 12618–12628
21 Sawaya, M. R. and Kraut, J. (1997) Loop and subdomain movements in the mechanism of *Escherichia coli* dihydrofolate reductase: crystallographic evidence. Biochemistry **36**, 586–603
22 Venkitakrishnan, R. P., Zaborowski, E., McElheny, D., Benkovic, S. J., Dyson, H. J. and Wright, P. E. (2004) Conformational changes in the active site loops of dihydrofolate reductase during the catalytic cycle. Biochemistry **43**, 16046–16055
23 Osborne, M. J., Schnell, J., Benkovic, S. J., Dyson, H. J. and Wright, P. E. (2001) Backbone dynamics in dihydrofolate reductase complexes: role of loop flexibility in the catalytic mechanism. Biochemistry **40**, 9846–9859
24 Falzone, C. J., Wright, P. E. and Benkovic, S. J. (1994) Dynamics of a flexible loop in dihydrofolate-reductase from *Escherichia coli* and its implication for catalysis. Biochemistry **33**, 439–442
25 McElheny, D., Schnell, J. R., Lansing, J. C., Dyson, H. J. and Wright, P. E. (2005) Defining the role of active-site loop fluctuations in dihydrofolate reductase catalysis. Proc. Natl. Acad. Sci. U.S.A. **102**, 5032–5037
26 Fierke, C. A., Johnson, K. A. and Benkovic, S. J. (1987) Construction and evaluation of the kinetic scheme associated with dihydrofolate reductase from *Escherichia coli*. Biochemistry **26**, 4085–4092
27 Miller, G. P. and Benkovic, S. J. (1998) Stretching exercises: flexibility in dihydrofolate reductase catalysis. Chem. Biol. **5**, R105–R113
28 Cummins, P. L. and Gready, J. E. (2001) Energetically most likely substrate and active-site protonation sites and pathways in the catalytic mechanism of dihydrofolate reductase. J. Am. Chem. Soc. **123**, 3418–3428
29 Castillo, R., Andres, J. and Moliner, V. (1999) Catalytic mechanism of dihydrofolate reductase enzyme: a combined quantum-mechanical/molecular-mechanical characterization of transition state structure for the hydride transfer step. J. Am. Chem. Soc. **121**, 12140–12147
30 Garcia-Viloca, M., Truhlar, D. G. and Gao, J. (2003) Importance of substrate and cofactor polarization in the active site of dihydrofolate reductase. J. Mol. Biol. **327**, 549–560
31 Garcia-Viloca, M., Truhlar, D. G. and Gao, J. (2003) Reaction-path energetics and kinetics of the hydride transfer reaction catalyzed by dihydrofolate reductase. Biochemistry **42**, 13558–13575
32 Thorpe, I. F. and Brooks, C. L. (2003) Barriers to hydride transfer in wild type and mutant dihydrofolate reductase from *E. coli*. J. Phys. Chem. B **107**, 14042–14051
33 Thorpe, I. F. and Brooks, C. L. (2004) The coupling of structural fluctuations to hydride transfer in dihydrofolate reductase. Proteins Struct. Funct. Bioinform. **57**, 444–457
34 Rod, T. H., Radkiewicz, J. L. and Brooks, C. L. (2003) Correlated motion and the effect of distal mutations in dihydrofolate reductase. Proc. Natl. Acad. Sci. U.S.A. **100**, 6980–6985
35 Rod, T. H. and Brooks, C. L. (2003) How dihydrofolate reductase facilitates protonation of dihydrofolate. J. Am. Chem. Soc. **125**, 8718–8719
36 Agarwal, P. K., Billeter, S. R. and Hammes-Schiffer, S. (2002) Nuclear quantum effects and enzyme dynamics in dihydrofolate reductase catalysis. J. Phys. Chem. B **106**, 3283–3293
37 Cameron, C. E. and Benkovic, S. J. (1997) Evidence for a functional role of the dynamics of glycine-121 of *Escherichia coli* dihydrofolate reductase obtained from kinetic analysis of a site-directed mutant. Biochemistry **36**, 15792–15800
38 Swanwick, R. S., Shrimpton, P. J. and Allemann, R. K. (2004) Pivotal role of Gly^{121} in dihydrofolate reductase from *Escherichia coli*: the altered structure of a mutant enzyme may form the basis of its diminished catalytic performance. Biochemistry **43**, 4119–4127
39 Maglia, G., Javed, M. H. and Allemann, R. K. (2003) Hydride transfer during catalysis by dihydrofolate reductase from *Thermotoga maritima*. Biochem. J. **374**, 529–535
40 Stone, S. R. and Morrison, J. F. (1982) Kinetic mechanism of the reaction catalyzed by dihydrofolate reductase from *Escherichia coli*. Biochemistry **21**, 3757–3765
41 Miller, G. P. and Benkovic, S. J. (1998) Strength of an interloop hydrogen bond determines the kinetic pathway in catalysis by *Escherichia coli* dihydrofolate reductase. Biochemistry **37**, 6336–6342
42 Bell, R. P. (1980) The Tunnel Effect in Chemistry, pp. 88–105, Chapman and Hall, London
43 Knapp, M. J., Rickert, K. and Klinman, J. P. (2002) Temperature-dependent isotope effects in soybean lipoxygenase-1: correlating hydrogen tunneling with protein dynamics. J. Am. Chem. Soc. **124**, 3865–3874
44 Jonsson, T., Glickman, M. H., Sun, S. J. and Klinman, J. P. (1996) Experimental evidence for extensive tunneling of hydrogen in the lipoxygenase reaction: implications for enzyme catalysis. J. Am. Chem. Soc. **118**, 10319–10320
45 Borgis, D. and Hynes, J. T. (1993) Dynamic theory of proton tunneling transfer rates in solution: general formulation. Chem. Phys. **170**, 315–346
46 Antoniou, D. and Schwartz, S. D. (1998) Activated chemistry in the presence of a strongly symmetrically coupled vibration. J. Chem. Phys. **108**, 3620–3625
47 Antoniou, D. and Schwartz, S. D. (2001) Internal enzyme motions as a source of catalytic activity: rate-promoting vibrations and hydrogen tunneling. J. Phys. Chem. B **105**, 5553–5558

48 Knapp, M. J. and Klinman, J. P. (2003) Kinetic studies of oxygen reactivity in soybean lipoxygenase-1. Biochemistry **42**, 11466–11475
49 Mincer, J. S. and Schwartz, S. D. (2003) A computational method to identify residues important in creating a protein promoting vibration in enzymes. J. Phys. Chem. B **107**, 366–371
50 Caratzoulas, S., Mincer, J. S. and Schwartz, S. D. (2002) Identification of a protein-promoting vibration in the reaction catalyzed by horse liver alcohol dehydrogenase. J. Am. Chem. Soc. **124**, 3270–3276
51 Sutcliffe, M. J. and Scrutton, N. S. (2002) A new conceptual framework for enzyme catalysis: hydrogen tunneling coupled to enzyme dynamics in flavoprotein and quinoprotein enzymes. Eur. J. Biochem. **269**, 3096–3102
52 Watney, J. B., Agarwal, P. K. and Hammes-Schiffer, S. (2003) Effect of mutation on enzyme motion in dihydrofolate reductase. J. Am. Chem. Soc. **125**, 3745–3750
53 Pu, J. Z., Ma, S. H., Gao, J. L. and Truhlar, D. G. (2005) Small temperature dependence of the kinetic isotope effect for the hydride transfer reaction catalyzed by *Escherichia coli* dihydrofolate reductase. J. Phys. Chem. B **109**, 8551–8556

Received 5 September 2005/11 October 2005; accepted 24 October 2005
Published as BJ Immediate Publication 24 October 2005, doi:10.1042/BJ20051464

PHILOSOPHICAL TRANSACTIONS OF THE ROYAL SOCIETY B

Phil. Trans. R. Soc. B (2006) **361**, 1317–1321
doi:10.1098/rstb.2006.1865
Published online 12 July 2006

Protein motions during catalysis by dihydrofolate reductases

Rudolf K. Allemann[1,*], Rhiannon M. Evans[1], Lai-hock Tey[1], Giovanni Maglia[2], Jiayun Pang[1,2], Robert Rodriguez[1,2], Paul J. Shrimpton[2] and Richard S. Swanwick[1]

[1]*School of Chemistry, Cardiff University, Main Building, Park Place, Cardiff CF10 3AT, UK*
[2]*School of Chemistry, University of Birmingham, Edgbaston, Birmingham B15 2TT, UK*

Dihydrofolate reductase (DHFR) maintains the intracellular pool of tetrahydrofolate through catalysis of hydrogen transfer from reduced nicotinamide adenine dinucleotide to 7,8-dihydrofolate. We report results for pre-steady-state kinetic studies of the temperature dependence of the rates and the hydrogen/deuterium-kinetic isotope effects for the reactions catalysed by the enzymes from the mesophilic *Escherichia coli* and the hyperthermophilic *Thermatoga maritima*. We propose an evolutionary pattern in which catalysis progressed from a relatively rigid active site structure in the ancient thermophilic DHFR to a more flexible and kinetically more efficient structure in *E. coli* that actively promotes hydrogen transfer at physiological pH by modulating the tunnelling distance. The *E. coli* enzyme appeared relatively robust, in that kinetically severely compromised mutants still actively propagated the reaction. The reduced hydrogen transfer rates of the extensively studied Gly121Val mutant of DHFR from *E. coli* were most likely due to sterically unfavourable long-range effects from the introduction of the bulky isopropyl group.

Keywords: hydrogen transfer; kinetic isotope effects; protein dynamics; catalysis; enzymes

1. INTRODUCTION

5,6,7,8-Tetrahydrofolate (H_4F) is required for the biosynthesis of thymidylate, purines and several amino acids. Its intracellular levels are maintained through the nicotinamide adenine dinucleotide phosphate (NADPH)-dependent reduction of 7,8-dihydrofolate (H_2F) catalysed by the ubiquitous enzyme dihydrofolate reductase (DHFR; figure 1). This enzyme has therefore been a long-standing pharmacological target and hence has been studied extensively by X-ray crystallography, nuclear magnetic resonance (NMR) spectroscopy and computation (Sawaya & Kraut 1997; Casarotto *et al.* 1999; Feeney 2000; Radkiewicz & Brooks 2000; Agarwal *et al.* 2002*a*,*b*; Shrimpton & Allemann 2002; Benkovic & Hammes-Schiffer 2003; Garcia-Viloca *et al.* 2003*a*,*b*; Shrimpton *et al.* 2003; Thorpe & Brooks 2003, 2004; Venkitakrishnan *et al.* 2004; McElheny *et al.* 2005; Pu *et al.* 2005). While structural studies of enzymes have significantly influenced our view of catalysis, the static three-dimensional pictures provided by these studies do not incorporate the wide range of dynamical motions that occur in proteins. DHFR has recently served as a paradigm for the development and testing of concepts that relate the enormous catalytic power of enzymes to their dynamic properties.

Several studies of DHFR have indicated the importance of its dynamic properties for catalysis. DHFR from *Escherichia coli* (EcDHFR) is a monomeric enzyme consisting of four α-helices, eight β-sheets and four mobile loops (figure 2). The enzyme is separated into two domains, the adenosine binding domain and the loop domain. Previous studies have indicated the central role of the M20, the FG (residues 116–132) and the GH (residues 142–150) loops for the catalytic activity and mechanism of DHFR. The M20 loop adopts the closed conformation in the reactive ternary complex when both H_2F and NADPH are bound (Sawaya & Kraut 1997). This conformation is stabilized through hydrogen bonds between residues in the M20 and the FG loops. The backbone nitrogen atoms of these loops displayed high dynamic mobility in NMR relaxation experiments, which has been interpreted to suggest a connection between the dynamic properties of these loops and the catalytic behaviour of DHFR (Epstein *et al.* 1995; Osborne *et al.* 2001). The relationship between movements of these loops and catalysis has been probed by site-directed mutagenesis. Replacement of Gly121, a highly mobile residue located in the middle of the FG loop over 19 Å from the active site, with Val or Leu slowed the hydride transfer rate dramatically and weakened the binding of NADPH (Cameron & Benkovic 1997). While being strictly conserved in all prokaryotic DHFRs, Gly121 does not appear to form any interactions with other residues. Molecular dynamic (MD) simulations of EcDHFR revealed a strong correlation between the movement of the catalytically important M20 and FG loops (Radkiewicz & Brooks 2000). These correlated motions were observed only in reactive complexes of the enzyme and absent in the product complex. Mixed quantum mechanical molecular mechanic simulations and genomic sequence analysis have identified a network

* Author for correspondence (allemannrk@cardiff.ac.uk).

One contribution of 16 to a Discussion Meeting Issue 'Quantum catalysis in enzymes—beyond the transition state theory paradigm'.

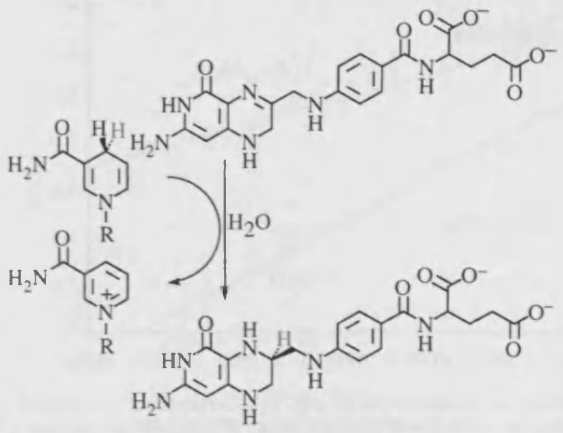

Figure 1. DHFR catalyses the transfer of H-Re from nicotinamide adenine dinucleotide phosphate (NADPH) to 7,8-dihydrofolate (H_2F).

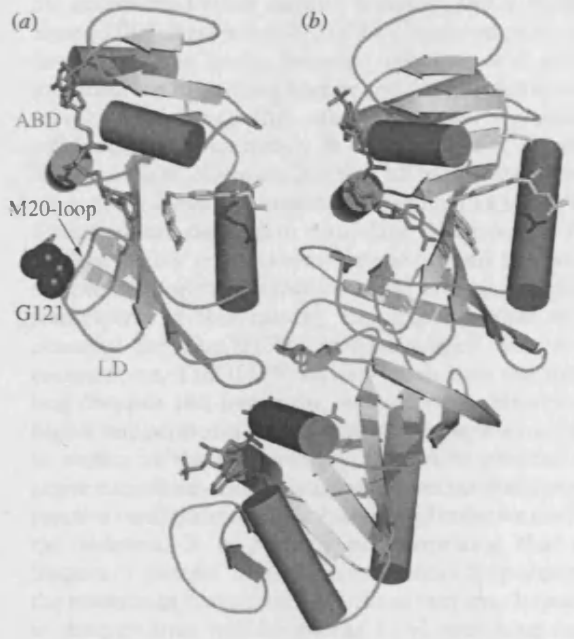

Figure 2. Sketch of the structures of (*a*) EcDHFR and (*b*) TmDHFR. The active site of EcDHFR is located between the ABD and the LD. Substrate, cofactor, and the position of Gly121 in the FG loop of EcDHFR are indicated.

of hydrogen bonds and van der Waals contacts from Asp122 on the surface of the protein to the active site (Agarwal *et al.* 2002*b*). This network may facilitate hydride transfer, suggesting a direct link between the motion of the FG loop and the catalytic events in the active site. In good agreement with the kinetic measurements, computation revealed a significant increase in the energy barrier for the hydride transfer of the Gly121 to Val mutant (EcDHFR-G121V) relative to the wild-type enzyme (DHFR; Watney *et al.* 2003).

2. RESULTS AND DISCUSSION

(a) *Hydride transfer in DHFR from* T. maritima *and* E. coli

The measurement of the temperature dependence of the kinetic isotope effects (KIEs) of the hydride transfer

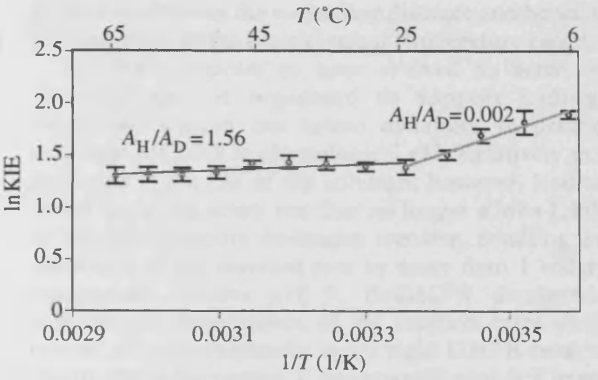

Figure 3. Temperature dependence of the kinetic isotope effects for hydrogen transfer catalysed by TmDHFR (Maglia & Allemann 2003).

catalysed by DHFR is a sensitive method to probe the influence of protein dynamics on the chemistry of the reaction. Here, we report the results of such measurements for the monomeric DHFR from *E. coli*, its catalytically compromised G121V-mutant and DHFR from *Thermatoga maritima* (TmDHFR). Unlike its mesophilic homologue, this thermophilic enzyme, which unfolds at *ca* 80 °C—almost 30 °C above the melting temperature of EcDHFR (Maglia *et al.* 2003)—is the only dimeric DHFR known at present (figure 2; Dams *et al.* 2000). Mutants that increase the proportion of the monomer of TmDHFR display significantly reduced thermal stability (Rodriguez & Allemann 2006, unpublished data). The dimerization interface involves the catalytically important M20 and the FG loops and the steady state turnover rate of TmDHFR is reduced by approximately 1 order of magnitude relative to the enzyme from *E. coli* at their respective physiological temperatures (Maglia *et al.* 2003).

The hydride transfer rates for the reduction of H_2F during Tm- and EcDHFR catalysis were measured as a function of temperature by fluorescence resonance energy transfer from the protein to the reduced nicotinamide moiety of NADPH. For TmDHFR, a biphasic temperature dependence was observed at pH 7.0 with a break point at approximately 25 °C (figure 3; Maglia & Allemann 2003; Maglia 2004). Below 25 °C the KIE increased with decreasing temperature, while above 25 °C the KIE was temperature-independent, at least within the relatively narrow range of experimentally accessible temperatures. The ratio of the Arrhenius pre-exponential factors, which was obtained from the extrapolation of the temperature dependence of the KIE, was inverse for the lower temperature range ($A_H/A_D = 0.002$) and close to unity above 25 °C ($A_H/A_D = 1.56$). The activation energies of hydride and deutride transfer were obtained from the temperature dependence of the reaction rates to the empirical Arrhenius equation. For the temperature range from 25 to 65 °C E_A^H and E_A^D for hydride and deuteride transfer were similar ($E_A^H = 53.5$ kJ mol^{-1}; $E_A^D = 56.0$ kJ mol^{-1}), while below 25 °C the difference of the activation energies increased owing to an increased activation energy for deuteride transfer.

Several theoretical approaches to hydrogen transfer have been proposed that treat the hydrogen coordinate

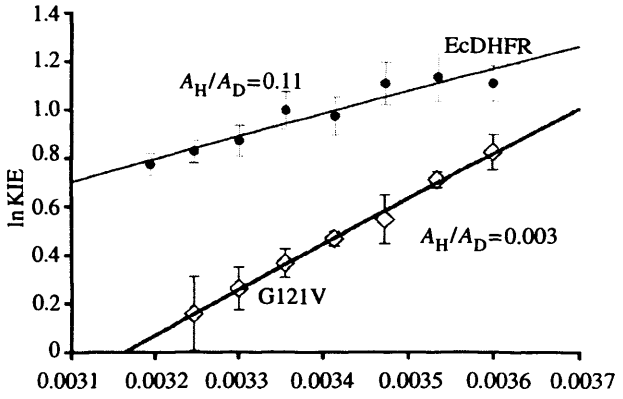

Figure 4. Comparison of the T-dependence of hydrogen transfer of EcDHFR and EcDHFR-G121V at pH 7.0 (Swanwick *et al.* 2006).

completely quantum mechanically and incorporate various degrees of heavy atom motions that modulate the tunnelling barrier (Bruno & Bialek 1992; Borgis & Hynes 1996; Agarwal *et al.* 2002*b*). In one such model, a distinction was made between motions that actively modulate the tunnelling barrier and passive motions that merely help bring the substrates into the reactive configurations (Kuznetsov & Ulstrup 1999; Knapp & Klinman 2002; Klinman 2003). This model predicts that when active dynamic motions are dominant and generate a temperature-dependent tunnelling distance, the KIEs become highly temperature-dependent and the ratio of the pre-exponential factors becomes inverse. Within the framework of this model, the experimental results observed for TmDHFR catalysis suggest that at low temperature, TmDHFR actively modulates the tunnelling distance and hence the reaction rates. However, at higher temperatures, the rigidity of the enzyme necessary to ensure its thermal stability appears to prevent such active tunnelling, and only passive motions that generate reactive configurations of substrate and cofactor promote the reaction. It is perhaps not surprising that low-frequency protein modes become more important for the reaction at lower temperatures as they may be excited at temperatures well below the C–H stretching mode, the excitation of which is much more temperature-dependent. A molecular dynamical simulation of the TmDHFR catalysed reaction at 5, 25 and 65 °C using ensemble-averaged variational transition state theory with multidimensional tunnelling confirmed significant contributions from H-tunnelling at all temperatures, with the relative contributions to the overall reaction rate decreasing with increasing temperatures (Pang *et al.* 2006).

H and D transfer catalysed by the mesophilic EcDHFR at pH 7.0 revealed a monophasic and relatively strong dependence of the reaction rates on the temperature resulting in activation energies of $E_A^H = 29.9$ kJ mol^{-1} and $E_A^D = 37.7$ kJ mol^{-1} leading to an inverse pre-exponential factor $A_H/A_D = 0.108$ and temperature-dependent primary KIEs (figure 4; Swanwick *et al.* 2006). Within the dynamic model proposed by Knapp & Klinman (2002), the inverse A_H/A_D and the temperature dependence of the KIEs observed here suggest a dynamic active site for EcDHFR at pH 7.0 that, unlike the active site of TmDHFR, actively modulates the tunnelling distance and hence the reaction rates in the physiological temperature range.

EcDHFR appears to have evolved an active site structure that is organized to support hydrogen tunnelling and to use active dynamics to promote hydrogen transfer at physiological pH. Relatively small increases in the pH of the solution, however, lead to a stiffening of the active site that no longer allows DHFR to actively promote hydrogen transfer, resulting in a reduction of the reaction rate by more than 1 order of magnitude. Above pH 9, EcDHFR displayed a temperature dependence of the reaction rates similar to that of the structurally more rigid DHFR from the thermophilic bacterium *T. maritima* (Knapp & Klinman 2002; Sikorski *et al.* 2004), suggesting that they both relied on passive motions only to generate active site configurations conducive to hydrogen transfer. These observations may suggest an evolutionary pattern in which catalysis progressed from a relatively rigid active site structure of DHFR from the ancient thermophile *T. maritima* to a more flexible and kinetically more efficient structure in *E. coli* that actively promotes hydrogen transfer at physiological pH.

(b) *Basis of reduced activity of EcDHFR-G121V*

Gly121 in the FG loop of DHFR is on the exterior of the protein and approximately 19 Å from the centre of the enzyme. Several studies have shown that replacement of this residue can lead to significant reductions of the hydride transfer rates. Together with NMR and computational studies, these results have been interpreted as evidence for the existence of a network of coupled dynamic motions that include residues in exterior loops of DHFR and promote hydride transfer. Replacement of Gly121 has been proposed to lead to alterations in the network of coupled motions and altered dynamic properties of the enzyme resulting in a reduction of its catalytic efficiency (Watney *et al.* 2003).

Similar to the wild-type EcDHFR, a relatively strong temperature dependence of the hydride transfer rates and the KIEs was observed between 5 and 35 °C for catalysis by the mutant (Swanwick *et al.* 2006). The rates increased almost threefold in the temperature range leading to activation energies of $E_A^H = 23.3$ and $E_A^D = 39.0$ kJ mol^{-1} for H- and D-transfer, respectively, and temperature-dependent KIEs (figure 4). Together with the strongly inverse pre-exponential factors ($A_H/A_D = 0.0025$), these results suggested that the reaction occurred with a significant contribution from the quantum mechanical tunnelling coupled to active dynamic motions.

Our observations indicated that, while replacing residue 121 in DHFR with Val leads to a significant reduction in the rate of hydrogen transfer, the general mechanism by which the reaction is coupled to the environment is unaltered, at least in a qualitative sense. This was in good agreement with MD simulations and CD and fluorescence experiments which had suggested that conformational changes that have been transmitted to the active sites as a consequence of the geometric constraints imposed by the bulky isopropyl group in EcDHFR-G121V may be the reason for the reduced catalytic efficiency of the mutant (Swanwick *et al.* 2004; Thorpe & Brooks 2004).

The pre-steady-state measurements of the hydride transfer event in EcDHFR-G121V catalysis revealed an isotope insensitive step before hydride transfer that occurred with a rate constant of approximately 3.5 s^{-1} at ambient temperature and could be interpreted as a conformational change (Cameron & Benkovic 1997; Swanwick *et al.* 2006). Thorpe and Brooks suggested previously that substrate and cofactor and NADPH populate preferentially a region of configuration space of EcDHFR from which the reaction can take place (Thorpe & Brooks 2004). In EcDHFR-G121V, however, NADPH and H_2F are postulated to become trapped in unproductive configurations (Swanwick *et al.* 2004). The temperature dependence of the hydride transfer indicates that once NADPH and H_2F are bound in the reactive configuration, both mutant and wild-type actively promote hydride transfer.

In summary, analysis of homologous DHFRs and their mutants has provided evidence that hydrogen transfer occurs to a significant amount by quantum mechanical tunnelling promoted by the environment. Structural changes as a consequence of mutations of EcDHFR appear to give rise to changes in these promoting motions leading to reduced hydrogen transfer efficiencies as a consequence of greatly changed ratios of pre-exponential factors. On the other hand, in the hyperthermophilic DHFR from *T. maritima*, the necessary stability against thermal denaturation appears to result in a rigid and hence less efficient enzyme.

The invaluable support of Donald Truhlar and Jiali Gao and stimulating discussions with Amnon Kohen are gratefully acknowledged. This work was generously supported by the BBSRC and Cardiff University.

REFERENCES

Agarwal, P. K., Billeter, S. R. & Hammes-Schiffer, S. 2002*a* Nuclear quantum effects and enzyme dynamics in dihydrofolate reductase catalysis. *J. Phys. Chem. B* **106**, 3283–3293. (doi:10.1021/jp020190v)

Agarwal, P. K., Billeter, S. R., Rajagopalan, P. T. R., Benkovic, S. J. & Hammes-Schiffer, S. 2002*b* Network of coupled promoting motions in enzyme catalysis. *Proc. Natl Acad. Sci. USA* **99**, 2794–2799. (doi:10.1073/pnas.052005999)

Benkovic, S. J. & Hammes-Schiffer, S. 2003 A perspective on enzyme catalysis. *Science* **301**, 1196–1202. (doi:10.1126/science.1085515)

Borgis, D. & Hynes, J. T. 1996 Curve crossing formulation for proton transfer reactions in solution. *J. Phys. Chem.* **100**, 1118–1128. (doi:10.1021/jp9522324)

Bruno, W. J. & Bialek, W. 1992 Vibrationally enhanced tunneling as a mechanism for enzymatic hydrogen transfer. *Biophys. J.* **63**, 689–699.

Cameron, C. E. & Benkovic, S. J. 1997 Evidence for a functional role of the dynamics of glycine-121 of *Escherichia coli* dihydrofolate reductase obtained from kinetic analysis of a site-directed mutant. *Biochemistry* **36**, 15 792–15 800. (doi:10.1021/bi9716231)

Casarotto, M. G., Basran, J., Badii, R., Sze, K. H. & Roberts, G. C. K. 1999 Direct measurement of the pK(a) of aspartic acid 26 in *Lactobacillus casei* dihydrofolate reductase: implications for the catalytic mechanism. *Biochemistry* **38**, 8038–8044. (doi:10.1021/bi990301p)

Dams, T., Auerbach, G., Bader, G., Jacob, U., Ploom, T., Huber, R. & Jaenicke, R. 2000 The crystal structure of dihydrofolate reductase from *Thermotoga maritima*: molecular features of thermostability. *J. Mol. Biol.* **297**, 659–672. (doi:10.1006/jmbi.2000.3570)

Epstein, D. M., Benkovic, S. J. & Wright, P. E. 1995 Dynamics of the dihydrofolate-reductase folate complex: catalytic sites and regions known to undergo conformational change exhibit diverse dynamical features. *Biochemistry* **34**, 11 037–11 048. (doi:10.1021/bi00035a009)

Feeney, J. 2000 NMR studies of ligand binding to dihydrofolate reductase. *Angew. Chem. Int. Ed.* **39**, 290–312. (doi:10.1002/(SICI)1521-3773(20000117)39:2<290::AID-ANIE290>3.0.CO;2-1)

Garcia-Viloca, M., Truhlar, D. G. & Gao, J. 2003*a* Importance of substrate and cofactor polarization in the active site of dihydrofolate reductase. *J. Mol. Biol.* **327**, 549–560. (doi:10.1016/S0022-2836(03)00123-2)

Garcia-Viloca, M., Truhlar, D. G. & Gao, J. 2003*b* Reaction-path energetics and kinetics of the hydride transfer reaction catalyzed by dihydrofolate reductase. *Biochemistry* **42**, 13 558–13 575. (doi:10.1021/bi034824f)

Klinman, J. P. 2003 Dynamic barriers and tunneling. New views of hydrogen transfer in enzyme reactions. *Pure Appl. Chem.* **75**, 601–608.

Knapp, M. J. & Klinman, J. P. 2002 Environmentally coupled hydrogen tunneling—linking catalysis to dynamics. *Eur. J. Biochem.* **269**, 3113–3121. (doi:10.1046/j.1432-1033.2002.03022.x)

Kuznetsov, A. M. & Ulstrup, J. 1999 Proton and hydrogen atom tunnelling in hydrolytic and redox enzyme catalysis. *Can. J. Chem.* **77**, 1085–1096. (doi:10.1139/cjc-77-5-6-1085)

Maglia, G. 2004 The importance of molecular dynamics in dihydrofolate catalysis. Ph.D. thesis, University of Birmingham.

Maglia, G. & Allemann, R. K. 2003 Evidence for environmentally coupled hydrogen tunneling during dihydrofolate reductase catalysis. *J. Am. Chem. Soc.* **125**, 13 372–13 373. (doi:10.1021/ja035692g)

Maglia, G., Javed, M. H. & Allemann, R. K. 2003 Hydride transfer during catalysis by dihydrofolate reductase from *Thermotoga maritima*. *Biochem. J.* **374**, 529–535. (doi:10.1042/BJ20030412)

McElheny, D., Schnell, J. R., Lansing, J. C., Dyson, H. J. & Wright, P. E. 2005 Defining the role of active-site loop fluctuations in dihydrofolate reductase catalysis. *Proc. Natl Acad. Sci. USA* **102**, 5032–5037. (doi:10.1073/pnas.0500699102)

Osborne, M. J., Schnell, J., Benkovic, S. J., Dyson, H. J. & Wright, P. E. 2001 Backbone dynamics in dihydrofolate reductase complexes: role of loop flexibility in the catalytic mechanism. *Biochemistry* **40**, 9846–9859. (doi:10.1021/bi010621k)

Pang, J., Pu, J., Gao, J., Truhlar, D. G. & Allemann, R. K. 2006 Hydride transfer reaction catalyzed by hyperthermophilic dihydrofolate reductase is dominated by quantum mechanical tunneling and is promoted by both inter- and intramonomeric correlated motions. *J. Am. Chem. Soc.* **128**, 8015–8023. (doi:10.1021/ja061585l)

Pu, J. Z., Ma, S. H., Gao, J. L. & Truhlar, D. G. 2005 Small temperature dependence of the kinetic isotope effect for the hydride transfer reaction catalyzed by *Escherichia coli* dihydrofolate reductase. *J. Phys. Chem. B* **109**, 8551–8556. (doi:10.1021/jp051184c)

Radkiewicz, J. L. & Brooks, C. L. 2000 Protein dynamics in enzymatic catalysis: exploration of dihydrofolate reductase. *J. Am. Chem. Soc.* **122**, 225–231. (doi:10.1021/ja9913838)

Sawaya, M. R. & Kraut, J. 1997 Loop and subdomain movements in the mechanism of *Escherichia coli* dihydrofolate reductase: crystallographic evidence. *Biochemistry* **36**, 586–603. (doi:10.1021/bi962337c)

Shrimpton, P. & Allemann, R. K. 2002 Role of water in the catalytic cycle of *E. coli* dihydrofolate reductase. *Protein Sci.* **11**, 1442–1451. (doi:10.1110/ps.5060102)

Shrimpton, P., Mullaney, A. & Allemann, R. K. 2003 Functional role for Tyr 31 in the catalytic cycle of chicken dihydrofolate reductase. *Proteins Struct. Funct. Genet.* **51**, 216–223. (doi:10.1002/prot.10370)

Sikorski, R. S., Wang, L., Markham, K. A., Rajagopalan, P. T. R., Benkovic, S. J. & Kohen, A. 2004 Tunneling and coupled motion in the *Escherichia coli* dihydrofolate reductase catalysis. *J. Am. Chem. Soc.* **126**, 4778–4779. (doi:10.1021/ja031683w)

Swanwick, R. S., Shrimpton, P. J. & Allemann, R. K. 2004 Pivotal role of Gly 121 in dihydrofolate reductase from *Escherichia coli*: the altered structure of a mutant enzyme may form the basis of its diminished catalytic performance. *Biochemistry* **43**, 4119–4127. (doi:10.1021/bi036164k)

Swanwick, R. S., Maglia, G., Tey, L.-h. & Allemann, R. K. 2006 Coupling of protein motions and hydrogen transfer during catalysis by *Escherichia coli* dihydrofolate reductase. *Biochem. J.* **394**, 259–265. (doi:10.1042/BJ20051464)

Thorpe, I. F. & Brooks, C. L. 2003 Barriers to hydride transfer in wild type and mutant dihydrofolate reductase from *E. coli*. *J. Phys. Chem. B* **107**, 14 042–14 051. (doi:10.1021/jp035734n)

Thorpe, I. F. & Brooks, C. L. 2004 The coupling of structural fluctuations to hydride transfer in dihydrofolate reductase. *Proteins Struct. Funct. Bioinform.* **57**, 444–457. (doi:10.1002/prot.20219)

Venkitakrishnan, R. P., Zaborowski, E., McElheny, D., Benkovic, S. J., Dyson, H. J. & Wright, P. E. 2004 Conformational changes in the active site loops of dihydrofolate reductase during the catalytic cycle. *Biochemistry* **43**, 16 046–16 055. (doi:10.1021/bi048119y)

Watney, J. B., Agarwal, P. K. & Hammes-Schiffer, S. 2003 Effect of mutation on enzyme motion in dihydrofolate reductase. *J. Am. Chem. Soc.* **125**, 3745–3750. (doi:10.1021/ja028487u)